The University Of Sheffield.

Photodynamic inactivation of bacterial pathogens – exploring the powers of light

A thesis submitted in part fulfilment for the degree of Doctor of Philosophy.

Department of Molecular Biology and Biotechnology.

The University of Sheffield

Peter G Walker

Bsc (Hons) The University of Leicester

Abstract

This alternative format thesis presents two manuscripts investigating the use of photodynamic inactivation (PDI) as an innovative non-antibiotic approach to inactivate bacterial pathogens. The first published paper investigates the effectiveness of an immobilised copper-based photosensitiser as a novel photo-antimicrobial to kill pathogenic bacteria using visible light. Photosensitisers which produce reactive oxygen species under light excitation have emerged as an efficient way to kill microorganisms in water, yet the majority of photosensitising metal complexes uses transition metal complexes which are compromised when immobilised to a surface, meaning photosensitiser purification remains problematic. These findings presented here for the first time show that a copper-based photosensitiser immobilised onto the surface of silica is effective in reducing both Gram-positive and Gram-negative bacteria in solution. This example of an immobilised copper photosensitiser used for light driven bacterial killing demonstrates the potential of transition metal complexes as low-cost efficient photo-antimicrobials which has the potential for use in water purification systems. The second manuscript investigates the susceptibility of the foodborne pathogen *Campylobacter jejuni* to killing by photodynamic inactivation. We have shown that the presence of oxygen sensitive enzymes coupled with an abundance of light absorbing photosensitiser makes *C. jejuni* much more susceptible to the effects of PDI than other Gram-negative pathogens. In the absence of endogenous photosensitisers, we have shown Copper-conjugate photosensitisers can also be applied to efficiently kill bacterial pathogens by visible-light excitation. Given we are approaching the end of the antibiotic era, the application and understanding of these alternative pathogen reduction treatments is becoming ever more important. The findings presented here demonstrate that photodynamic inactivation could be used to remove *C. jejuni* from the surface of chicken skin which in turn could reduce the prevalence of this widespread pathogen. In this study, we aimed to characterise the global bacterial response to photooxidative stress, uncovering the molecular targets which become inactivated during PDI, as well as the cellular responses expressed to protect these enzymes. Given the microaerophilic nature of *C. jejuni,* this pathogen has an innate sensitivity to stress, yet little is understood how this stress-sensitive pathogen can survive across the range of oxygen tensions required to become a successful gastrointestinal pathogen. In the third chapter of unpublished work, we aim to utilise new techniques to uncover novel regulatory proteins which control the bacteria's ability to survive and thrive across a range of oxygen tensions as it passes between its hosts. The results described herein further the knowledge of this widespread foodborne pathogen and highlight the potential of PDI to kill pathogenic bacteria.

Acknowledgements

Firstly, I need to thank Professor Dave Kelly, for giving me this opportunity and being a great mentor and friend throughout my time here. You have made this experience truly unforgettable in so many ways and I can honestly say there would be no other supervisor I would rather have worked alongside. A mention also has to go to Professor Julia Weinstein for her help as a co-supervisor.

To everyone who has ever thrown on a dirty lab coat in F1, you have made this process thoroughly enjoyable and it has been a pleasure working with you all. A particular shout out must go to Dr Aidan Taylor, for taking me from a truly shoddy scientist, to not one of the worst!

I also need to give a particular mention to my dad, for bribing me with an iPod back in high school so that I took triple science instead of PE, without which, I probably wouldn't have made it this far! And of course, to the rest of my family, for encouraging me from the very beginning and always showing an interest in what I do.

And finally, a huge thanks to Siobhan, for supporting me all the way through and mostly putting up with the perpetual moaning and mood swings which come part and parcel with *Campylobacter* research!

And to those new students picking this dusty black book off the shelf, enjoy it, the freedom of thought you get during your PhD is truly the greatest part of the job.

PGW

2020

Presentations

Peter Walker, Julia Weinstein and David J. Kelly. Violet-blue light as a novel probe to reveal mechanisms of oxidative damage in *Campylobacter jejuni.* CHRO, Nantes France, September 2017, poster presentation

Peter Walker, Julia Weinstein and David J. Kelly. Photodynamic inactivation as a new tool to reduce *Campylobacter* infections, European Society of Photobiology (ESP) Congress, Pisa Italy, September 2017, poster presentation (awarded ESP fellow sponsorship).

Peter Walker, Aidan Taylor, Julia Weinstein and David J. Kelly. Photodynamic Inactivation of *Campylobacter jejuni* - an innate sensitivity. CHRO, Belfast Ireland, September 2019, oral presentation (awarded SfAM presidents fund sponsorship)

Peter Walker, Aidan Taylor, Julia Weinstein and David J. Kelly. Photosensitiser abundance and iron-sulphur cluster enzyme's dictate the sensitivity of *Campylobacter jejuni* to photodynamic inactivation. European Society of Photobiology Congress, Barcelona Spain, September 2019, oral presentation (awarded ESP fellow sponsorship).

Abbreviations:

Abs_{xxx}	absorbance at xxx nm
aa	amino acid
Amp	ampicillin
APS	ammonium persulphate
ATP	adenine triphosphate
BHI	brain heart infusion
bp	base pair
BSA	bovine serum albumin
BTS	Brucella broth with added tryptone & serine
°C	degrees Celsius
cat	chloramphenicol acetyl transferase
cDNA	complementary DNA
CFE	cell free extract
Cj	*Campylobacter jejuni*
cm	centimetre
Cm	chloramphenicol
CO_2	carbon dioxide
CP	coproporphyrin
Da	Dalton
dH_2O	distilled water
DMSO	dimethyl sulphoxide
DNA	deoxyribonucleic acid
DNase	deoxyribonuclease
DTT	dithiothreitol
EDTA	ethylenediamine tetra-acetic acid
ETC	electron transport chain
EPR	electron paramagnetic resonance
Fe-S	iron sulphur
Fur	ferric uptake regulator
g	gram
$HO^{\cdot}$	hydroxyl radical
H_2O	water
H_2O_2	hydrogen peroxide
Hyd	hydrogenase
Hp	*Helicobacter pylori*
HPLC	high performance liquid chromatography
IPTG	isopropyl β-D-1-thiogalactopyranoside
ISA	isothermal assembly
kan	kanamycin
kb	kilobase
kDa	kiloDalton
l	litre
J	joules
LacZ	ß-galactosidase
LB	Luria-Bertani
LOS	lipooligosaccharide
LPS	lipopolysaccharide
M	molar
MB	methylene blue
mg	milligram

MH	Muller-Hinton
MHS	Muller-Hinton with 20 mM serine
mm	millimetre
mM	millimolar
mRNA	messenger ribonucleic acid
ms	millisecond
mV	millivolts
mW	milliwatts
MW	molecular weight
µg	microgram
µl	microlitre
µM	micromoles
NAD(P)H	nicotinamide adenine dinucleotide (phosphate) reduced
ng	nanogram
nm	nanometer
nM	nanomolar
NMR	nuclear magnetic resonance
NO	nitric oxide
O_2^-	superoxide
OD_{XXX}	optical density at XXX nm
OM	outer membrane
ORF	open reading frame
Oor	2-oxoglutarate : acceptor oxidoreductase
OOPS	orthogonal organic phase separation
PAGE	polyacrylamide gel electrophoresis
PBS	phosphate buffered saline
PCR	polymerase chain reaction
pH	hydrogen potential
Pi	isoelectric point
PMF	proton motif force
Por	pyruvate:acceptor oxidoreductase
qRT-PCR	quantitative reverse transcriptase PCR
RBP	RNA binding protein
RBPome	RNA binding proteome
ROS	reactive oxygen species
RNA	ribonucleic acid
RNAse	ribonuclease
RPM	revolutions per minute
RT	room temperature
s	second
SDS	sodium dodecyl sulphate
Sec	general secretory pathway
T6SS	type VI secretion system
TCA	tricarboxylic acid cycle
TCR	two-compnent regulator
TEMED	N,N,N',N'-tetramethyl- ethane-1,2-diamine
Tris	tris(hydroxymethyl)aminomethane
UV	ultraviolet
v/v	concentration, volume/volume
WT	wild-type
w/v	concentration, weight/volume
x g	multiplied by gravitational force

Contents

Chapter 1: Introduction

1.1 *Campylobacter jejuni* discovery

Although *Campylobacters* were not recognised as human pathogens up until the early 1970s, they have probably caused illness in man for centuries. First reports of *Campylobacter* infection date back to 1886, where a German scientist described a spiral bacterium in the colons of children who had died of what they termed 'cholera infantum'(Escherich, 1886). The bacterium was later identified as a cause of abortive infection in cattle, with isolates originally named *Vibrio fetus,* based on its morphological similarity to *Vibrio* species (Smith, 1919). The first well documented human outbreak of *Campylobacter* infection occurred at an Illinois prison, where 355 inmates were affected by a milk-borne outbreak of diarrhea, with *Vibrio* like organisms identified as the causative agent (Levy, 1946). Elizabeth King was the first to study human strains in detail, characterising a classic *Vibrio fetus* and a similar but distinct group with different biochemical and antigenic characteristics termed 'related *vibrio'* (King, 1957). King noted that V*ibrio fetus* does not grow at the optimal growth temperature for 'related *vibrio*' of 42^{o}C and that the serological properties of the two strains were distinctly different (King, 1962). Following King's discovery, only 12 cases of 'related *vibrio*' were reported in the literature up until 1972 (Butzler, 2004). King believed that the infection was not as rare as the reports suggested as fecal cultures from patients often tested negative as selective culture techniques necessary for the isolation of this organism had not yet been developed, meaning the infection was mainly diagnosed from the blood of bacteraemic patients. It took a further 10 years before isolation of 'related *vibrio'* from fecal samples was accomplished and the scale of this endemic pathogen was understood (Butzler *et al*., 1973). The 'related *vibrio*' were later re-named as *Campylobacter,* derived from the Greek word *Kampylos* meaning curved rod and the species name *jejuni,* defining the site where the organism does its damage, namely the jejunum and the ileum.

1.2 The ε-proteobacteria

Campylobacter species belong to the Gram-negative epsilon class of proteobacteria, which include the families *Helicobacteraceae* and *Campylobacteraceae.* Members of this family have characteristically small genomes (1.6-2.0 mega bases) and often establish long-term associations with their hosts, sometimes resulting in pathogenic consequences. The family *Helicobacteraceae* consist of five genera: *Helicobacter, Sulfuricurvum, Sulfurimonas, Sulfurovum, Thiovulum* and *Wolinella.* The genus *Wolinella* containing a single species *Wolinella succinogenes,* typically colonise cattle as a commensal. Though no current evidence suggests that *Wolinella* is pathogenic itself, it has been found to contain many genes identified as

virulence factors in other pathogenic bacteria such as *C. jejuni* 'antigen B'. The genus *Helicobacter* includes the species *Helicobacter pylori,* which are known to cause peptic ulcers and gastritis but will live as a commensal in over half of the human population. The *Campylobacteraceae* family is a diverse group of environmental, commensal and pathogenic bacteria which comprises of three genera: *Arcobacter, Campylobacter* and *Sulfurospirillum.* The genus *Campylobacter* consists of 25 species which have widespread ecological distribution, typically found as commensals in domesticated animals and poultry but are pathogenic in the human host. All species in this order are microaerobic, with an optimum growth temperature ranging from 30-42 ^{o}C and a low GC content (29-47%) (Debruyne, *et al.,* 2008). Morphologically, cells are spiral shaped curved rods around 0.5-5 µm in lengh and 0.2-0.8 µm wide as shown in Figure 1. This curved spiral nature combined with a single polar unsheathed flagella make cells highly motile allowing movement in a corkscrew motition. *Campylobacters* have a respiratory and chemoorgnaotrophic metabolism, deriving energy from amino acids and tricarboxylic acid (TCA) cycle intermediates, but are generally unable to derive energy from carbohydrates such as glucose.

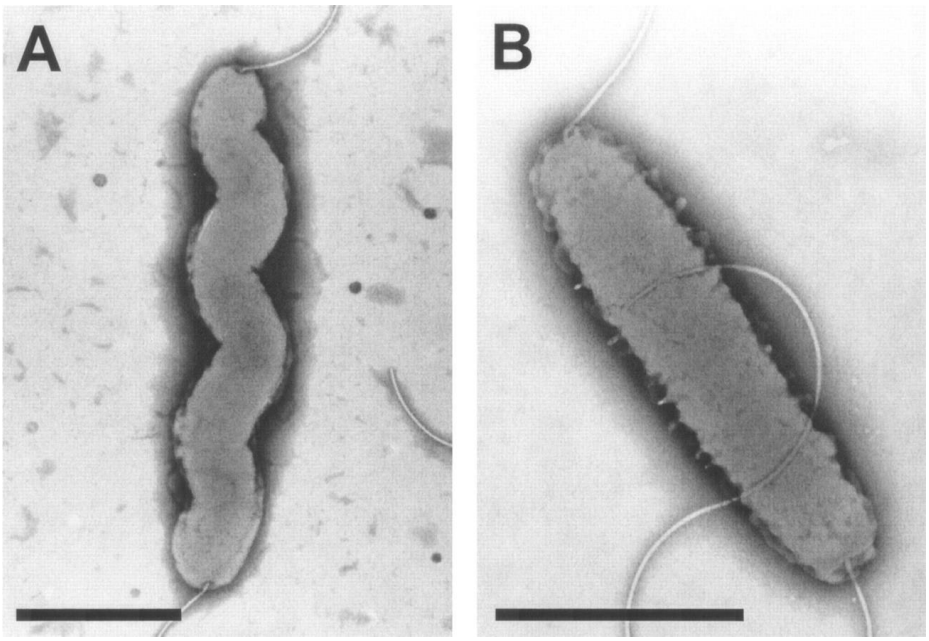

Figure 1: *Campylobacter jejuni* NCTC 11168 cell morphologies. (A) NCTC 11168-O the original clinical isolate of the wild type strain obtained by Skirrow. (B) NCTC 11168-GS – a varient of the 11168-O strain used to produce the Parkhill geneome sequence (Parkhill *et al.*, 2000). The variant cells are negatively stained; black bars represent 1 µm. Images reproduced from Gaynor *et al.*, 2004.

1.2 *Campylobacter jejuni* strains and genome analysis

The complete genome sequence of *C. jejuni* strain NCTC 11168 was sequenced and published by Parkhill *et al* in 2000 and has since been re-analysed and re-annotated (Parkhill *et al*., 2000, Gundogdu *et al*., 2007). This relatively small genome is 1,641,481 bp long, has a GC content of 30.6 % and codes for 1643 open reading frames (ORFs) (of which 19 are predicted to be pseudogenes) and 54 stable RNA species. With 94.3% of the genome being coding sequences, the *C. jejuni* genome is far denser than many other prokaryotic sequences due to an almost complete lack of functional insertion sequences or repetitive DNA sequences (Parkhill *et al*., 2000).

Despite the NCTC 11168 reference strain being the most commonly used *C. jejuni* strain in the UK, the strain differs in many aspects from the original isolate obtained by Skirrow. Most notably, the NCTC 11168 strain has been described as a poor or non-coloniser of young chickens after mutations in its genome for adaptation to growth in broth (Ahmed *et al*., 2002)(Gaynor *et al*., 2004). Since this finding, a second strain, *C. jejuni* 11168-H, has been selected under *in vitro* conditions for increased motility which also shows high-level intestinal colonisation (Karlyshev *et al*., 2002). Analysis of the genome sequence of hyper motile 11168-H strain shows that mutations in *maf5, flaA* (motility and flagellation) and *kpsM* (capsule deficiency) eliminate colonisation, whereas *pglH* (general glycosylation system deficient) reduced but did not eliminate colonisation (Jones *et al*., 2004). The highly pathogenic 81-176 strain contains 35 genes which are either pseudogenes or absent in the genome of the 11168 reference strain. Most are involved in either pathogenic or specific metabolic roles such as dimethyl sulphoxide (DMSO) reductase, a glycerol-3-phosphate transporter (GlpT) and γ-glutamyltranspeptidase (*ggt*). As well as inter-strain variation, genetic variation between reference strains has been reported by Sheppard *et al* who compared 23 11168 reference *Campylobacter* genomes from labs across the UK, finding considerable phenotypic variation in motility, morphology, invasion and susceptibility to ampicillin (Pascoe *et al*., 2019). This phenotypic variation between strains is driven by SNPs between clones during the process of sub culturing isolates, creating the opportunity for genetic variability. In some lab strains, putative identical isolates varied by up to 281 SNPs in 15 genes compared with the most recent reference strain (Pascoe *et al*., 2019).

1.3 *Campylobacter jejuni* Metabolism

Until recently, it was suggested that *C. jejuni* isolates are unable to catabolise sugars, especially glucose, due to the lack of glucokinase (Glk) and phosphofructokinase (PfkA) of the classical Embden-Meyerhof-Parnas (EMPs) glycolysis pathway (Parkhill *et al*., 2000)(Velayudhan & Kelly, 2002). However, it was recently shown that 30-50 % of *C. jejuni* strains can utilise L-fucose as a

carbon and energy source (Stahl *et al*., 2011, Muraoka & Zhang, 2011). More recently, it was shown that *Campylobacter coli* isolates can utilise glucose as a growth substrate, with isolates exhibiting specific fitness advantages including stationary-phase survival and biofilm production (Vegge *et al*., 2016). However, only 1.7 % of > 6,000 genomes sequenced from diverse range of both *C. jejuni* and *C. coli* isolates have been shown to contain the complete set of genes required for the Entner-Doudoroff (ED) pathway (Vegge *et al*., 2016).

With the absence of a complete glycolytic pathway, amino acids form the primary source of carbon for *C. jejuni,* with serine being the most favoured. The presence of an active serine transporter, (SdaC) and dehydratase (SdaA) allows serine to be efficiently converted to pyruvate which is fed into the citric acid cycle (CAC) by conversion to acetyl-CoA as shown in Figure 2 (Velayudhan *et al*., 2004). In the presence of serine (as well as lactate and pyruvate), *C. jejuni* can inhibit the utilisation of other carbon sources through an active catabolite repression mechanism. In the presence of Serine, there is transcriptional repression of several central metabolic enzymes by the regulatory proteins RacR and CsrA. All other amino acids catabolised by *C. jejuni* are converted to aspartate before deamination by *aspA* to enter the TCA cycle as fumarate (Guccione *et al*., 2008). Growth of *C. jejuni* in complex medium occurs in the sequential manner of serine, aspartate, asparagine, glutamate with proline representing a 'secondary substrate' only being utilised during stationary phase (Wright *et al*., 2009).

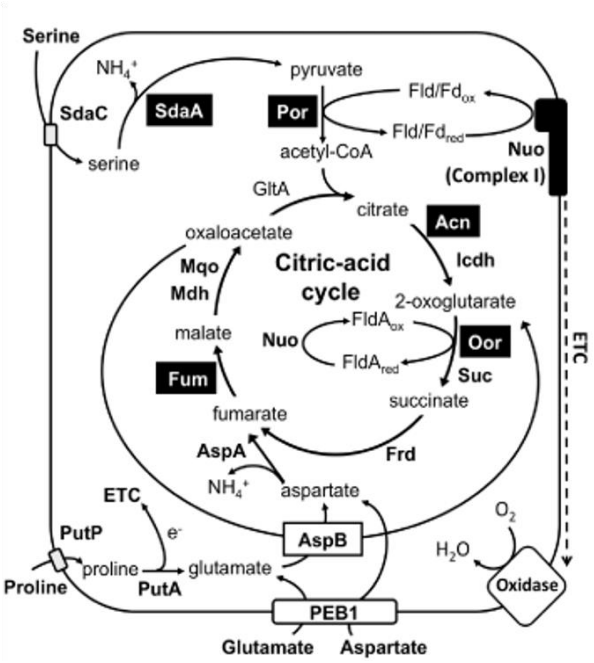

Figure 2 Schematic of the central carbon metabolism of *C. jejuni* showing the key enzymes and transporters involved in the citric acid cycle. Note, Fe-S cluster enzymes are highlighted in black, showing the susceptibility of the pathway to oxidative damage (Kendall *et al*., 2014).

Although amino acids from the main source of carbon, studies have shown *C. jejuni* strains can transport and catabolise organic acids such as acetate, lactate and pyruvate when carbon becomes limiting in the later stages of growth (Guccione *et al*., 2008, Wright *et al*., 2009). Proton NMR studies show that upon entering stationary phase, *C. jejuni* isolates switch from acetate excretion to acetate uptake and utilise the Acetyl-CoA synthase (Acs) enzyme to convert acetate back to acetyl-CoA (Wright *et al*., 2009).

1.5 Electron transport chain

Although *C. jejuni* strains can carry out substrate-level phosphorylation, they are unable to grow by a purely fermentative metabolism, therefore growth must occur by electron transport linked oxidative phosphorylation. The three essential components of the electron transport chain are a primary dehydrogenase to accept electrons from the appropriate donor, a terminal reductase to reduce an electron acceptor, and a membrane soluble quinone to facilitate electron transfer between the two. Despite its small genome size, *Campylobacter* spp. have a surprisingly complex and highly branched electron transport chain with a wide variety of electron donor systems to feed electrons into the quinone pool as well as a range of terminal reductases that allow the use of electron acceptors other than oxygen. The complexity of this electron transport system allows for greater energy conservation and supports the bacteria to grow under a wide range of environmental niches due to greater metabolic flexibility (Weingarten *et al*., 2008)(Taylor & Kelly, 2019). A variety of organic electron donors and molecular hydrogen feeds electrons into the menaquinone pool which feeds electrons to the membrane bound cytochrome *bc1* complex. This highly conserved proton-translocating, quinol-cytochrome *c* reductase (Qcr) receives electrons from the low potential menaquinone and transfers them to cytochrome *c* accompanied by a proton gradient across the cytoplasmic membrane (Taylor & Kelly, 2019). Oxygen reduction occurs through either the cbb_3-type oxidase which transfers electrons from the Qcr complex or through the *bd*-type CioABY enzyme which directly couples menaquinol oxidation to oxygen reduction (Liu & Kelly, 2015) (Jackson *et al*., 2007).

1.5.1 *c*-type cytochromes

Early studies of the *Campylobacter* respiratory chain observed the presence and abundance of cytochromes in the periplasm (Hoffman & Goodman, 1982). It has since been well understood that *Campylobacters* are very rich in *b*- and *c*-type cytochromes and it is the abundance of these species in the periplasm which gives packed *C. jejuni* cells their pronounced pink colour. There are two types of cytochrome *c* found among prokaryotic and eukaryotic organisms: cytochromes which are tightly associated with a redox centre of oxidases/reductases such as the cytochrome bc_1 complex and the water soluble protein present in the periplasm of gram negative bacteria

and the thylakoid lumen of some chloroplasts (Thöny-Meyer, 1997). Examples of enzyme assciated cytochrome *c* include the cytochrome *c* peroxidase which was recently shown to exploit H_2O_2 as a terminal oxidant in the form of anaerobic respiration. The mechanism involves ferrous cytochrome *c* providing electrons for the cytochrome *c* peroxidase system to reduce hydrogen peroxide to water. This both promotes flux through the electron transport chain and reduces the levels of peroxide which can pass through membrane porins and induce oxidative damage in the cytoplasm (Khademian & Imlay, 2017). The soluble or membrane associated *c*-type cytochromes catalyse various redox and electron transfer reactions, namely the electron transfer between the bc_1 and the *cb*-type oxidase.

The characteristic *c*-type cytochrome CXXCH sequence motif allows the formation of two thioester bonds between the two cysteine sulphurs (also called the haem attachment motif where 'X' represents any residue). Sequence analysis of the *C. jejuni* 11168 genome by Liu and Kelly (2015) revealed a total of 16 *c*-type cytochromes of which 5 had unknown function (CccA (*Cj1153*), CccB (*Cj1020*), CccC (*Cj0037*), CccD (*Cj0158*) and CccE (*Cj0854*)) (Liu & Kelly, 2015). Haem blots of periplasmic preparations showed that CccA (9.5 kDa) is the most abundant of all the *c*-type cytochromes in *C. jejuni*. This putative mono-haem cytochrome *c* CccA has been shown to bridge the electron flux from the bc_1 to the terminal oxidase (Liu & Kelly, 2015). Interestingly, the deletion of *cccA* gives an interesting phenotype in that the bacteria can no longer synthesize any other periplasmic *c*-type cytochrome. As CccA is involved in electron transfer between the bc_1 and the *cb* oxidase complex, a CccA deletion causes an influx of electrons into the periplasm which causes the accumulation of ROS, which inhibits haem ligation to other cytochromes in the periplasm (Liu & Kelly, 2015).

1.5.2 *c*-type cytochrome biogenesis

A *c* type cytochrome typically has two cysteines in the CXXCH motif of the protein linked by two thioester bonds to the two vinyl groups of haem, providing stability to the cytochrome, preventing loss or denaturation of the haem. Before haem can attach to the apocytochrome, cytosolic haem must be delivered to through a periplasmic haem chaperone so that haem can be attached to apocytochrome in the periplasm. This process occurs in three essential steps: (i) the translocation of haem b and the apocytochrome polypeptide across the cytoplasmic membrane, (ii) the periplasmic reduction of cysteine residues in the haem c attachment motif of the apocytochrome in the periplasm, and (iii) the formation of covalent bonds between haem b and sulphur atoms of the two cysteine residues in the -CXXCH- motif (Taylor & Kelly, 2019). There are three pathways known to assemble a cytochrome *c*, with prokaryotes using either systems I or II. The *Epsilonproteobacteria,* along with *Beta*- and *Gammaproteobacteria* utilise

the Ccs (cytochrome c synthase) system or System II. The Ccs system is composed of four membrane-bound proteins with at least one transmembrane segment. The cytochrome *c* synthase is formed from CcsA and CcsB which acts as a haem-protein ligase, transporting reduced haem *b* from the cytoplasm to the periplasm. The apocytochrome polypeptide is transported by the Sec pathway in the reduced thiol state where it then becomes oxidised in the periplasm. CcsX then reduces the cysteines residues in the CXXCH haem attachment motif using electrons derived from cytoplasmic thioredoxin via the membrane bound thiol reductase DsbD protein. The CcsAB cytochrome synthase can then recognise the reduced cysteine residues in the CXXCH haem attachment motif and form thioester bonds between reduced apocytochromes and the reduced vinyl groups of the haem.

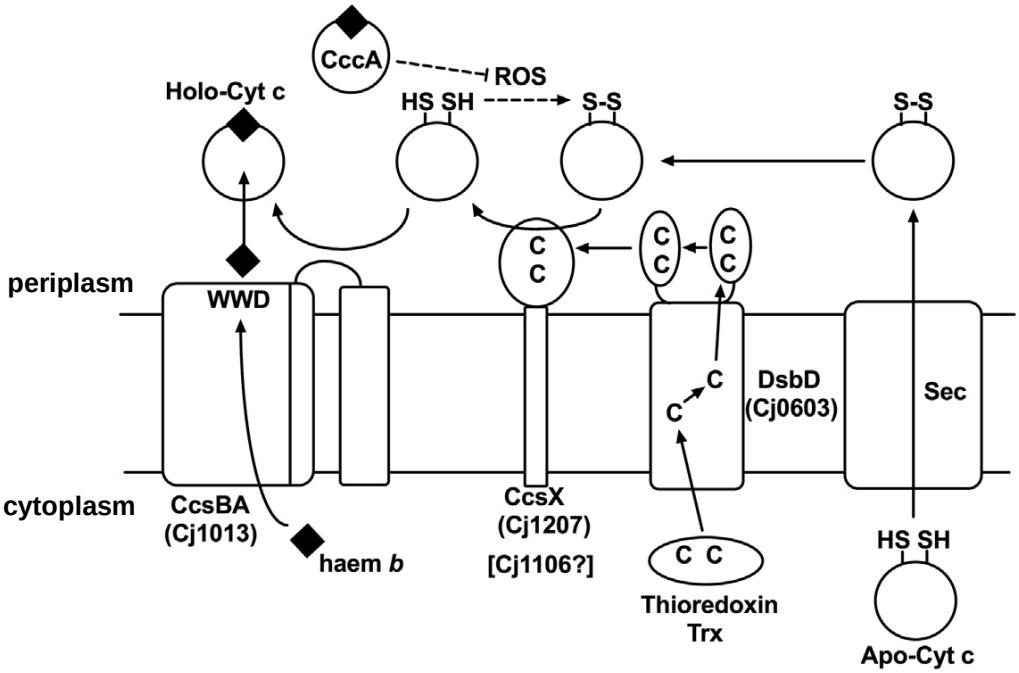

Figure 3 - Model for system II cytochrome *c* biogenesis in *C. jejuni* NCTC11168. Apocytochromes are transported to the periplasm via the Sec systems where they immediately become oxidised. The thiol-disulphide redox module required to break the disulphide bond between the two cysteine residues of the CXXCH is shown. Electrons derived from cytoplasmic thioredoxin, donates hydrogens to the DsbD system, which then induces a redox chain through conserved cysteines to the periplasm. The cytochrome *c* synthase, CcsBA transports haem *b* from the cytoplasm and ligates it to the reduced apocytochrome *c.* CccA prevents oxidation of the CXXCH motif which would prevent the ligation of the apocytochrome to haem (Taylor & Kelly, 2019).

The periplasmic *c* type cytochrome CccA has been found to play a major role in facilitating the covalent attachment of the apocytochrome to haem. As previously mentioned, deletion of *CccA (cj1153)* results in an almost complete loss of all other c-type cytochromes, a pleiotropic phenotype more like that seen in *ccsX* mutants in other bacteria (Taylor & Kelly, 2019). This phenotype could however be rescued by growth in the presence of reducing agents such as L-cysteine or dithiothreitol. It was also shown that the *cccA* mutant had increased ROS production and excessive oxidative stress damage, leading to the hypothesis that in the absence of CccA, the cysteine residues of the apocytochrome CXXCH motif become oxidised, preventing covalent attachment of haem.

1.5.3 Haem biosynthesis

Haems are tetrapyrroles, a family of compounds that includes corrins, chlorins, chlorophylls and bacteriochlorophylls. Cytochromes are quantitatively the predominant haem proteins in most prokaryotes, with haem *b* being the most abundant tetrapyrrole (Panek & O'Brian, 2002). In most bacteria, haem demand is met by biosynthesis rather than by acquisition from the environment although this is not universal. Lactic acid bacteria and *Enterococcus faecalis* possess genes encoding apohemoproteins but rely on haem uptake systems as they cannot synthesize their own haem (Baureder & Hederstedt, 2013). *C. jejuni* also possess a complete haem uptake system, capable of transporting haem across the outer membrane through a TonB/ExbB like complex, encoded in the gene cluster *cj1613-cj1617* (Parkhill *et al*., 2000). However, the absence of linkage of the haem transport system to other genes associated with the haem metabolic pathway suggest that iron nutrition rather than haemin utilisation is the main purpose of the acquisition system in *C. jejuni* (Ridley *et al*., 2006).

The synthesis of haem entails nine reactions which convert glutamyl-tRNA to protoporphyrin IX. The first step in the tetrapyrrole biosynthetic pathway is the synthesis of the first committed pathway intermediate, 5-aminolevulinic acid (ALA). There are two independent biosynthetic routes for the formation of ALA with all prokaryotes except Alphaproteobacteria utilising the C5 pathway. The C5 pathway converts glutamyl-tRNA into the liable glutamate-1-semialdehyde (GSA) by glutamyl-tRNA reductase (GtrR) or HemA which is then converted into ALA by glutamate-1-semialdehyde-2,1-aminomutase (GsaM) or HemL. The three steps from ALA to uroporphyrin III are well conserved and are thought to be the evolutionary core of haem biosynthesis. From uroporphyrin III, protoheme is synthesised first by the conversion of uroporphyrinogen III into coproporphyrinogen III followed by the oxidative decarboxylation of coproporphyrinogen III to protoporphyrinogen IX. The terminal step of haem synthesis is the

insertion of ferrous iron into the protoporphyrin IX macrocycle by the ferrochelatase encoded by *hemH* to produce protoheme IX (haem).

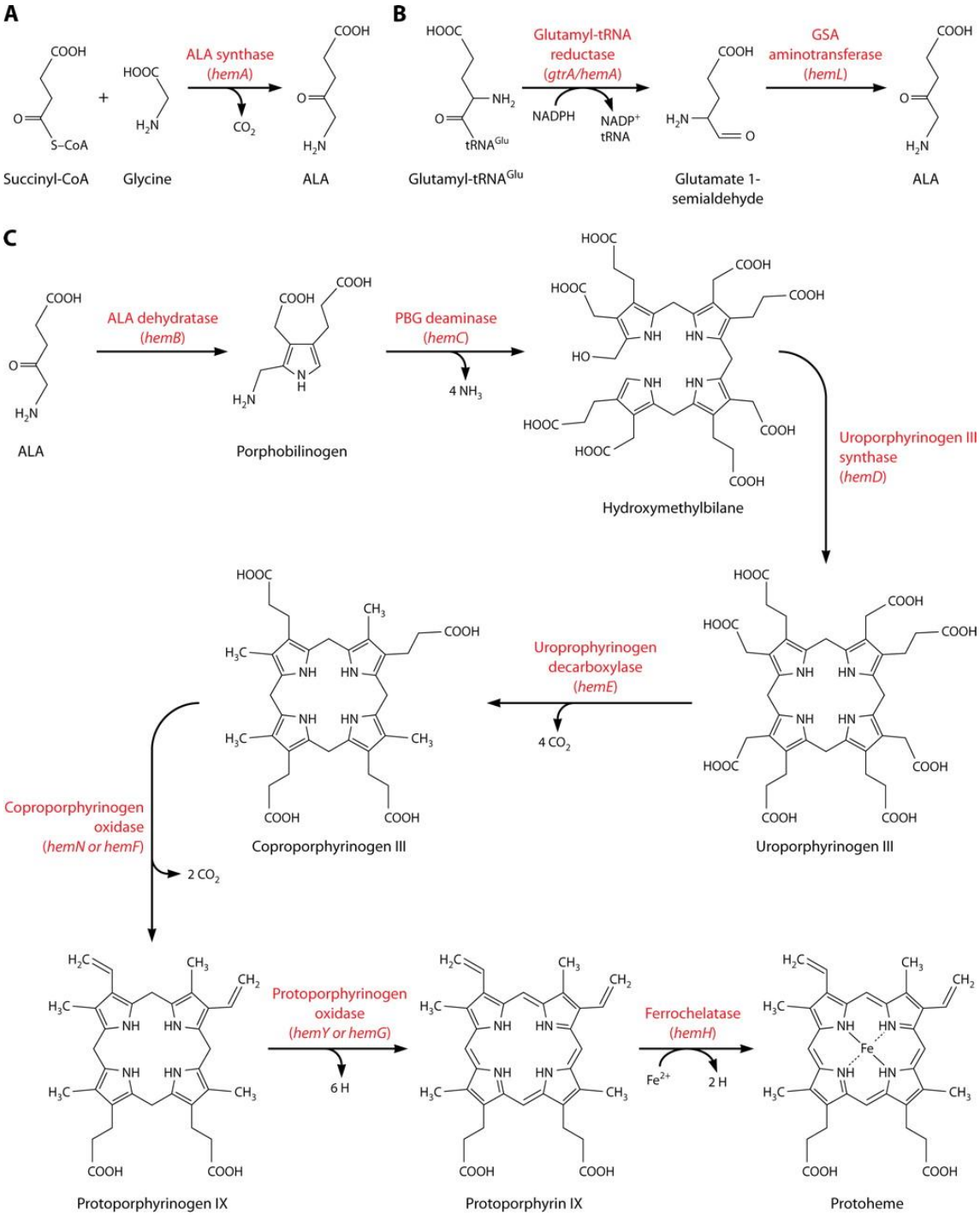

Figure 4 – Schematic of the prokaryotic haem biosynthesis pathway – A- Succinyl-CoA and glycine are converted into ALA by ALA synthase in the C4 pathway for 5-aminolevulinic acid (ALA) synthesis present in α-proteobacteria. B- The C5 ALA synthesis pathway utilised by all other prokaryotes converting glutamyl-tRNAGlu to ALA GtrA/HemA and HemL. C- The highly conserved haem biosynthesis pathway converting ALA to protoheme (Anzaldi & Skaar, 2010).

Given the high redox potential of haem, expression at high quantities can become toxic, therefore tight regulation of tetrapyrrole biosynthesis is essential. The regulation of the haem biosynthetic pathway is controlled in part by the abundance of its end product at the levels of transcription, protein stability, and enzyme activity. Under standard conditions, the activity of HemA (glutamyl-tRNA reductase) which catalyses the first dedicated step in haem synthesis is the rate limiting reaction for the tetrapyrrole pathway flux. Recent studies have shown that HemA levels can respond to haem sufficiency through an allosteric feedback mechanism (Jones & Elliott, 2010). When intracellular levels of haem are sufficient, HemA will bind haem, becoming vulnerable to rapid degradation by the ClpAP and Lon protease, decreasing flux through the pathway (Jones & Elliott, 2010).

As well as autoregulation through its end product, the tetrapyrrole biosynthesis pathway must respond to increasing demand for haem proteins in response to environmental changes. For the bacterial response to oxidative stress, cells upregulate detoxification enzymes such as catalase and peroxidases to detoxify ROS, which utilise a haem prosthetic group. Recent proteome profiles of glucose grown *E. coli* reveal that in unstressed cells catalase represents 7-10% of the haem bound proteome (Mancini & Imlay, 2015). In order to meet the haem demand upon induction of these highly upregulated detox enzymes, tetrapyrrole synthesis must be maintained or elevated to provide the prosthetic group for the peroxidase. The problem however lies with the fact H_2O_2 stress derives almost exclusively from iron, as Fenton chemistry produces free hydroxyl radicals, therefore cellular adaption to H_2O_2 is centred around minimising the levels of intracellular ferrous iron driven by the DNA-protective iron storage protein Dps. Typically, most biosynthetic pathways are synthesised with excess capacity, therefore little product dependant feedback is required, but as protoporphyrin IX metalation is dependent on iron, upregulation of the ferrochelatase in response to oxidative stress is critical to maintain haem supply to the peroxidases (Prather & Martin, 2008). In *E. coli,* induction of the *ppfC* and *cgdC* genes, encoding ferrochelatase and the O_2-dependent coproporphyrinogen oxidase are induced in response to oxidative stress by the H_2O_2 response regulator OxyR (Mancini & Imlay, 2015). In *B. subtilis,* the major peroxide regulator PerR controls expression of the *hemAXCDBLH* operon, and following the oxidation of PerR by H_2O_2, the regulator becomes inactivated, resulting in derepression of the *hem* operon, providing the prosthetic group for cellular peroxidases (Mongkolsuk & Helmann, 2002). It was shown that a *perR* mutation has a growth phenotype due to the haem sequestration from the increased catalase abundance due to derepression of the *katA* gene. This highlights that despite the derepression of the *hem* operon, increased catalase abundance overwhelms the cells tetrapyrrole biosynthesis pathway

due to the substantial quantity of haem which is committed to KatA synthesis (Faulkner *et al*., 2012).

1.6 Microaerobic growth

Like many other Epsilon proteobacteria, *Campylobacters* are typical microaerophiles, meaning they require oxygen for growth but are sensitive to high oxygen concentrations and thus grow best at partial oxygen tensions of 3-10 % (Kelly, 2001). Although this unusual physiological characteristic restricts the bacterium under atmospheric oxygen concentrations, it does offer the pathogen a niche for surviving at low oxygen concentrations like that found in the avian gut. Despite *C. jejuni* being equipped with various enzymes which facilitate oxygen-independent respiration using alternative electron acceptors to oxygen, it cannot grow in strictly anaerobic conditions (Véron *et al*., 1981). The inability to support anaerobic growth is in part due to the requirement of low amounts of oxygen for deoxyribonucleotide synthesis, catalysed by a single "aerobic-type" class I ribonucleotide reductase (Sellars *et al*., 2002). The sensitivity of *C. jejuni* to high oxygen concentrations is primarily due to the possession of several oxygen and ROS sensitive metabolic enzymes systems which are essential for growth.

1.6.1 Oxoacid: acceptor oxidoreductase

In eukaryotes and most aerobes, the oxidative decarboxylation of pyruvate and 2-oxoglutarate to their respective acyl-CoA derivatives is carried out by NADH-dependent dehydrogenase complexes, which are oxygen-stable. Like many anaerobic and microaerobic bacteria, *C. jejuni* does not utilise 2-oxoacid dehydrogenases and instead relies on 2-oxoacid acceptor oxidoreductases. These enzymes evolved much earlier than the multi-enzyme NADH-dependent dehydrogenase complexes and use flavodoxin or ferredoxin as electron acceptors (Weerakoon *et al*., 2009). The pyruvate: acceptor oxidoreductase (Por) responsible for the oxidative decarboxylation of pyruvate to acetyl-CoA and the 2-oxoglutarate: acceptor oxidoreductase (Oor) responsible for the analogous conversion of 2-oxoglutarate to succinyl-CoA are two crucial reactions, central to carbon metabolism which utilise these alternative enzyme complexes. The use of these acceptor: oxidoreductase complexes is particularly significant as they are iron-sulphur cluster containing enzymes which are highly susceptible to damage by molecular oxygen or reactive oxygen species. *C. jejuni* utilises multiple oxygen sensitive 2-oxoacid acceptor oxidoreductases for essential TCA cycle reactions as shown in Figure 2, but the Por and Oor enzymes are far more sensitive to oxygen and ROS damage than other TCA cycle oxidoreductase such as SdaA (Kendall *et al*., 2014). Although Por and Oor are partially protected from oxygen damage by the hemerythrin proteins HerA (*cj0241c*) and HerB (*cj1224*), once damaged through

exposure to high ROS or oxygen concentrations, no mechanisms have been found to repair and restore Por and Oor activity.

1.6.2 Iron-sulphur clusters and reactive oxidants

Iron-sulphur (Fe-S) cluster cofactors are exploited for a wide range of biochemical functions as they provide an excellent redox active catalyst under anaerobic conditions. Their ability to cycle between ferrous (Fe^{2+}) and ferric (Fe^{3+}) iron oxidation states as well as binding of oxygen or nitrogen atoms in organic substrates makes them a well-equipped catalyst (Meyer, 2008). They are utilised for a variety of biochemical functions including iron or oxygen sensing, electron transfer and redox catalysts (Roche *et al*., 2013). Clusters can exist in multiple forms from simple single iron atom ligands, rhombic ligands [2Fe-2S] and the more common cubic [4Fe-4S] forms. Due to their low redox potential, these complexes can readily interact with ROS, causing oxidation of exposed Fe^{2+} iron to Fe^{3+}, forming unstable $[4Fe\text{-}4S]^{3+}$ oxidation state, resulting in the release of free iron shown in Figure 5. The interaction between released ferrous iron and ROS mediates the generation of the highly reactive and extremely damaging hydroxyl radical, through Fenton chemistry.

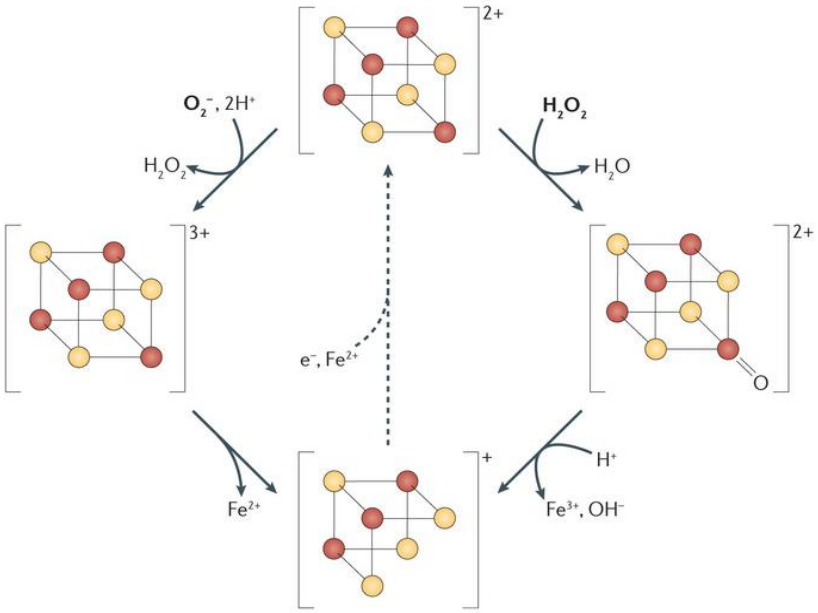

Figure 5 – Fe-S cluster damage by reactive oxidants. The exposed Fe^{2+} atom in a $[4Fe\text{-}4S]^{2+}$ cluster is oxidized by a reactive oxidant such as superoxide (O_2^-) resulting in the formation of hydrogen peroxide (H_2O_2) and conversion of the cluster to an unstable $[4Fe\text{-}4S]^{3+}$ species (left pathway). Release of free Fe^{2+} results in an inactive $[3Fe\text{-}4S]^{1+}$ enzyme and free Fe^{2+} which can drive Fenton chemistry. Alternatively, H_2O_2 can oxidise the cluster, creating a transient ferryl species which abstracts a second electron from the cluster resulting in the inactive $[3Fe\text{-}4S]^{1+}$ cluster (right pathway) (Imlay, 2006).

1.7 Defence against ROS

Despite the possession of multiple oxygen sensitive [4Fe-4S] cluster enzymes, *Campylobacters* are respiratory pathogens which prefer to use oxygen as an electron acceptor. In order to withstand highly variable oxygen concentrations and resist oxidative stress during transmission or infection, they must employ a full complement of oxidative stress defence enzymes to protect these oxygen sensitive enzyme complexes. The nature of damage induced by molecular oxygen is not self-evident as the structural molecules from which organisms are made are essentially unreactive with O_2. The toxicity of molecular oxygen derives from the formation of partially reduced reactive oxygen species (ROS) generated by the stepwise reduction of molecular oxygen (Imlay, 2013). During aerobic metabolism, the auto-oxidation of respiratory dehydrogenases generates superoxide radicals (O_2^-) which are mildly reactive physiologically. In the presence of cellular iron, H_2O_2 can interact with ferrous iron mediating the generation of the highly reactive and extremely damaging hydroxyl radicals ($\bullet OH^-$). In addition, *C. jejuni* are exposed to superoxide, nitric oxide and other ROS and RNS derivatives through activation of neutrophils, which are recruited to the gut in large numbers as part of the immune response against pathogenic bacteria. The ability of *C. jejuni* to combat the deleterious effects of ROS depends on the expression of inducible detoxification enzymes which convert harmful reactive oxygen intermediates into less harmful or inert products.

1.7.1 Superoxide defence

The metalo-enzyme superoxide dismutase (SOD), which catalyses the conversion of superoxide radicals to hydrogen peroxide, is one of the bacterial cells first line of defence against the toxic effects of reactive oxygen intermediates. Bacteria commonly contain two types of SOD, either MnSOD (SodA) or FeSOD (SodB). Unlike most enteric pathogens, *C. jejuni* expresses a single SodB, which utilises an iron cofactor for the two-step reaction:

i) Fe^{3+}- SOD + O_2- → Fe^{2+}-SOD + O_2

ii) Fe^{2+}-SOD + O_2- +2H+ → Fe^{3+}- SOD + H_2O_2

The SOD of *C. jejuni* has an additional 20-amino acid elongated C-terminal which is thought to allow the organism to associate SOD with the cells surface and flagella, providing a first line defence against oxidative stress during infection (Esposito *et al*., 2008). Mutational studies have shown deletion of *sodB* results in hypersensitivity towards O_2^- as well as H_2O_2 and cumene hydroperoxide, oxidants that are not detoxified by SodB (Palyada *et al*., 2009). It is thought the increased sensitivity to H_2O_2 comes from the accumulation of endogenous superoxide anions produced during normal metabolism. These anions then oxidise [4Fe-4S] cluster complexes,

releasing catalytic ferrous iron, promoting Fenton chemistry resulting in the release of free radicals.

1.7.2 Peroxide defence

The defence system for scavenging peroxides is slightly more complex as several enzymes such as catalases (KatA) and peroxiredoxins (AhpC, Tpx and Bcp) are involved in preventing H_2O_2 levels reaching lethal concentrations. Peroxides must be inactivated effectively since they are major contributors to the formation of highly toxic hydroxyl radicals. *C. jejuni* expresses a single monofunctional haem-containing catalase, *katA* which non-reductively converts hydrogen peroxide to oxygen and water as shown the following reaction: (Po refers to the porphyrin ring).

i) $[Po\text{-}Fe^{3+}] + H_2O_2 \rightarrow [Po^{+}\text{-}Fe^{4+}=O] + H_2O_2$

ii) $[Po^{+\bullet} - Fe^{4+}= O] + H_2O_2 \rightarrow [Po\text{-}Fe^{3+}] + H_2O + O_2$

In this two-step reaction, one molecule of H_2O_2 initially oxidises the KatA haem group to generate H_2O, an oxyferryl species and a porphyrin cation radical. A second molecule of H_2O_2 is then used as a reductant to regenerate the original enzyme, resulting in the release of H_2O and O_2 (Chelikani *et al*., 2004). However, at low concentrations of H_2O_2, the catalytic cycle of catalases can stall, with the haem trapped in its intermediate ferryl/radical form which can act as a potential oxidant, taking electrons from surrounding polypeptides (Putnam *et al*., 2000). As expected, deletion of the *C. jejuni katA* gene abolishes catalase activity and results in hypersensitivity to H_2O_2 compared with wild-type cells (Palyada *et al*., 2009).

Although catalases are used as the major detoxifiers of peroxides at high concentrations, other H_2O_2 detoxification enzymes also contribute to limit oxidative damage. In contrast to catalases, alkyl hydroperoxide reductase (Ahp) does not form dangerous oxidizing species and is therefore the more effective scavenger during low level peroxide stress. Ahp reduces reactive hydroperoxides to H_2O through an active site cysteine that is oxidized to sulfenic acid. Stationary phase *C. jejuni ahpC* $^{-}$ mutants show increased sensitivity to cumene hydroperoxide as well as significantly reduced aerotolerance compared with wild-type cells (Baillon *et al*., 1999). Two other peroxiredoxins widespread in bacteria include thiol peroxidase (Txp) and bacterioferritin co-migratory protein (Bcp). Tpx and Bcp are cytoplasmic proteins which can utilise a wide variety of peroxides as substrates such as hydrogen peroxide, organic peroxides and lipid peroxides. Single mutants in both *tpx* and *bcp* genes resulted in poorer growth than wildtype under high aeration conditions. Growth was dramatically reduced under microaerobic conditions and almost completely under high aeration in the Δ*tpx* Δ*bcp* double mutant (Atack *et al*., 2008). These findings suggest despite their overlapping functions, each individual enzyme contributes

to the defence against peroxide stress, providing a fitness advantage during colonisation (Flint *et al*., 2014).

1.7.3 Singlet oxygen defence

Singlet oxygen is the most unstable of all ROS and can form from energy transfer reactions to molecular oxygen either from excited endogenous photosensitisers or as by products from certain enzyme catalysis (Ziegelhoffer & Donohue, 2009). Given the limited diffusion radius of $^1O_2$ from its site of generation, the localisation of the photosensitiser often determines the biological target of damage. Singlet oxygen will react with a range of biological targets including DNA, RNA and lipids though proteins form the major biological target owing to their abundance and high rate constants for reaction with $^1O_2$ (Wilkinson *et al*., 1995). Reactions with proteins occurs most favourably with Tyr, His and Trp side chains, forming protein radicals which can propagate oxidative damage (Davies, 2003). These protein peroxides are problematic for enzymatic removal as these residues are typically buried in protein structures, explaining their long-lived nature when generated within cells. Singlet oxygen derived peptide peroxides have been shown to be removed by glutathione peroxidase, in the presence of reduced glutathione (GSH), with protein thiols acting as major direct and indirect reductants for protein and peptide peroxides (Morgan *et al*., 2004).

Both phototropic and non-phototrophic bacteria utilise pigments to counteract photooxidative stress in the form of carotenoids which act to directly quench $^1O_2$ (Domonkos *et al*., 2013). *Staphylococcus aureus* has a high concentration of the carotenoid pigment staphyloxanthin which is able to perform an antioxidant action against oxidant-based reactions (Clauditz *et al*., 2006)(Costa *et al*., 2013). Studies have shown that mutant strains unable to produce staphyloxanthin are more susceptible to oxidative stress and that *S. aureus* strains with a high relative concentration of staphyloxanthin are more resistant to photooxidative stress (Bartolomeu *et al*., 2016). Given the small genome of *C. jejuni,* it lacks the presence of any recognised singlet oxygen scavenging carotenoids, and instead may employ other non-specific radical quenching proteins which have yet to be characterised.

1.7.4 Protein damage response

Methionine residues are frequently damaged by oxidative stress due to the presence of highly oxidisable sulphur atom (Denkel *et al*., 2011). Under oxidative stress, peptidyl and free methionine is converted to a mixture of methionine-S- (Met-S-SO) and methionine-R-sulfoxides (Met-R-SO) which differ due to the asymmetry of the sulphur atom in the lateral chain. These oxidized methionine diastereoisomers form much poorer substrates for methionine aminopeptidase than the reduced form, preventing the correct folding of newly synthesised

proteins. Oxidised methionine residues Met-S-SO and Met-R-SO are repaired by methionine sulfoxide reductases, MsrA and MsrB respectively. These Msr enzymes are highly conserved in both eukaryotes and prokaryotes and appear to be required for full resistance to oxidative and nitrosative stress in *C. jejuni* by protecting key methionine rich proteins such as KatA, AhpC, GroEL and Trx1. The *C. jejuni msrA/B* double mutant shows hypersensitivity to peroxide and superoxide mediated stress as no repair of oxidized methionine residues can take place (Atack & Kelly, 2008). Complementation of the Msr mutants restored wildtype sensitivity when studied using disc assays with hydrogen peroxide, cumene hydroperoxide, methyl viologen, SNP and diamide. This highlights the importance of Msr repair mechanisms in repairing cellular components damaged by oxidative stress to allow successful colonization and virulence.

As well as repair of specific oxidised residues, bacteria also employ the non-specific, heat shock response (HSR) proteins to repair damaged or aggregated proteins under oxidative stress. There are two groups of heat shock proteins: the ATP dependant proteases which degrade unfolded peptides and molecular chaperones which promote correct protein folding. The Lon and Clp proteolytic complexes degrade stress damaged proteins utilising an ATPase driven peptidase, with a *clpP lon* double mutant showing significant increases in the levels of aggregated proteins (Cohn *et al*., 2007). The expression of heat shock response proteins is controlled by binding of the heat shock repressor HcrA to the CIRCE (controlling inverted repeat of chaperone expression) element. HrcA instability under stress conditions leads to dissociation of HcrA from the CIRCE element, causing increased expression of heat shock genes. A feedback loop regulates heat shock protein expression as the protein chaperones GroEL, GroES upregulated by the dissociation of HrcA from the CIRCE element, act to refold fold HrcA under unstressed conditions to repress the expression of the regulon. Another negative HSR regulator HspR, bound to the HAIR (HspR associated inverted repeat) sequence, represses the heat shock response genes in association with DnaK. Under stress, unfolded proteins compete with HspR for DnaK, resulting in decreased HspR repression, increasing expression of the heat shock response genes.

1.7.5 Oxidative stress regulators

In most Gram-negative bacteria, the oxidative stress defence mechanisms are regulated by the superoxide- and peroxide- sensing regulators SoxRS and OxyR respectively. In *C. jejuni*, these regulators are absent and only the peroxide-sensing regulator (PerR) has been identified (Van Vliet *et al*., 1999). PerR is related to the ferric-uptake repressor (Fur) and requires either iron or manganese as a regulatory metal iron. PerR senses H_2O_2 by Fe^{2+}-catalysed oxidation of two histidine residues in its regulatory binding site, causing Fe^{2+} release and rapid induction of PerR regulated genes (Lee and Helmann, 2006). Inactivation of PerR results in constitutive expression

of *katA* and *ahpC*, and increased resistance to peroxide stress as shown in Figure 6 (Palyada *et al*., 2009). Interestingly, transcriptome analysis of the PerR mutant showed differential expression of a large group of genes in the absence of iron, suggesting PerR may also regulate in an iron independent manner (Butcher *et al*., 2015).

The *C. jejuni* ferric uptake regulator, Fur, which usually mediates bacterial iron-responsive gene regulation is also involved in the direct regulation of oxidative stress defence genes *katA* and *ahpC*. Analysis of *fur*$^{-}$ and *perR*$^{-}$ mutants have shown there is significant overlap between the iron, Fur and PerR regulons. This is best shown in the case of the *katA* gene where both Fur and Per regulons must be deleted for the gene to be fully derepressed and unresponsive to iron repression (Butcher *et al*., 2015). The capability of iron to produce reactive oxygen species via the Haber-Weiss and Fenton reactions explains why the iron uptake and oxidative stress responses are under the same metalloregulatory proteins. Other *C. jejuni* oxidative stress regulators have been identified such as CosR (Campylobacter oxidative stress regulator), an OmpR-type regulator essential for *C. jejuni* viability (Raphael *et al*., 2005). Proteomic studies have shown *cosR* expression is reduced after exposure to paraquat, suggesting a role for CosR in the oxidative stress response of *C. jejuni* (Garénaux *et al*., 2008). Recently it has been shown that the MarR-type transcriptional regulators RrpA and RrpB also pay a role in controlling both the *C. jejuni* oxidative and aerobic stress response, with mutants in either *rrpA or rrpB* showing reduced *katA* expression (Gundogdu *et al*., 2015).

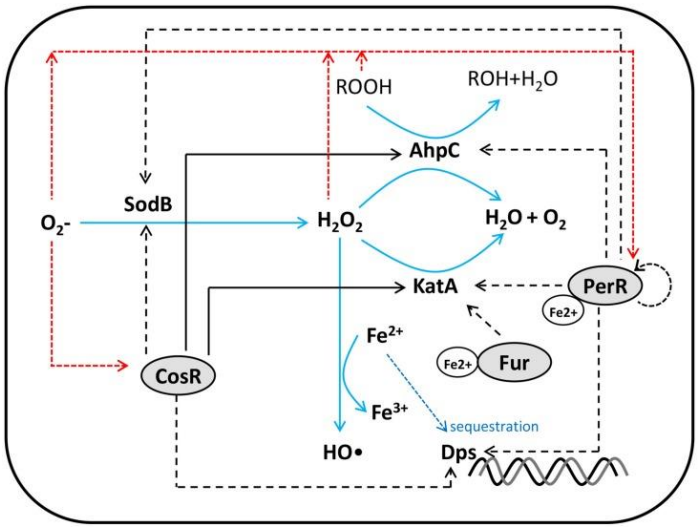

Figure 6 – Schematic showing oxidative stress response regulators PerR, Fur and CosR. Positive and negative regulations are indicated by black solid and black dotted lines respectively with red dotted lines showing transcriptional/translational downregulation by ROS (Kim *et al*., 2015). This diagram does not include the more recently discovered transcriptional regulators RrpA RrpB (Gundogdu *et al*., 2015).

1.8 Pathogenicity of *C. jejuni*

1.8.1 Epidemiology and Virulence

Campylobacter jejuni typically resides in the intestinal tracts of many wild and agriculture-associated animals, with poultry flocks forming the main transmission route to humans. Most cases of sporadic *C. jejuni* infection occur through the handling or consumption of undercooked chicken meat, or cross-contamination of other foods with raw poultry fluid. Infections in humans are characterized by the invasion and inflammation of the colonic epithelium, causing severe but typically self-limiting acute gastrointestinal illness. Chronic inflammation of the intestinal tract causes ulcerative colitis and colonic crypt abscesses which can resolve in most patients but is life threatening immune-compromised individuals. Furthermore, roughly 1 in 1,000 individuals infected with *C. jejuni* develop serious acute inflammatory polyneuropathies such as Guillain-Barré syndrome, which is the leading cause of acute neuromuscular paralysis since the eradication of polio (Nyati & Nyati, 2013)(Buzby *et al*., 1997).

1.8.2 Motility and Adhesion

Virulence in *C. jejuni* is heavily dependent on chemotactic motility with mutants deficient in chemotaxis and/or motility displaying defects in colonisation and the ability to cause persistent infections in animal models (Golden & Acheson, 2002) (Hendrixson & DiRita, 2004). Motility is driven by the action of a bipolar flagellum, composed of O-linked glycosylated flagellin which propels the cell through the intestinal mucus, bring cell adhesins into close proximity to attachment sites on intestinal epithelial cells. In order to migrate through the visco-elastic mucus gel layer, the C. *jejuni* flagellum is equipped with additional components to generate power for creating a higher level of torque for flagellar rotation and motility relative to other bacteria (Burnham & Hendrixson, 2018). Three large multimeric disk structures composed of FlgP, PflA and PflB surround the MotAB stator motor complex which powers rotation via proton transport providing torque to the flagella rotor. The *C. jejuni* motor incorporates 17 stators in its motor compared with the typical 11 stators, orienting the greater number of stators at a greater radial distance from the central motor axis, providing a higher torque to drive through the thick mucus gel layer (Beeby *et al*., 2016).

Campylobacters use amino acid components of the mucus layer such as L-glutamate, L-serine, L-cysteine and L-aspartate as chemo attractants, to direct chemotaxis and increase motility (Alemka *et al*., 2012). Recent studies have demonstrated that mucins modulate the pathogenicity of *C. jejuni,* determining whether the bacteria adopt a commensal or pathogenic mode of existence. The production of mucus by T29-MTX-E12 cells promoted higher levels of adhesion, invasion, and translocation to the basolateral aspects of cells compared with parental

HT29 cells that lack a mucus layer infected with *C. jejuni* (Alemka *et al*., 2010). *C. jejuni* utilises surface adhesins such as the periplasmic binding protein PEB1, the flagella secreted protein FlaC and two fibronectin-binding proteins CadF and FlpA to attach to epithelial cell adhesins. Once through the mucus layer, *C. jejuni* can invade intestinal epithelial cells by altering host cell biology to promote its uptake in a microtubule-dependent, actin-independent manner (Oelschlaeger *et al*., 1993). Once internalised, *C. jejuni* must survive and replicate inside a modified membrane compartment known as the *Campylobacter*-containing vesicle (CCV) by undergoing physiological changes in oxygen sensitivity and metabolism to allow survival (Cróinín & Backert, 2012).

1.8.3 Protein glycosylation

Although previously considered a eukaryotic phenomenon, it has been discovered that many pathogens which colonise the mucosal linings of the human body with relatively small genomes devote significant proportions of their genome content to glycoconjugate biosynthesis. *C. jejuni* has two separate glycoprotein modification systems: an *O*-linked protein glycosylation system which modifies the extracellular flagellar filament, and the N-linked general protein glycosylation system which modifies extra-cytoplasmic proteins (Szymanski & Wren, 2005). *O*-linked flagellin glycosylation is essential for flagellins to polymerize into the extracellular filament for motility, although the role glycosylation plays in filament assembly is still not yet understood. Flagellin glycosylation is confined to 19 serine and threonine residues along the central domain of the flagellin protein, covering a total of 10 % of the FlaA glycoprotein mass, yet studies have shown only three to five glycosylated residues are essential for filament formation, motility or autoagglutination (Ewing *et al*., 2009).

Originally thought to play a role in LPS biosynthesis, the *N*-linked general glycosylation system has been shown to modify dozens of relatively average or low abundant periplasmic and outer membrane proteins with a specific glycan. Unlike *O*-linked, *N*-linked glycosylation appear to be highly conserved among Proteobacteria, lacking putative phase-variable genes driving variation (Szymanski *et al*., 1999). N-linked glycosylation of surface proteins reduces degradation by extracellular proteases and facilitates binding with the C-type lectin receptor MGL and certain macrophage cells to limit the production of interleukin-6 (IL-6) during infection. Mutation of the *N*-linked glycosylation system reduces the ability of *C. jejuni* to adhere to and invade *in vitro* cultured eukaryotic cells or colonise the intestines of chickens (Golden & Acheson, 2002, Guerry *et al*., 2006). An alternative role proposed for the *N*-linked glycosylation system is that free glycan incorrectly bound to proteins functions as an osmoprotectant during osmotic stress. As only 10 % of the glycan produced for *N*-linked glycosylation is attached to protein, the remaining

90 % is found as free glycan in the periplasm acting as a cellular defence in both the protein-linked and free states (Nothaft *et al*., 2009).

1.8.4 Iron homeostasis

Iron is an essential micronutrient for all living organisms, playing an essential role in cellular metabolism, gene regulation, enzyme catalysis and protein structure stabilisation. During colonisation of the intestinal tract, pathogens are under a near continual iron deficiency due to competition from the host and normal microbiota. For an intestinal pathogen to successfully colonise its host, it must employ a competitive iron acquisition system, to bind and transport extracellular iron. Although *C. jejuni* does not produce iron chelating compounds to sequester ferric iron, it does produce several iron scavenging uptake systems which sequester exogenous ferrochrome and enterochelin from other bacteria and haem compounds, which might be released in the site of inflammation (Holmes *et al*., 2005). Several iron acquisition systems have been identified in *C. jejuni,* including the Fe(II) ABC transporter (FeoB), a haemin/haemoglobin-uptake system (ChuA) and a ferric enterobactin uptake receptor (CfrA) (Miller *et al*., 2009). Animal model studies have shown the importance of FeoB, ChuA and CfrA for successful colonisation, demonstrating the importance of iron-uptake for host pathogenicity (Miller *et al*., 2009). Although iron is essential for growth, excess iron in combination with oxygen can generate ROS via Fenton and Haber–Weiss reactions which damage proteins, lipids and DNA. Thus, iron uptake needs to be tightly regulated to prevent iron associated oxidative damage. The balance between iron uptake and free radical formation is controlled by the ferric uptake regulator (Fur) and the iron response peroxide regulator Per as mentioned in section 1.7.5.

1.9 Control Strategies

1.9.1 *C. jejuni* prevalence in the food chain

Epidemiological assessment studies have reported that handling, preparation and consumption of broiler meat may account for up to 30% of human cases of campylobacteriosis, while 50–80% may be attributed to the chicken reservoir as a whole (Panel & Biohaz, 2010). Despite *C. jejuni* residing in the cecum and colon of chicken, during processing, the intestinal track may rupture or leak, transferring the intestinal fluid onto the skin. Transmission from animal host to humans also comes via faecal contamination, through the transfer of host intestinal gut flora to water supplies or to the surface of the meat carcass during slaughtering. Previous studies have shown the bacteria can grow in the cervices and channels on the surface of the meat at room temperature, increasing the risk to consumers if chicken is inadequately stored (Scherer *et al*., 2006). Quantitative risk assessment models have shown that a 2-log reduction in *C. jejuni* numbers on broiler carcases could result in a significant reduction (30 times less) in the incidence rate of campylobacteriosis (Rosenquist *et al*., 2003). The resistance of *Campylobacter* to clinical antibiotics including macrolides and fluoroquinolones, the major drugs of choice for treating human campylobacteriosis, raises an urgent need for novel strategies to control and prevent *Campylobacter* colonisation in poultry.

1.9.2 Farm to fork strategy

Reduction of *Campylobacter*-positive flocks from broiler houses has been found to be the most relevant strategy to reduce the number of human *Campylobacter* infections as the farm is the preliminary site of *Campylobacter* entry into the production (Skarp *et al*., 2016). A review outlining the major risk factors which determine the incidence rate of *Campylobacter* infection in broiler hens found that flock thinning, slaughter in the summer months, and bird age were the main factors which determine *Campylobacter* colonization (Lawes *et al*., 2012, Tustin *et al*., 2011). Following these reports, the EFSA outlined their multi-layered intervention strategy often termed ‘farm to fork’, which targets multiple areas of the infection cycle. The first point of intervention acts to prevent *Campylobacter* entering the flock, primarily through increased biosecurity, then failing that, reducing flock susceptibility to infection through food additives and vaccination, then finally targeting post-harvest measures such as improved processing and decontamination.

1.9.2 Bacteriocins

Bacteriocins are short cationic antimicrobial peptides with broad-spectrum activity produced by bacteria to inhibit the growth of closely related strains. Despite the broad diversity in sequence and structure, bacteriocins share a common mechanism of killing by disruption of membrane

integrity (Yeaman & Yount, 2003). Bacteriocins first interact with target cells through initial electrostatic interactions, followed by the disruption of the structure and function of the bacterial membrane, permeating the lipid biolayer and forming a transmembrane pore. There are at least 4 purified bacteriocins known to reduce *Campylobacter* colonisation in poultry, with the most effective being Enterococcin E-760 isolated from *Enterococcus durans* (Line *et al*., 2008). Enterococcin administered to broiler hens 4 days prior to analysis was able to reduce *Campylobacter* counts of 5.15-8.36 $\log_{10}$ CFU/g from the untreated control group to undetectable levels (below 2 $\log_{10}$ CFU/g) in the Enterococcin treated group (Line *et al*., 2008). Although slight E-760 resistance was detected in some *C. coli* strains (MIC = 64 mg l^{-1}), bacteriocin resistance in *Campylobacter* strains is generally difficult to develop and studies have shown that *C. jejuni* mutants with low bacteriocin resistance are not stable (Caldwell *et al*., 2008, Hoang *et al*., 2011). Despite the success of bacteriocin trials *in vitro,* the high costs associated with industrial purification of antimicrobial peptides has meant bacteriocins have not been implemented as a control strategy on a commercial scale. Unfortunately, studies assessing the inhibitory effect of solely viable bacteriocin expressing strains *L. salivarius* (NRRL B-30514) and *P. polymyxa* (NRRL B-30509) observed no CFU reduction, compared with the 6 $\log_{10}$ reduction observed in purified bacteriocin treated groups (Line *et al*., 2008).

1.9.3 Vaccination

Despite substantial research towards the development of an effective *Campylobacter* vaccine, currently there are no products on the market to reduce *Campylobacter* loads in the gastrointestinal tract of chickens. The development has been hindered by multiple factors including the lack of a small animal model, high genetic variability and the presence of LOS ganglioside mimics which can induce human autoimmune disorders. Multiple vaccine candidates have made it to clinical trials including the recombinant flagellin rFla-MBP, the recombinant protein ACE 393 and capsule-conjugate (CJCV), yet none have advanced past phase II clinical trials (Poly *et al*., 2019). Recently a patent has been submitted for a glycoconjugate vaccine which combines the conserved *C. jejuni* N-glycan with a protein carrier, GlycoTag (Tox-GT). Chickens exposed to the ToxC-GT glycoconjugate showed up to 10-log reduction in *C. jejuni* colonisation and all induced N-glycanspecific IgY responses (Nothaft *et al*., 2016). As N-glycan is the only glycoconjugate structure conserved among all *C. jejuni* isolates, the resulting immune response is cross protective, making ToxC-GT vaccination an excellent strategy to reduce *C. jejuni* infection in poultry, yet further trials are required before this treatment can be implemented.

1.9.4 Decontamination of carcasses

At the final stages of processing before carcasses are delivered to the consumer, physical or chemical decontamination offers the last resort to remove *Campylobacter* from the surface of meat to reduce the transmission of infection. The European commission currently allows decontamination treatments to be considered if a substance is shown to be safe and effective, yet no chemical decontamination treatments are currently authorised by the EU (European Commission, 2004). Other countries outside the EU have resorted to the use of chemical decontamination of raw poultry, using lactic acid, chlorine dioxide and acidified sodium chlorite which is often used as a substitute to good hygiene practices. Given the risk of accumulation of carcinogenic trihalomethanes, such as chloroform, there remains great uncertainty surrounding the use of chlorine related decontaminants in poultry (Couri *et al.*, 1982). Additionally, for most chemical decontaminates, the beneficial effect increases during chilled storage, meaning in regions which require chemical decontaminates to be removed after application (including the EU), the beneficial effects are most likely lost (Cox & Pavic, 2010). Overall current chemical interventions show poor efficiency and lack consumer confidence which has driven the need for alternative interventions to reduce *Campylobacter* abundance on the surface of poultry. Physical decontamination methods including increasing/decreasing temperature or exposure to radiation are safer alternatives to chemical decontamination. Freezing poultry to -20^{o}C is used to treat *Campylobacter* colonised flocks in some countries, and has been shown to reduce CFU by approximately 2 $\log_{10}$ units with minimal impact on the quality of the meat (Georgsson *et al.*, 2006). Currently, UK poultry producers utilise a combination of steam and ultrasound to reduce *Campylobacter* numbers on the surface of meats which is effective at reducing CFU by approximately 1.5-2 $\log_{10}$ cycles (Rosenquist *et al.*, 2009). Although the steam and ultrasound treatment is relatively efficient in producing low levels of waste water, the machinery required to generate high pressure steam and ultrasound is expensive and costly to maintain. Irradiation systems using gamma and x-rays can be relatively inexpensive machines to install and can be controlled by the flick of a switch, yet the risk of damage to human skin and the poor penetration of light at these low wavelengths make these irradiation systems impractical for industrial use. Although multiple intervention strategies have been implemented across the world as shown in Table 2, there has been no clear 'golden bullet' which is both safe and effective at reducing *Campylobacter* on the surface of meats.

Intervention Strategy	Efficacy for Campylobacter reduction	References
Lactic acid (2%)	0.74 log10 reduction	(Riedel *et al.*, 2009)
Acidified sodium chlorite (1200 mg/l)	1.75 log10 reduction (spray)	(Kere Kemp *et al.*, 2001)
Chlorine dioxide (50-100 mg/l)	0.99 -1.21 log10 reduction	(Hong *et al.*, 2008)
Trisodium phosphate	1.03 log10 reduction (spray)	(Bashor *et al.*, 2004)
Acidified electrolysed oxidising water	1.07 log10 reduction	(Kim *et al.*, 2005)
Hot water immersion	1.25 log10 reduction	(Bull *et al.*, 2006)
Steam ultrasound	1.3-2.51 log10 reduction	(Rosenquist *et al.*, 2009)
Freezing for 3 weeks	2.18 log10 reduction	(Georgsson *et al.*, 2006)

Table 2 - Approved chemical and physical intervention strategies used around the world and their corresponding decontamination efferences. Reduction efficiencies represent CFU reductions comparing untreated poultry skin with *C. jejuni* CFU levels around 4-6 $\log_{10}$ CFU on the surface of skin with chemically or physically decontaminated skin.

1.9.5 Violet-blue light

Recently it emerged that photodynamic inactivation (PDI) which involves killing by violet-blue light could be a novel intervention strategy to remove *Campylobacter* species from surfaces (Murdoch *et al.*, 2010). Results demonstrated that *C. jejuni* is far more sensitive to violet/blue light than other gram-negative enteric pathogens. This result coupled with the safety-in-use advantages of visible (non-ultraviolet wavelength) light suggest 405 nm violet/blue light could be a promising new technology to decontaminate *Campylobacter* from surfaces without the use of chemicals or cost intensive treatments.

1.10 Photodynamic inactivation

1.10.1 Discovery

The concept of photodynamic inactivation (PDI) was accidently discovered in 1900 by Oscar Raab, a medical student working on the toxicity of acridine orange on the freshwater protozoa *Paramecium spp.* His results were initially highly variable and non-reproducible despite multiple replicates (Defty & Orpin, 2011). His supervisor Hermann von Tappeiner, noticed that the observed toxicity was dependent on the time of the day and the amount of daylight, given this was the only changing parameter. Later, von Tappeiner applied this light dependant phenomenon for treatment of skin carcinomas, coining the treatment the "photodynamic phenomenon"(Jesionek , 1905). Since then, PDI has been used as a tool for the treatment of various skin carcinomas and age related macular degeneration (Dai *et al*., 2009). Most recently, as the end of the antibiotic era gets closer, PDI has emerged as an innovative, non-antibiotic approach to inactivate pathogenic bacteria, independent of existing antibiotic resistance status.

1.10.2 Photochemistry

The basic principle of the PDI involves the excitation of a photosensitiser with visible light of the correct wavelength, which generates ROS through transfer energy or electrons after excitation to molecular oxygen. Photosensitisers are molecules formed by one or more light-sensitive π electron-rich macrocycles, with strong absorption bands (higher than 30,000 M^{-1} cm^{-1}) (De Freitas & Hamblin, 2016). Upon irradiation with light of a specific wavelength, the photosensitizer undergoes a transition from a low energy ground state to an excited singlet state followed by the reversal of the excited electron's spin, known as intersystem crossing to the excited triplet state (Sharman *et al*., 1999). This triplet state is less energetic than the excited singlet state, but has a considerably longer lifetime, as the excited electron is in a parallel spin to its former paired electron, and may not immediately fall back down (Dai, *et al*., 2011).The extended lifetime of the excited triplet state means it can undergo electron transfer reactions with biomolecules to produce ROS through two different pathways as shown in Figure 7. Photochemical reactions of the triplet state are divided into two different pathways, the type I mechanism involving electron transfer from the excited photosensitiser to O_2, forming O_2^- which undergoes further transfer to form H_2O_2 and $^{\bullet}OH$, or type II reactions which involves energy transfer to molecular oxygen to generate singlet oxygen $^1O_2$. After excitation and ROS generation, the photosensitiser passes back to the ground state, ready to absorb a new photon and generate more ROS. Thus, one photosensitiser can generate thousands of oxygen radicals before being destroyed.

Porphyrins are commonly used photosensitisers as they have a strong absorption band in the visible wavelength, they are relatively photostable so can undergo numerous photoexcitation reactions and have a high ROS yield upon illumination with high intensity violet/blue light (Wainwright, 2008). Broadly speaking, tetrapyrrole based photosensitisers have a preference to undergo Type II photoexcitation to generate $^1O_2$, whereas non-tetrapyrrole based photosensitisers favour Type I reactions (Maisch *et al*., 2007, Yamakoshi *et al*., 2003, Regensburger *et al*., 2010). Porphyrin based photosensitisers have a high redox potential therefore they primarily undergo energy transfer reactions via type II photoexcitation, whereas methylene blue (MB) base photosensitisers have a low redox potential, making them good electron acceptors following the type I pathway (Kasimova *et al*., 2014). Although various studies have been conducted to determine the specific ratio of type I or type II photosensitisers, the perceived lack of specificity of ROS quenchers or electron paramagnetic resonance (EPR) spin traps used to distinguish the photochemical reaction preference means it remains difficult to determine the true ratio of a given photosensitiser (Maisch *et al*., 2005, Tavares *et al*., 2011). The exact microbial targets of light generated ROS depend on the whether the bacteria have an abundance of endogenous photosensitisers which can be excited to generate oxygen radicals or if the photosensitiser needs to be supplied exogenously. As most ROS generated are highly reactive and cannot travel far from the site of generation, the localisation of the excited photosensitiser often determines the biomolecules damaged.

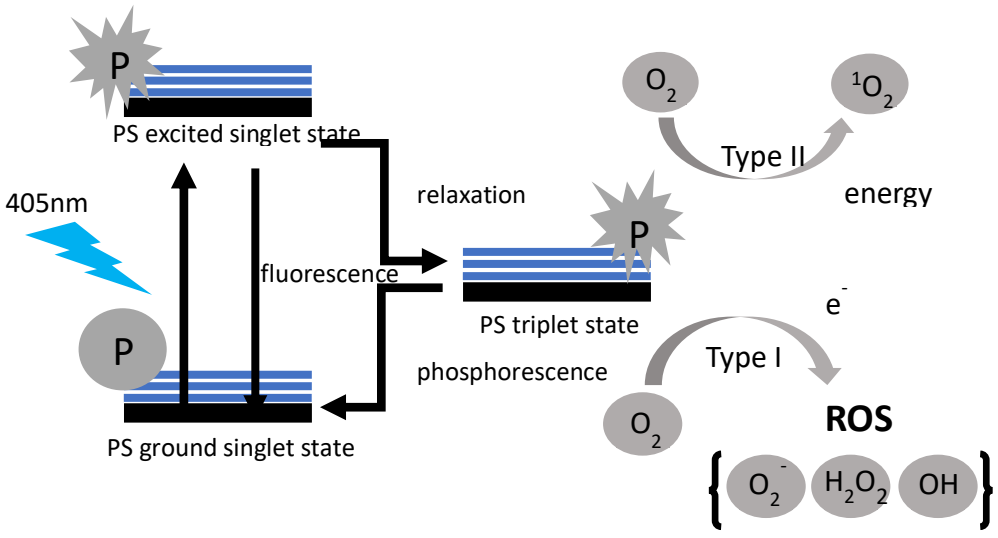

Figure 7 – Photochemical generation of oxidising species: Excitation of photosensitizer (P) by specific wavelength of light (405nm) produces excited triplet singlet state which releases electrons as it transitions back to ground state trough type I and type II electron transfer reactions.

1.11 Exogenous photosensitisers to kill bacteria

Antimicrobial PDI using exogenous photosensitisers is a growing approach to treat skin and mucosal infections, using non-toxic dyes or photosensitizer molecules which can be activated by visible light to generate ROS. Due to the broad range of photooxidative targets, PDI can be used to treat multi-drug resistance strains without the development of resistance (Hamblin & Hasan, 2004). Despite the continuing rise of MDR strains, light activated antimicrobials have been widely ignored and currently only three photo antimicrobial agents have received clinical approval (methylene blue (MB), toluidine blue O, and indocyanine green). The main limitations to PDI is that the delivery of visible light is almost by definition a localised process, therefore treatments are exclusively aimed at localised diseases, and arpre ineffective at treating systematic infections such as bacteraemia.

Due to the short lifetime of ROS and its limited diffusion length, the oxidative targets of PDI depend on the respective localisation of the photosensitiser. For photosensitisers which stay in close proximity to the bacterial cell or actively bind to the bacterial membrane through electrostatic interactions, oxidative damage occurs to the cytoplasmic membrane, disrupting membrane transporters and lipids (Cieplik *et al*., 2018). There have been several reports that show photosensitisers do not need to penetrate the bacterial membrane to exert oxidative damage intracellularly. If singlet oxygen is generated in sufficient quantities near to the bacterial membrane, it will diffuse into the cell and damage intracellular ROS susceptible structures (Arenas *et al*., 2013).

For photosensitisers which bind and diffuse across the bacterial membrane, intracellular ROS sensitive components such as DNA and iron sulphur clusters form the main sites of damage. It has been well reported that gram-negative bacteria are less sensitive to PDI than gram-positives as their outer membrane restricts the transport of anionic photosensitiser molecules into the cytoplasm, where light generated radicals can damage ROS susceptible targets. Recent fluorescent microscopy studies have reported that photosensitiser uptake is dependent on the photooxidative damage to bacterial cell membranes, increasing permeability, therefore allowing intracellular uptake of photosensitisers (Gollmer *et al*., 2017). However, other studies have shown that the phenothiazinium photosensitiser methylene blue locates intracellularly, as the addition of efflux pump inhibitors to *S. aureus* and *P. aeruginosa* increased photodynamic inactivation efficiency (Tegos *et al*., 2008). Given the large molecular size and lipophilicity of most tetrapyrrole photosensitisers, it seems reasonable that the main targets for PDI are external cytoplasmic membrane structures. Only when the cytoplasmic membranes become

sufficiently leaky following prolonged oxidative damage, will photosensitisers become internalised and exert photooxidative damage on cytoplasmic protein and DNA complexes.

1.12 Endogenous photosensitisers

It has been frequently reported that some bacteria accumulate porphyrins under certain conditions, deeming them more susceptible to PDI than other bacteria. The two mechanisms which bacteria naturally accumulate photoactive porphyrins occur either through haem acquisition or tetrapyrrole biosynthesis. The anaerobic oral pathogens *Porphyromonas* and *Prevotella* spp depend largely on external haem to satisfy their demand for iron. Unlike other gram-negative bacteria, *Porphyromonas* do not produce siderophores and instead employ specific outer membrane receptors and proteases to bind and transport haem (Olczak *et al*., 2005). Once internalised, the bacteria will store acquired haem proteins as iron-containing haem aggregates hematin, until iron can be stripped from the tetrapyrrole centre, releasing iron-free protoporphyrin IX (PPIX) as a by-product (Shah & Gharbia, 1993). As the bacteria strip hematin to meet their iron demands, they accumulate PPIX, which increases their photosensitivity, however, if sequestered haem is maintained as hematin, they will not become photosensitive as iron containing tetrapyrroles do not carry out the appropriate photochemistry.

The alternative route for porphyrin accumulation is through poor regulation of the haem biosynthesis pathway, leading to the accumulation of the haem intermediates coproporphyrin and PPIX (with a minor contribution from uroporphyrin) (Melo & Johnsson, 1982). The anaerobic bacteria *Propionibacterium acnes* have been known to accumulate fluorescent porphyrins, which causes a proinflammatory response in humans, commonly known as acne vulgaris. Although it has been suggested that the *deoR* repressor element upstream of the porphyrin biosynthesis operon regulates porphyrin synthesis in *P. acnes*, no differences were observed in sequence or expression levels of this repressor in strains with both high and low porphyrin production (Barnard *et al*., 2020). This suggests there are additional factors which regulate the differential porphyrin production in *P. acnes* which is not yet understood.

Recent reports have shown that *H. pylori* also naturally accumulates sufficient photoactive porphyrins to allow it to be efficiently killed after illumination with blue light (Hamblin *et al*., 2005). Like *Propionibacterium, Helicobacter* generates excess porphyrins through intermediates of the haem biosynthetic pathway as opposed to haem acquisition systems as tetracarboxylic protoporphyrinogen IX and coproporphyrinogen III form the main intracellular tetrapyrrole structures which can't be produced from dicarboxylic porphyrin obtained from exogenous haem (Battisti *et al*., 2017). HPLC analysis showed that *H. pylori* excrete coproporphyrin (CP) and protoporphyrin into the supernatant during growth, with increasing levels of tetrapyrrole

excretion occurring in the later phases of growth, consistent with that reported in *P. acnes* (Hamblin *et al*., 2005). Despite *Helicobacter* and *Propionibacterium* generating similar levels of intracellular CP and PPIX, *Helicobacter* species are more than 100 fold more sensitive to PDI than *P. acnes* (Hamblin *et al*., 2005). As there are so few examples of natural porphyrin-producing photosensitive bacteria, it is difficult to determine the physiological differences between the two bacteria which determine their differential susceptibilities. However, a recent review exposed the difficulties in cross-comparing killing efficiencies between different labs as large variations can occur using different illumination setups, highlighting a need for a more standardised approach to studying PDI (Hessling *et al*., 2017). Endogenous porphyrins can also be produced in high quantities after incubation with the haem precursor 5-aminolaevulinic acid (ALA). Analysing the porphyrin content of ALA induced content of *S. aureus* and *E. coli* cultures found CP and PPIX form the main overproduced tetrapyrrole intermediates with coproporphyrin being preferentially excreted into the supernatant whereas protoporphyrin forms intracellular aggregates (Nitzan & Kauffman, 1999).

1.13 Bacterial response to photooxidation

The bacterial response to photooxidative stress is largely dependent on the localisation of the photosensitiser and the photochemical preference of the photosensitiser for type I or type II photoexcitation. Bacteria can respond to ROS generated through type I photoexcitation through upregulation of the oxidative stress regulon to detoxify superoxide, peroxide and hydroxyl radicals. A study by Maisch *et al* 2018 looked at the viability of *sobB* deficient mutants in *E. coli* in response to exogenously generated ROS from photosensitisers with either type I photoexcitation preference (MB) or type II (PPIX based TMPyP). They found that *sod*$^{-}$ mutants were more susceptible to type I PDI than WT, and this phenotype could be rescued by the addition of ROS quenchers (Tabrizi *et al*., 2018). However, there was little difference in the survival rates between wild-type and *sod*$^{-}$mutants under type II PDI, with PPIX based TMPyP. Also, ROS quenchers did not generate a significant difference in survival rate like that seen using type I PDI (Faraj Tabrizi *et al*., 2018). This effect may be partially explained by the intracellular localisation of MB compared to the membrane localised TMPyP, as exogenously generated ROS will not be efficiently quenched by intracellular superoxide dismutase.

Bacterial antioxidant enzymes are ineffective at scavenging ROS generated through the type II pathway as singlet oxygen is simply molecular oxygen at the lowest lying electronic excited state (+0.98 eV). This excitation energy is sufficient to induce oxidative damage through formation of protein peroxides, protein unfolding and enzyme inactivation (Gomes *et al*., 2013)(Dosselli *et al*., 2012). These damages have been shown by enzyme assays of NADH and succinate

dehydrogenases or through quantification of protein carbonylation and lipid peroxidation (Du *et al*., 2012, Sharma *et al*., 2008, Dosselli *et al*., 2012). Although bacterial carotenoids have been shown to directly quench $^1O_2$ among other ROS species, there has been no evidence of an adaptive response to PDI through upregulation of carotenoid defence genes (Sun *et al*., 2020).

The first study to assess the global response to photooxidative stress induced by the extracellularly located PPIX based TMPyP photosensitiser in *S. aureus* highlighted the selective damage caused by membrane localised, porphyrin-based photosensitisers. Dosselli *et al*. showed that sublethal PDI influenced the expression of proteins involved in bacterial metabolism, forcing a switch to a fermentative glycolytic metabolism, yet enzyme assays showed selective oxidative damage to specific enzymes of these pathways prevented the exchange (Dosselli *et al*., 2012). Additionally, a 4-fold increase in catalase abundance was detected between bacteriostatic and bactericidal light doses, showing the response of antioxidant proteins only occurs once significant damage has occurred. This finding was supported by Maisch *et al*. who found PDI using TMPyP photosensitisers had no relevant influence on the upregulation of *S. aureus* superoxide defence genes (Tabrizi *et al*., 2018).

Given the inability of the oxidative stress regulon to detoxify $^1O_2$, bacterial defence proteins have been shown to be upregulated to prevent the damage induced by type II photoexcitation. Using the type II photosensitiser Toluidine Blue O (TBO), Hamblin *et al.* found a 7-fold increase in the protein chaperone GroEL and a 3-fold increase in the bacterial heat shock protein DnaK (Huang, *et al*., 2011). By exposing *E. coli* and *E. faecalis* to a heat pre-treatment, they were able to see a 2 $\log_{10}$ and a 4 $\log_{10}$ reduction in TBO mediated PDI respectively, suggesting heat shock protein upregulation may form a possible mechanism for resistance. To reveal the molecular targets of type II-based photoexcitation in *Salmonella enterica,* Buchovec *et al.* monitored the expression of 33 stress- related genes by RT qPCR following PDI with the exogenous chlorophyllin based photosensitiser (Buchovec *et al*., 2017). They found significant upregulation of defence enzymes involved in adaption to oxidative and acid stress (*oxyR, ahpC, grxA, sulA, atpC, groEL*). There have been multiple studies across numerous bacterial pathogens to try induce resistant phenotypes towards PDI through repeated passages of treatment and regrowth (Lauro *et al*., 2002, Pedigo *et al*., 2009, Tavares *et al*., 2010). The inability to isolate resistance genes and response networks may be due to fundamental limitations in the experimental design. Bacteria acquire resistance towards a given antimicrobial when they are continuously exposed to low or sub-antimicrobial doses for a prolonged period which is often difficult to maintain when using exogenous photosensitisers. A superior approach would be to identify resistance determinants

using a transcriptomic approach, studying PDI in bacteria which naturally accumulate porphyrin photosensitisers, to remove the variation seen from exogenously supplied photosensitisers.

Aims of this study

We have selected *C. jejuni* as a model system to study the global response to PDI as this bacterium appears to be innately sensitive to photooxidative stress due to the accumulation of endogenous porphyrin species (Murdoch *et al*., 2010). Given ROS generated by PDI in this bacterium accumulates intracellularly, it offers a clean system to study the intracellular response to photooxidative stress at the site of damage. Given the lack of a clear mechanism of damage for PDI in pathogenic bacteria, we aim to uncover for the first time which molecular targets become inactivated following photooxidative stress as well as the cellular responses expressed to defend them.

Specific Objectives:

- To characterise the major endogenous photosensitisers in *C. jejuni* which differentiate it from other non-light sensitive bacteria using HPLC and whole cell spectroscopy.
- To identify which enzyme and protein complexes in *C. jejuni* are damaged by photooxidative stress through specific enzyme assays and protein blots.
- To characterise the global transcriptional response to photooxidative stress using RNAseq across a range of 405 nm light doses.
- To identify which response proteins and enzymes protect the bacteria from photooxidative stress by characterising the light sensitivity of appropriate mutants.
- To assess the efficiency of other exogenous photosensitisers at killing bacterial pathogens which lack an abundant endogenous photosensitiser.

Chapter 2: Materials and Methods

2.1 Materials

Chemicals were obtained from Alfa Aesar, Duchefa, Invitogen, Melford, Oxiod, Sigma-Aldrich, Thermo-Fisher scientific and VWR. Molecular biology reagents were supplied by Ambion, Bioline, Invitrogen, New England Biolabs and Promega. Gasses were supplied by BOC.

2.2 Organisms used in this study

All bacterial strains used in this study are listed in Table 2.1. *Campylobacter jejuni* strains were stored at -80°C in Brain Heart Infusion (BHI) broth (Oxoid) containing 20% [v/v] glycerol as a cryoprotectant. *E. coli, S. aureus and P. aeruginosa* strains were stored at -80°C in Luria-Bertani (LB) broth (Oxoid) containing 25% [v/v] glycerol as a cryoprotectant.

2.2.1 *E. coli* strains used in this study

Escherichia coli strain	**Genotype/description**	**Source**
MG1655	F- λ-*ilvG- rfb*-50 *rph*-1 – wild type K12	Invitrogen
DH5α™	F– Φ80*lac*ZΔM15 Δ(*lac*ZYA-*arg*F) U169 *rec*A1 *end*A1 *hsd*R17 (rK–, mK+) *pho*A *sup*E44 λ– *thi*-1 *gyr*A96 *rel*A1	Invitrogen
BL21 (DE3)	F– *omp*T *hsd*SB(rB–, mB–) *gal dcm* (DE3)	Invitrogen
Top10	Protein expression strain. *hsdR mcrA lacZΔM15*	Invitrogen
BL21 (pET21a-*cj1384c*)	BL21 cells containing pET21a. C-terminal His-tagged *cj1384c*	This study
BL21 (pET28a-*cj1384c*)	BL21 cells containing pET28a. N-terminal His-tagged *cj1384c*	This study
Top10 (pBAD-*cj184c*)	Top10 cells containing pBAD. N-terminal His-tagged *cj1384c*	This study

Table 2.1 List of *E. coli* strains used in this study with the genotype listed in column 2.

2.2.2 Other strains used in this study

Strain	Genotype/description	Source
***Pseudomonas aeruginosa* PA01**	Wild type wound isolate	Professor Colin Manoil transposon library (University of Washington)
***Staphylococcus aureus* SH1000**	Wild type pathogen	Professor Simon Foster (University of Sheffield)
***Helicobacter pylori* 26695**	Wild type pathogen	Professor David Kelly (University of Sheffield)

Table 2.2 List of other organisms used in this study with the genotype listed in column 2.

2.2.2 *C. jejuni* strains used in this study

Campylobacter jejuni	**Strain description**	**Source**
Wild type NCTC11168	Laboratory wild type strain, original human clinical isolate	Parkhill *et al.,* 2000
Wild type NCT11168-H	Hypermotile human clinical isolate	Karlyshev *et al.,* 2002
Wild type 81116	Genetically stable strain	Pearson *et al.,* 2007
Wild type 81-176	Highly virulent strain with pVir and pTet plasmids	Hofreuter *et al.,* 2006
Δcj0012	NCT11168-H *rrc cj0012* deletion :: Kan	This study
Δcj0045	NCT11168-H *cj0045* deletion :: Cat	This study
Δcj0169	NCT11168-H *sodB cj0169* deletion :: Kan	This study
Δcj0241c	NCT11168-H *hemB cj0241c* deletion :: Kan	This study
Δcj0271	NCT11168-H *bcp cj0271* deletion :: Kan	This study
Δcj0322	NCT11168-H *perR cj0322* deletion :: Kan	This study
Δcj0334	NCT11168-H *ahpC cj0334* deletion :: Kan	This study
Δcj0400	NCT11168-H *fur cj0400* deletion :: Kan	This study

Δcj0504 metK+	NCT11168-H *hemH cj0504 metK* complementation :: Cat	This study
Δcj0779	NCT11168-H *tpx cj0779* deletion :: Kan	This study
Δcj0737	NCT11168-H *cj0737* deletion :: Cat	This study
Δcj1153	NCT11168-H *cj1153* deletion :: Kan	This study
Δcj1262	NCT11168-H *cj1262* deletion :: Kan	This study
Δcj1385	NCT11168-H *katA cj1385* deletion :: Kan	This study
Δcj1385 pRRA	NCT11168-H *katA cj1385* complement :: a*pr*	This study
Δcj1534c	NCT11168-H *dps cj1534c* deletion :: Kan	This study
Cj1673c	NCT11168-H *recA cj1673c* deletion :: Kan	This study

Table 2.3 List of *C. jejuni* strains used in this study with the strain description listed in column 2.

2.3 *Campylobacter* growth medium preparation

Campylobacter was routinely grown on Columbia blood agar base (Oxoid) containing 5% lysed horse blood with 10 µg ml^{-1} amphotericin-B and vancomycin and selective antibiotics (where required) were added when media had cooled to approximately 50°C. Growth medium was prepared with distilled water (dH_2O) following manufacturer's recipes and sterilised by autoclaving (121°C, 20 mins, 15 psi). Plates were stored at 4°C for up to 1 month. Liquid cultures of *C. jejuni* were routinely grown in Brucella broth (Oxoid) supplemented with 20 mM L-serine and 1% Tryptone (Oxoid) prior to autoclaving and is referred to as BTS broth.

2.4 *Escherichia coli, S. aureus* and *P. aeruginosa* growth medium

Escherichia coli, S. aureus and P. aeruginosa was grown routinely at 37 °C on LB agar (Oxoid) which was made according to manufacturer's instructions. Liquid cultures were grown in LB broth.

2.5 Antibiotics

Antibiotics (purchased from Sigma-Aldrich, Melford or Duchefa) were dissolved in sterile distilled water (sdH_2O) and filter sterilised through 0.2 µm filters except from chloramphenicol which was dissolved in ethanol. Drop-wise addition of 10 M NaOH was required for dissolving

Amphotericin B. Stock solutions (1000 x concentrated) were stored at 4 °C and were used at the following working concentrations: amphotericin B and vancomycin 10 µg ml^{-1}, kanamycin 30-50 µg ml^{-1}, chloramphenicol 30 µg ml^{-1} and carbenicillin 50-100 µg ml^{-1}.

2.6 Growth of *C. jejuni*

2.6.1 Batch culture

Campylobacter jejuni strains were grown at 42 °C in microaerobic conditions (10% [v/v] O_2, 10% [v/v] CO_2 and 80% [v/v] N_2) in a MACS-VA500 Incubator (Don Whitley Scientific Ltd, UK). Typically, *C. jejuni* strains were grown on blood agar plates for 1-2 days before being used to inoculate 30 ml or 300 ml BTS broth medium in 100 ml or 500 ml conical flasks respectively mixed by continuous orbital shaking at 140 rpm on a SeaStar® orbital shaker. Cultures were supplemented with 10 µg ml^{-1} amphotericin-B and vancomycin. Growth medium was pre incubated in microaerobic atmosphere for 12 hours prior to inoculation with a microaerobically grown liquid starter culture or a day-old blood agar plate.

2.6.2 Chemostat culture

Continuous cultures were grown in an Infors HT Labfors 3 chemostat, controlled by Infors Iris 5 software (Infors, Switzerland). *Campylobacter jejuni* was grown in L-serine limited defined medium as previously described by (Guccione *et al*., 2017). Culture volume was maintained at 37°C in 885 ml, with proportional mixing of compressed air and 10 % v/v CO_2 (nitrogen balanced) maintained an oxygen tension of 5% O_2 v/v, sufficient for 100% aerobiosis with a stirring rate of 350 rpm (Guccione *et al*., 2010). pH was maintained at pH 7.4, as imposed by the phosphate buffered medium measured by an internal probe. The vessel was inoculated to on OD_{600} of 0.1 and allowed to grow without turnover for 6 hours until an OD_{600} of around 0.6 was reached. At this point, growth medium is fed into the vessel at a dilution rate of 0.2 l $hour^{-1}$ until a steady state of 5 vessel volumes of turnover was achieved. Once at steady state, cell cultures were extracted and used for analysis.

2.7 Growth of *S. aureus, P. aeruginosa* and *E. coli*

All strains were routinely cultured aerobically at 37°C on LB broth or agar plates sterilised by autoclaving and supplemented with appropriated antibiotics. Liquid cultures were shaken at 200 rpm.

2.8 DNA manipulation

2.8.1 DNA isolation and purification

Genomic DNA was isolated using GeneElute bacterial genomic DNA extraction kit (Sigma). Plasmid DNA was extracted from *E. coli* strains using Qiagen Miniprep (Qiagen, UK) and the

QIAquick PCR purification kit (Qiagen) was used for DNA extraction from agarose gel and cleaning up of PCR reactions. All kits were used following the manufacturer's instructions.

2.8.2 Polymerase chain reaction

Standard PCR reactions were carried out in a final volume of 20 µl in one of two types of PCR reaction. Phusion (Thermo) was used for high fidelity cloning and MyTaq (Bioline) was used for colony screening of mutants. All primers were purchased from Sigma.

Each reaction was made up of the following components.

Component	**µl (Phusion PCR)**	**µl (MyTaq PCR)**
2X Polymerase solution	10 µl (Phusion)	10 µl (MyTaq)
100 µM Primer solutions	1 µl	1 µl
Template DNA	10 ng	1 colony
dH_2O	7	7

The PCR conditions used are shown below, conditions were occasionally modified according to requirements. The PCR reactions were performed in a 36 well (Applied Biosystems) thermal-cycler.

Step	Temperature	Duration	Cycles	Description
1	98°C 95°C	5 minutes	1	Initial Denaturation
2	98°C	10 seconds	32	Denaturation
	50-60°C	20 seconds		Annealing
	72°C 72°C	1 minute kb^{-1}		Extension
3	72°C	5 minutes	1	Final Extension
4	4°C	Hold	1	Final Hold

Table 2.4 PCR conditions and extension times

2.8.3 Primers used in this study

***C. jejuni* 11168 ISA knockout primers**	
Δcj0012* F1 *fwd	GAGCTCGGTACCCGGGGATCCTCTAGAGTCACAACCCATCAAGTTGTT
Δcj0012* F1 *rev	AAGCTGTCAAACATGAGAACCAAGGAGAATATGTAAAGCACCAAAAGAGTA
Δcj0012* F2 *fwd	GAATTGTTTTAGTACCTAGCCAAGGTGTGCTCTACTTCATTGCCACATT
Δcj0012* F2 *rev	AGAATACTCAAGCTTGCATGCCTGCAGGTCGGAATACAGATTAAAGCATCA
Δcj0045* F1 *fwd	GAGCTCGGTACCCGGGGATCCTCTAGAGTCAACACAGTTGCAATTAAAATAC
Δcj0045* F1 *rev	AAGCTGTCAAACATGAGAACCAAGGAGAATCTTGAATGTTTAGAGCTAAATC
Δcj0045* F2 *fwd	GAATTGTTTTAGTACCTAGCCAAGGTGTGCAGTTCATTTGGATTATTTTGAT
Δcj0045* F2 *rev	AGAATACTCAAGCTTGCATGCCTGCAGGTCGAAATAGAGCTTGAAATTGC
Δcj0169* F1 *fwd	GAGCTCGGTACCCGGGGATCCTCTAGAGTCATAGACTTATATCAAGGCTGG
Δcj0169* F1 *rev	AAGCTGTCAAACATGAGAACCAAGGAGAATATGTTTTCCATGATGATAGC
Δcj0169* F2 *fwd	GAATTGTTTTAGTACCTAGCCAAGGTGTGCTGCTCATATTAACTGGGAA
Δcj0169* F2 *rev	AGAATACTCAAGCTTGCATGCCTGCAGGTCGAATTAGGAGATATGATGTGAA
Δcj0241c* F1 *fwd	GAGCTCGGTACCCGGGGATCCTCTAGAGTCGGCGAAACAGATATAGAAGA
Δcj0241c* F1 *rev	AAGCTGTCAAACATGAGAACCAAGGAGAATCGTTGGTTCATTAAAGAGA
Δcj0241c* F2 *fwd	GAATTGTTTTAGTACCTAGCCAAGGTGTGCACATACAGCCAAAGAAGATT
Δcj0241c* F2 *rev	AGAATACTCAAGCTTGCATGCCTGCAGGTCTGATCAAAATACACACCCT
Δcj0271* F1 *fwd	GAGCTCGGTACCCGGGGATCCTCTAGAGTCAGTTGCATCTTTAAAATCAAC
Δcj0271* F1 *rev	AAGCTGTCAAACATGAGAACCAAGGAGAATACAAGCTTCTGTAGTGCAA
Δcj0271* F2 *fwd	GAATTGTTTTAGTACCTAGCCAAGGTGTGCAACAGGTAAGATTGCTCAA
Δcj0271* F2 *rev	AGAATACTCAAGCTTGCATGCCTGCAGGTCAGCAAACTGTCTTTGAGTG
Δcj0322* F1 *fwd	GAGCTCGGTACCCGGGGATCCTCTAGAGTCCTTGTGAGATAAAACTTGGTAA
Δcj0322* F1 *rev	AAGCTGTCAAACATGAGAACCAAGGAGAATTAAGCATTTGTAGTAATTCCAT
Δcj0322* F2 *fwd	GAATTGTTTTAGTACCTAGCCAAGGTGTGCCGTCAATCATCTGTCTGTT

Δcj0322* F2 *rev	AGAATACTCAAGCTTGCATGCCTGCAGGTCTGTTTAGAATTTAAATCATGATG
Δcj0334* F1 *fwd	GAGCTCGGTACCCGGGGATCCTCTAGAGTCAATATTATCACGACTTGGTTG
Δcj0334* F1 *rev	AAGCTGTCAAACATGAGAACCAAGGAGAATAATCTTGAACAATTTCATTGT
Δcj0334* F2 *fwd	GAATTGTTTTAGTACCTAGCCAAGGTGTGCTGAAGGTATGAAAGCTAACC
Δcj0334* F2 *rev	AGAATACTCAAGCTTGCATGCCTGCAGGTCTAAACCTTTTAGAGGATTGATT
Δcj0400* F1 *fwd	GAGCTCGGTACCCGGGGATCCTCTAGAGTCGGTATTATCAATGGTTTGATAA
Δcj0400* F1 *rev	AAGCTGTCAAACATGAGAACCAAGGAGAATCCACATTTTCTATCAGCAT
Δcj0400* F2 *fwd	GAATTGTTTTAGTACCTAGCCAAGGTGTGCGTGTTTGTGGTGATTGTAATA
Δcj0400* F2 *rev	AGAATACTCAAGCTTGCATGCCTGCAGGTCCTTCGACATTCATTATCATATC
Δcj0542* F1 *fwd	GAGCTCGGTACCCGGGGATCCTCTAGAGTCTTAGGACTTGCTTTTCAGAT
Δcj0542* F1 *rev	AAGCTGTCAAACATGAGAACCAAGGAGAATACAAAAGCAACAATTTCAAC
Δcj0542* F2 *fwd	GAATTGTTTTAGTACCTAGCCAAGGTGTGCAAGCGATACAGTGATTAATG
Δcj0542* F2 *rev	AGAATACTCAAGCTTGCATGCCTGCAGGTCCATTAGAAATTCACGACATC
Δcj0737* F1 *fwd	GAGCTCGGTACCCGGGGATCCTCTAGAGTCTTAAAGATGTAAATATCGATTTG
Δcj0737* F1 *rev	AAGCTGTCAAACATGAGAACCAAGGAGAATAGAGGTATGGATAGTCCCA
Δcj0737* F2 *fwd	GAATTGTTTTAGTACCTAGCCAAGGTGTGCCATCAAATCAATATGTAGGAAT
Δcj0737* F2 *rev	AGAATACTCAAGCTTGCATGCCTGCAGGTCCCTTCATCAATGTAACCAT
Δcj0779* F1 *fwd	GAGCTCGGTACCCGGGGATCCTCTAGAGTCAGGACAAGTTGGACTTTATG
Δcj0779* F1 *rev	AAGCTGTCAAACATGAGAACCAAGGAGAATCTTCTACTGAATTTCCTTTAAGT
Δcj0779* F2 *fwd	GAATTGTTTTAGTACCTAGCCAAGGTGTGCAGTGTTGCAAGTGATTTTG
Δcj0779* F2 *rev	AGAATACTCAAGCTTGCATGCCTGCAGGTCAGTTCCACAAAATCTACAAAC
Δcj1153* F1 *fwd	GAGCTCGGTACCCGGGGATCCTCTAGAGTCACCTTCTAAATGCGGACAAT
Δcj1153* F1 *rev	AAGCTGTCAAACATGAGAACCAAGGAGAATACTACTAATAATTTTTTCAT
Δcj1153* F2 *fwd	GAATTGTTTTAGTACCTAGCCAAGGTGTGCAAAATAATTTCTAAAAAAGG

Δcj1153* F2 *rev	AGAATACTCAAGCTTGCATGCCTGCAGGTCCTTTAAAAAAAGCCATCAAA
Δcj1385* F1 *fwd	GAGCTCGGTACCCGGGGATCCTCTAGAGTCTTGCACAAACTAATGGAAT
Δcj1385* F1 *rev	AAGCTGTCAAACATGAGAACCAAGGAGAATGTTATCAGCTATAATGTTTCCA
Δcj1385* F2 *fwd	GAATTGTTTTAGTACCTAGCCAAGGTGTGCTCTATGGAAGGAGTTGATG
Δcj1385* F2 *rev	AGAATACTCAAGCTTGCATGCCTGCAGGTCAGTTCACACATAGGTAAGTATCC
cj0322 pRRA fwd	ACACCAATTGTTGGCGGTATAGAAAGTT
cj0322 pRRA rev	ACACTCTAGACCTTATTTTGCTTAATGACAC
cj0400 pRRA fwd	ACACCAATTGGATCGTATTGGTGGCTT
cj0400 pRRA rev	ACACTCTAGACAAACATTTATATTTTTACCTTTG
Δcj1534c* F1 *fwd	GAGCTCGGTACCCGGGGATCCTCTAGAGTCTTAACTCCTATTGCACTCATT
Δcj1534c* F1 *rev	AAGCTGTCAAACATGAGAACCAAGGAGAATCATCTGCTTGCATTTGTA
Δcj1534c* F2 *fwd	GAATTGTTTTAGTACCTAGCCAAGGTGTGCTACTACAACAGCTGCTTTTG
Δcj1534c* F2 *rev	AGAATACTCAAGCTTGCATGCCTGCAGGTCTCTTCAAACCCATTTACATT
Δcj1673c* F1 *fwd	GAGCTCGGTACCCGGGGATCCTCTAGAGTCATCAAAGCATTGGTGGTAT
Δcj1673c* F1 *rev	AAGCTGTCAAACATGAGAACCAAGGAGAATTTAGAGTGGTTTTACCTGAAC
Δcj1673c* F2 *fwd	GAATTGTTTTAGTACCTAGCCAAGGTGTGCATTGCAGATGAAATCACAA
Δcj1673c* F2 *rev	AGAATACTCAAGCTTGCATGCCTGCAGGTCCTTGAAAATCTACATTGTTGTT
Kan cassette *fwd*	ATTCTCCTTGGTTCTCATGTTTGACAGCTTAT
Kan cassette *rev*	GCACACCTTGGCTAGGTACTAAAACAATTCAT
Chl cassette *fwd*	ATTCTCCTTGGTTCTCATGTTTGACAGCTTGAATTCCTGCAGCCCGGGGG
Chl cassette *rev*	GCACACCTTGGCTAGGTACTAAAACAATTCACTAGTGGATCCCGGGTACC
Protein expression primers	
Cj1384c* pET21a *fwd NdeI	TATAACATATGTCAGTTTTGGTTATTGGTG

Cj1384c* pET21a *rev XhoI	TATAACTCGAGACCTTTATAGCAAGAAAATTCTT
Cj1384c* pET28a *fwd NdeI	TATAACATATGTCAGTTTTGGTTATTGGTG
Cj1384c* pET28a *rev XhoI	TATAACTCGAGTCTTTAACCTTTATAGCAAGAA
Cj1384c* pBAD *fwd XhoI	ATACTCGAGTCAGTTTTGGTTATTGGTG
Cj1384c* pET21a *rev EcoRI	TATAAGAATTCTTAACCTTTATAGCAAGAAAATT

Table 2.5 Table showing primers used in this study with primer sequence shown in column 2.

2.8.4 Agarose gel electrophoresis

DNA was analysed by agarose gel electrophoresis. Agarose gel (0.8-2% [w/v]) was dissolved in TEA buffer (40 mM Tris-acetate pH 8.0, 1 mM EDTA). Ethidium bromide (0.1 µg ml^{-1}) was added to visualise DNA fragments. DNA samples were mixed with 6X loading buffer (Bioline) and loaded into wells alongside the 1 Kb hyperladder-1 (Bioline) as a size marker. Separation of DNA occurred using a constant voltage of 120 V for 35 minutes in 1X TEA buffer. A Gene Flash gel documentation system (Sygene) was used to view DNA. For extraction of DNA from agarose gels after electrophoresis, DNA bands were excised with a scalpel and extracted using a QIAquick® Gel Extraction Kit (Qiagen).

2.8.5 Restriction digestion of DNA

Digestion of DNA from PCR products and plasmids are carried out using NEB enzymes according to manufacturer's instructions. Typically a reaction lasted 2-4 hours at 37°C using 20-100 units of enzyme. Digested samples were then separated by agarose gel electrophoresis for analysis or purification using a QIAquick® Gel Extraction Kit (Qiagen). To decrease the vector only background during cloning, shrimp alkaline phosphatase (rSAP) (NEB) was used to catalyse the dephosphorylation of 5´ and 3´ ends of digested plasmid DNA. The 5´ phosphoryl termini are required by ligases therefore phosphatase treatment prevents re-circularisation and self-ligation of plasmids. Sodium phosphate treatment was performed following manufacturer's instructions and the enzyme heat inactivated after treatment.

2.8.6 Ligation of DNA

DNA quantification was carried out in a Genova Nano Spectrophotometer (Jenway) and the volumes required for an approximate 3:1 ratio of vector : insert was calculated. Ligation reactions were performed in 20 µl, containing appropriate vector : insert volumes, 1 µ T4 DNA ligase (Thermo), 2 µl of the associated 10X buffer, made up to 20 µl with water. Reactions were incubated at room temperature for 2-3 hours.

2.8.7 Sequencing of DNA

DNA samples were sequenced using an external drop off sequencing service (GATC-Biotech®). Samples were prepared following GATC standard protocol with read lengths typically 0.8-1.2kb.

2.8.7 Isothermal Assembly Cloning

Isothermal Assembly (ISA) cloning, based on the method described by Gibson (2009), was used to generate constructs for *C. jejuni* mutagenesis. This *in vitro* recombination system inactivates the gene of interest by insertion of a resistance cassette into the reading frame by a double homologous cross-over between the resistance cassette and the mutant allele. The HiFi DNA assembly cloning kit (NEB) was used for ISA reactions to improve efficiency of DNA assembly.

For *C. jejuni* knockout mutants, 4 fragments for HiFi DNA assembly were prepared as follows. pGEM3Zf(-) was digested with *Hinc*II and phosphatase treated using rSAP. The desired antibiotic resistance (Ab^R) cassette was PCR amplified using kan-ISA, apr-ISA, cat-ISA primers. 50 bp primers (30 bp adapter plus 20 bp gene of interest) were designed to amplify flanking regions of the gene of interest from *C. jejuni* 11168-H typically removing most of the ORF. The left flanking region termed fragment 1 (F1; beginning of gene of interest plus upstream flanking DNA) and fragment 2 (F2; end of gene of interest plus downstream flanking DNA). The adapter sequences used when amplifying F1 and F2 primers were designed such that the adjacent DNA fragments to be joined share single stranded terminal sequence overlaps. All PCR reactions were performed using Phusion polymerase (Thermo) and purified using QIAquick PCR purification kit (Qiagen). For isothermal assembly of the fragments, the 2 X HiFi master mix (NEB) was combined with 12.5 ng of HincII digested pGEM3ZF, resistance cassette at a 2:1 ratio (insert: vector) and flanking regions at a 4:1. Fragments were incubated at 50°C for 1 hour in a ProFlex thermal-cycler (Applied Biosystems). The resulting DNA was transformed into competent *E. coli* DH5α and selected on solid LB medium containing the appropriate selective antibiotic. Correct constructs were checked by DNA sequencing and then transformed into Wild-type or mutant *C. jejuni* 11168-H strains by electroporation and selected on blood agar with the appropriate resistance. Colonies were screened by PCR to confirm the correct insertion of the cassette into the genome.

2.8.8 Preparation of chemically competent *E. coli*

Escherichia coli cells were made competent by the method of (Hanahan, 1983). *Escherichia coli* was grown in LB broth at 37°C to mid-exponential phase (OD_{600} ~ 0.6). Cells were incubated on ice for 15 minutes and pelleted by centrifugation (6000 x g, 20 minutes, 4°C). The supernatants were discarded and pellets resuspended in 50 ml RF1 solution (100 mM KCl, 50 mM $MnCl_24H_2O$, 30 mM CH_3COOK, 10 mM $CaCl_2{\cdot}2H_2O$, 15 % [w/v] glycerol; adjusted to pH 5.8 with 0.2 M acetic acid). Cells were then incubated on ice for 15 minutes, then centrifuged (6000 x g, 20 minutes, 4°C) and resuspended in 8 ml RF2 solution. solution (10 mM MOPS, 10 mM KCl, 75 mM $CaCl_2{\cdot}2H_2O$, 15% [w/v] glycerol; adjusted to pH 6.8 with 5 M NaOH). Cells were then incubated for a further 15 minutes on ice before being aliquoted in to pre-chilled Eppendorfs and stored at – 80°C.

2.8.9 Transformation of competent *E. coli*

A 100 µl aliquot of chemically competent cells were thawed on ice and 10-20 ng of plasmid DNA was added and mixed gently. Competent cells were incubated on ice for 2 minutes then heat shocked at 42°C for 45 seconds, then placed back on ice for 2 minutes. 1 ml of LB broth was added before cells were incubated at 37°C 200 rpm for 1 hour. Cells were then harvested by centrifugation (5000 x g 5 minutes), resuspended in 200 µl LB broth and plated onto selective LB agar. Cells were grown overnight at 37°C and positive transformants were selected by colony PCR.

2.8.10 Plasmids used in this study

Plasmid	Description	Resistance	Source
pGEM®3Zf(-)	Standard cloning vector used for making mutagenesis constructs. MCS in frame with *lac* operon to allow blue/white colour selection	Amp	Promega
pRRA	*C. jejuni* complementation vector allowing insertion into the *cj0046* pseudogene locus	Apr	(Cameron & Gaynor, 2014)
pET28a(+)	Used for over-expression of proteins with N-terminal His-tag and thrombin cut site under control of IPTG inducible T7 promoter	Kan	Novagen
pET21a(+)	Used for over-expression of proteins with C-terminal His-tag under control of IPTG inducible T7 promoter	Amp	Novagen
pBADHisA	Expression vector to over-express proteins with an N-terminal His-tag through a L-arabinose inducible promotor	Amp	ThermoFisher

Table 2.6 Table showing plasmids used in this study with resistance cassette shown in column 2

2.8.11 Preparation of chemically competent *C. jejuni*

Campylobacter jejuni was grown on blood agar plates overnight, scrapped off and resuspended in 1 ml BTS broth. The cells were pelleted by centrifugation (15,000 x g, 5 minutes, 4°C), resuspended in 1 ml ice cold wash buffer (15% [v/v] glycerol, 9% [w/v] sucrose). This wash step was repeated three times before a final resuspension in 300 µl chilled wash buffer. The cells were then separated into 100 µl aliquots and stored at -80°C.

2.8.12 Transformation of competent *C. jejuni*

100 µl of competent *C. jejuni* was thawed on ice and mixed with 500 ng plasmid DNA, the mixture was then incubated on ice for 20 minutes. The reactions were transferred to pre-chilled electroporation cuvettes (Bio-Rad), electroporated with a pulse of 25 F, 2.5 kV and 200 Ω, giving time constants for 4 – 5 ms in a Gene pulsar chamber (Bio-Rad®) and returned immediately to ice. 100 µl of BTS broth was added to the electroporated cells and the cells were then plates onto a non-selective blood agar and grown overnight. Cells were then harvested into 1 ml BTS broth, centrifuged (14,000 rpm, 5 min, RT), resuspended in 200 µl BTS broth and plated (100 µl) in duplicate onto selective blood agar. Plates were incubated for 2-5 days until individual colonies formed. Positive transformants were re-plated onto selective blood agar and screened by PCR.

2.8.13 Whole cell RNA extraction and purification

Campylobacter jejuni was grown in triplicate in BTS broth culture to an OD_{600} ~ 0.6 under standard conditions unless otherwise stated. RNA was extracted using the TRIzol max bacterial RNA isolation kit (Invitrogen). The only modification was 5 ml of mid-log culture was extracted and treated instead of the recommended 1.5 ml. Purified RNA was treated with DNAse using the Turbo-DNA free kit (Ambion) to remove any DNA contaminates according to the manufacturer's instructions. RNA concentration and purity were assessed using a NanoDrop 2000c spectrophotometer (Thermo). Treated samples were matched to 10 ng μl^{-1} in DEPC treated nuclease free water (Thermo) and stored at -80°C. RNA samples were checked for contaminating DNA by performing a PCR reaction with and without reverse transcriptase.

2.8.14 Real time quantitative reverse transcriptase PCR

Gene-specific primers (see Table 2.5) were designed to amplify a 100-300 bp fragment within the target genes, with the *gyrA* gene being used as a reference. RT-PCR primer specificity was checked by comparison to the *C. jejuni* genome using BLAST (Johnson *et al*., 2008) and confirmed by PCR amplification of a single band. The primers were diluted to 25 µM in nuclease free water prior to use. RT-PCR reactions were carried out using a Sensifast SYBR Lo-Rox one step kit (Bioline, UK) in 20 µl, containing 10 µl Sensifast SYBR 2x buffer, 0.2 µl of each forward and

reverse primer, 0.4 µl RNAse inhibitor, 0.2 µl reverse transcriptase and 2 µl of RNA or DNA template. The reaction mix was made up to 20 µl with nuclease free water (Thermo) and RT-PCR reactions were performed in a MicroAmp® 96-well optical reaction plate (ABI prism). Each RNA reaction was repeated in triplicate and reactions using genomic DNA for the standard curve were replicated in duplicate. PCR amplification was carried out in a Stratagene MX3005p thermal cycler (Agilent) at 45°C for 10 minutes; 95°C for 2 minutes followed by 40 cycles of 95°C for 20 seconds; 55°C for 30 seconds and 72°C for 20 seconds. Transcriptomic data is collected with the associated MxPRO QPCR software (Agilent). A standard curve for each gene was produced using a series of gDNA dilutions. The relative levels of transcript of the target genes were calculated following the protocol for the Standard Curve Method in the *User Bulletin* #2 (*ABI Prism 7700 Sequence Detection System*, Subject: Relative Quantification of Gene Expression) provided by Applied Biosystems. Target gene expression was normalised to *gyrA* expression, which is constitutive and acts as an internal control. No-template reactions were included as negative controls.

2.8.15 Microarray analysis

Campylobacter samples for transcriptomic analysis were grown from an overnight starter culture in 6 well plates to an OD_{600} 0.6. At mid-log growth phase, samples were taken after 0, 10, 30 or 60 minutes of either 405 nm light exposure or dark treatment by harvesting 6 ml from each well. Samples were mixed with a prechilled 1:20 phenol/ethanol [v/v] RNA protection solution. RNA was extracted as described in section 2.8.13 and DNase treated as recommended by the suppliers. RNA (8 µg) from experimental samples was used to prepare Cy5-dUTP (Amersham) labelled cDNA with Superscript III reverse transcriptase (Invitrogen) following manufacturer's instructions. Genomic DNA (2 µg) for Type II microarray analysis was Cy3-dUTP (Amersham) labelled with the Klenow fragment (40 U/µl) (Invitrogen). gDNA and cDNA were mixed and purified using PCR purification kit (Qiagen) as described in 2.8.1 and concentrated by speed vacuum. Hybridisation buffer (100 µl Ocimum Biosolutions) was added to the gDNA/cDNA mix and heated to 95°C for 3 minutes. This mix was hybridised to a *C. jejuni* NCTC 11168 Agilent microarray slide (Agilent Technologies) for 16 hours at 42°C. The slides were washed with (2x SSC + SDS buffer (300 mM NaCl, 30 mM sodium citrate +0.04% SDS), 0.1 X SSC and 0.2 X SSC and dried via centrifugation. Slides were scanned using an Agilent DNA microarray scanner (Agilent). Each condition was performed with at least 3 biological replicates and dye swap experiments were not performed as all genomic DNA was labelled with Cy3-dUTP and all cDNA samples labelled with Cy5-dUTP. The mean values for each channel normalised and $\log_{10}$-transformed per spot, dividing by control channel, per chip to 50th percentile. Normalised values were used to calculate the ratio of each VB light exposed experimental timepoint to its dark control. Data

was processed using Genespring GX 11.5. Genes exhibiting greater than twofold change in abundance at one or more timepoints with a p value of ≤ 0.05 were deemed to be differentially regulated. The Benjamini Hochberg test was used to correct for false positives.

2.8.16 RNAseq

Campylobacter jejuni samples for RNAseq analysis were grown from an overnight starter culture. Cells were harvested by centrifugation and resuspended in 50 ml BTS to an OD_{600} 0.1 and added to 6 well plates (Greiner), 5 ml per well. After growth to mid-log (OD_{600} 0.6) phase, the T0 timepoint was taken and cells were exposed to 405 nm light with samples taken after 15 and 30 minutes light exposure. At each timepoint, 1.5 ml of culture was harvested from each well and centrifuged (12,000 g, 2 min, 4°C). The resulting supernatant was removed, and cell pellets were immediately frozen by submerging in liquid nitrogen for 45 seconds. Frozen cell pellets were stored at -80°C before being sent for sequencing. RNA extraction, purification, library preparation and next generation sequencing was done by Genewiz (Genewiz UK). Data was processed using the Galaxy server (Galaxy UK) by performing quality control on each read to remove bad reads, followed by read trimming to remove Illumina sequencing adaptors. Reads were then mapped to the genome using the Genbank *Campylobacter jejuni NCTC 11168 (ATCC 700819)* reference genome. Read counts per genome feature were calculated and then normalised to calculate the ratio of each VB light exposed experimental timepoint to the T0 timepoint. Genes exhibiting greater than twofold change in abundance at one or more timepoints with a p value of ≤ 0.05 were deemed to be differentially regulated. The Benjamini Hochberg test was used to correct for false positives.

2.9 Preparation of *C. jejuni* cell fractionations

2.9.1 Preparation of cell free extracts

Campylobacter jejuni was grown overnight in three 250ml BTS broth cultures under standard conditions. Cells were harvested by centrifugation (12,000 x g, 5 minutes) and resuspended in 10 mM Tris-HCl pH 7.4, 500 mM NaCl. Cells were lysed either by 4 x 20 s sonication with frequency of 16 amplitude microns using a Soniprep 150 ultrasonic disintegrator (SANYO) or by French press (SIM Aminco). Cell debris was removed by centrifugation (14,000 x g, 10 minutes) and the resulting cell free extract was stored at 4°C prior to use.

2.9.2 Periplasm preparation by osmotic shock

For periplasm preparation, three 250ml mid-log BTS broth cultures were harvested by centrifugation (12,000 x g, 15 minutes, 4°C) and resuspended gently in 2 ml STE buffer (20% sucrose, 20mM Tris pH 8, 1mM EDTA) and incubated at room temperature with gentle shaking for 30 minutes. Cells were centrifuged (12,000 x g, 5 minutes) and the supernatant was removed.

The pellet was then resuspended in 2 ml of ice-cold 10 mM Tris-HCl (pH 8), incubated at 4°C for 2 hours with gentle shaking at 15 r.p.m and centrifuged (12,000 x g, 20 minutes, 4°C). The supernatant was collected and used immediately or stored at -20°C.

2.10 Protein manipulation

2.10.1 Protein concentration determination

Soluble (cell-free) protein concentration was determined using a Bio-Rad Protein Assay Kit (based on the Bradford Assay method, Bradford 1976). For approximate determination of cell free protein concentration, the method was adapted as follows: 0.5-10 µl of protein solution was added to a 1 ml cuvette containing 0.2 ml Bio-Rad Dye Reagent Concentrate with 0.8 ml MiliQ water. The cuvette was mixed by inversion and absorbance was measured at 595 nm. Using the formula: (OD_{595} x 15)/volume of protein (µl), protein concentration (mg ml^{-1}) was calculated.

For more accurate determination of soluble protein from whole cell free extracts, protein concentration was measured by modification of the Lowry method (Markwell *et al.,* 1978). A standard curve of BSA was generated and the protein concentration of whole cells was determined using this reference. 50 µl of cell suspension (diluted to the appropriate range) and BSA standards were added to a 96-well plate, mixed with 150 µl of Solution C formed by 100 parts of Solution A (2% [w/v] sodium carbonate, 0.4% [w/v] sodium hydroxide, 0.16% [w/v] sodium potassium tartrate, 1% [w/v] SDS) mixed with 1 part Solution B (4% [w/v] cupric sulphate) in a 100:1 ratio to give Solution C. After a 1 hour incubation at room temperature with constant shaking, 15 µl of Folin & Ciocalteu's phenol reagent (Sigma-Aldrich) was added. After a further incubation of 45 minutes shaking at room temperature, absorbance was measured at 600 nm using a SpectraMax plate reader (Molecular devices). Protein concentrations were calculated by comparison to a BSA standard curve using the following equation:

$M = Abs280_{nm} – Abs320_{nm} / \varepsilon$

Where:

M – Molar concentration

E – Extinction coefficient

The extinction coefficient for each protein was calculated from the complete amino acid sequence using the ExPasy ProtParam service (http://web.expasy.org/protparam/).

2.10.2 SDS-polyacrylamide gel electrophoresis

SDS-PAGE was performed using the Mini-Protean Tetra system (Bio-Rad), 15% resolving gels were prepared (30% [w/v] acrylamide with 0.8% [w/v] bis-acrylamide was diluted in 1 M Tris-HCl pH 8.8, 10% [w/v] SDS and dH_2O to create a 375 mM Tris-HCl pH 8.8, 0.1% [w/v] SDS, 15% acrylamide mixture). Addition of 0.1% (w/v) ammonium persulphate (APS) and 0.01 % N,N,N',N'-Tetramethylethylenediamine (TEMED) initiated polymerization. The components were mixed by inversion and pipetted into assembled gel casts. 100% Ethanol was added to the top of the mixture to ensure a level spread, this was removed using filter paper before the stacking gel was loaded. Stacking gels (6%) were prepared by dilution of 30% (w/v) acrylamide/0.8% (w/v) bisacrylamide with 1 M Tris-HCl pH 6.8, 10% (w/v) SDS and distilled water to create a 125 mM Tris-HCl pH 6.8, 0.1% (w/v) SDS, 6% acrylamide mixture. Polymerisation was initiated as above. Components were mixed by inversion and the stacking gel was added on top of the resolving gel before the addition of a 10-well comb. The comb was removed from the set gel, which was placed in a gel tank containing 1 x running buffer (25 mM Tris, 0.1 % [w/v] SDS, 250 mM glycine).

Protein samples were prepared by boiling for 2 minutes in an equal volume of sample buffer (60 mM Tris-HCl pH 6.8, 0.005% [w/v] bromophenol blue, 2% [w/v] SDS, 5% [v/v], 10% [w/v] glycerol, β-mercaptoethanol). Samples were loaded into the gel with the prestained EZ-Run protein ladder (Bioline). The samples were separated by electrophoresis initially at 90 V for 10 minutes to allow passage through the stacking gel followed by 180 V until the tracking dye had reached the bottom of the gel. Gels were stained with coomassie brillaint blue (50% [(/v) methanol, 10% [v/v] glacial acetic acid, 0.1% [w/v] coomassie brilliant blue (Sigma-Aldrich)) and de-stained (50% [v/v] methanol, 10% [v/v] glacial acetic acid) until individual bands were visible.

2.10.3 Western blotting

Periplasmic protein samples or cell-free extracts were separated by SDS-PAGE (section 2.10.2) and transferred to a nitrocellulose membrane (Hybond-C Extra, Amersham Biosciences) using a Mini Trans-Blot Electrophoretic Cell (Bio-Rad) according to manufacturer's instructions. The transfer of protein was carried out at a constant voltage of 100 V for 90 minutes at 4°C in ice cold transfer buffer (25 mM Tris, 190 mM glycine, 20% [v/v] methanol). All immuno-detection steps were carried out at room temperature with constant agitation. PBS-T20 buffer (25 mM Tris-HCl pH 7.4, 137 mM NaCl, 2.7 mM KCl, 0.1% Tween 20) was used as both a base for blocking agent (5% dried skimmed-milk powder, incubated overnight) and for washing (15 minutes and 2 x 5 minutes).

2.10.4 Detection of c-type cytochromes by enhanced chemiluminescence (Haem blot)

The protocol was according the paper by Vargas (Vargas., 1993). Samples were electroblotted from the SDS-PAGE gel to a nitrocellulose membrane (see section 2.10.3). Then, the membrane was washed with 1X PBS for 5 minutes at room temperature to remove excess methanol and SDS and transferred into a exposure cassette (Amersham Biotech). Solution A and B of the enhanced chemiluminescence kit (ECL, GE healthcare) was mixed before adding onto the nitrocellulose membrane. The membrane was exposed for different time intervals on a ChemiDoc Gel Imaging System until the signal could easily visualised.

2.12 Assays of specific enzyme activity

2.12.1 Sample preparation

Anaerobic cell free extracts of C*. jejuni* cultures were prepared by pelleting 30 ml of OD_{600} culture (12,000 x g, 10 minutes, 4^{o}C) in a 50 ml falcon tube. The supernatant was then carefully removed and Suba-Seal Septa (Sigma) was applied and the headspace was sparged for 2 minutes with nitrogen. The sparged pellets were resuspended in 1 ml of anaerobic Tris-HCl buffer (100 mM pH 8 made anaerobic by sparging with nitrogen). A 1 ml aliquot of an O_2 scavenging system (10% [w/v] glucose, 5 µg ml^{-1} glucose oxidase (Sigma), 10 µg ml^{-1} catalase (Sigma)) was added to the cell suspension and left for 10 minutes before sonication on ice (10 µm, 3 x 20 s) using a Soniprep 150 MSE. The cell sonicate was pelleted by centrifugation (12,000 x g, 10 minutes, 4^{o}C) and the resulting CFE was transferred to a pre-sparged anaerobic vessel and kept on ice. The protein concentration was determined as described in section 2.10.1.

2.12.2 Pyruvate and 2-oxoglutarate: acceptor oxireducatase enzyme activity

Por and Oor rates were measured by utilising the electrons produced during the conversion of 2-oxoacid to its acyl-CoA derivative to reduce methyl-viologen, resulting in a colour change measured at 585 nm. The assay substrates (100 mM Tris-HCl pH 8, 2 mM $MgCl_2.6H_2O$, 0.2 mM CoA-SH (Sigma), 0.1 mM thiamine pyrophosphate (Sigma), 1 mM methyl-viologen (Sigma)) were spared for 10 minutes in a 1 ml Quartz cuvette (Hellma) before the CFE was added. The reaction mixture was mixed by inversion and a drift rate was taken using a Shimadzu UV-240 dual-wavelength scanning spectrophotometer (Shimadzu). The assay was started by the addition of either 5 mM sodium pyruvate (Sigma) or 2-oxoglutarate (α-ketoglutaric acid, Sigma). The extinction coefficient of methyl-viologen at 585 nm (11.8 M^{-1} cm^{-1}) was used to calculate the specific enzyme activity.

2.12.3 Rate calculation

The following equation was used to calculate the final specific activity (mol min^{-1} mg $protein^{-1}$) of each enzyme:

$$\frac{\text{Absorbance change (abs } min^{-1}) \times 1000}{\text{Extinction coefficient } (M^{-1}\ cm^{-1}) \times \text{CFE Con}^{c} \text{ (mg } ml^{-1}) \times \text{Volume CFE (µl)} \times \text{Cuvette path length (cm)}}$$

2.14 *Campylobacter jejuni* live cell assays

2.14.1 Growth rate experiments

Campylobacter jejuni NCTC 11168 wild type and mutant cells from frozen glycerol stocks were grown on blood agar and harvested to inoculate a 30 ml starter culture. The overnight starter broth culture was used to inoculate Brucella Tryptone Serine (BTS) medium to an OD_{600} 0.1, with readings taken every hour for 12 hours with a final reading at 24 hours. All optical density readings were measured using a Jenway® 6705 UV spectrophotometer with each growth curve done in triplicate.

2.14.2 Light exposure viability assays

High intensity 405 nm light was produced by a Thorlabs' M405L3 mounted fiber-coupled LED with a nominal wavelength of 405 nm and a bandwidth of ~20 nm at full half width maximum. Power density (J cm^{-2}) was measured using a Thorlabs 5310C thermal power sensor 200 mm away from the light source at the position the sample cuvette is mounted. Light sensitivity experiments were carried out on mid-log bacterial broth culture resuspended in sodium phosphate buffer to an OD_{600} of 0.1. A 300 µl volume of bacterial suspension was pipetted into a 1 ml cuvette (Sarstedt) and exposed to 405 nm light at varying intensities for 30 minutes. Viability was calculated by counting the number of colony forming units (C.F.U) after appropriate dilution on Campylobacter blood free selective agar plates (CCDA), counting their number per ml. The survival rate was calculated according to the equation N/N0 = survival fraction, where N0 is the C.F.U at zero illumination and N1 is the C.F.U following illumination.

2.14.3 Detecting reactive oxygen species

2',7'-Dichlorodihydrofluorescin diacetate (Sigma) was used to detect the production of ROS. The non-polar dye, DCFH-DA is taken up and converted into the polar derivative DCFH by cellular esterases. DCFH is non fluorescent but is switched to highly fluorescent DCF upon oxidation by intracellular ROS such as hydrogen peroxide, hydroxyl, and peroxyl radicals. A stock solution of 2 mM (w/v) DCFH-DA in 1% DMSO was prepared and kept on ice. Mid log cells resuspended in

NaPhos buffer to an OD 0.1 were mixed with 10 µM (final concentration) DCFH-DA and illuminated for varied time periods. After illumination, cells were analysed using a Varian carry eclipse spectrophotometer (Varian) exciting at 485 nm and measuring emission at 530 nm.

2.14.4 Disc diffusion assays

Campylobacter jejuni cells were grown to mid-log OD_{600} 0.6 in BTS broth. Cells were harvested by centrifugation and used to inoculate cooled Muller Hinton agar (Sigma) with added 20 mM Serine to an OD_{600} ~ 0.1. The inoculated Muller Hinton agar was poured into 90 mm single vented petri dishes (Thermo) and left to partially set before a 6 mm antibiotic assay sterile disc (Whatman) was added to the center of the plate. When set, 10 µl of either 1 M H_2O_2 or 10 mM PBS control was added to the center of the disc. Plates were then inverted and incubated for 2-3 days before the exclusion zone around the disc was measured.

2.15 Chromophore biochemical analysis

2.15.1 Differential cytochrome *c* spectroscopy

To determine the *c*-type cytochrome content in the periplasm, dithionite-reduced *minus* air oxidised difference spectroscopy was performed. The concentration of periplasmic extract was 1 mg ml^{-1} in a 1 ml volume per quartz cuvette. For analysis of oxidised *c*-type cytochromes absorbance spectra, purified cytochrome extract was treated with 10 mM hydrogen peroxide or 10 mM sodium hypochlorite for 5 minutes at room temperature before spectroscopy was performed. Spectra were measured using a Shimadzu UV-2401 dual wavelength scanning spectrophotometer (Shimadzu) at room temperature. Reduced minus oxidised scans were carried out from 400 to 700 nm after the addition of sodium dithionite.

2.15.2 Differential whole cell spectroscopy

Strains were grown to mid-log growth phase before harvesting by centrifugation (12,000 x g, 5 minutes). Cells were resuspended in sodium phosphate buffer (20 mM pH 7.2) to an OD_{600} 0.1. Absorbance spectra was read using Olis CLARiTY UV/Vis spectrophotometer which uses an integrating cavity for measurements of turbid samples. Difference spectra was obtained by subtracting the sodium ascorbate oxidized (10 mM) from the dithionite reduced (10 mM) absorbance spectra.

2.15.3 Pigment analysis by High performance liquid chromatography (HPLC)

The method for extraction and analysis of porphyrin species from bacteria developed by Fyrestam *et al* (Fyrestam *et al*., 2015) was adapted for this study. After cell cultures were harvested by centrifugation, cell pellets were resuspended in Tris/EDTA buffer (5 mM Tris-HCl, 10 mM EDTA, pH 7.2) for 1 h in the dark. Formic acid was added at equal volume to precipitate

proteins and lower pH. Cells were lysed by 3 x 20 seconds sonication in a with frequency of 16 amplitude microns using a Soniprep 150 ultrasonic disintegrator (SANYO) and centrifuged at 2500 g to pellet bacterial debris. The supernatant containing the porphyrins was loaded onto a pre-conditioned C18 SPE cartridge, washed with ammonium acetate, and eluted with acetone:formic acid 9:1(v/v). Samples were loaded on to an Agilent-1200 series HPLC system in conjunction with a Nova-Pak C18 reverse phase column (4 mm particle size, 3.9 mm 3 150 mm; Waters, USA).

2.16 Orthogonal organic phase separation (OOPS)

Campylobacter jejuni cells were grown in a chemostat culture for 5 rounds of replication as described in Section 2.6.2. Once at a steady state, 15 ml of culture was extracted and mixed with 15 ml of NaPhos Buffer pH 7.2, 42°C and immediately cross linked at 254 nm (CL-1000 Ultraviolet Crosslinker, UVP) for a dose of 525 J cm^{-2} in a 50 ml square plate. An additional 5 ml of steady state culture was spun down at 15,000 g, 5 minutes and RNA was extracted for qRT-PCR analysis as described in section 2.8.13. Once crosslinked, cells were pelleted by centrifugation (5 minutes at 15,000 g) and resuspended in 100 µl Trizol® before 500 µl of 0.5 mm glass beads (Sigma) were added to each sample. Cells were then lysed by mechanical lysis using a Mini-Beadbeater (Biospec) for 3 x 30 seconds treatment, resting on ice between treatments. Following lysis, 1 ml of Trizol® was added to each tube before samples were homogenised vertexing. Supernatants were transferred to a fresh Eppendorf (avoiding glass bead uptake) and centrifuged for 6,000 g, 5 minutes 4°C. The supernatant was then transferred to a new tube leaving the unlysed cells as a pellet. For phase separation, 200 µl of chloroform (Fisher) was added before each sample was vortexed and separated by centrifugation for 15 minutes at 12,000 g at 4°C. After separation, the upper aqueous phase containing non-cross linked RNA was transferred to a new Eppendorf and RNA was precipitated by phenol/chloroform extraction. The lower organic phase containing non-cross linked proteins was removed leaving an interphase containing protein-RNA adducts. This phase separation was repeated a further 2 times before the RNA-protein adducts were precipitated by the addition of nine volumes of methanol and pelleted by centrifugation at 14,000 g for 10 minutes.

For RNA analysis, precipitated interfaces were incubated with 300 µl of proteinase K buffer (30 mM Tris-HCl (pH 8), 10 mM EDTA) and 30 µl proteinase K (Sigma) for 2 hours at 50°C. Samples were cooled and released RNA was purified using phenol/chloroform phase separation. For RNA binding protein analysis, the precipitated interphase was resuspended in 100 mM triethylammonium bicarbonate (TEAB), 1 % SDS, 1 mM $MgCl_2$ for 20 minutes at 95°C. Samples were disrupted by ultrasonication (Biorupter®) for 15 minutes to solubilise the interphase.

Solubilised interphases were then cooled and digested with 2 µg RNase A (Thermo Fisher) for 3 hours at 37^{o}C. Another 2µg of RNase mix was added and incubated overnight at 37^{o}C. Once RNA has been digested, released proteins were recovered by a final round of phase separation, with the organic phase collected and precipitated using methanol precipitation.

Chapter 3: Appleby *et al*.

Cu(I) diimine complexes as antibacterial photosensitisers operating in water under visible light

Martin V. Appleby**, Peter Walker**, Dylan Pritchard, Sandra van Meurs, Carly M. Booth, Michael D. Ward, David Kelly, Julia A. Weinstein

Preface

In collaboration with Prof Julia Weinstein from the University of Sheffield Department of Chemistry, we tested the antimicrobial properties of novel photosensitisers against a variety of bacterial pathogens. By binding metal-based photosensitisers to the surface of silica nanoparticles, we aimed to use these immobilised photosensitisers as a water treatment method to kill bacterial pathogens using visible light. The Copper photosensitiser complex (complex 1) was selected for use as a water treatment agent as it displays high ROS production upon photoexcitation and is more photostable than other previously characterised photosensitisers. We found that the silica bound complex 1 was effective in killing both *E. coli* MG1655 and *S. aureus* SH1000 after exposure to 405 nm light with killing efficiencies comparable to the 'gold standard' photosensitiser methylene blue (MB). The optimum photosensitiser concentration and photoexcitation period was also determined for the complex 1 bound silica photosensitiser. This study highlights the potential of silica bound photosensitisers as a novel water sanitation agent which could potentially be utilised as a household water treatment system in developing countries which lack the infrastructure to provide safe drinking water.

Authors contributions

The synthesis and binding of the complex 1 to silica was carried out by Martin Appleby and Julia Weinstein with minor contributions from other authors. The experiments which determined the phototoxicity of the free and immobilised complex 1 was designed and conducted by Peter Walker and supervised by David Kelly. All microbiology was performed solely by Peter Walker using photosensitiser complexes synthesised by Martin Appleby.

The manuscript was written by Martin Appleby, Peter Walker, David Kelly and Julia Weinstein. Figures 1-2 and supporting information 1-6 were produced by Martin Appleby, Dylan Pritchard, Sandra van Meurs, Carly M. Booth, Michael D. Ward and Julia A. Weinstein. Figures 3-5 were produced by Peter Walker. The manuscript has been published in Materials Advances Chemistry in November 2020.

Materials Advances

ROYAL SOCIETY OF CHEMISTRY

PAPER

View Article Online
View Journal | View Issue

Cite this: *Mater. Adv.*, 2020, **1**, 3417

Cu(I) diimine complexes as immobilised antibacterial photosensitisers operating in water under visible light†

Martin V. Appleby,[a] Peter G. Walker,[b] Dylan Pritchard,[a] Sandra van Meurs,[a] Carly M. Booth,[a] Craig Robertson,[a] Michael D. Ward,[c] David J. Kelly*[b] and Julia A. Weinstein*[a]

A complex of an Earth-abundant metal, copper, immobilised on silica offers a remarkably efficient way to kill bacteria in water under visible light, the first example of lighter transition metal complexes to do so. Photosensitisers which produce reactive oxygen species under light are emerging as an efficient way to kill microorganisms in water, yet the majority of photosensitising metal complexes are based on rare transition metals. Moreover, the efficiency of most solution-based photosensitisers is greatly compromised upon immobilisation on solid support, which is essential for safe treatment. Photosensitisers based on inexpensive metal complexes, such as those of Cu, Ni or Fe, usually have too short excited state lifetime to react efficiently with oxygen and are ineffective in production of reactive oxygen species. Here, we demonstrate that complexes of Cu(I) can be used as efficient photosensitisers for killing bacteria in water under visible light, when immobilised on surfaces, using as an example of [Cu(I)(xantphos)(dmp)]tfpb (**1**) [xantphos = 4,5-bis(diphenylphosphino)-9,9-dimethyl-xanthine, dmp = 2,9-dimethyl-1,10-phenanthroline, and tfpb = tetrakis(3,5-bis-(trifluoromethyl)-phenyl)borate] immobilised on silica, **1**-silica. In contrast to many short-lived Cu(I) complexes, a sterically-hindered coordination centre in **1** leads to a relatively long excited state lifetime of >200 ns, which enables **1** to efficiently photosensitise singlet oxygen (29%). Upon irradiation, **1**-silica (55 μM) shows high antibacterial activity against both a Gram-negative bacterium *E. coli*, and a Gram-positive bacterium *Staphylococcus aureus* (*S. aureus*, the Methicillin Resistant strain MRSA 315), both of which commonly occur in water. 99.99% killing of *S. aureus* was observed after only 15 min of irradiation with 17.5 mW cm^{-2} light, with 99.9999% ('complete') killing achieved after 2 h. For *E. coli*, 99.99% killing was achieved after 2 h, and 99.9999% after 3 h of irradiation. Thus **1**-silica exceeds the ≥99.99% threshold set by WHO for the "highly protective" antibacterial agents. This first example of an immobilised Cu(I) complex used for light-driven bacterial killing demonstrates the potential of Earth-abundant transition metal complexes as low-cost efficient photo-antibacterial agents.

Received 28th August 2020,
Accepted 12th November 2020

DOI: 10.1039/d0ma00642d

rsc.li/materials-advances

Introduction

Clean water, sanitation and water scarcity are major issues worldwide, as highlighted in the UN Sustainable Development Goal 6.[1] According to the UN, 1.8 billion people (25% of the global population) do not have access to a clean water source free from contamination.[2] The situation could be much improved with proper water sanitation, however many regions where these problems occur lack access to proper water management systems and infrastructure. Developing point-of-use solutions/household water treatments to purify water on a local scale is one potential way of dealing with this problem.[3,4] However, many current solutions are either very inefficient, or require large amounts of power.[3–5]

There is a clear and urgent need to develop efficient, scalable, and ideally inexpensive antibacterial agents for water treatment. Utilizing sunlight for water purification could provide a cheap and clean way of providing water disinfection.

So far, this has been achieved *via* solar disinfection,[6–8] which uses high energy UV light, that is absorbed by pathogens themselves including bacteria. Inspired by the ground-breaking developments in photodynamic therapy (PDT) of cancer,[9] researchers are turning to development of photosensitisers,

[a] *Department of Chemistry, University of Sheffield, Sheffield S3 7HF, UK. E-mail: Julia.Weinstein@sheffield.ac.uk*
[b] *Department of Molecular Biology and Biotechnology, University of Sheffield, UK. E-mail: D.Kelly@sheffield.ac.uk*
[c] *Department of Chemistry, University of Warwick, Coventry CV4 7AL, UK*

† Electronic supplementary information (ESI) available. See DOI: 10.1039/d0ma00642d

compounds that absorb light that bacteria do not absorb themselves, for use as antibacterial agents.[10] Photosensitisers are ideally non-toxic to living organisms without light, but become toxic upon irradiation with light of an appropriate wavelength which promotes the photosensitiser into its excited state, PS*. One of the most common mechanisms of toxicity involves PS* reacting with dissolved oxygen, leading to production of reactive oxygen species (ROS). The two most damaging ROS are considered singlet oxygen ($^1O_2$) and the hydroxyl radical anion, as bacterial resistance to other ROS often occurs.[11]

The key requirements for a photosensitiser are efficient absorption of visible light, photostability, and an excited state with a sufficiently long lifetime to interact with oxygen dissolved in water by means of a bimolecular reaction; hundreds of nanoseconds is the lower limit of the excited state lifetimes needed to be practically relevant (see ESI† for estimation of lifetimes based on Stern–Volmer equation). Transition metal complexes with diimine ligands have been proven as excellent photosensitisers in applications such as anti-cancer PDT, as they possess a long-lived metal-to-ligand charge transfer (MLCT) excited state with triplet multiplicity. This triplet MLCT state is populated, usually with high efficiency, from the initially formed singlet excited state due to strong spin–orbit coupling of the central atom that promotes intersystem crossing.

Currently-used photosensitisers include organic compounds[9,10] (which usually possess nanosecond excited-state lifetimes), porphyrins, and complexes of the 2nd and 3rd row transition metals (including Ir, Ru, Pt, Pd and Os)[12–23] which are either rare, expensive, or both. More accessible alternatives are therefore beginning to be developed as photosensitisers.[24–30] Metal ions such as Ag^+,[31,32] metal oxides such as ZnO,[33] and complexes based on various metal ions including Cu(I),[34] have shown to be toxic to bacteria without light;[31,32,34] whilst inherently phototoxic metal nanoparticles have been used together with photosensitisers to promote the photoactivated production of ROS to initiate bacterial killing.[33,35] Other well-known photosensitisers include porphyrins,[36,37] such as derivatives of Zn(II) porphyrazine, or 5,10,15,20-tetrakis(1-methylpyridinium-4-yl)porphyrin tetra-iodide (tetra-Py^+-Me), which have also been used for water treatment with good results: for example, tetra-Py^+-Me at 10 μM achieved a reduction of 99.999% of *E. coli* after 120 min of irradiation with artificial white light (380–700 nm).

It is important to immobilise the photosensitiser on a support as this would eliminate the need to remove the sensitiser from water post-irradiation, but the immobilisation should not compromise the photosensitisation of ROS.[38,39] Several organic photosensitisers, including BODIPY-derivatives immobilised on Nylon or polyacrylonitrile nanofibers,[40] porphyrin derivatives immobilised on polyethylene elastomer or nanofibrillated cellulose (NFC) have shown efficient killing of bacteria, viruses, and other pathogens, often with 6 $\log_{10}$ efficiency, primarily on surfaces.[41,42] A summary of the currently available immobilised photosensitisers is given in Table S9 in the ESI,† with the most relevant ones being used for comparison in the discussion section below.

Most of the transition metal photosensitisers reported to date for water purification are, however, only active in solution. To develop them towards practical systems requires a 1st row transition metal complex that generates ROS efficiently under visible light, is photostable, not soluble in water, and can be immobilised on a solid support.

The class of compounds which is particularly promising in this regard are tetracoordinate Cu(I) diimine complexes, which absorb well in the UV/visible region due to an MLCT transition, and are potentially easy to modify at the periphery of the ligands, either to tune the energy of the absorption band or to attach functional groups which allow immobilisation onto a surface. However, Cu(I) diimine complexes often have excited state lifetimes that are too short to be of practical value for photosensitisation of ROS, often due to geometric distortion of a pseudo-tetrahedral ground-state geometry to a pseudo square-planar one in the MLCT excited state:[43–48] this distortion creates a vacant coordination site[43,44] for interaction with a solvent molecule (exciplex formation) which quenches the excited state,[44] the process which has recently been observed directly by ultrafast spectroscopic methods.[47,48] To ''lock'' the molecule in its tetrahedral ground-state geometry and prevent its geometry changing in the excited state, and thereby achieve long-lived excited states in Cu(I) complexes, sterically hindering ligands are required whose interlocking stops the angle between the two ligand planes from changing in the excited state.[49]

This approach was first demonstrated in 1980: the sterically-hindering ligand 2,9-dimethyl-1,10-phenanthroline (dmp) yields the complex $[Cu(dmp)_2]^+$ with an excited-state lifetime of 85 ns in deoxygenated DCM.[44] There are now many examples of longer-lived excited states in Cu(I) complexes of various composition.[30,45,49–55] Recent studies have shown that Cu(I) complexes containing one diimine ligand, and one diphosphine ligand such as 4,5-bis(diphenylphosphino)-9,9-dimethyl-xanthine (xantphos), which has a large bite angle and high steric hindrance, can have even longer excited state lifetimes (ns–μs).[56–60] Cu(I) complexes are being increasingly used as photosensitisers in photocatalysis,[24,25,30,51,61–73] and dyes-sensitised solar cells.[74] They are also used as antitumor[75–78] and antibacterial agents[79–85] due to their innate dark toxicity. However, utilisation of their photosensitisation properties for PDT or antimicrobial PDT has been overlooked so far.

Here, we overturn the perception that only complexes of rare transition metals can be good photosensitisers, and that they do not work well when immobilised on a surface. We present the first example of a Cu(I) complex used as photosensitiser for antibacterial action in water, immobilised on silica support. We demonstrate the high light-induced antibacterial activity of the well-known complex [Cu(I)(xantphos)(dmp)]tfpb (**1**) [tfpb = tetrakis(3,5-bis(trifluoromethyl)phenyl)borate][51,59,66,70,72] which has been previously examined as an oxygen sensor.[59] The antibacterial action of **1** was tested on a Gram-negative bacterium, *Escherichia coli* (*E. coli*, strain MG1655),[5,86,87] and a Gram-positive bacterium *Staphylococcus aureus* (*S. aureus*, the Methicillin Resistant strain MRSA 315), both of which commonly occur in water. We determine the yield of photosensitised $^1O_2$ generation by **1**, and demonstrate $>99.9999\%$ ($>6\log_{10}$) killing of both *S. aureus*

and *E. coli* in presence of the complex **1** immobilised on silica particles, upon irradiation with blue light. To be classified as protective against bacteria according to WHO, an agent is required to achieve a $\geq 2 \log_{10}$ killing, and to be highly protective $\geq 4 \log_{10}$ is required, and this system comfortably exceeds both thresholds.[87]

Results and discussion

Complex **1** as its BF_4^- salt was synthesised following the known procedure, although the reaction was scaled up from 100 mg of product[59] to 2.81 g. $[Cu(CH_3CN)_4]BF_4$ was reacted with xantphos in DCM to form a solution of $[Cu(xantphos)(CH_3CN)_2]BF_4$.

This was followed by an addition of a solution of dmp in DCM, to yield $[Cu(xantphos)(dmp)]BF_4$ as a yellow solid. The salt $[Cu(xantphos)(dmp)]BF_4$ was re-dissolved in methanol, and a solution of Na(tfpb) in methanol solution added to yield complex **1** as a yellow solid, Fig. 1. The $tfpb^-$ counterion was chosen as it has been previously shown that the complex **1**, with $tfpb^-$ as counterion, has a longer excited state lifetime in the solid state than does $[Cu(xantphos)(dmp)]BF_4$.[59] Neither salt is water-soluble, which is important to prevent the leaching of the compound from the solid support into water. Complex **1** was characterised by UV/Vis absorption spectroscopy, steady-state and time-resolved emission spectroscopy, high-resolution mass-spectrometry, and multinuclear NMR spectroscopy. The analytical data agree with those published previously.[51,59,66,70,72]

The properties of complex **1** are summarised in Table S1 in the ESI;† the absorption and emission spectra in acetonitrile solution, in the solid state, and when immobilised on silica, are shown in Fig. 2. The absorption maximum of **1** in acetonitrile is 378 nm, with a tail into the visible region; the emission maximum from the ^{3}MLCT excited state occurs at *ca.* 550 nm. The excited state lifetime increases from 64 ns in aerated acetonitrile solution to 220 ns in deoxygenated solution. Assuming the concentration of dissolved of oxygen in acetonitrile to be 2.42 mM,[88] the quenching constant of the excited state by oxygen, k_q, was estimated as $4.6(5) \times 10^9$ M^{-1} s^{-1}.

The quantum yield of singlet oxygen production, $\phi_{^1O_2}$, by complex **1** in acetonitrile solution was measured directly, under excitation with a 355 nm (8 ns pulses) laser, by detecting the emission from photo-generated singlet oxygen at 1270 nm. The $\phi_{^1O_2}$ value determined relative to a standard, perinaphthenone ($\phi_{^1O_2} = 100\%$)[89] was 0.29 (±0.07), see Fig. S11 and S12 (ESI†). The relatively high quantum yield for singlet oxygen production explains the previously reported use of this compound as an oxygen sensor.[59]

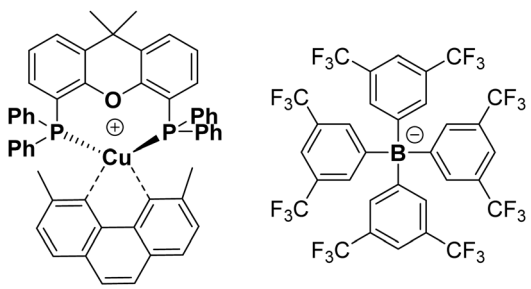

Fig. 1 Chemical structure of complex **1** with counterion $tfpb^-$. Structure of complex **1** obtained by single crystal X-ray crystallography, which is fully consistent with that published previously, is given in the ESI,† Fig. S8. CCDC 2012235.

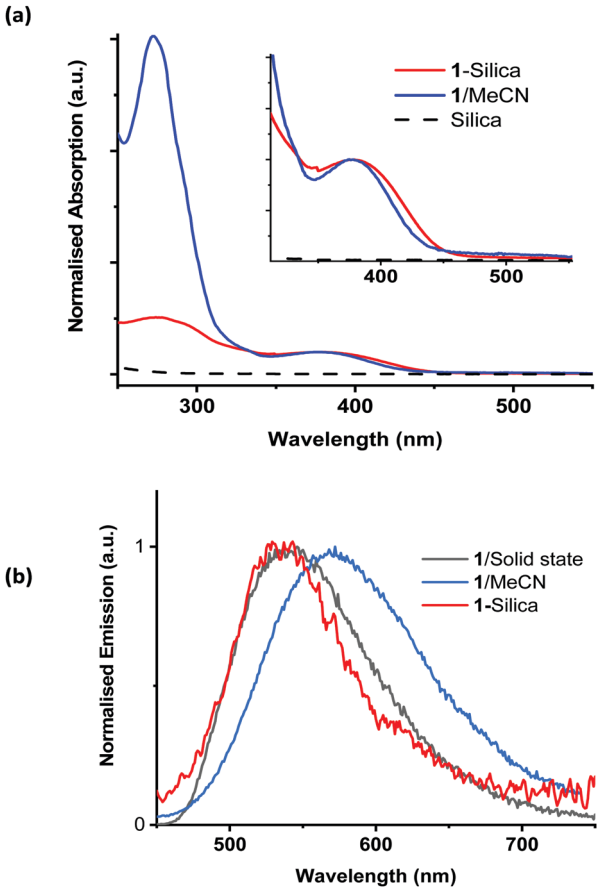

Fig. 2 (a) Normalised (to OD at 380 nm) absorption spectra of **1** in MeCN and diffuse reflectance spectra of pure silica and **1**-silica (55 μM); and (b) emission spectra of **1** in MeCN solution, in the solid state, and of **1**-silica, excitation wavelength 400 nm. The MLCT absorption band of **1**-silica is somewhat broader than that of **1** in solution, as is typical for solid-state spectra. A small shift to higher energies in the emission spectra of **1** in solid state and on silica *vs.* that in solution is observed, indicating emission from a relaxed configuration in solution.

To avoid contaminating the water with the photosensitiser, it is beneficial to immobilise it on a solid support. The chosen support for these experiments was chromatography grade silica (40–63 μm, VWR chemicals), due to its high stability, ready availability, and low cost. The silica used had an average pore size of 60 Å and a surface area of 400 m^2 g^{-1}. Complex **1** was immobilised on silica (**1**-silica) by drying a concentrated solution of **1** in DCM onto the silica by slow rotary evaporation. For **1**, 1 mg ml^{-1} corresponds to 583 μM. For **1**-silica, prepared as described above, 1 mg ml^{-1} is equivalent to 11 μM of complex **1** (see Experimental part for detail). The size of the $[Cu(xantphos)(dmp)]^+$ ion estimated from X-ray crystallographic data, Fig. S8 (ESI†), is smaller than the pore size of the silica,

therefore some of the complex may have loaded inside the pores. The diffuse reflectance spectra, emission spectra, and emission excitation spectra all confirmed that the complex has been immobilised on the silica support (Fig. 2).

The presence of the photosensitiser on the silica substrate was also confirmed by solid state NMR spectroscopy, using the nuclei ^{13}C and ^{31}P (for the complex ion); ^{11}B, ^{13}C and ^{19}F (for the anion); and ^{29}Si (for the solid support). The spectra are shown in ESI,† Fig. S3–S7.

Comparative magic angle spinning (MAS) solid state NMR spectra were performed on complex **1**, on silica gel without complex **1**, and on **1**-silica. In each of the high-abundance, high-sensitivity nuclei (^{11}B, ^{19}F and ^{31}P) the signals were clearly retained from complex **1** to the **1**-silica, even if slight shifts in position were observed on adsorption on the solid support and fine structure was lost. This was especially the case for the ^{31}P spectra where the signal for complex **1** shows coupling to two NMR active Cu nuclei (^{63}Cu and ^{65}Cu),[90] but when adsorbed on the silica support the signal is broadened to a wide envelope at the same chemical shift, giving confidence that the complex has been adsorbed. The reason for this broadening will partly be loss of crystallinity (tendency towards amorphous structure and associated shorter relaxation time) and partly due to signal-to-noise considerations, as the loading of complex **1** on the solid support is only 10 mg per 500 mg silica.

The same behaviour was observed for the low-abundance, low sensitivity nucleus ^{13}C: a highly resolved ^{13}C NMR spectrum for **1** in the solid state was changed to a severely broadened spectrum with comparable chemical shifts for **1**-silica.

Direct determination of $^1O_2$ production from **1**-silica by measuring $^1O_2$ emission at 1270 nm was not possible due to laser scattering from the silica particles. Instead, an indirect method that relies on the sensor Singlet Oxygen Sensor Green (SOSG, Invitrogen/Molecular Probes) was used: this sensor molecule is not emissive in solution, however, upon reaction with $^1O_2$, a brightly emissive product is formed.[91] The emission intensity of the sensor increased as the irradiation time of the suspension increased (Fig. S9 and S10, ESI†). The suspension was irradiated with a 405 nm diode with irradiance 10 mW cm^{-2} with the total radiant exposure equal to 6 J cm^{-2} after 600 s (Fig. 3). Whilst it is not possible to determine the $\phi_{^1O_2}$ from **1**-silica as the exact amount of the PS interacting with light cannot be determined accurately, the steady increase in probe emission intensity with irradiation time in the presence of a photosensitiser is significantly larger than upon irradiating the probe alone (Fig. 3). This observation confirms that adsorbed complex **1**-silica produces $^1O_2$ on light irradiation. A control experiment where SOSG was activated by a known $^1O_2$ photosensitiser, $[Ru(bpy)_3]Cl_2$ ($\phi_{^1O_2}$ in aerated water 0.41)[92] also confirms this conclusion.

S. aureus cultures were grown to mid-log growth phase before exposure to 405 nm light in 12-well plates with continuous shaking. For each experiment, bacterial viability reduction was compared against *S. aureus* cultures exposed without added photosensitiser as well as cultures treated with the well-characterised photosensitiser methylene blue (MB). No toxicity of the light alone for the *S. aureus* was observed, Fig. 4. A reduction from 10^{10} to 10^5 CFU ml^{-1} in presence of 50 μM of methylene blue was observed. Addition of 1 mg ml^{-1} (583 μM) of **1** (suspension) causes a 10-fold reduction of CFU in the dark or after irradiation with 405 nm light for 2 hours; thus small dark toxicity and no light toxicity at this concentration of **1** are observed. Increasing the concentration of **1** from 583 μM to 2917 μM causes significant dark toxicity, but no additional light toxicity, Fig. S13 (ESI†). It is clear that **1** alone displays some dark toxicity only at very large concentrations, but is not acting as a photosensitiser against *S. aureus* under any conditions studied.

In contrast to the free compound **1**, immobilised **1**-silica at 1 mg ml^{-1} or 5 mg ml^{-1} shows no dark toxicity towards *S. aureus*, Fig. 4. The lack of dark toxicity when the complex is immobilised

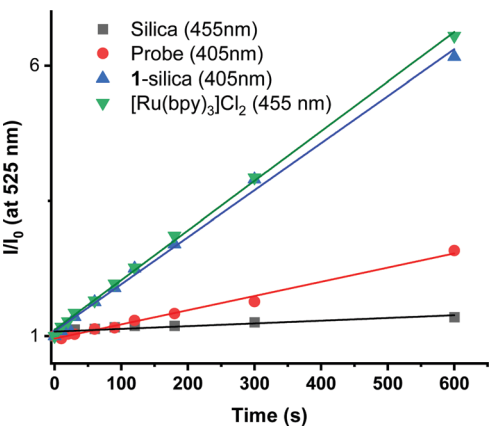

Fig. 3 Relative emission intensity of SOSG probe (λ_{max} = 525 nm) in water as a function of irradiation time. Probe (1 nM, -square-), $[Ru(bpy)_3]Cl_2$ in solution (1.56 μM, -upside down triangle-); silica suspension (5 mg ml^{-1}, -circle-); **1**-silica suspension (5 mg ml^{-1}, 55 μM, -triangle-).

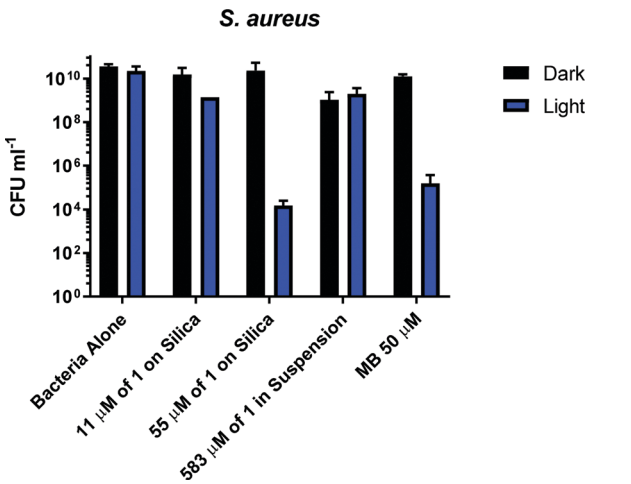

Fig. 4 Bacterial viability assay measuring the colony forming units of *S. aureus* on its own and in the presence of **1**-silica: 1 mg ml^{-1} (equivalent to 11 μM of complex **1**) and 5 mg ml^{-1} (equivalent to 55 μM of complex **1**), 5 mg ml^{-1} of complex **1** in suspension (583 μM) and methylene blue (MB) (50 μM). Assay without irradiation for 2 hours (black bars) and after irradiation for 2 hours with 405 nm light at 17.5 mW cm^{-2}, total dose 126 J cm^{-2} (blue bars).

on silica may be attributed to the much lower overall amount of the Cu-complex present. This also suggests that any leaching from the complex would have minimal effect on bacteria due to the highest loading (55 μM **1**-silica) being only 1% of the concentration of **1** in suspension (583 μM) required to achieve $\sim 1\log_{10}$ of killing, Fig. 4. Exposure of *S. aureus* to 405 nm light for 2 h in presence of **1**-silica at 1 mg ml^{-1} leads to a 100-fold reduction in CFU, and to $6\log_{10}$ reduction in presence of 5 mg ml^{-1} of **1**-silica.

In order to identify the amount of **1**-silica required for optimal bacterial killing, experiments were conducted at different concentrations, from zero to 40 mg ml^{-1}. All samples had a starting CFU value of 10^6–10^7 and were irradiated with a 405 nm diode at 17.5 mW cm^{-2} for 30 min, Fig. 5. Fig. 5b shows that maximum killing of *S. aureus* is achieved using 5 mg ml^{-1} of **1**-silica, and that any further increase in the amount of photosensitiser does not have an effect [note that 1 mg ml^{-1} was not causing any killing even at longer exposure times, Fig. 4]. In contrast, only a small reduction in CFU, up to a factor of 10, was observed for the Gram-negative *E. coli* at high concentrations of **1**-silica after irradiation for 30 min, Fig. 5a. *E. coli* killing was be achieved at longer exposure times using 5 mg ml^{-1} of **1**-silica (Fig. 6a). It has been reported previously that Gram-negative bacteria with an outer lipid/protein membrane are less susceptible to killing using exogenous photosensitisers such as **1**-silica, as the outer membrane presents an additional barrier to protect the cell against extracellular generated ROS.[93]

In order to determine the time required to achieve complete killing of both bacterial strains at the $6\log_{10}$ level, time-dependent measurements were performed (Fig. 6). The coloured bars in Fig. 6a show that *E. coli* killing ($4\log_{10}$ reduction) was observed after 2 h of irradiation with 405 nm light, and $5\log_{10}$ reduction was achieved after 3 h of 405 nm irradiation.

No dark toxicity of **1**-silica towards *E. coli* was observed after 1 h, with a 100-fold reduction in CFU after 3 hours. This result suggests that the killing of *E. coli* is due to a light-activated process. Killing of *S. aureus* was observed after only 15 min of exposure to 405 nm light, with a $4\log_{10}$ reduction in CFU, Fig. 6b. Irradiation for 120 min led to reduction of *S. aureus* CFU to 10^2, the detection limit of the experiment, corresponding to a $6\log_{10}$ reduction of *S. aureus*. The dark toxicity of **1**-silica towards *S. aureus* was a 100-fold reduction in CFU after 30 min, a value which remained unchanged after 120 min. Thus, killing of *S. aureus* is also due to a light-activated process.

Finally, to establish the toxicity of light alone, killing of the bacteria when irradiated with 405 nm light in the presence and in the absence of the photosensitiser are compared in Fig. 6 (pink bars). Killing of *E. coli* to $6\log_{10}$ is observed when the photosensitiser is present, with only 10-fold reduction in CFU using light irradiation alone. For *S. aureus*, light alone causes some killing at exposure times of 60 min and longer, but the presence of photosensitiser increases the light-induced killing 1000-fold, Fig. 6b. As both *S. aureus* and *E. coli* contain low levels of photo-excitable endogenous porphyrin molecules synthesised by the haem biosynthesis pathway, low levels of

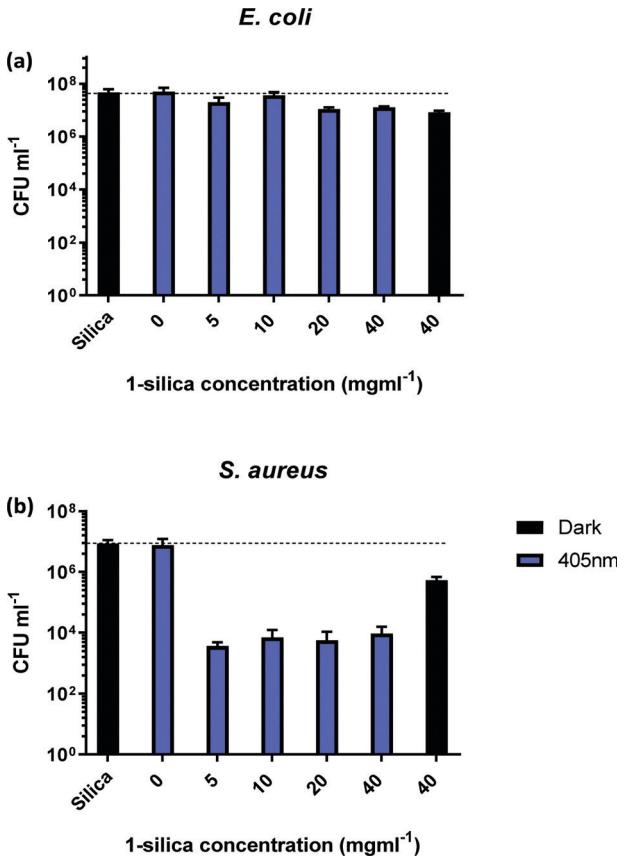

Fig. 5 Colony forming units (CFU ml^{-1}) for (a) *E. coli* and (b) *S. aureus*, as a function of exposure to different amounts of compound **1** adsorbed on silica (**1**-silica). Blue bars: irradiation with 405 nm light, 17.5 mW cm^{-2}, 30 min. Black bars: no irradiation. All experiments performed in triplicate. 1 mg ml^{-1} of complex **1**-silica is equivalent to 11 μM of complex **1**.

light-dependent killing by irradiation alone can be expected. However, neither *S. aureus* nor *E. coli* have sufficient concentrations of endogenous porphyrin molecules to allow for bacterial killing ($4\log_{10}$ reduction) using light alone, suggesting that the method of killing is *via* light activated **1**-silica photosensitisation (Fig. 6a). It has been reported that Gram-negative bacteria with an outer lipid/protein membrane biolayer are less susceptible to killing using exogenous photosensitisers such as **1**-silica as the outer membrane presents an additional permeability barrier to protect the cell against extracellular generated ROS.[94]

One possible light-dependent mechanism of bacterial killing with complex **1** is based on an oxidative burst that occurs upon illumination and will initially target extracellular structures in close proximity to the silica-immobilised photosensitiser which cannot penetrate the cell.[95] The positively charged **1**-silica will be brought to close proximity with the negatively charged bacterial surface to induce damage to extracellular cell envelope structures and biomolecules may be the primary site of damage, eventually causing death by cell lysis.

The lipophilic nature of **1** could also lead to potentially disruption of the bacterial lipid cell membranes (cytoplasmic membrane, and/or outer membrane in Gram-negative bacteria)

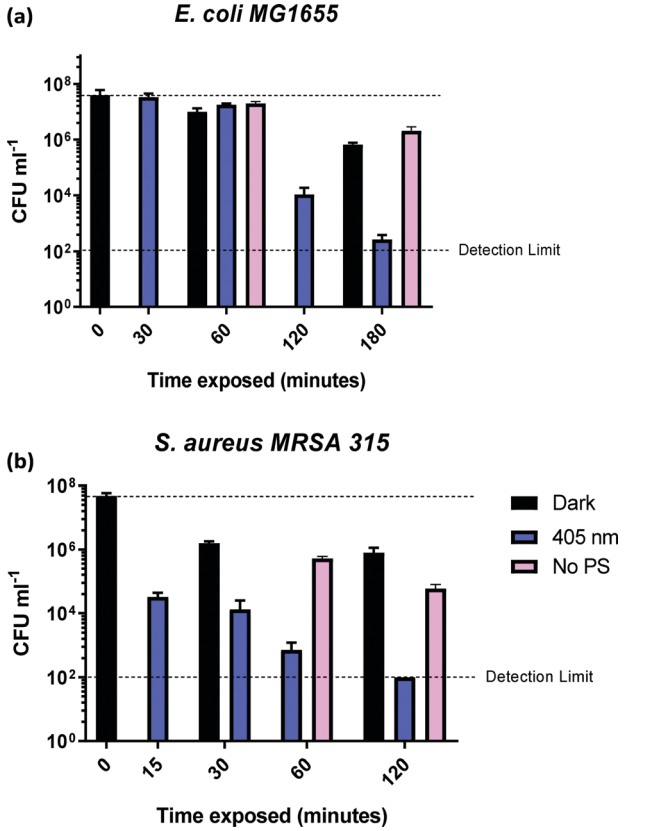

Fig. 6 Colony forming units (CFU ml^{-1}) for (a) *E. coli* MG1655 and (b) *S. aureus* MRSA 315, in presence of 5 mg ml^{-1} of **1**-silica as a function of irradiation time with 405 nm light, 17.5 mW cm^{-2} (blue bars) and in the absence of 5 mg ml^{-1} of **1**-silica (pink bars).

in a light-independent manner. It is well-established that some lipophilic cations, for example of the triphenylphosphonium class[96] can enter bacterial cells in a process driven by the cytoplasmic membrane potential (negative inside) and have even been conjugated to photosensitisers to increase their antibacterial effect in the cytoplasm.[97] Multiple active transporters may also exist for many large cationic lipophilic molecules.[98] The very small degrees of dark toxicity of **1** towards *S. aureus* and *E. coli* (Fig. 4–6) could be due to the direct membrane insertion, depolarisation and downstream cellular disruption caused by these processes should the compound be free in solution free rather than silica bound. In the latter case, it is clear that dark toxicity is much smaller than the degree of light-induced killing. We also note that whilst some dark toxicity has been observed at the 10^8 CFU ml^{-1} initial concentration of bacteria, no dark toxicity has been detected for 10^{10} CFU ml^{-1} initial concentration, even at 583 μM of **1** which would correspond to the $\sim 3.50 \times 10^{17}$ molecules ml^{-1}.

The stability of **1**-silica in water was confirmed by time-dependent spectrophotometric investigation: **1**-silica subjected to vigorous stirring and irradiation with light for up to 21 h did not show any leaching of the compound from silica support into water (within experimental uncertainty), see Part S6 in the ESI.† Therefore, it is unlikely that dark toxicity stems from an unbound photosensitiser.

While it is difficult to compare the efficiency of different photosensitisers already reported in the literature, due to the different conditions used, some observations can be made. It has previously been shown that 10 mg l^{-1} of methylene blue, MB, reduced the population of *E. coli* by 99.5% after 30 min of irradiation in solution, with sunlight with a total dose of 743 W m^{-2}.[94] However, immobilisation on multiple supports, including silica, led to greatly reduced bacteria killing potency of MB compared to that in solution. MB immobilised on polystyrene achieved a 97.5% reduction of CFU in 60 min of irradiation with white light,[99] whilst for MB immobilised on silica (20 g l^{-1} of silica, 0.5 mg g^{-1} of MB on silica, equivalent to 31 μM of MB) only 65% reduction of CFU after 60 min (unknown irradiance) was observed, which will not be sufficient for practical use.[99] In comparison, the **1**-silica used at comparable concentrations (5 mg ml^{-1}, equivalent to 55 μM of **1**) achieves a 4 orders of magnitude more efficient killing of *E. coli*, >99.9999%.

Several immobilised photosensitisers have shown high killing under comparable conditions as **1**-silica (Table S7, ESI†). For example, an organic photosensitiser BODIPY immobilised on Nylon leads to 99.9999% killing of MRSA under 400–700 nm light (30 min, 72 J cm^{-2}), however it is photobleaching in the process.[38] Photobleaching of BODIPY occurs at 118 J cm^{-2}, half the total dose needed for 99.95% reduction of the Gram negative bacteria *A. baumannii.* Porphyrin derivatives, especially 5-(4-aminophenyl)-10,15,20-tris-(4-*N*-methylpyridinium)porphyrin (A_3B^{3+}) and its Zn-metallated derivative, (Zn-A_3B^{3+}) immobilised on polyethylene elastomer or nanofibrillated cellulose (NFC) have shown efficient killing of various pathogens, including MRSA and *E. coli*, with 99.9999% efficiency after 60 min of irradiation with a total dose of 234 and 288 J cm^{-2} respectively;[41] (*cf.* **1**-silica which requires 120 min for MRSA and 180 min for *E. coli* to achieve 99.9999% killing with a total dose of 126 J cm^{-2} and 189 J cm^{-2} respectively).

Another organic photosensitiser, 9,10-anthraquinone-2-carboxylic acid bound to silica, ANT-SiO_2,[100] at a concentration of 700 μM caused reduction of 10^6 CFU ml^{-1} of *E. coli* after 110 min irradiation with 365 nm light, 3.85 mW cm^{-2} (total radiation exposure of 25.41 J cm^{-2}), following an initial induction period of 60 min. In comparison, 90 min irradiation of TiO_2 at 365 nm, 3.85 mW cm^{-2}, led to a total inactivation of bacteria with no induction period. The difference between TiO_2 (no induction time) and ANT-SiO_2 photosensitiser on silica (induction time) in treatment of *E. coli* was attributed to the different ROS generated directly by TiO_2 in comparison to the ROS produced *via* photosensitisation in ANT-SiO_2.[100]

Recent work (2019/2020) on transition metal complexes for antibacterial action has included Re, Ir and Ru complexes in solution. Re-derivatives (5.8–11.6 μM, 365 nm light, 1 h, 3 J cm^{-2}) were shown to inhibit bacterial growth for both *E. coli* and *S. aureus*.[101] Ir(III) tris-diimine complexes of the structure $[Ir(phen)_2(R\text{-}phen)]^{3+}$, where R-phen = 3,8-dipyrenylphenanthroline and 3-pyrenylphenanthroline, caused 50% killing

of *S. aureus* at 0.17 and 0.16 μM respectively when irradiated with visible light to a dose of 35 J cm^{-2}.[23] $[Ru(bpy\text{-}TMEDA)_3]^{8+}$, 15 μM, achieved a 6.87 $\log_{10}$ reduction of *S. aureus* in PBS buffer after 20 min of irradiation at 470 nm, 22 mW cm^{-2} for a total dose of 27 J cm^{-2}.[102] Whilst some of these transition metal photosensitisers are very efficient in killing of bacteria, all of the above systems have been studied in solution and therefore cannot be compared directly to **1**-silica.

Perhaps the closest comparison to **1**-silica as a transition metal complex is $[(4,7\text{-diphenyl-}1,10\text{-phenanthroline})_3Ru]^{2+}$, RDP^{2+}, bound to porous silicone (pSil).[18] The immobilised RDP^{2+} photo-sensitiser was used with a loading of 1–30 mg g^{-1} inside a micro-reactor with a Xe lamp and a cut-off filter letting through wave-lengths >373 nm. The total irradiation of 2 kW m^{-2} delivered for 9 h to water flowing with the rate of 15 ml h^{-1} resulted in an inactivation rate of *E. coli* of 1.1×10^5 CFU h^{-1} l^{-1}.[18] In our work, **1**-silica achieved the rate of killing of $\sim 5 \times 10^7$ CFU h^{-1} l^{-1}, under 405 nm irradiation with power density of 17.5 W m^{-2}, although direct comparisons are difficult due to different setups used in our work and in that reported previously. Detailed summary of immobilised photosensitisers is given in Table S9 in the ESI.†

Overall, the data presented in Fig. 4–6 show that the bacterial killing is caused by a combination of the surface-bound photosensitiser **1**-silica and light. Given the relatively high quantum yield of $^1O_2$ production by compound **1** in solution (29%), singlet oxygen is likely the primary ROS involved in the killing of both bacteria, although contributions from other types of ROS cannot be ruled out.[11]

Conclusions

The first example of efficient killing of bacteria in water by an immobilised copper photosensitiser has been demonstrated. This simple, easy to make and easy to scale up copper(I) complex, which has a moderately long excited-state lifetime of 220 ns, has been shown to produce singlet oxygen upon irradiation with visible light in aqueous media. Significant killing of the Gram-positive bacterium, *S. aureus* (MRSA 315), with 99.99% killing observed after only 15 min, and 99.9999% ('complete') killing observed after 2 h. For a Gram-negative bacterium *E. coli* (MG1655), significant killing of 99.99% was achieved after 2 h of irradiation, and 99.9999% ('complete') killing after 3 h. Thus the complex immobilised on silica achieved significant light-induced killing of both Gram-positive and Gram-negative bacteria of a level considered "highly protective" by WHO standards (>4 $\log_{10}$ reduction).[87]

This first example of application of Cu(I) complexes for photoactivated bacterial killing in water under visible light demonstrates the potential of this class of compounds as low-cost, immobilised antibacterial agents. These results could initiate future developments of Earth-abundant complexes for diverse antibacterial treatments (aPDT), such as water purification or surface disinfection, providing a long-sought replacement of rare transition metals.

Experimental

Reagents

Reagents were obtained from commercial sources and used without further purification unless stated otherwise. The starting materials of $[Cu(CH_3CN)_4](BF_4)$, dmp, xantphos and Na(tfpb) were purchased from Sigma-Aldrich. The solvents (DCM, MeOH, diethyl ether) used were purchased from commercial sources and were not purified further before use. Chromatography grade silica was purchased from VWR chemicals (particle size 40–63 μm, pore size 60 Å, surface area 400 m^2 g^{-1}). Singlet Oxygen Sensor Green (Molecular Probes) was purchased from ThermoFisher Scientific (https://www.thermofisher.com/order/catalog/product/S36002#/S36002).

Synthesis of complex 1

[Cu(xantphos)(dmp)](tfpb) **1** was synthesised following the literature procedure.[59] $[Cu(CH_3CN)_4](BF_4)$ (50 mg, 0.16 mmol) was added to a solution of xantphos (92 mg, 0.16 mmol) in DCM (20 ml). The solution was then stirred for 2 hours. Adding dmp (33 mg, 0.16 mmol) to the solution caused it to turn yellow. The solution was then stirred for a further hour. The product was precipitated by addition with diethyl ether and separated *via* vacuum filtration to give a bright yellow powder. This powder was then dissolved in MeOH (20 ml) and sodium tetrakis[3,5-bis(trifluoromethyl)-phenyl]borate (tfpb) (0.164 g, 0.185 mmol) was added. The solution was then stirred for 1 hour at room temperature. Upon addition of water, bright yellow crystals of complex **1** was yielded (0.114 g, 0.146 mmol). The method was later scaled up to produce 2.81 g, 1.64 mmol of **1**.

[Cu(xantphos)(dmp)]tfpb: ^1H NMR (400 MHz, $CDCl_3$) δ 8.17 (d, J = 8.2 Hz, 2H), (7.74 s, 8H), 7.70 (s, 2H), 7.65 (dd, J = 7.8, 1.1 Hz, 2H), 7.51 (s, 4H), 7.41 (d, J = 8.3 Hz, 2H), 7.26–7.13 (m, 6H), 7.09–6.95 (m, 16H), 6.95–6.84 (m, 2H), 2.25 (s, 6H), 1.74 (d, J = 7.1 Hz, 6H). m/z (ES^+) 849.6 (100%, M^+).

Preparation of complex 1-silica

A solution of 10 mg of complex **1** in 10 ml of DCM was added onto 500 mg of silica, stirred, and rotary-evaporated. The resulting yellow powder was left to dry overnight, during which time no weight loss has been observed. The resulting concentration is 11 mM of complex **1** per gram of silica.

Determination of singlet oxygen quantum yield using a singlet oxygen sensor green probe (SOSG, 2′,7′-dichlorofluorescin)

100 μg of SOSG probe was dissolved in 100 μL of MeOH to make a stock solution of SOSG of concentration ~1.65 mM. For each experiment, 20 μl of the stock solution was added to 3 ml of water giving SOSG concentration of ~11 nM. The 1.56 μM solution of $[Ru(bpy)_3]Cl_2$ in water was used. For the suspensions of complex **1** and **1**-silica, 5 mg ml^{-1} was used.

The experiment was conducted using standard 1 cm path-length cuvettes, with 3 ml solution. The samples were stirred using a magnetic stirrer plate and irradiated with a 405 or 455 nm diode with an irradiance of 10 mW cm^{-2}. The data were recorded using a Jobin-Yvon FluoroMax-4 Spectrofluorometer at the same time points for each sample (0, 10, 20, 30, 60, 90, 120, 180, 300

and 600 s). The emission intensity at the emission maximum of the probe (525 nm) was plotted against irradiation time as a ratio against the emission intensity at $t = 0$, before the irradiation.

Quantum yield of singlet oxygen production

Singlet oxygen was detected through measurement of the singlet oxygen emission band at ~1275 nm. Complex **1** in acetonitrile solution (MeCN) was excited by the third harmonic of a Q-Switch Nd:YAG laser (λ = 355 nm, ~8 ns pulse length, laser model LS-1231M from LOTISII). The time-resolved signal of $^1O_2$ luminescence at 1275 nm was detected by a liquid nitrogen cooled InGaAs photodiode of $\varnothing$ 3 mm active area (J22D-M204-R03M-60-1.7, Judson Technologies). The output from the photodiode was coupled into a low-noise current amplifier (DLPCA-200, FEMTO Messtechnik GmbH). The amplifier output signal was recorded with a digital oscilloscope (TDS 3032B Tektronix) and transferred to a computer. To selectively detect the $^1O_2$ emission, the high-contrast bandpass optical filter (1277 nm centre wavelength, 28 nm FWHM, custom-made by Izovac, Belarus) was fitted in front of the InGaAs photodiode. To increase the light collection efficiency, the spherical broadband mirror was set behind the sample to reflect the NIR emission through the sample towards the detector.

The quantum yield of singlet oxygen production $(\phi_{^1O_2})$ is determined by comparing the initial amplitude of the emission signal of $^1O_2$ generated when irradiating the air-equilibrated solution of complex **1** and that of the standard (perinaphthenone, $\phi_{^1O_2} = 100\%$ (acetonitrile)).[89] The emission lifetime for $^1O_2$ sensitised by the complex and the standard must be similar (within the range 70–90 μs in acetonitrile) to confirm that $^1O_2$ does not react with the photosensitiser in its ground state. The optical densities of the complex and a standard are matched at 355 nm, and the same solvent was used for both compounds. The experiments are performed at a series of excitation energies ranging from 20 μJ to 500 μJ per pulse. The $\phi_{^1O_2}$ values are obtained in the low-energy limit whilst the intensity of the emission increases linearly with the laser power.

A correction is applied to the calculated initial intensities to account for small discrepancies in the optical density of the compound and standard solutions at 355 nm:

$$\text{corrected initial amplitude} = \frac{\text{experimentally determined amplitude}}{1 - 10^{\text{OD}_{355}}} \quad (1)$$

values of $\phi_{^1O_2}$ are calculated at each power by using eqn (2) and the average of the values stated is taken as the singlet oxygen yield.

$$\phi_{^1O_2}(\text{compound}) = \frac{\text{corrected initial amplitude (comp.)}}{\text{corrected initial amplitude (stand.)}} \phi_{^1O_2}(\text{standard}) \quad (2)$$

^{1}H NMR spectroscopy in solution

^{1}H spectra were measured using a 400 MHz Bruker Avance 400 spectrometer. The complexes were dissolved in spectroscopic grade deuterated chloroform ($CDCl_3$) or acetonitrile (CD_3CN) and calibrated against the residual solvent peak.

Solid-state NMR spectroscopy

Solid-state NMR spectroscopy was carried out using a Bruker AVANCE III HD NMR spectrometer operating at 500.13 MHz ^{1}H frequency, using 4 mm zirconia rotors and a magic angle spinning (MAS) rate of 10 kHz on a dual resonance (HX-type) MAS-probe. For those experiments using cross-polarisation (CP), a contact time of 2 ms was used and the relaxation delay for each sample was individually determined from a proton T1 measurement (setting the relaxation delay to 5 × T1 for the measurement). Spectra with high-power decoupling (^{31}P) were acquired with a longer relaxation delay of 30 s (T1 not determined) and single-pulse experiments (^{19}F) were acquired with 10 s relaxation delay (T1 not determined). Transients were collected until sufficient signal-to-noise was obtained. Values of the chemical shifts are referenced to adamantane in ^{13}C (magnetic field set to place the higher shift resonance of adamantane at 38.48 ppm).

Diffuse reflectance and UV-visible absorption spectroscopy

Diffuse reflectance spectra were recorded using a Varian Cary 5000 spectrophotometer. A Praying Mantis™ Diffuse Reflectance Accessory was used to hold the solid samples in the spectrophotometer. The UV-Vis spectra were recorded using a Cary 50 Bio Spectrometer and sample solutions in a quartz cuvette with a path length of 1 cm.

Emission spectroscopy and emission lifetime experiments

Emission and excitation spectra were collected using a Horiba Jobin Yvon Fluromax-4 spectrofluorometer. Solutions were placed in 1 cm path length quartz cuvette. Emission lifetime experiments were conducted with an Edinburgh Instruments mini-tau Edinburgh Instrument set-up using 405 nm, 75 ps diode laser as an excitation source.

Bacterial strains and growth conditions

S. aureus MRSA 315 and *E. coli* MG1655 were cultured aerobically at 37 °C in Luria-Bertani (LB) broth (Oxoid) sterilised by autoclaving. Liquid cultures were shaken at 200 rpm. Cultures were grown to mid-log growth phase (2–3 hours) before samples were collected.

Light exposure viability assays

High intensity 405 nm light was produced by an LED with a nominal wavelength of 405 nm and a bandwidth of ~20 nm at full half width maximum. Power density (J cm^{-2}) was measured using a Thorlabs 5310C thermal power sensor at the position the samples were exposed, 5 cm away from the light source. Light sensitivity experiments were carried out on mid-log bacterial broth culture resuspended in sodium phosphate buffer (20 mM pH 7.2) to an OD_{600} of 0.1. For each condition tested, 1 ml of mid-log cell culture was added into 12 well plates containing the appropriate photosensitiser tested. Each condition was tested in triplicate with three technical replicates per

repeat. Viability was calculated by counting the number of colony-forming units (C.F.U.) after appropriate dilution on LB agar plates, counting their number per ml.

Conflicts of interest

There are no conflicts to declare.

Acknowledgements

We thank the EPSRC (capital equipment award to Lord Porter Laser Laboratory), the BBSRC (DTP funding to P. J. W.), the Grantham Centre for Sustainable Futures (studentship to M. V. A.), and the University of Sheffield for support.

Notes and references

1 United Nations, 2015, 16301, pp. 1–35.
2 World Health Organization and UNICEF, 2017, pp. 1–110.
3 S. Loeb, R. Hofmann and J. H. Kim, *Environ. Sci. Technol. Lett.*, 2016, **3**, 73–80.
4 P. R. Hunter, *Environ. Sci. Technol.*, 2009, **43**, 8991–8997.
5 World Health Organization, 2011, pp. 1–543.
6 V. Alipour, L. Rezaei, M. R. Etesamirad, S. Rahdar, M. R. Narooie, A. Salimi, J. Hasani, R. Khaksefidi, S. A. Sadat and H. Biglari, *J. Global Pharma Technol.*, 2017, **9**, 40–46.
7 W. Heaselgrave and S. Kilvington, *Acta Trop.*, 2011, **119**, 138–143.
8 A. Carratalà, A. D. Calado, M. J. Mattle, R. Meierhofer, S. Luzi and T. Kohn, *Appl. Environ. Microbiol.*, 2016, **82**, 279–288.
9 D. Phillips, *Pure Appl. Chem.*, 2011, **83**, 733–748; N. Manav, P. E. Kesavan, M. Ishida, S. Mori, Y. Yasutake, S. Fukatsu, H. Furuta and I. Gupta, *Dalton Trans.*, 2019, **48**, 2467–2478; J. M. Fernandez, M. D. Bilgin and L. I. Grossweiner, *J. Photochem. Photobiol., B*, 1997, **37**, 131–140; see also, *Coord. Chem. Rev.*, 2019, **379**, 1–160 (special issue, Ed. J. F. Lovell); see also, *J. Photochem. Photobiol., B*, 2015, **150**, 1–68.
10 M. Wainwright, T. Maisch, S. Nonell, K. Plaetzer, A. Almeida, G. P. Tegos and M. R. Hamblin, *Lancet Infect. Dis.*, 2017, **17**, e49–e55; H. Abrahamse and M. R. Hamblin, *Biochem. J.*, 2016, **473**, 347–364; S. K. Sharma, T. H. Dai and M. R. Hamblin, in *Antimicrobial Drug Discovery: Emerging Strategies*, ed. A. Tegos and E. Mylonakis, 2012, CABI, Wallingford, pp. 310–322.
11 F. Vatansever, W. C. M. A. de Melo, P. Avci, D. Vecchio, M. Sadasivam, A. Gupta, R. Chandran, M. Karimi, N. A. Parizotto, R. Yin, G. P. Tegos and M. R. Hamblin, *FEMS Microbiol. Rev.*, 2013, **37**, 955–989.
12 F. Manjón, D. García-Fresnadillo and G. Orellana, *Photochem. Photobiol. Sci.*, 2009, **8**, 926–932.
13 D. García-Fresnadillo, Y. Georgiadou, G. Orellana, A. M. Braun and E. Oliveros, *Helv. Chim. Acta*, 1996, **79**, 1222–1238.
14 M. Thandu, C. Comuzzi and D. Goi, *Int. J. Photoenergy*, 2015, **2015**, 1–22.
15 F. Manjón, M. Santana-Magaña, D. García-Fresnadillo and G. Orellana, *Photochem. Photobiol. Sci.*, 2014, **13**, 397–406.
16 R. Bonnett, M. A. Krysteva, I. G. Lalov and S. V. Artarsky, *Water Res.*, 2006, **40**, 1269–1275.
17 A. I. Silverman, B. M. Peterson, A. B. Boehm, K. McNeill and K. L. Nelson, *Environ. Sci. Technol.*, 2013, **47**, 1870–1878.
18 M. E. Jiménez-Hernández, F. Manjón, D. García-Fresnadillo and G. Orellana, *Sol. Energy*, 2006, **80**, 1382–1387.
19 L. Villén, F. Manjón, D. García-Fresnadillo and G. Orellana, *Appl. Catal., B*, 2006, **69**, 1–9.
20 S. L. Rosado-Lausell, H. Wang, L. Gutiérrez, O. C. Romero-Maraccini, X. Z. Niu, K. Y. H. Gin, J. P. Croué and T. H. Nguyen, *Water Res.*, 2013, **47**, 4869–4879.
21 F. Manjón, M. Santana-Magaña, D. García-Fresnadillo and G. Orellana, *Photochem. Photobiol. Sci.*, 2010, **9**, 838–845.
22 D. García-Fresnadillo, *ChemPhotoChem*, 2018, **2**, 512–534.
23 L. Wang, S. Monro, P. Cui, H. Yin, B. Liu, C. G. Cameron, W. Xu, M. Hetu, A. Fuller, S. Kilina, S. A. McFarland and W. Sun, *ACS Appl. Mater. Interfaces*, 2019, **11**, 3629–3644.
24 R. Giereth, W. Frey, H. Junge, S. Tschierlei and M. Karnahl, *Chem. – Eur. J.*, 2017, **23**, 17432–17437.
25 A. J. J. Lennox, S. Fischer, M. Jurrat, S. P. Luo, N. Rockstroh, H. Junge, R. Ludwig and M. Beller, *Chem. – Eur. J.*, 2016, **22**, 1233–1238.
26 S. Garakyaraghi, E. O. Danilov, C. E. McCusker and F. N. Castellano, *J. Phys. Chem. A*, 2015, **119**, 3181–3193.
27 S. Garakyaraghi, P. D. Crapps, C. E. McCusker and F. N. Castellano, *Inorg. Chem.*, 2016, **55**, 10628–10636.
28 C. E. McCusker and F. N. Castellano, *Inorg. Chem.*, 2013, **52**, 8114–8120.
29 C. E. McCusker and F. N. Castellano, *Inorg. Chem.*, 2015, **54**, 6035–6042.
30 S. Garakyaraghi, C. E. McCusker, S. Khan, P. Koutnik, A. T. Bui and F. N. Castellano, *Inorg. Chem.*, 2018, **57**, 2296–2307.
31 J. R. Morones-Ramirez, J. A. Winkler, C. S. Spina and J. J. Collins, *Sci. Transl. Med.*, 2013, **5**(190), 1–11.
32 A. V. Domínguez, R. A. Algaba, A. M. Canturri, Á. R. Villodres and Y. Smani, *Antibiotics*, 2020, **9**(36), 1–10.
33 Y. Xiang, C. Mao, X. Liu, Z. Cui, D. Jing, X. Yang, Y. Liang, Z. Li, S. Zhu, Y. Zheng, K. W. K. Yeung, D. Zheng, X. Wang and S. Wu, *Small*, 2019, **15**, 1900322.
34 A. Kyzioł, A. Cierniak, J. Gubernator, A. Markowski, M. Jezowska-Bojczuk and U. K. Komarnicka, *Dalton Trans.*, 2018, **47**, 1981–1992.
35 X. An, N. Naowarojna, P. Liu and B. M. Reinhard, *ACS Appl. Mater. Interfaces*, 2020, **12**, 106–116.
36 M. Bartolomeu, S. Reis, M. Fontes, M. G. P. M. S. Neves, M. A. F. Faustino and A. Almeida, *Water*, 2017, **9**, 630.
37 L. Sobotta, J. Dlugaszewska, D. Ziental, W. Szczolko, T. Koczorowski, T. Goslinski and J. Mielcarek, *J. Photochem. Photobiol., A*, 2019, **368**, 104–109.
38 F. Cieplik, D. Deng, W. Crielaard, W. Buchalla, E. Hellwig, A. Al-Ahmad and T. Maisch, *Crit. Rev. Microbiol.*, 2018, **44**, 571–589.
39 N. Maldonado-Carmona, T. S. Ouk, M. J. F. Calvete, M. M. Pereira, N. Villandier and S. Leroy-Lhez, *Photochem. Photobiol. Sci.*, 2020, **19**, 445–461.

40 K. R. Stoll, F. Scholle, J. Zhu, X. Zhang and R. A. Ghiladi, *Photochem. Photobiol. Sci.*, 2019, **18**, 1923–1932.
41 D. R. Alvarado, D. S. Argyropoulos, F. Scholle, B. S. T. Peddinti and R. A. Ghiladi, *Green Chem.*, 2019, **21**, 3424–3435.
42 B. S. T. Peddinti, F. Scholle, R. A. Ghiladi and R. J. Spontak, *ACS Appl. Mater. Interfaces*, 2018, **10**, 25955–25959.
43 M. W. Blaskie and D. R. Mcmillin, *Inorg. Chem.*, 1980, **19**, 3519–3522.
44 D. R. McMillin, J. R. Kirchhoff and K. V. Goodwin, *Coord. Chem. Rev.*, 1985, **64**, 83–92.
45 M. T. Miller, P. K. Gantzel and T. B. Karpishin, *Inorg. Chem.*, 1999, **38**, 3414–3422.
46 M. T. Miller, P. K. Gantzel and T. B. Karpishin, *J. Am. Chem. Soc.*, 1999, **121**, 4292–4293.
47 L. X. Chen, G. B. Shaw, I. Novozhilova, T. Liu, G. Jennings, K. Attenkofer, G. J. Meyer and P. Coppens, *J. Am. Chem. Soc.*, 2003, **125**, 7022–7034.
48 M. Iwamura, S. Takeuchi and T. Tahara, *Acc. Chem. Res.*, 2015, **48**, 782–791.
49 M. Schmittel and A. Ganz, *Chem. Commun.*, 1997, 999–1000.
50 M. Sandroni, Y. Pellegrin and F. Odobel, *Chimie*, 2016, **19**, 79–93.
51 M. Heberle, S. Tschierlei, N. Rockstroh, M. Ringenberg, W. Frey, H. Junge, M. Beller, S. Lochbrunner and M. Karnahl, *Chem. – Eur. J.*, 2017, **23**, 312–319.
52 K. Soulis, C. Gourlaouen, C. Daniel, A. Quatela, F. Odobel, E. Blart and Y. Pellegrin, *Polyhedron*, 2018, **140**, 42–50.
53 M. T. Miller, P. K. Gantzel and T. B. Karpishin, *Angew. Chem., Int. Ed.*, 1998, **37**, 1556–1558.
54 M. T. Miller, P. K. Gantzel and T. B. Karpishin, *Inorg. Chem.*, 1998, **37**, 2285–2290.
55 M. T. Miller and T. B. Karpishin, *Inorg. Chem.*, 1999, **38**, 5246–5249.
56 S. Keller, F. Brunner, J. M. Junquera-Hernández, A. Pertegás, M. G. La-Placa, A. Prescimone, E. C. Constable, H. J. Bolink, E. Ortí and C. E. Housecroft, *ChemPlusChem*, 2018, **83**, 143.
57 M. Alkan-Zambada, S. Keller, L. Martínez-Sarti, A. Prescimone, J. M. Junquera-Hernández, E. C. Constable, H. J. Bolink, M. Sessolo, E. Ortí and C. E. Housecroft, *J. Mater. Chem. C*, 2018, **6**, 8460–8471.
58 S. Keller, A. Prescimone, H. Bolink, M. Sessolo, G. Longo, L. Martínez-Sarti, J. M. Junquera-Hernández, E. C. Constable, E. Ortí and C. E. Housecroft, *Dalton Trans.*, 2018, **47**, 14263–14276.
59 C. S. Smith, C. W. Branham, B. J. Marquardt and K. R. Mann, *J. Am. Chem. Soc.*, 2010, **132**, 14079–14085.
60 S. M. Kuang, D. G. Cuttell, D. R. McMillin, P. E. Fanwick and R. A. Walton, *Inorg. Chem.*, 2002, **41**, 3313–3322.
61 A. Rosas-Hernández, C. Steinlechner, H. Junge and M. Beller, *Green Chem.*, 2017, **19**, 2356–2360.
62 Y. Yamazaki, T. Onoda, J. Ishikawa, S. Furukawa, C. Tanaka, T. Utsugi and T. Tsubomura, *Front. Chem.*, 2019, **7**, 288.
63 J. Kim, D. R. Whang and S. Y. Park, *ChemSusChem*, 2017, **10**, 1883–1886.
64 C. Minozzi, A. Caron, J. C. Grenier-Petel, J. Santandrea and S. K. Collins, *Angew. Chem., Int. Ed.*, 2018, **57**, 5477–5481.
65 M. M. Cetin, R. T. Hodson, C. R. Hart, D. B. Cordes, M. Findlater, D. J. Casadonte, A. F. Cozzolino and M. F. Mayer, *Dalton Trans.*, 2017, **46**, 6553–6569.
66 R. Giereth, I. Reim, W. Frey, H. Junge, S. Tschierlei and M. Karnahl, *Sustainable Energy Fuels*, 2019, **3**, 692–700.
67 B. Wang, D. P. Shelar, X. Z. Han, T. T. Li, X. Guan, W. Lu, K. Liu, Y. Chen, W. F. Fu and C. M. Che, *Chem. – Eur. J.*, 2015, **21**, 1184–1190.
68 B. J. McCullough, B. J. Neyhouse, B. R. Schrage, D. T. Reed, A. J. Osinski, C. J. Ziegler and T. A. White, *Inorg. Chem.*, 2018, **57**, 2865–2875.
69 Y. R. Zhang, X. Yu, S. Lin, Q. H. Jin, Y. P. Yang, M. Liu, Z. F. Li, C. L. Zhang and X. L. Xin, *Polyhedron*, 2017, **138**, 46–56.
70 Y. Zhang, M. Heberle, M. Wächtler, M. Karnahl and B. Dietzek, *RSC Adv.*, 2016, **6**, 105801–105805.
71 Y. Zhang, L. Zedler, M. Karnahl and B. Dietzek, *Phys. Chem. Chem. Phys.*, 2019, **21**, 10716–10725.
72 Y. Zhang, P. Traber, L. Zedler, S. Kupfer, S. Gräfe, M. Schulz, W. Frey, M. Karnahl and B. Dietzek, *Phys. Chem. Chem. Phys.*, 2018, **20**, 24843–24857.
73 O. Reiser, *Acc. Chem. Res.*, 2016, **49**, 1990–1996.
74 C. Dragonetti, M. Magni, A. Colombo, F. Fagnani, D. Roberto, F. Melchiorre, P. Biagini and S. Fantacci, *Dalton Trans.*, 2019, **48**, 9703–9711.
75 R. Starosta, A. Bykowska, A. Kyziol, M. Plotek, M. Florek, J. Król and M. Jezowska-Bojczuk, *Chem. Biol. Drug Des.*, 2013, 579–586.
76 U. K. Komarnicka, S. Kozieł, P. Zabierowski, R. Kruszyński, M. K. Lesiów, F. Tisato, M. Porchia and A. Kyzioł, *J. Inorg. Biochem.*, 2020, **203**, 110926.
77 V. Gandin, M. Porchia, F. Tisato, A. Zanella, E. Severin, A. Dolmella and C. Marzano, *J. Med. Chem.*, 2013, **56**, 7416–7430.
78 D. Mahendiran, N. Pravin, N. S. P. Bhuvanesh, R. S. Kumar, V. Viswanathan, D. Velmurugan and A. K. Rahiman, *ChemistrySelect*, 2018, **3**, 7100–7111.
79 U. A. Khan, A. Badshah, M. N. Tahir and E. Khan, *Polyhedron*, 2020, **181**, 114485.
80 O. Evangelinou, A. G. Hatzidimitriou, E. Velali, A. A. Pantazaki, N. Voulgarakis and P. Aslanidis, *Polyhedron*, 2014, **72**, 122–129.
81 T. S. Lobana, J. K. Aulakh, H. Sood, D. S. Arora, I. Garcia-Santos, M. Kaur, C. E. Duff and J. P. Jasinski, *New J. Chem.*, 2018, **42**, 9886–9900.
82 P. R. Chetana, B. S. Srinatha, M. N. Somashekar and R. S. Policegoudra, *J. Mol. Struct.*, 2016, **1106**, 352–365.
83 L. Tabrizi and H. Chiniforoshan, *New J. Chem.*, 2017, **41**, 10972–10984.
84 M. K. Rauf, Imtiaz-ud-Din, A. Badshah, M. Gielen, M. Ebihara, D. de Vos and S. Ahmed, *J. Inorg. Biochem.*, 2009, **103**, 1135–1144.
85 P. R. Chetana, B. S. Srinatha, M. N. Somashekar, R. S. Policegoudra, R. Rao, B. Maity and S. M. Aradhya, *Int. J. Pharm. Sci. Rev. Res.*, 2013, **21**, 355–363.
86 N. J. Ashbolt, *Toxicology*, 2004, **198**, 229–238.
87 World Health Organization, 2011, pp. 1–68.
88 C. Franco and J. Olmsted, *Talanta*, 1990, **37**, 905–909.

89 R. Schmidt, C. Tanielian, R. Dunsbach and C. Wolff, *J. Photochem. Photobiol., A*, 1994, **79**, 11–17.
90 F. Asaro, A. Camus, R. Gobetto, A. C. Olivieri and G. Pellizer, *Solid State Nucl. Magn. Reson.*, 1997, **8**, 81–88.
91 S. Kim, M. Fujitsuka and T. Majima, *J. Phys. Chem. B*, 2013, **117**, 13985–13992.
92 C. Tanielian, C. Wolff and M. Esch, *J. Phys. Chem.*, 1996, **100**(16), 6555–6560.
93 F. Sperandio, Y.-Y. Huang and M. Hamblin, *Recent Pat. Anti-Infect. Drug Discovery*, 2013, **8**, 108–120.
94 A. T. Cooper and D. Y. Goswami, *J. Sol. Energy Eng.*, 2002, **124**, 305–310.
95 T. Maisch, S. Hackbarth, J. Regensburger, A. Felgenträger, W. Bäumler, M. Landthaler and B. Röder, *J. Ger. Soc. Dermatology*, 2011, **9**, 360–366.
96 D. G. Nicholls and S. J. Ferguson, *Bioenergetics*, 4th Edn, 2013.
97 R. Bresolí-Obach, I. Gispert, D. G. Peña, S. Boga, Ó. Gulias, M. Agut, M. E. Vázquez and S. Nonell, *J. Biophotonics*, 2018, **11**, e201800054.
98 S. Jindal, L. Yang, P. J. Day and D. B. Kell, *BMC Microbiol.*, 2019, **19**, 1–16.
99 A. Savino and G. Angeli, *Water Res.*, 1985, **19**, 1465–1469.
100 A. K. Benabbou, C. Guillard, S. Pigeot-Rémy, C. Cantau, T. Pigot, P. Lejeune, Z. Derriche and S. Lacombe, *J. Photochem. Photobiol., A*, 2011, **219**, 101–108.
101 A. Frei, M. Amado, M. A. Cooper and M. A. T. Blaskovich, *Chem. – Eur. J.*, 2020, **26**, 2852–2858.
102 Y. Feng, W. Z. Sun, X. S. Wang and Q. X. Zhou, *Chem. – Eur. J.*, 2019, **25**, 13879–13884.

Chapter 4: Walker *et al.*

Photodynamic inactivation of *Campylobacter jejuni*: exploiting an innate sensitivity

Peter Walker, Aidan Taylor, Julia Weinstein, David Kelly

Preface

A recent study by Murdoch *et al.* 2010 found that *Campylobacter jejuni* is more sensitive to photooxidative stress than other bacterial pathogens. As *C. jejuni* is the leading cause of bacterial gastroenteritis worldwide, its control is of great significance, especially as antibiotic resistant strains are emerging. In this study we set out to characterise why *C. jejuni* is more sensitive to photooxidative stress than other bacteria and to understand the bacterial response to light generated radicals. We demonstrate that *C. jejuni* has an abundance of endogenous porphyrin species which can be excited by light to generate ROS. We highlight the ROS sensitive targets which are damaged by light generated radicals and the transcriptional response induced to protect these complexes. This work outlines for the first time the global bacterial response to photooxidative stress and explains why this bacteria represents the perfect target for bacterial photodynamic inactivation.

Author contributions

Peter Walker and David Kelly devised the study and wrote the manuscript. All experiments were conducted by Peter Walker with contributions from Aidan Taylor for the construction of the 405 nm diodes. The heat map displaying global transcriptomic changes after photooxidative stress was created with assistance from the University of Sheffield bioinformatics core. The Figure displaying transcription factor responses predicted using TFInfer software was created by Professor Jeff Green. All other Figures were produced by Peter Walker.

This manuscript has not yet been submitted to a Journal.

Mechanisms underlying the innate sensitivity of the food-borne pathogen *Campylobacter jejuni* to photodynamic inactivation by violet-blue light

Peter Walker[1], Aidan J. Taylor[1], Andrew Hitchcock[1], Joseph P. Webb[1], Julia Weinstein [2], and David J. Kelly[1]*

INTRODUCTION

Campylobacter jejuni is a microaerophilic Gram-negative pathogen which causes human campylobacteriosis, one of the most widespread zoonotic enteric diseases worldwide [1]. Campylobacters colonise the intestinal tracts of many wild bird species and agriculture-associated animals, with poultry flocks forming the main transmission route to humans. Most cases of sporadic *C. jejuni* infection occur through the handling or consumption of undercooked chicken meat, or cross-contamination of other foods with raw poultry fluid [2]. Infections in humans are characterised by the invasion and inflammation of the colonic epithelium, causing severe but typically self-limiting acute gastrointestinal illness. Chronic inflammation of the intestinal tract causes ulcerative colitis and colonic crypt abscesses which can resolve in most patients but is life threatening in immune-compromised individuals. Furthermore, roughly 1 in 1,000 individuals infected with *C. jejuni* develop serious acute inflammatory polyneuropathies such as Guillain-Barré syndrome, which is the leading cause of acute neuromuscular paralysis since the eradication of polio [3]. Despite the threat to human health, current control strategies have largely failed to reduce the prevalence of *Campylobacter* in the food chain [4]. As a result, around 1% of the population across North America, Australia and Europe become infected each year [1].

Epidemiological assessment studies have reported that handling, preparation and consumption of broiler meat may account for up to 30% of human cases of campylobacteriosis, while 50–80% may be attributed to the chicken reservoir as a whole [5]. Despite *C. jejuni* residing in the caecum and colon of chickens, during

processing, the intestinal tract may rupture or leak, transferring the intestinal fluid onto the skin. Previous studies have shown the bacteria can grow in cervices and channels on the surface of the meat at room temperature, increasing the risk to consumers if chicken is inadequately stored [6]. Control of *Campylobacter* infections focuses on all stages of poultry production, from broiler house cleansing to chlorine treated meats [7,8], yet no intervention strategies have been shown to be fully successful under commercial conditions.

One novel possibility for control is photodynamic inactivation (PDI), which has emerged as an innovative, non-antibiotic approach to inactivate pathogenic bacteria [10, 11]. The basic principle of antimicrobial PDI is the combination of visible or near infrared light, oxygen, and a photosensitiser that can absorb and transfer energy or electrons after excitation to molecular oxygen, which in turn generates reactive oxygen species (ROS). It is these three requisites, combined with the cells innate sensitivity to ROS, which dictates the susceptibility to killing by PDI [12]. It has increasingly been reported that some bacteria harbour sufficiently high concentrations of endogenous photosensitizers for them to be inactivated by irradiation with violet-blue (VB) light [13, 14]. Haem intermediates in the form of metal-free, fluorescent tetrapyrroles including coproporphyrin III, protoporphyrin IX (PPIX) and uroporphyrin III have been identified as one of the primary endogenous photosensitizers responsible for bacterial photoinactivation [13].

Murdoch et al. [XX] reported that *C. jejuni* was far more sensitive to killing by 405 nm VB light than either *Escherichia coli* or *Salmonella enteritidis* and it has been proposed that this could be used to remove *C. jejuni* from surfaces or chicken skin. Photodynamic inactivation could thus present an attractive method to specifically target *C. jejuni*, but the identity of the endogenous photosensitizers and the reasons for this differential sensitivity have not been investigated. Given the potential of this treatment to reduce *Campylobacter* prevalence in the food chain, we have investigated the factors which

make the bacteria susceptible and the mechanisms which they employ to respond. Here, we identify flavin and PPIX as the major endogenous photosensitizers for VB light in *C. jejuni*. Using a time-course transcriptomic profile, the bacterial response to endogenous ROS generation at both bacteriostatic and bactericidal light doses was reflected in a range of differentially expressed genes, some of which represent novel, previously uncharacterised components of the oxidative stress response. We also show that *c*-type cytochromes and at least two key iron-sulphur cluster enzymes (pyruvate and 2-oxoglutarate oxidoreductase; POR and OOR) used in the unique citric-acid cycle of *C. jejuni* are important targets of light induced oxidative damage. For the first time, the key components unique to this widespread pathogen, which make it highly susceptible to blue light killing, are described.

RESULTS

Differential susceptibility of *C. jejuni* to violet-blue light, analysis of chromophores and light-induced ROS generation

We first confirmed that *C. jejuni* NCTC is more susceptible to killing by PDI than a range of other bacterial pathogens, as originally reported by Murdoch et al. (2010), by comparing the light-induced reduction in viability of *E. coli* MG1655*, Staphylococcus aureus* SH1000*, Pseudomonas aeruginosa* PA01 and *C. jejuni* 11168H*.* After exposure of broth grown cells to 48 J cm^{-2} of 405 ± 5 nm light, there was a ~ 5.8 $\log_{10}$ CFU ml^{-1} reduction in *C. jejuni* samples compared to only a ~ 1 $\log_{10}$ CFU ml^{-1} reduction seen in the other bacterial pathogens (Figure 1A). Two other commonly studied *C. jejuni* strains (81-176 and 81116) showed the same high susceptibility as the *C. jejuni* NCTC11168H strain (Figure 1A). Populations of *C. jejuni* NCTC11168H were also rapidly killed on the surface of chicken skin by light from a high intensity 405 nm diode, with a 2.2 $\log_{10}$ CFU ml^{-1} reduction in viability achieved after 60 s and a further reduction to below the detection limit after a 120 s dose of 405 ± 5 nm light (Figure 1B).

In order to examine whether the increased sensitivity of *C. jejuni* to 405 nm light correlated with an increase in ROS generation, total intracellular ROS levels in *C. jejuni* and *E. coli* were qualitatively assessed. Exposure to 405 nm light resulted in a dose dependant increase in fluorescence from the probe 2,7-dichlorodihydrofluorescein diacetate (DCFDA) in both *C. jejuni* and *E. coli* suggesting a photoexcitation induced ROS increase (Figure 1C). However, there was significantly higher DCFDA-based fluorescence in *C. jejuni* cells compared with *E. coli* (normalised by cell protein concentration) at every dose, suggesting 405 nm light exposure in *C. jejuni* results in higher intracellular ROS generation.

One reason why *C. jejuni* may be more susceptible to killing by 405 nm light than the other bacterial pathogens examined could be due to a higher abundance of specific photoexcitable chromophores able to generate intracellular ROS. Whole cell

absorbance spectra show *C. jejuni* has a strong absorption peak centred at 418 nm, that is not present in the other bacteria examined here, along with diagnostic alpha- and beta bands at xxx and yy nm typical of c-type cytochromes, which closely match the absorption spectrum of the purified cytochrome *c* CccA (*cj1153*), the most abundant *c*-type cytochrome in *C. jejuni* 11168 [16] (Figure 1D). The high abundance of *c*-type cytochromes in the periplasm of *C. jejuni* is well known and may be attributed to its highly branched electron transport chain which allows growth with a wide range of environmental electron donors and acceptors [16, 17]. However, *c*-type cytochromes themselves cannot carry out the appropriate photochemistry to generate ROS [18], but the abundance of haem bound to cytochrome *c* in the periplasm means *C. jejuni* will likely have a higher abundance of photoactive haem biosynthesis intermediates which feed the *c*-type cytochrome biosynthetic pathway. The composition and abundance of photoactive haem intermediates, which potentially confers the differential photosensitivity of *C. jejuni* was investigated.

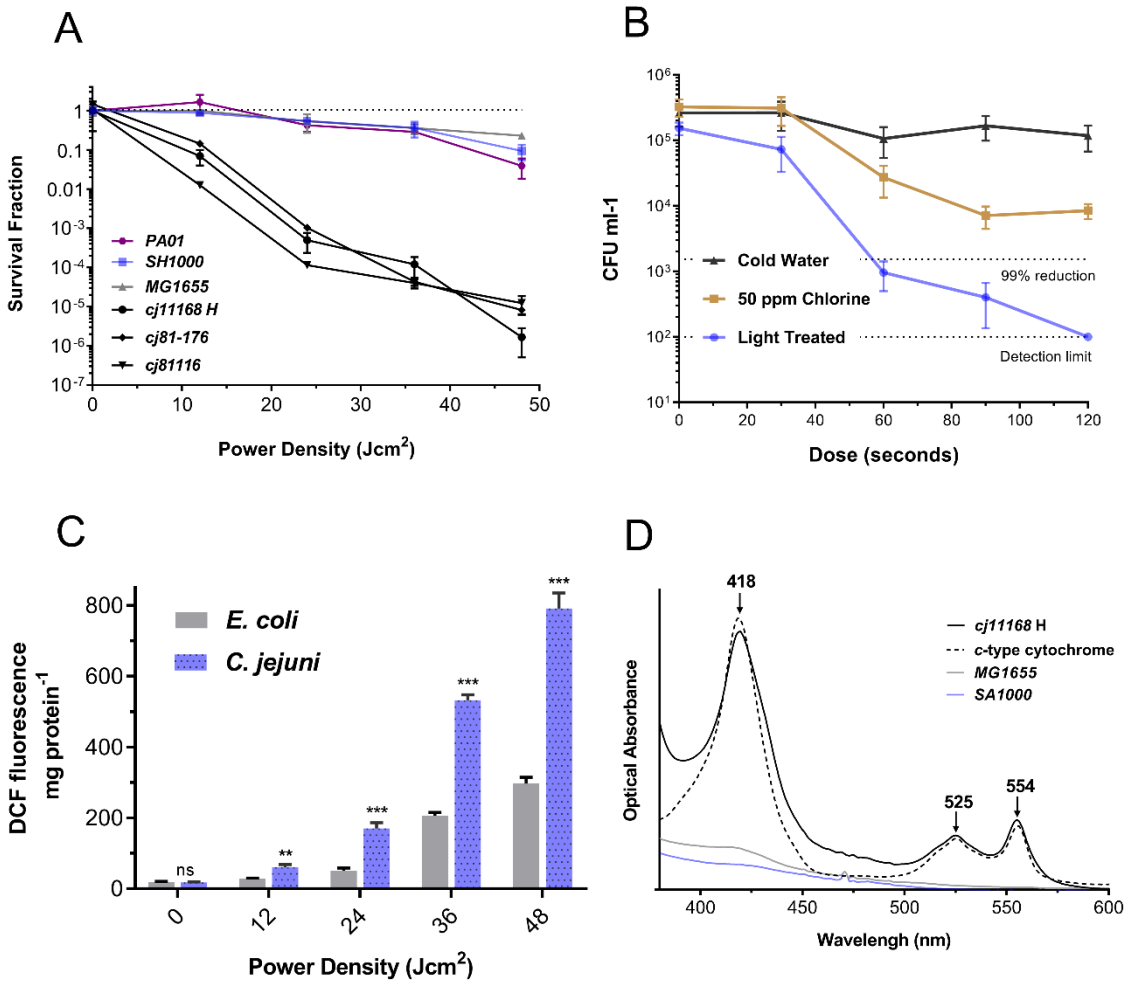

Figure 1 (A) Comparison of photoinactivation using 405 nm laser light of *C. jejuni* 11168H, *S. aureus* SH1000, *E. coli* MG1655 *P. aeruginosa* PA01 grown in liquid medium as described in the experimental procedures. Values are means of three independent experiments and bars are standard errors. (B) Viability changes of *C. jejuni* on the surface of chicken skin after exposure to either cold water, 50 ppm chlorine or 405 nm light over a period of 2 minutes. Values are means of three independent experiments and bars are standard errors. (C) Comparison of ROS accumulation in *C. jejuni* and *E. coli* after photoinactivation with 405 nm laser light. Bacteria were loaded with 10 µM DCFDA and exposed to 405 nm light for varied doses before fluorescence was measured. Background fluorescence was subtracted from each value shown. DCFDA was exposed to 405 nm light in buffer alone but no fluorescence increase was detected. Values are means of three independent replicates and bars are standard errors. Significant differences are shown between *C. jejuni* and *E. coli* samples as either **P≤ 0.01 or ***P≤ 0.001 or ns for no significance. (D) Dithionite-reduced minus ascorbate oxidised whole cell difference spectra of *C. jejuni* 11168H (black spectrum), *E. coli* MG1655 (grey spectrum), *S. aureus* SH1000 (blue spectrum), and purified *Campylobacter* CccA (*cj1153c*) c-type cytochrome (dotted spectrum). Cells were grown in liquid medium to mid-log growth phase and resuspended in sodium phosphate buffer (1 mg ml^{-1} total protein). Soret (418 nm), beta- (525 nm) and alpha- (554 nm) bands are arrowed.

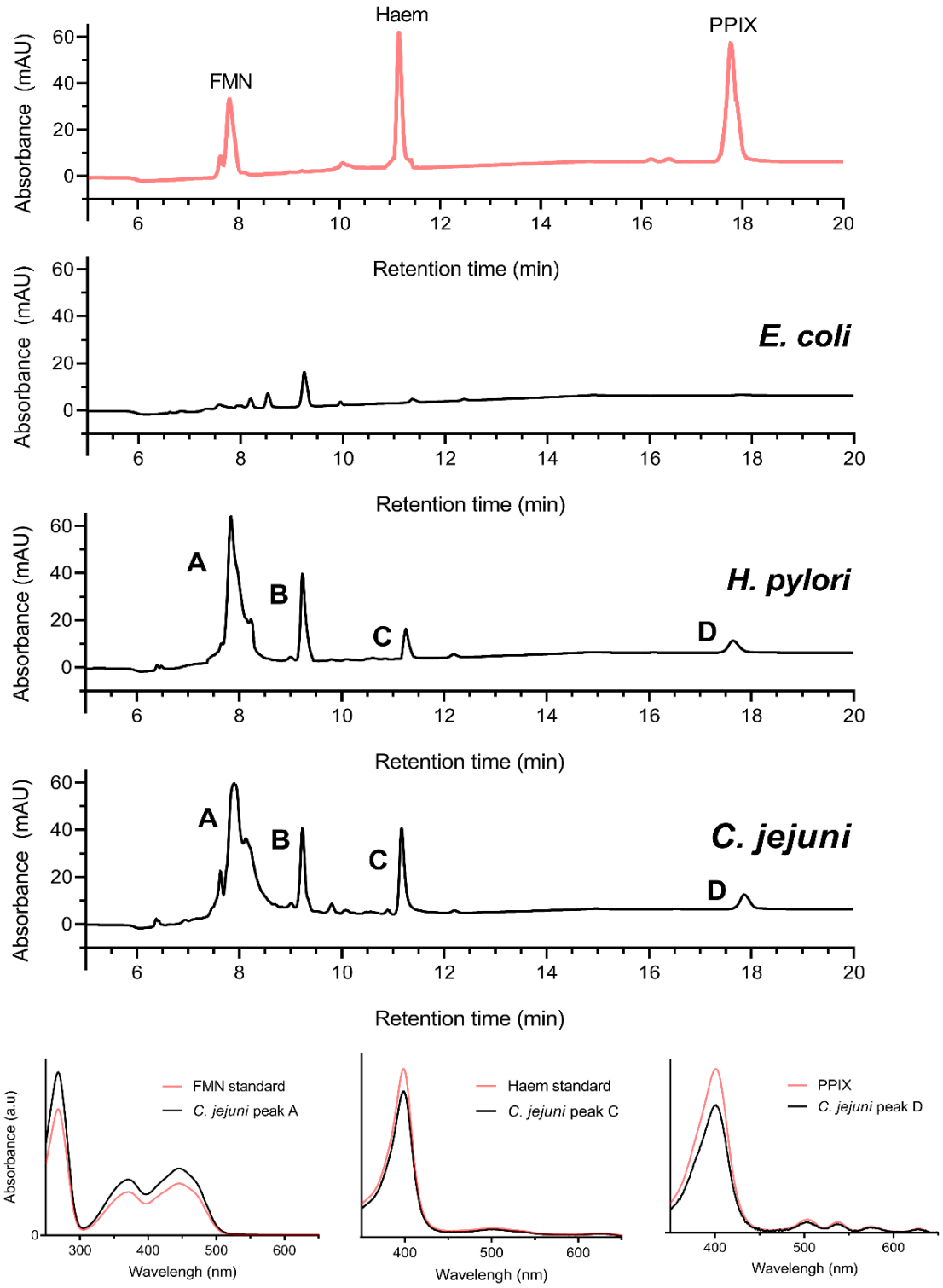

Figure 2 Top HPLC trace in red shows chromatographic analyses of the three standards FMN, haem and PPIX dissolved in 6M formic. The three black chromatograms show pigment extracts from *E. coli, H. pylori* and *C. jejuni* with pigments detected by the absorption at 405 nm. Samples were normalised based on protein concentration before pigments were extracted using acidified methanol and subject to reverse phase HPLC analysis.

.

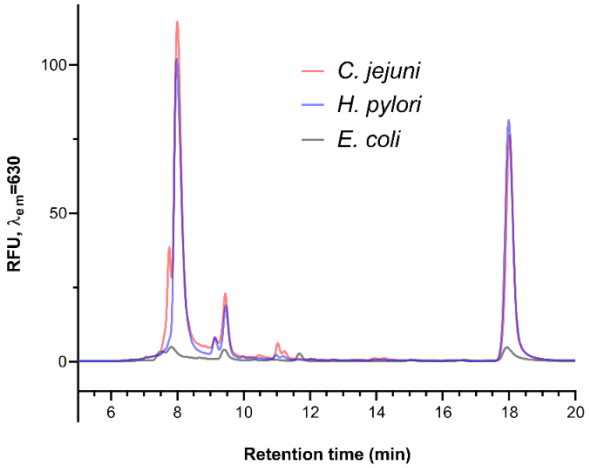

Figure 3 HPLC pigment analysis of *C. jejuni, H. pylori, S. aureus* and *E. coli* extracts scanning for species with an emission intensity at 630 nm after excitation at 405 nm. Samples were normalised based on protein concentration before pigments were extracted using acidified methanol extraction and subject to reverse phase HPLC analysis.

Flavin and protoporphrin IX are the major photoactive species in *C. jejuni*

We compared the composition of potential violet-blue light absorbing photosensitisers in *C. jejuni* with those extracted from *H. pylori*, a closely related epsilonproteobacterium previously shown to excrete porphyrin and *E. coli*. Pigment extracts were analysed by reverse phase HPLC with absorbance detection at 405 nm (Figure 2). The *C. jejuni* chromatogram showed 4 distinct peaks with retention times that match those extracted from the closely related *H. pylori.* Peak retention times and UV-VIS absorbance spectra of peaks A, C and D closely corresponded to those of flavin mononucleotide (FMN), haem B and protoporphyrin XI (PPIX) standards respectively. The absorption spectrum of peak B could not be matched against any known standards and remains unidentified. The chromatogram from *E. coli* showed a much lower abundance of 405 nm absorbing chromophores compared to *C. jejuni* or *H. pylori*. Porphyrins and flavins fluoresce strongly in the red region of the spectrum when excited by blue light. Therefore, the fluorescence emission intensities of the HPLC eluates at 635 nm were compared, with excitation at 405 nm (Figure 3). The two largest emission peaks detected in *C. jejuni* and *H. pylori* correspond to FMN and PPIX (Figure 3). The

abundant peak C identified in *C. jejuni* extracts which matches the haem B standard is likely dissociated haem from the abundant periplasmic *c*-type cytochromes. By comparison, the *E. coli* chromatogram shows only a small peak of fluorescence at 18 min, corresponding to PPIX.

_c_-type cytochromes are targets of photo-oxidative damage in intact cells

Although unable to carry out the primary photochemistry to generate ROS, the particular abundance of *c*-type cytochromes in the periplasm of *C. jejuni* does present a possible target for photo-oxidative damage. Heme is ligated to apocytochromes *c* through a CXXCH attachment motif, and the Cys-heme thioether bonds are sensitive to oxidation. Therefore, the effect of violet-blue light on the integrity of periplasmic *c*-type cytochromes was investigated by exposing intact cells to 405 nm light at increasing doses. Reduced minus oxidised absorbance spectra of *C. jejuni* periplasmic extracts made from these cells (Figure 4A) showed a dose dependent decrease in the intensity of the *c*-type cytochrome Soret absorption peak (418 nm), beta peak (525 nm) and alpha peak (554 nm) after exposure to 405 nm light. Absorbance spectra of purified CccA (*cj1153*), the most abundant *c*-type cytochrome in *C. jejuni* and the major contributor to the intact cell spectrum (ref), before and after a 21 J cm^{-2} 405 nm light dose showed there was no reduction in the intensity of the 418 nm Soret peak, suggesting periplasmic *c*-type cytochromes are not intrinsically light sensitive (Figure 4B). In contrast, when CccA was treated with 10 mM hydrogen peroxide, there was a large reduction in the intensity of the 418 nm Soret absorption peak, due to dissociation of the heme. These controls support the conclusion that the reduction in the cytochrome absorbance in *C. jejuni* cells is specifically due to photo-oxidative damage. Heme blots of SDS-PAGE gels of the *C. jejuni* periplasmic extracts show a dose dependant decrease in the intensity of heme-reactive bands following 405 nm light treatment, particularly in the case of the most abundant periplasmic cytochromes CccA and CccC (Figure 4C). Taken together, the data suggest that during illumination,

sufficient ROS is generated in the periplasm to oxidise cytcohrome *c* Cys-heme bonds, releasing the heme.

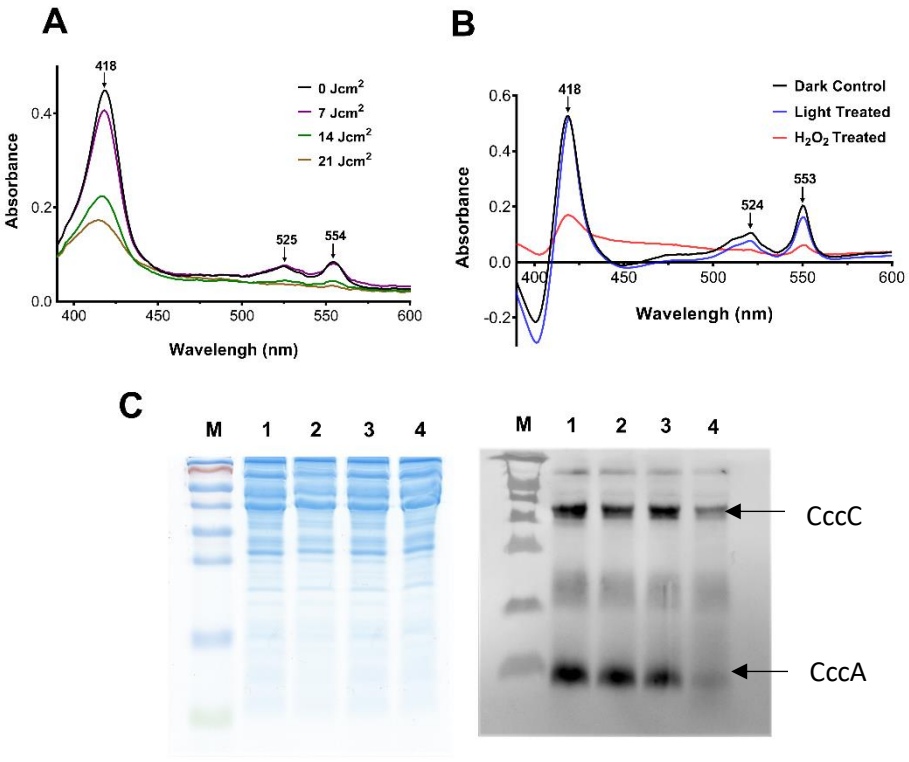

Figure 4. (A) The UV-vis absorbance spectra of *C. jejuni* periplasmic extract (1 mg ml^{-1} protein) after varied doses of 405 nm light. The cytochrome *c* Soret (418 nm), beta- (525 nm) and alpha- (554 nm) bands are arrowed. (B) The UV-vis dithionite reduced minus ascorbate oxidised absorbance spectra of purified *C. jejuni* CccA (*cj1153c) c*-type cytochrome in sodium phosphate buffer before and after 21 J cm^{-2} 405 nm light treatment (blue line) or 10 mM hydrogen peroxide treatment (red line). (C) 15% SDS-PAGE gel of periplasmic proteins (15 µg per lane) from cells grown in Brucella Broth were exposed to varied doses of 405 nm light. Left panel: stained by Coomassie blue. Right panel: haem blot (30 seconds exposure). Lane M, pre-stained protein markers; lane 1, wild-type 0 J cm^{-2}; lane 2, wild-type 7 J cm^{-2}, lane 3, wild-type 14 J cm^{-2}, lane 4, wild-type 21 J cm^{-2}. The positions of CccA and CccC (identified by their mass) are indicated by arrows.

Key iron-sulphur cluster enzymes are inactivated upon exposure to violet-blue light

Unlike most aerobic bacteria, microaerophilic campylobacters including *C. jejuni* do not utilise 2-oxoacid dehydrogenases for the oxidative decarboxylation of pyruvate and 2-oxoglutarate to their respective acyl-CoA derivatives but instead rely on the iron-sulphur cluster containing 2-oxoacid: acceptor oxidoreductases (Figure 5A). These key enzymes are highly vulnerable to oxidative damage [15]. We investigated whether light generated ROS could damage these enzymes *in vivo*, by measuring the activity of both pyruvate:acceptor oxidoreductase (Por) and 2-oxoglutarate:acceptor oxidoreductase (Oor). Three light doses were selected to assess photooxidative damage to Por and Oor in *C. jejuni.* A sublethal dose which elevated intracellular ROS levels, prevented bacterial growth but did not induce killing, a bactericidal dose which induced greater intracellular ROS levels and induced 1 $\log_{10}$ CFU reduction, and a more lethal dose which induced a >2 $\log_{10}$ CFU reduction and caused a large increase in ROS (Figure 5B, 5C). A 62% reduction in activity of Por (0.75 ± 0.11 versus 0.28 ± 0.07 μmol $min^{-1}mg^{-1}$ protein) and a 58% reduction in Oor (0.23 ± 0.05 versus 0.095 ± 0.008 μmol $min^{-1}mg^{-1}$ protein) following a sublethal light dose of 7 J cm^{-2} and a complete loss of activity in both enzymes after a lethal dose of 21 J cm^{-2} was observed (Figure 5D).

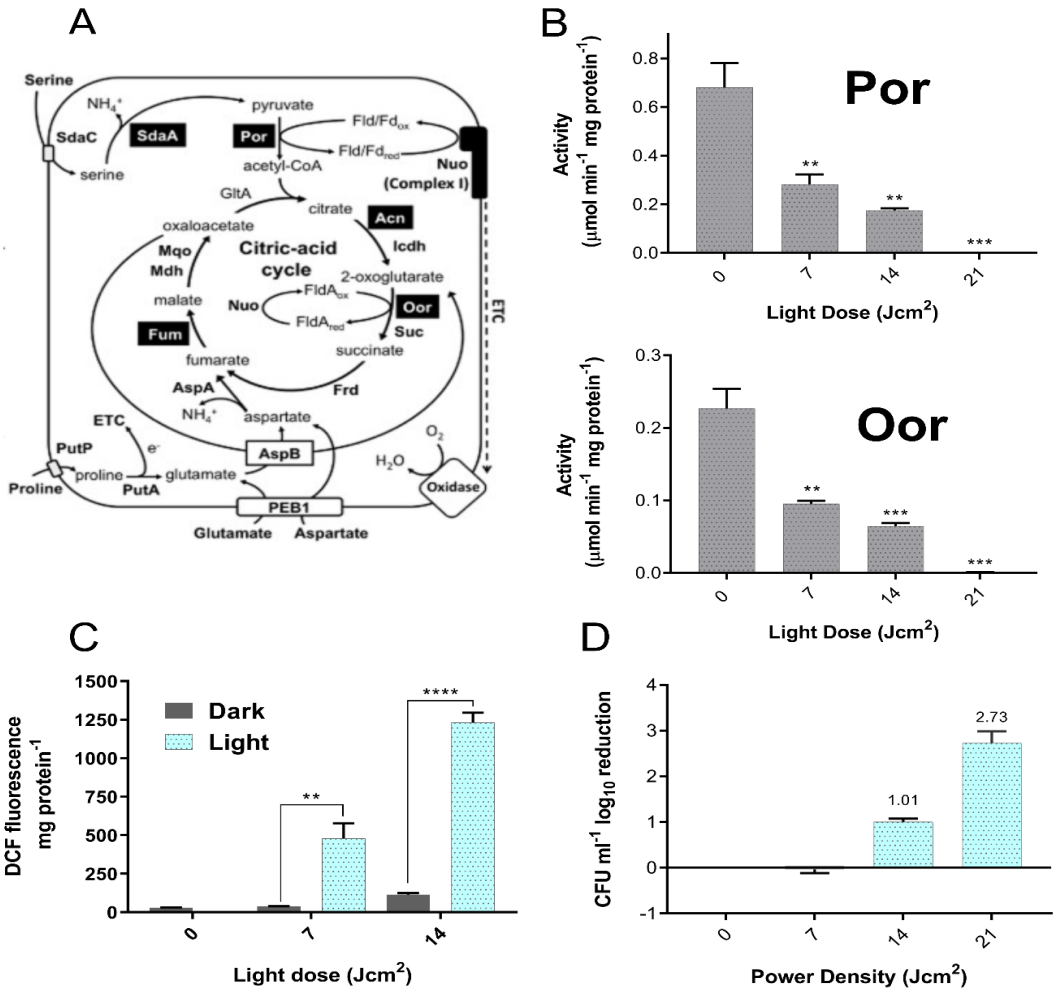

Figure 5. (A) Central carbon metabolism of *C. jejuni* taken from Kendall et al[15]. The key enzymes are shown next to the reaction they catalyse. Fe-S cluster enzymes are highlighted in black text boxes. Key: SdaC, serine transporter; SdaA, serine dehydratase; Por, pyruvate:acceptor oxidoreductase; GltA, citrate synthase; Acn, aconitase; Icdh, isocitrate dehydrogenase; Nuo, flavodoxin/ferredoxin: quinone oxidorectase; Mqo, malate:quinone oxidoreductase; Mdh, malate dehydrogenase; Oor, 2-oxoglutarate:acceptor oxidoreductase; Suc, succinyl-CoA synthetase; Fum, fumarase; Frd, fumarate reductase [Note: in *C. jejuni* there is no succinate dehydrogenase and the type B fumarate reductase is bi-directional[19]; (B) Activities of key iron sulphur cluster enzymes, Por, pyruvate:acceptor oxidoreductase and Oor, 2-oxoglutarate:acceptor oxidoreductase in anaerobic cell-free extracts prepared from mid-log *C. jejuni* cells. Cells were exposed to 405 nm light in 6-well plates at varied light doses (J cm^{-2}) before cells were lysed and enzyme activities were measured as described in *Experimental procedures.* (C) The histograms represent the mean activities from three independent cultures, with error bars showing standard deviation. Significant differences are shown as either $^{**}P \leq 0.01$ or $^{***}P \leq 0.001$. C. $\log_{10}$ CFU reduction in *C. jejuni* 11168H after exposure to increasing doses of 405 nm light (irradiance 28 mW cm^2). (D) Comparison of ROS accumulation in *C. jejuni* after photoinactivation with 405 nm laser light. Bacteria were loaded with 10 µM DCFDA and exposed to 405 nm light for varied doses before fluorescence was measured. Background fluorescence was subtracted from each value shown. DCFDA was exposed to 405 nm light in buffer alone but no fluorescence increase was detected. Values are means of three independent replicates and bars are standard errors. Significant differences are shown between dark and light treated samples as either **P≤ 0.01 or ***P≤ 0.001 or ns for no significance.

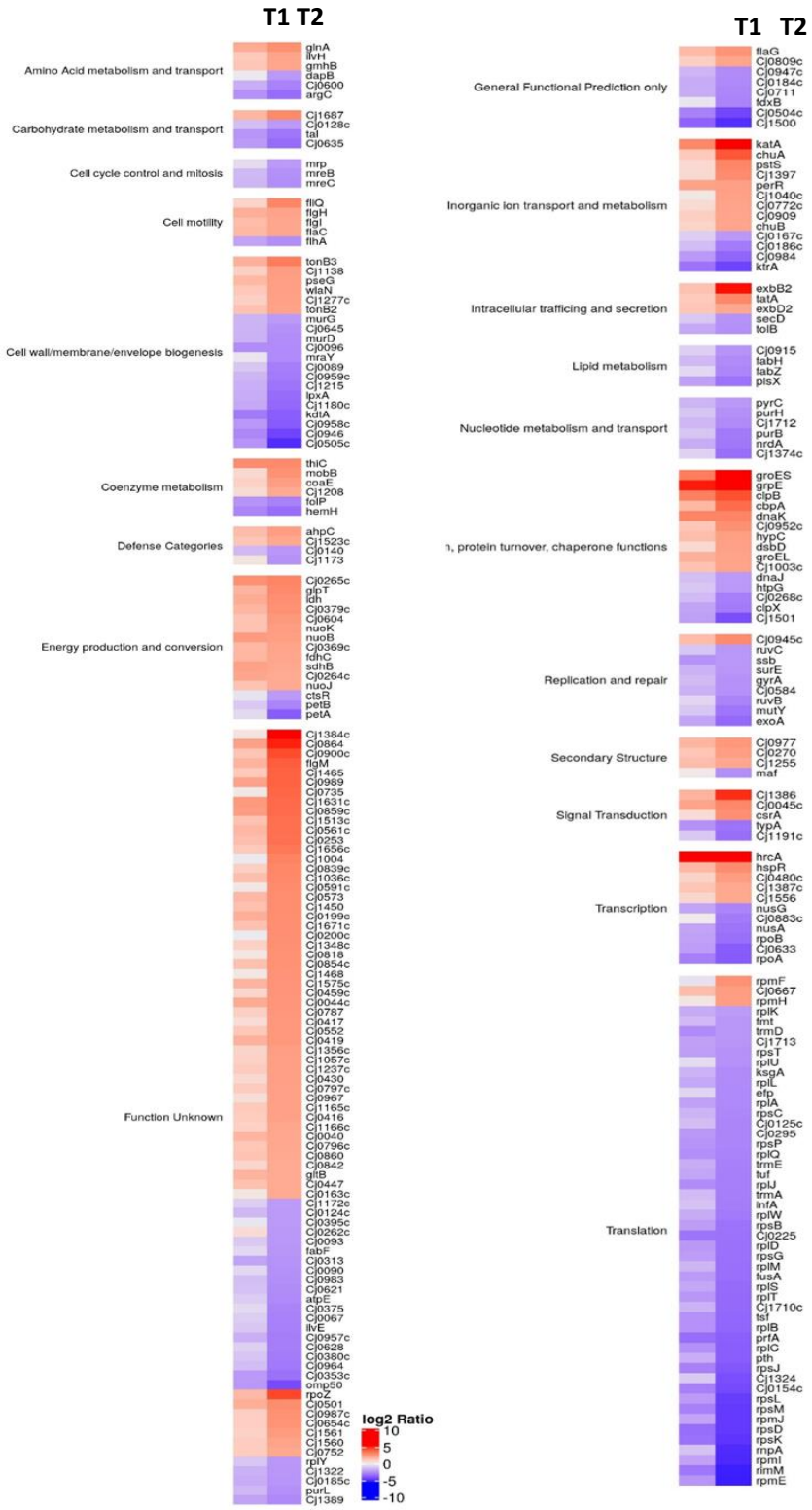

Figure 6. A. Global view of gene expression changes after exposure to a bacteriostatic light dose (T1) for 15 minutes, 7 J cm^{-2} and the bactericidal dose (T2) for 30 minutes, 14 J cm^{-2}. Genes are grouped by functional categories according to the Sanger Center *C. jejuni* genome database. Only genes with a significant fold change ≥ ±2 log_2 are plotted. Each row represents one gene and each column represents the expression profile at each timepoint (the mean fold change in expression ratio of the technical replicates). An increasing red intensity denotes a gene for which expression is significantly increased compared with T0 and increasing blue intensity indicates a gene which expression was significantly decreased compared with T0.

Transcriptome analysis reveals that that *C. jejuni* has a two-stage response to violet-blue light

In order to assess global gene expression changes in response to photooxidative stress induced by exposure to 405 nm VB light, the transcriptome profile of *C. jejuni* NCTC1168H was investigated by RNAseq using Illumina sequencing of cDNA libraries prepared from mRNA extracted from cells treated with bacteriostatic (15 min exposure, 7 J cm^{-2}) and bactericidal (30 min exposure, 14 J cm^{-2}) doses of 405 nm light, as used in Figure 6. As shown in Figure 5C, these doses progressively elevated intracellular ROS levels as measured by DCFDA fluorescence. The full dataset is shown in Supporting Information Table 1. Genes that were changed in expression ≥ 4-fold with a false discovery rate adjusted p-value ≤ 0.05 compared to a dark control at time 0 are shown in Figure 6.

Under bacteriostatic photooxidative stress at the 15 min time-point, the most striking upregulation was observed for several genes encoding proteins involved in the cellular response to global protein damage, including the chaperone encoding genes *grpE, groES, groEL, clpB, dnaK* and their associated transcriptional regulators *hrcA* and to a lesser extent *hspR*, as shown in Figure 6. The expression of *grpE, groES, groEL* and *clpB* continued to increase at 30 min exposure, joined by *cbpA* (encoding a DnaJ-like protein).

At 30 min, when more ROS has accumulated and the light dose becomes bactericidal, by far the largest gene expression increase was seen for *cj1384c* (log_2FC= 8.46; 352-fold), encoding a protein of unknown function that is part of a small gene cluster also containing the *katA* gene for the peroxide degrading enzyme catalase (*cj1385*) and an ankyrin repeat protein encoding gene *cj1386*, that has been shown to function in heme trafficking to KatA. These genes were both also much more highly expressed at the 30 min time-point compared to15 min. Other genes encoding known oxidative stress protective proteins were also found to increase in expression from the first to the

second time-point (e.g. *ahpC, rrc*) but to a lesser extent compared to *katA*. Amongst some other notable genes increasing in expression under VB-light were *cj0864* (*dsbA2*), *dsbB* and *dsbD*, involved in the periplasmic disulfide bond system and *exbB2/exbD2/tonB2/tonB3*, encoding proteins transducing energy from the inner membrane to the outer membrane for TonB dependent uptake systems. In addition, *csrA*, controlling the translation of many key metabolic and stress related proteins in *C. jejuni* was also up-regulated. Many other genes of currently unknown function were also upregulated. As expected, the major classes of genes that were down-regulated upon VB-light exposure, particularly at the 30 min (bactericidal) time-point were those associated with cell growth and the cell-cycle, including protein translation, cell wall and envelope biogenesis, lipid metabolism and also DNA synthesis.

Analysis of transcription factor activity underlying the gene expression changes by probabilistic modelling

To investigate the transcriptional regulation driving the differential gene expression observed we employed a probabilistic modeling tool (TFInfer) for genome-wide inference of transcription factor (TF) activities from transcriptomic data[23]. TFInfer is a state space model that uses a binary connectivity matrix linking genes to TFs with changes in gene expression. Gaussian prior distributions are placed over each TF activity and then a factorized variational approximation is applied to infer the posterior distributions of TF activities that account for the observed changes in gene expression. A connectivity matrix was first constructed based on the known and putative *C. jejuni* transcription factors. Genes controlled directly or indirectly by these regulators were obtained by literature searches. For 18 putative transcription factors (CbrR; Cj0258; Cj0394; Cj0422; Cj0480; Cj0571; Cj0883; Cj1036; Cj1042; Cj1172, Cj1227; Cj1410; Cj1491; Cj1505; Cj1533; Cj1561; Cj1563, Cj1608) the complete composition of their regulons was not known at the time of writing, although phenotypic analysis of mutants

has been carried out in several cases. Elimination of these putative transcription factors left 19 transcription regulators in the connectivity matrix Supplementary Figure 2, which was used to facilitate inference of the changes in transcription factor activities that underpinned the expression profiles of 1592 genes after exposure to low and then high intensity blue light (transcript abundance being normalized to those of cultures grown in the dark). According to TFInfer, eight of the 19 transcription factors did not respond to blue light (Cj0440, Cj1387(HeuR), Cj1546(RrpA), CosR, CprR, HrcA, ModE and NssR). For those that were predicted to respond, three patterns were evident in Supplementary Figure 2, (i) a rapid and sustained change in activity at low and high doses of VB-light; (ii) a higher response at the high compared to low light dose and (iii) a change in response only at the high light dose. The strongest response at 7 J cm^{-2} (bacteriostatic light dose) was predicted for the repressor HspR. HspR activity decreased, which explains the large increase in the expression of several protein chaperone genes controlled by it, including *grpE*, *clpB, dnaK, groEL* and *groES*[24], suggesting that protein damage is a consequence of the initial exposure to low intensity blue light. The expression of groES and groEL is also controlled by HrcA and although HrcA activity was not predicted to change by TFInfer, *hrcA* gene expression was the highest of all genes after 7 J cm^{-2} VB-light exposure. CmeR (resistance to bile salts), FhlA (motility and virulence), FlgR (flagella biosynthesis), Fur (iron-homeostasis), PerR (oxidative stress), PhoR (phosphate) and RacR (central and respiratory metabolism) also responded at 15 min exposure to blue light but their responses were amplified at the 30 min time-point. The strong PerR and Fur responses are consistent with the observed regulatory pattern of *katA* and *cj1386*, while *cj1384c* has previously been shown to be regulated by Fur. Interestingly, there are two MarR type oxidative stress regulators in *C. jejuni* but only RrpB (Cj1556) and not RrpA (Cj1546) showed a significant blue-light response. Importantly, RrpB regulates *katA, perR* and *hspR* expression. Finally, DccR only responded after exposure to high intensity blue light at

the 30 min time-point. DccR is important for colonisation of mice and controls the expression of several genes encoding extra-cytoplasmic proteins.

These inferred changes in transcription factor activities suggest a complex, multi-phasic response to blue light, illustrated in Supplementary Figure 2 for genes upregulated 4-fold or more, in which the initial low intensity exposure invokes a response to protein damage/mis-folding, mediated by HspR, followed by an increasingly strong oxidative stress response and changes to the extra-cytoplasmic proteome, when the light intensity was increased.

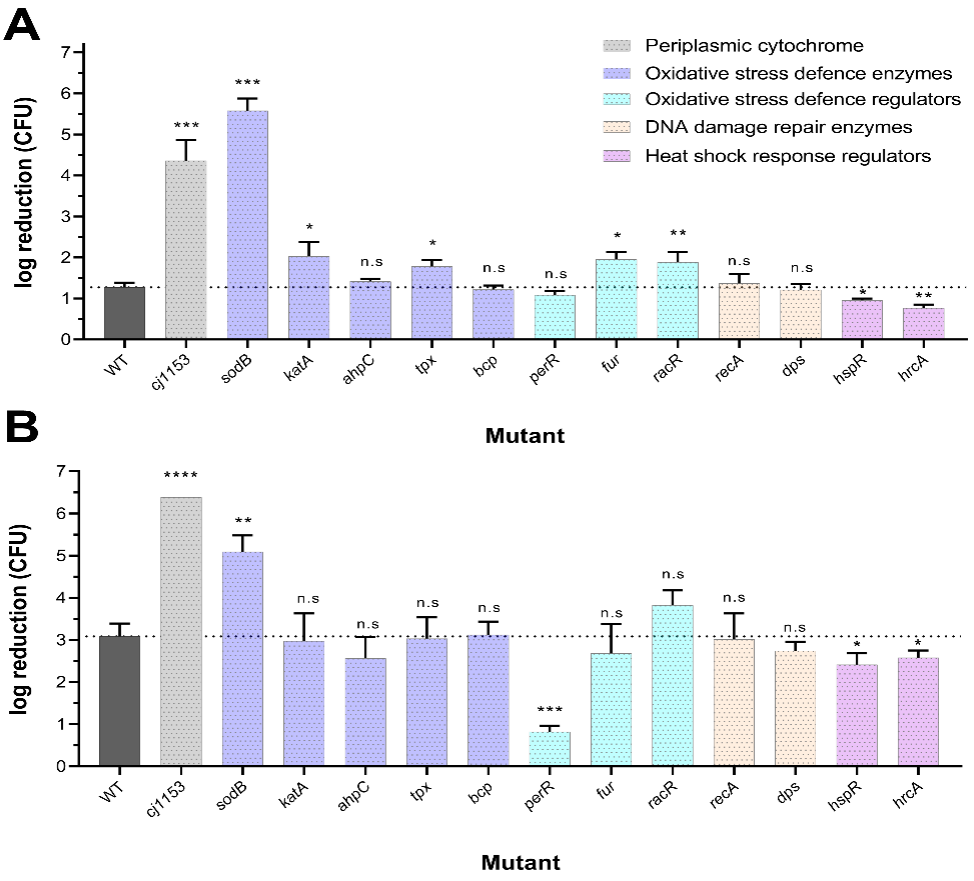

Figure 7 Photodynamic inactivation of *C. jejuni* stress defence mutants after either 12 J cm^{-2} (A) or 24 J cm^{-2} (B) 405 nm light exposed for 20 minutes. Cells were resuspended in sodium phosphate buffer to an OD_{600} 0.1. Results show log reduction means after 20 minutes light exposure (*n* = 9). Dotted line shows WT log reduction as reference. All mutants were resuspended to a similar starting CFU shown in Supplementary Figure 3. Significant differences calculated by student t test shown as either *P ≤ 0.05, **P ≤ 0.01 or ***P ≤ 0.001.

Susceptibility of deletion mutants to VB-light highlights key proteins involved in photo-oxidative stress defence

To determine if some of the significant genes identified from the RNAseq analysis are important in defence against VB-light, the effect of illumination on the viability of deletion mutants in several stress defence enzymes and key regulators (*katA, ahpC, perR, fur, racR, hspR, hrcA*) was investigated. We also constructed mutants in other genes that were not regulated by VB-light according to our data but which we hypothesised might play a role in the response (*sodB, tpx, bcp, cj1153, recA, dps*). Despite repeated attempts, it was not possible to obtain a deletion mutant in the *cj1384c* gene.

The genes encoding the upregulated protein chaperones GroEL/ES and ClpB are known to be essential in *C. jejuni*, but knockout mutations of the heat shock response regulators *hrcA* and *hspR* were successfully constructed. qRT-PCR analysis showed that deletion of *hrcA* resulted in a 25-fold increase in *groEL* expression compared to the wild type strain. Deletion of *hspR* increased expression of *groEL* 18-fold and *grpE* 53-fold when compared to the wild type strain (Supplementary Figure 1). This might be predicted to enhance survival under VB-light, and both the *hrcA* and *hspR* mutants showed a slight but significant decrease in susceptibility compared to WT after a 12 J cm^{-2} light dose shown in Figure 7.

Of genes involved in oxidative stress defence, deletion of the superoxide dismutase gene *sodB* resulted in the most striking phenotype, with ~5.6 and ~5.0 log10 reductions in viability at X and Y respectively, compared to ~1.25 log10 for the WT. The picture was different for genes involved in peroxide defence; of the mutants lacking one of the peroxide degrading thiol peroxidase enzymes AhpC, Tpx or Bcp, only the *tpx* mutant showed a slightly more susceptible phenotype at X, which may be due to a degree of redundancy in the function of these enzymes. A catalase (*katA*) mutant was also slightly more susceptible than WT at X. A peroxide-sensing regulator (*perR)* mutant

was found to be significantly more resistant to VB-light than WT (consistent with the role of PerR as a repressor of several oxidative stress defence genes), but this was only apparent at the higher light dose used here in Figure 7. Taken together, these results suggest superoxide defence is important at all light doses that induce ROS formation but peroxide stress defence might assume greater importance at higher intracellular ROS levels. Deleting genes associated with DNA repair or protection (*recA* and *dps*) had no significant effect on VB-light sensitivity. The hypothetical genes *cj0737* and *cj0045* identified as being significantly upregulated in the RNAseq showed no significant differences in the log reduction to WT when deleted.

Finally, the evidence presented in Figure 7 suggested that the periplasmic c-type cytochrome CccA (c*j1153*) is a target for photo-oxidative damage and our previous work has shown that a *cj1153* mutant has increased intracelluar ROS levels. In Figure 7 it is clear that this mutant is highly susceptible to VB-light at both 12 and 24 J cm^2. Possible reasons for this phenotype are considered in the discussion.

Discussion

Photodynamic inactivation is clearly an effective method to kill *Campylobacter* spp., yet the factors which dictate the susceptibility of these bacteria were not previously understood. We have shown that PDI can effectively remove *Campylobacter* from the surface of chicken skin, with CFU reductions much greater than chlorine treatment. Given the current interest in chlorine treated meats and the prevalence of *Campylobacter* in the food chain, this study was designed to uncover why *C. jejuni* is more susceptible than other pathogens and to characterise the global bacterial response to photooxidative stress.

In this study we have shown in whole cell spectra of *Campylobacter* extracts there is a strong absorption peak at 418 nm, which is not present in other non-light sensitive bacteria. We propose that this peak is due the abundance of soluble or membrane associated *c*-type cytochromes, due to the alignment of the Soret, -beta and -alpha bands in the dithionite reduced spectra with purified CccA, the most abundant periplasmic *c*-type cytochrome[16]. The presence of *c*-type cytochromes in the periplasm is not a feature exclusive to *Campylobacters*, though it is thought their abundance reflects the complex and highly branched electron transport chain of this bacterium. This greater abundance of *c*-type cytochromes in the periplasm will most likely require a higher rate of haem biosynthesis to feed the *c*-type cytochrome biosynthetic pathway. As *Campylobacters* lack a siderophore based haem acquisition system, haem attached to apocytochromes have to be synthesised intracellularly, which could result in a greater abundance of photoactive porphyrin intermediates. HPLC analysis shows *Campylobacter* has a greater abundance of the photosensitiser PPIX than non-light sensitive bacteria which will contribute to the increased sensitivity to 405 nm light.

Another photosensitiser identified in both *Campylobacter* and *Helicobacter* extracts was the enzyme cofactor flavin mononucleotide FMN. Previous studies have shown FMN can be a potent photosensitiser with a singlet oxygen quantum yield of ($\Phi\Delta$ =

0.51 ± 0.07)[20]. The increased abundance of FMN in both *Helicobacter* and *Campylobacter* comes from the use of flavodoxin and not NADH as an electron donor to the citric acid cycle. Both bacteria contain a single flavodoxin, FldA that is the electron carrier for Por and Oor and has a bound FMN cofactor. These unique physiological differences between *Campylobacter* spp. and other non-light sensitive bacteria would typically have little effect on fitness, but when combined with photodynamic treatment, we begin to see largescale differences between the susceptibility of these bacteria.

We have shown that *C. jejuni* has a much greater abundance of endogenous photosensitisers than other non-light sensitive bacteria, yet DCFDA fluorescence analysis shows light induced ROS increase also occurs in *E. coli* without significant reductions in CFU. The increased sensitivity in *C. jejuni* is not a result of deficiencies in the oxidative stress defences, as it has a full complement of oxidative stress defence enzymes. However, *C. jejuni* does utilise multiple oxygen sensitive respiratory complexes, which are highly sensitive to ROS damage. Enzyme kinetics of the iron sulphur cluster containing 2-oxoacid acceptor oxidoreductases Por and Oor in Figure 5, show a sharp reduction in activity after PDI, which will contribute to a significant shutdown of the citric acid cycle, starving the electron transport chain. The loss of an active citric acid cycle would not typically result in large CFU reductions in other bacteria, but as *Campylobacter* lacks the classical Embden-Meyerhof-Parnas glycolytic pathway, it loses its main source of electrons to the electron transport chain.

Another differentiating feature that was not previously associated with an increased sensitivity to reactive oxidants is the abundance of periplasmic *c*-type cytochromes in *C. jejuni.* Analysis of the cell free extracts after photooxidative stress shows a sharp reduction in the intensity of the 410 nm Soret peak associated with periplasmic *c*-type cytochromes. The periplasmic *c*-type cytochromes were studied by haem blotting of washed membrane preparations, which showed a decrease in the intensity of the haem

signals associated with the most abundant periplasmic cytochromes CccA and CccC. As the apo cytochrome is bound to haem by the highly oxidizable CXXCH sequence motif, light induced ROS accumulation can inhibit haem ligation to cytochromes in the periplasm, as well as damaging haem bound cytochrome *c,* which explains the decreases in the intensity of the haem bands. As CccA and CccC form the main electron carriers between the *bc*1 and the *cb*-type oxidase, there will be a sharp reduction in the activity of the electron transport chain which will greatly reduce bacterial viability.

After identifying the molecular targets that become inactivated during PDI, we investigated the transcriptional response to characterise the stress defence genes expressed to protect the ROS sensitive targets. We saw a sharp upregulation of the heat shock chaperone proteins *grpE* (logFC= 5.09), *groES* (logFC= 3.27) and *clpB* (logFC= 3.21) driven by a decrease in activity of the heat shock response repressors HrcA and HspR shown in Supplementary Figure 2. Given the preference of the two primary photosensitisers identified in *C. jejuni* to singlet oxygen generation (FMN $\Phi\Delta$ = 0.51 ± 0.07, PPIX $\Phi\Delta$ = 0.56 ± 0.07), it is likely that protein damage through oxidation and carbonylation will be the first PDI induced physiological effect, given the high reaction constant of singlet oxygen with proteins[20,21,25]. Previous reports in *E. coli* have shown the GroEL/ES chaperone complex are the most important heat shock response proteins in protecting against protein carbonylation, which explains their sharp upregulation[26]. When the light dose becomes bactericidal at the second timepoint, the largest gene expression changes are seen in the PerR regulated, uncharacterised gene *cj1384c* (logFC= 8.46) and the gene for the peroxide defence enzyme *katA* (logFC= 6.08) driven by a decreased repression by PerR. Despite multiple attempts to His tag purify or gene knockout *cj1384c,* no mutant vectors were successful in transformations, which only enables speculation about its function. Analysing the protein structure, it is possible that the small size of only 104 amino acids and the 7 exposed cysteine residues makes this protein a prime singlet oxygen scavenging

protein, which can be highly expressed to quench intracellular singlet oxygen, which cannot be detoxified enzymatically.

The mutant analysis of the other oxidative stress defence enzymes might also suggest a role for *cj1384c* in photooxidative stress defence. Mutations to the peroxide regulator *perR*, give rise to the largest resistance phenotype to PDI, yet mutations in the key peroxide defence enzymes regulated by *perR* (*katA, ahpC, tpx, bcp*) do not show a significant increase in sensitivity shown in Figure 7. Previous reports have shown *cj1384c* is regulated by both PerR and RacRS suggesting a role for *cj1384c* in oxidative stress defence[27,28]. It may be the case that the significant decrease in susceptibility of the *perR* mutant to PDI is driven by a very large upregulation of the proposed singlet oxygen quencher, *cj1384c*. Mutant analysis also highlights the role of the heat shock response regulon in defence against early stage PDI, with the heat shock regulator mutants *hrcA* and *hspR* both showing a significantly lower log reduction than WT after 12 J cm^{-2} 405 nm light. Knockout mutation of the sole superoxide defence enzyme SodB resulted in a large increase in sensitivity to PDI after a low dose of 12 J cm^{-2} as reported previously[29]. Interestingly, the periplasmic *c*-type cytochrome mutant *cj1153* showed a significant increase in susceptibility compared with WT with >3 log difference seen between WT and the *cj1153* mutant after 12 J cm^{-2} 405 nm light treatment. Previous studies have shown that the deletion of *cj1153* causes an increase in periplasmic ROS, due to the leakage of electrons from the bc_1 complex. This causes a loss of all periplasmic *c*-type cytochromes as the bacteria can no longer form the thioester bond required to covalently attach haem to the apocytochrome at the CXXCH motif[16]. As membrane associated PPIX has been shown to be a primary endogenous photosensitiser in *C. jejuni,* it is possible that photoexcitation of PPIX at the membrane causes an efflux of ROS to the periplasm, which overwhelms the already oxidatively stressed *cj1153* mutant, causing a dissociation of haem from apocytochromes.

In summary, this study is the first to outline the bacterial transcriptional response to photooxidative stress, which highlighted a two-pronged stress response to PDI. RNA sequencing identified uncharacterised genes which may play an important role in the defence against singlet oxygen radicals not recognised by the classical oxidative stress defence enzymes. Given the importance this technique could hold in reducing *Campylobacter* prevalence in the food chain, we have for the first time outlined the key components, unique to this microaerobic pathogen, which deem it innately susceptible to PDI.

Methods

Bacterial strains and growth conditions

C. jejuni strains were grown at 42 ^{o}C in microaerobic conditions (10% [v/v] O_2, 10% [v/v] CO_2 and 80% [v/v] N_2) in a MACS-VA500 Incubator (Don Whitley Scientific Ltd, UK). Typically, *C. jejuni* strains were grown on Columbia blood agar base (Oxoid) containing 5% lysed horse blood for 1-2 days. Liquid cultures of *C. jejuni* were routinely grown in Brucella broth (Oxoid) supplemented with 20 mM L-serine and 1% Tryptone (Oxoid) in 100 ml or 500 ml conical flasks respectively mixed by continuous orbital shaking at 140 rpm on a sea star orbital shaker. Cultures were supplemented antibiotics where appropriate: amphotericin-B (10 μg ml^{-1}), vancomycin (10 μg ml^{-1}), kanamycin (50 μg ml^{-1}) and chloramphenicol (20 μg ml^{-1}). Growth medium was pre-incubated in microaerobic atmosphere for 12 hours prior to inoculation with a microaerobically grown liquid starter culture or a day-old blood agar plate. For growth of *S. aureus, P. aeruginosa* and *E. coli,* strains were routinely cultured aerobically at 37^{o}C on LB broth or agar plates sterilised by autoclaving. Liquid cultures were shaken at 200 rpm. Cultures were grown to mid-log growth phase before samples were collected.

Light exposure viability assays

High intensity 405 nm light was produced by a Thorlabs' M405L3 mounted fibre-coupled LED with a nominal wavelength of 405 nm and a bandwidth of ~20 nm at full half width maximum. Power density (J cm^{-2}) was measured using a Thorlabs 5310C thermal power sensor 200 mm away from the light source at the position the sample cuvette is mounted. Light sensitivity experiments were carried out on mid-log bacterial broth culture resuspended in sodium phosphate buffer (20 mM pH 7.2) to an OD_{600} of 0.1. A 300 μl volume of bacterial suspension was pipetted into a 1 ml cuvette (Sarstedt) and exposed to 405 nm light at varying intensities for 30 minutes. Viability was calculated by counting the number of colony forming units (C.F.U) after appropriate

dilution on *Campylobacter* blood free selective agar (CCDA) or LB agar plates, counting their number per ml. The survival rate was calculated by dividing the C.F.U following illumination by the C.F.U at zero illumination.

Chicken skin viability assays

The method for *C. jejuni* enumeration on the surface of chicken skin was adapted from the Food Standards Agency (2015). Chicken leg-thigh pieces were purchased at a local retail market and were processed as follows: the chicken skin was removed from the leg-thigh pieces and 2.5 cm^2 medallions weighing approximately 500 mg were cut using a stainless steel coring tool. The skin medallions were washed with 70% ethanol then rinsed twice in sodium phosphate buffer (20 mM pH 7.2). For *C. jejuni* attachment, 1 ml of stationary phase *C. jejuni* culture (grown for 12 hours) was added to the centre of a sterile petri dish with the washed chicken skin placed directly on top. The skin was left for 30 seconds before the inoculated meat sections were transferred to a fresh petri dish and left for 30 minutes to allow for bacterial attachment. Once skin medallions were inoculated with *C. jejuni,* samples were either exposed to 405 nm light 5 cm away from the light source or placed in 50 ppm chlorine solution or ice-cold water. Once treated, samples were homogenised in 20 ml sodium phosphate buffer (20 mM pH 7.2) in a Potter pestle before the homogenised skin samples were serial diluted and plated onto CCDA agar plates. All samples were treated in triplicate with three technical replicates per triplicate.

Whole cell absorbance spectroscopy

Strains were grown to mid-log growth phase before harvesting by centrifugation (12,000 x g, 5 minutes). Cells were resuspended in sodium phosphate buffer (20 mM pH 7.2) to an OD_{600} 0.1. Absorbance spectra were obtained using an Olis CLARiTY UV/Vis spectrophotometer which uses an integrating cavity for measurements of turbid samples. Difference spectra were obtained by subtracting the sodium ascorbate oxidized (10 mM) from the dithionite reduced (10 mM) absorbance spectra.

Detecting reactive oxygen species

2',7'-Dichlorodihydrofluorescin diacetate (Sigma) was used to detect the production of ROS. The non-polar dye, DCFH-DA can be taken up and converted into the polar derivative DCFH by cellular esterases. DCFH is non fluorescent but is switched to highly fluorescent DCF upon oxidation by intracellular ROS such as hydrogen peroxide, hydroxyl, and peroxyl radicals. A stock solution of 2 mM (w/v) DCFH-DA in 1% DMSO was prepared and kept on ice. Mid log cells were resuspended in sodium phosphate buffer to an OD_{600} 0.1 were mixed with 10 µM (final concentration) DCFH-DA and illuminated for varied time periods. After illumination, cells were analysed using a Varian Carry Eclipse spectrophotometer (Varian) exciting at 485 nm and measuring emission at 530 nm. The protein abundance of cell extracts was determined using the Bradford Coomassie blue binding assay (Bio-Rad, Hemel Hempstead, UK) with DFC fluorescence was calculated per mg of protein.

Determination of intracellular porphyrin content by HPLC

The method for extraction and analysis of porphyrin species from bacteria developed by Fyrestam et al. (2015) was adapted for this study. After cell cultures were harvested by centrifugation, cell pellets were resuspended in Tris/EDTA buffer (5 mM Tris-HCl, 10 mM EDTA, pH 7.2) for 1 h in the dark. Formic acid was added at equal volume to precipitate proteins and lower pH. Cells were lysed by 3 x 20 seconds sonication in a with frequency of 16 amplitude microns using a Soniprep 150 ultrasonic disintegrator (SANYO) and centrifuged at 2500 g to pellet bacterial debris. The supernatant containing the porphyrins was loaded onto a pre-conditioned C18 SPE cartridge, washed with ammonium acetate, and eluted with acetone:formic acid 9:1(v/v). All porphyrins standards were obtained from Sigma and resuspended in 6 M formic acid. Samples were loaded on to an Agilent-1200 series HPLC system in conjunction with a Nova-Pak C18 reverse phase column (4 mm particle size, 3.9 mm 3 150 mm; Waters, USA). Reverse-phase HPLC was carried out using 350 mM ammonium acetate 30%

methanol as solvent A and 100% methanol as solvent B. Pigments were eluted with a linear gradient of solvent B (65–75%, 35 min) followed by 100% solvent B at a flow rate of 1 ml min^{-1} at 40°C. Pigment content was monitored by absorbance at 405 nm and fluorimetry (405 nm excitation and 635 nm emission).

Differential cytochrome *c* spectroscopy

C. jejuni cells grown from an overnight starter culture were harvested by centrifugation and resuspended in 200 ml BTS broth to an OD_{600} 0.1. Cell cultures were loaded into 6 well plates (Greiner), 8 ml per well, with one plate per condition. After growth to mid-log phase (OD_{600} 0.6), the T0 timepoint was taken and cells were exposed to 405 nm light with samples taken after 15 and 30 minutes light exposure (18 mW cm^2). Cells were then harvested by centrifugation and periplasmic extracts were prepared by osmotic shock by first resuspending gently in 2 ml STE buffer (20% sucrose, 20 mM Tris pH 8, 1 mM EDTA) and incubated at room temperature with gentle shaking for 30 minutes. Cells were centrifuged (12,000 x g, 5 minutes) and the supernatant was removed. The pellet was then resuspended in 2 ml of ice-cold 10 mM Tris-HCl (pH 8), incubated at 4ºC for 2 hours with gentle shaking at 15 r.p.m and centrifuged (12,000 x g, 20 minutes, 4ºC). The supernatant was collected, and protein concentration determined using the Bio-Rad Protein Assay Kit (BioRad). To determine the *c*-type cytochrome content in the periplasm, dithionite-reduced *minus* air oxidised difference spectroscopy was performed. The concentration of periplasmic extract was 1 mg ml^{-1} in a 1 ml volume per quartz cuvette. For analysis of oxidised *c*-type cytochromes absorbance spectra, purified cytochrome extract was treated with 10 mM hydrogen peroxide or 10 mM hypochlorite for 5 minutes at room temperature before spectroscopy was performed. Spectra were measured using a Shimadzu UV-2401 dual wavelength scanning spectrophotometer (Shimadzu) at room temperature. Reduced minus oxidised scans were carried out from 400 to 700 nm after the addition of sodium dithionite.

Detection of c-type cytochromes by enhanced chemiluminescence

Periplasmic protein samples were collected as described above. 1 mg ml^{-1} of periplasmic extract per condition were prepared by boiling for 2 minutes in an equal volume of sample buffer (60 mM Tris-HCl pH 6.8, 0.005% [w/v] bromophenol blue, 2% [w/v] SDS, 5% [v/v], 10% [w/v] glycerol, 5% β-mercaptoethanol). Samples were loaded into the gel with the prestained EZ-Run protein ladder (Bioline). The samples were separated by electrophoresis on a 15 % resolving gel initially at 90 V for 10 minutes to allow passage through the stacking gel followed by 180 V until the tracking dye had reached the bottom of the gel. Gels were stained with Coomassie brilliant blue (50% [(v/v) methanol, 10% [v/v] glacial acetic acid, 0.1% [w/v] Coomassie brilliant blue (Sigma-Aldrich)) and de-stained (50% [v/v] methanol, 10% [v/v] glacial acetic acid) until individual bands were visible. Samples were electroblotted from the SDS-PAGE gel to a nitrocellulose membrane. The membrane was then washed with 1X PBS for 5 minutes at room temperature to remove excess methanol and SDS and transferred into an exposure cassette (Amersham Biotech). Solution A and B of the enhanced chemiluminescence kit (ECL, GE healthcare) was mixed before adding onto the nitrocellulose membrane. The membrane was exposed for different time intervals on a ChemiDoc Gel Imaging System until the signal could easily visualised.

Pyruvate and 2-oxoglutarate: acceptor oxidoreductase enzyme activity

Cell cultures for anaerobic cell free extracts were prepared as above with either 0, 15, 30 or 60 minutes light exposure (18 mW cm^2). Cells were harvested by centrifugation and resuspended in 1 ml of nitrogen-sparged Tris-HCl buffer (0.1 M, pH 8), to which 0.5 ml of an oxygen-scavenging system [10% (w/v) glucose, 50 µg ml^{-1} glucose oxidase (Sigma, St. Louis, MO, USA), 10 µg ml^{-1} catalase (Sigma)] was then added. Cells were lysed by 3 x 20 s sonication with a frequency of 16 amplitude microns using a Soniprep 150 ultrasonic disintegrator (SANYO).Cell debris was removed by centrifugation (14,000 x g, 10 minutes) and the resulting cell free extract werestored at

4°C before enzyme rates were calculated. All enzyme assays were performed in a 1 ml total volume in stoppered quartz cuvettes (Hellma, Mullheim, Germany) using a Shimadzu UV-240 recording spectrophotometer (Shimadzu, Kyoto, Japan) with 20–100 µl of CFE per assay. The protein concentration of cell free extracts was determined using the Bradford Coomassie blue binding assay (Bio-Rad, Hemel Hempstead, UK). Por and Oor rates were measured by utilising the electrons produced during the conversion of 2-oxoacid to its acyl-CoA derivative to reduce methyl-viologen, resulting in a colour change measured at 585 nm. The assay substrates (100 mM Tris-HCl pH 8, 2 mM $MgCl_2.6H_2O$, 0.2 mM CoA-SH (Sigma), 0.1 mM thiamine pyrophosphate (Sigma), 1 mM methyl-viologen (Sigma)) were sparged for 10 minutes in a 1 ml Quartz cuvette (Hellma) before the cell free extract was added. The reaction mixture was mixed by inversion and a drift rate was taken using a Shimadzu UV-240 dual wavelength scanning spectrophotometer (Shimadzu). The assay was started by the addition of either 5 mM sodium pyruvate (Sigma) or 2-oxoglutarate (α-ketoglutaric acid, Sigma). The extinction coefficient of methyl-viologen at 585 nm (11.8 M^{-1} cm^{-1}) was used to calculate the specific enzyme activity.

RNAseq sample preparation and analysis

C. jejuni samples for RNAseq analysis were grown from an overnight starter culture. Cells were harvested by centrifugation and resuspended in 50 ml BTS to an OD_{600} 0.1 and added to 6 well plates (Greiner), 5 ml per well. After growth to mid-log (OD_{600} 0.6) phase, the T0 timepoint was taken and cells were exposed to 405 nm light with samples taken after 15 and 30 minutes light exposure (18 mW cm^2). At each timepoint, 1.5 ml of culture was harvested from each well and centrifuged (12,000 g, 2 min, 4ºC). The resulting supernatant was removed, and cell pellets were immediately frozen by submerging in liquid nitrogen for 45 seconds. Frozen cell pellets were stored at -80 ºC before being sent for sequencing. RNA extraction, purification, library preparation and next generation sequencing was done by Genewiz (Genewiz UK). Data was processed

using the Galaxy server (Galaxy UK) by performing quality control on each read to removed bad reads, followed by read trimming to remove Illumina sequencing adaptors. Reads were then mapped to the genome using the Genbank *Campylobacter jejuni subsp. jejuni* NCTC 11168 reference genome. Read counts per genome feature were calculated and then normalised to calculate the ratio of each VB light exposed experimental timepoint to the T0 timepoint. Genes exhibiting greater than twofold change in abundance at one or more timepoints with a p value of ≤ 0.05 were deemed to be differentially regulated. The Benjamini Hochberg test was used to correct for false positives.

Supplementary Figure 1

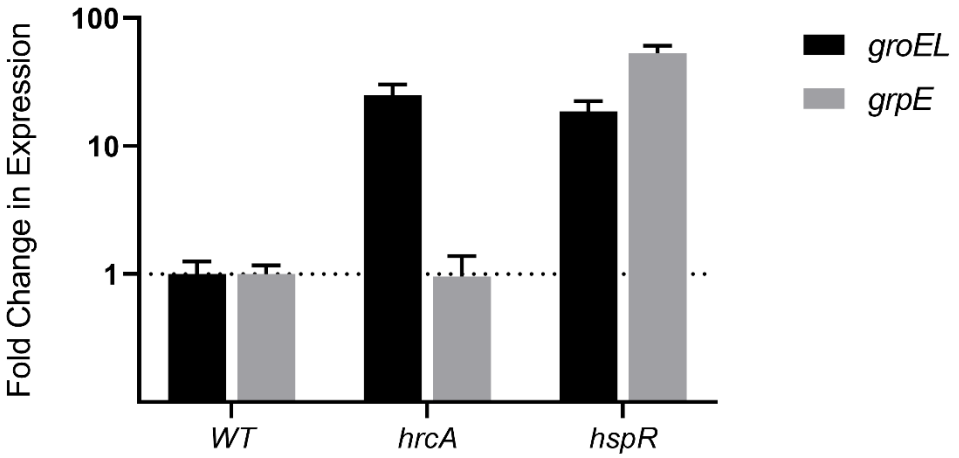

Supplementary Figure 1 – Comparison of expression levels of the protein chaperones *groEL* (black bars) and *grpE* (grey bars) in the heat shock regulator mutants *hrcA* and *hspR.* Expression levels are relative to *C. jejuni* WT cells. The dashed line represents the baseline level of expression.

Supplementary Figure 2

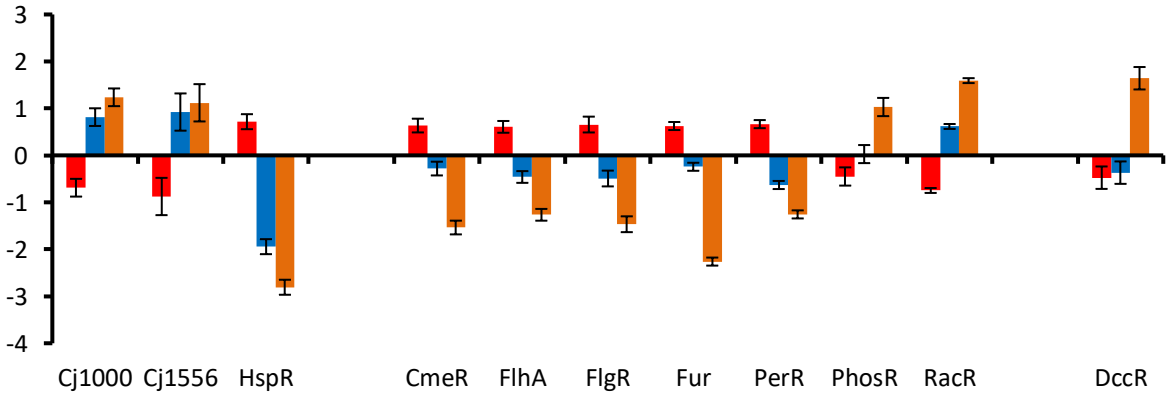

Supplementary Figure 2 - Predicted changes in transcription factor activities upon exposure of *C. jejuni* to blue light. Transcription factor responses were predicted using the TFInfer software by applying a connectivity matrix consisting of 19 transcription factors and their regulons (genes/proteins that are directly or indirectly regulated; see reference list for sources of information). The red bars show the predicted activities of the indicated transcription factors in unexposed cultures T0, the blue bars after exposure to a bacteriostatic light dose (T1) for 15 minutes, 7 J cm^{-2} and the brown bars showing a bactericidal dose (T2) for 30 minutes, 14 J cm^{-2}. The error bars represent the confidence intervals provided by the posterior distribution.

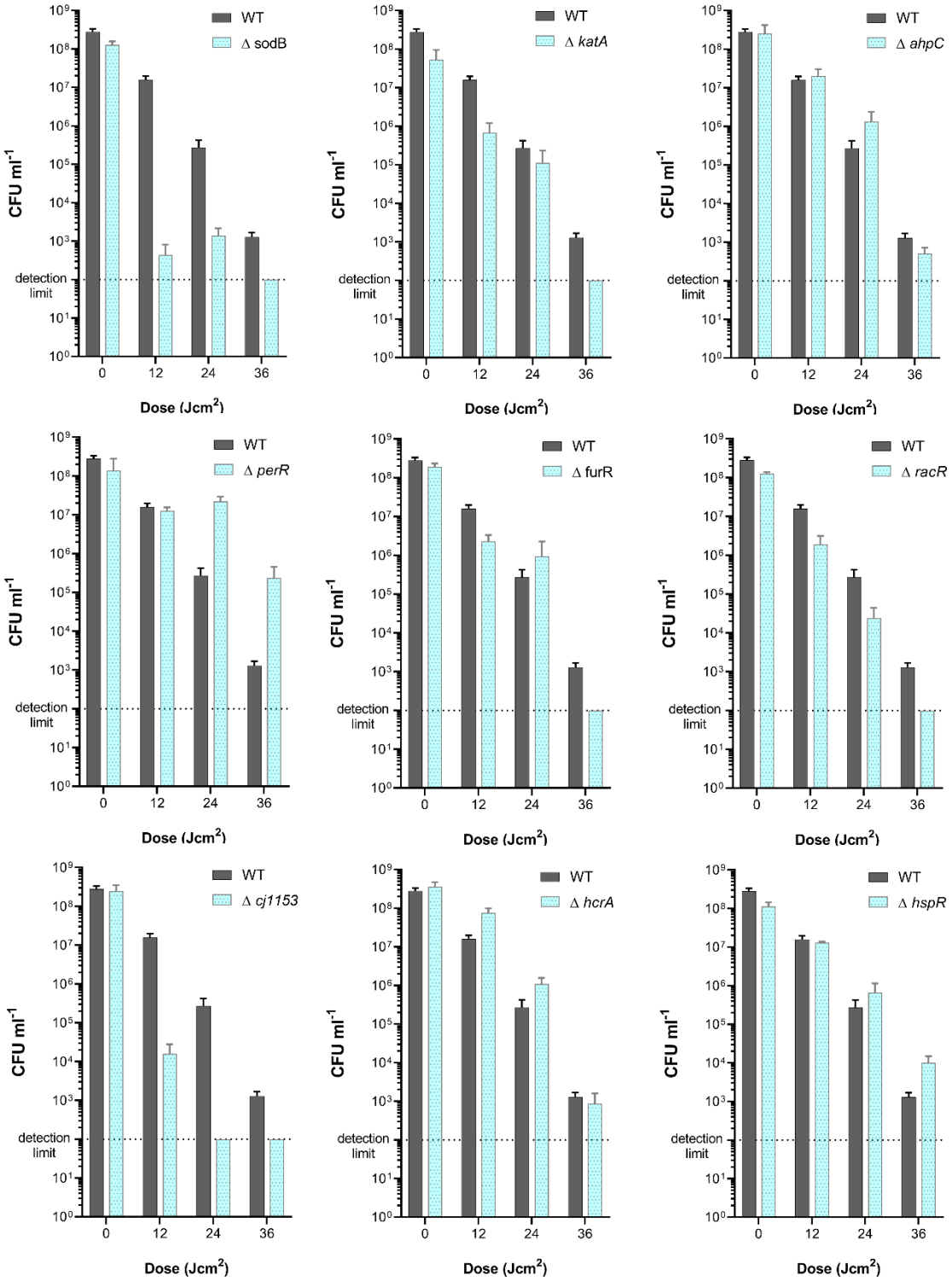

Supplementary Figure 3 - Photodynamic inactivation of WT and *C. jejuni* stress defence mutants. Results (n = 9) are shown as CFU means. Bars below the dashed line show CFU reduction below the detection limit.

Supplementary Table 1

https://drive.google.com/file/d/1acHCeRzGzqkj723o9h8rMEYlGAGYzVXl/view?usp=sharing

Full RNAseq dataset of photooxidative stress response.

References

1. Kaakoush, N. O., Castaño-Rodríguez, N., Mitchell, H. M. & Man, S. M. Global epidemiology of *Campylobacter* infection. *Clin. Microbiol. Rev.* (2015) *3,* 687–720

2. Luber, P., Brynestad, S., Topsch, D., Scherer, K. & Bartelt, E. Quantification of *Campylobacter* species cross-contamination during handling of contaminated fresh chicken parts in kitchens. *Appl. Environ. Microbiol.* (2006) *72,* 66-70

3. Buzby, J. C., Allos, B. M. & Roberts, T. The Economic Burden of *Campylobacter*-Associated Guillain-Barré Syndrome . *J. Infect. Dis.* (1997) *45,* 1-14

4. Wagenaar, J. A., French, N. P. & Havelaar, A. H. Preventing *Campylobacter* at the source: Why is it so difficult? *Clin. Infect. Dis.* (2013) *28,* 890-899

5. Panel, E. & Biohaz, H. Scientific Opinion on Quantification of the risk posed by broiler meat to human campylobacteriosis in the EU. *EFSA J.* 8, 1–89 (2010).

6. Scherer, K., Bartelt, E., Sommerfeld, C. & Hildebrandt, G. Comparison of different sampling techniques and enumeration methods for the isolation and quantification of *Campylobacter* spp. in raw retail chicken legs. *Int. J. Food Microbiol.* (2006) *34,* 77-89

7. Evans, S. J. & Sayers, A. R. A longitudinal study of C*ampylobacter* infection of broiler flocks in Great Britain. *Prev. Vet. Med.* (2000) *32,* 1-14

8. Riedel, C. T., Brøndsted, L., Rosenquist, H., Haxgart, S. N. & Christensen, B. B. Chemical decontamination of *Campylobacter jejuni* on chicken skin and meat. *J. Food Prot.* (2009) *45,* 77-89

9. Murdoch, L. E., MacLean, M., MacGregor, S. J. & Anderson, J. G. Inactivation of *Campylobacter jejuni* by exposure to high-intensity 405-nm visible light. *Foodborne Pathog. Dis.* (2010) *6,* 889-901

10. Jesionek A, T. von H. Zur Behandlung der Hautcarcinome mit fluoreszierenden Stoffen. *Dtsch Arch Klin Med*, (1905). 85, 223–239

11. Hamblin, M. R. & Hasan, T. Photodynamic therapy: A new antimicrobial approach to infectious disease? *Photochemical and Photobiological Sciences* (2004) *77,* 890-901

12. Dai, T., Huang, Y. Y. & Hamblin, M. R. Photodynamic therapy for localized infections-State of the art. *Photodiagnosis and Photodynamic Therapy* (2009) *771,* 1-15

13. Hamblin, M. R. *et al. Helicobacter pylori* accumulates photoactive porphyrins and is killed by visible light. *Antimicrob. Agents Chemother.* (2005) *75,* 601-651

14. Feuerstein, O., Ginsburg, I., Dayan, E., Veler, D. & Weiss, E. I. Mechanism of Visible Light Phototoxicity on *Porphyromonas gingivalis* and *Fusobacterium nucleatum*. *Photochem. Photobiol.* (2005) *31,* 301-333

15. Kendall, J. J., Barrero-Tobon, A. M., Hendrixson, D. R. & Kelly, D. J. Hemerythrins in the microaerophilic bacterium *Campylobacter jejuni* help protect key iron-sulphur cluster enzymes from oxidative damage. *Environ. Microbiol.* (2014) *56,* 431-451

16. Liu, Y. W. & Kelly, D. J. Cytochrome c biogenesis *in Campylobacter jejuni* requires cytochrome c6 (CccA; Cj1153) to maintain apocytochrome cysteine thiols in a reduced state for haem attachment. *Mol. Microbiol. 96*, 1298–1317 (2015).

17. Taylor, A. J. & Kelly, D. J. The function, biogenesis and regulation of the electron transport chains in *Campylobacter jejuni*: New insights into the bioenergetics of a major

food-borne pathogen. *Advances in Microbial Physiology* vol. 74 (Elsevier Ltd, 2019).

18. Tim, M. Strategies to optimize photosensitizers for photodynamic inactivation of bacteria. *J. Photochem. Photobiol. B Biol.* 150, 2–10 (2015).

19. Guccione, E. *et al.* Reduction of fumarate, mesaconate and crotonate by Mfr, a novel oxygen-regulated periplasmic reductase in Campylobacter jejuni. *Environ. Microbiol.* (2010) *32,* 771-802

20. Baier, J. *et al.* Singlet oxygen generation by UVA light exposure of endogenous photosensitizers. *Biophys. J.* (2006) *6,* 333-345

21. Nishimura, T. *et al.* Determination and analysis of singlet oxygen quantum yields of talaporfin sodium, protoporphyrin IX, and lipidated protoporphyrin IX using near-infrared luminescence spectroscopy. *Lasers Med. Sci.* (2020) *43,* 450-461

22. St. Denis, T. G., Huang, L., Dai, T. & Hamblin, M. R. Analysis of the bacterial heat shock response to photodynamic therapy-mediated oxidative stress. *Photochem. Photobiol.* (2011) *34,* 21-48

23. Shahzad Asif, H. M. *et al.* TFInfer: A tool for probabilistic inference of transcription factor activities. *Bioinformatics* (2010) *23,* 1136-1176

24. Holmes, C. W., Penn, C. W. & Lund, P. A. The hrcA and hspR regulons of *Campylobacter jejuni. Microbiology* (2010) *92,* 113-123

25. Maisch, T. *et al.* The role of singlet oxygen and oxygen concentration in photodynamic inactivation of bacteria. *Proc. Natl. Acad. Sci. U. S. A.* (2007) *86,* 1030-1454

26. Fredriksson, Å., Ballesteros, M., Dukan, S. & Nyström, T. Defense against protein carbonylation by DnaK/DnaJ and proteases of the heat shock regulon. *J. Bacteriol.* (2005) *61,* 1-14

27. Palyada, K. *et al.* Characterization of the oxidative stress stimulon and PerR regulon of *Campylobacter jejuni. BMC Genomics* (2009) *561,* 321-345

28. van der Stel, A. X. *et al.* The *Campylobacter jejuni* RacRS two-component system activates the glutamate synthesis by directly upregulating γ-glutamyltranspeptidase (GGT). *Front. Microbiol.* (2015) *37,* 801-854

29. Faraj Tabrizi, P., Wennige, S., Berneburg, M. & Maisch, T. Susceptibility of sodA- and sodB-deficient: *Escherichia coli* mutant towards antimicrobial photodynamic inactivation via the type I-mechanism of action. *Photochem. Photobiol.* (2018). *Sci. 17*, 352–362

30. Food Standards Agency. A microbiological survey of *Campylobacter* contamination in fresh whole UK- produced chilled chickens at retail sale- February 2014 to February 2015. *UK- wide survery campylobacter Contam. fresh chickens Retail.* (2015). *B4* 1-37

31. Fyrestam, J., Bjurshammar, N., Paulsson, E., Johannsen, A. & Östman, C. Determination of porphyrins in oral bacteria by liquid chromatography electrospray ionization tandem mass spectrometry. *Anal. Bioanal. Chem.* (2015) *407(23):* 7013–7023

Chapter 5: *Campylobacter* RNA Binding Proteins

5.1 Introduction

During its life-cycle, *C. jejuni* must be able to survive in both extremes of oxygen availability, from the hypoxic conditions during transfer and invasion of the host, to the severe oxygen limitation of the gastro-intestinal tract. The ability to cycle between a variety of environmental oxygen tensions remains a defining feature of the biology of this food-borne bacterium, perhaps dictating its success as a gastrointestinal pathogen. Enteric bacteria like *C. jejuni* protect themselves against the effects of the hyperoxic conditions during transmission using an arsenal of defences which eliminate harmful oxidants before they cause cellular damage. Yet, mechanisms of adaption must also be in place to survive the severe oxygen-limited conditions found at the mucosal matrix. Thus, understanding the mechanisms of adaption and regulators which control the switch between oxygen tensions is key to elucidating how *C. jejuni* can survive and cause disease.

In order to survive at low oxygen tensions, *C. jejuni* must undergo enzymatic and metabolic adaptions to allow survival in the severely oxygen limited gastro-intestinal tract. Terminal oxidases with a high oxygen affinity such as the cbb_3 type cytochrome *c* oxidase allow for better growth at lower oxygen levels than the low affinity *bd*-like quinol oxidase (CioAB or CydAB) (Guccione *et al*., 2017). As *C. jejuni* has a highly branched electron transport chain, the choice of terminal reductase also plays a significant role in survival under oxygen limitation, as for those less energetically favourable electron acceptors can be repressed in favour of more energy efficient electron carriers. Microarray analysis comparing gene expression between *C. jejuni* 11168-H batch culture cells with RNA extracted from cells growing in the chick cecum found significant upregulation of genes encoding alternative electron acceptors and the high affinity oxidase CcoNOPQ (Woodall *et al*., 2005). The regulatory network controlling the switch to low oxygen concentrations remains poorly understood in *C. jejuni* as it lacks the classic oxygen-sensing transcription factors FNR and ArcA found in other bacterial species (Crack *et al*., 2012). Of the three regulatory systems known to affect the expression of oxygen responsive electron transport genes, the RacRS two-component system is the most understood. Under oxygen limited conditions, the RacRS system represses genes involved in less energetically favourable fumarate respiration when the more energetically favourable electron acceptors such as nitrate and TMAO are present (van der Stel *et al*., 2015). Although there is no evidence to suggest that RacS has an oxygen sensing domain, it may be redox sensing, as its activity depends on an oxidation sensitive periplasmic disulphide bond (van Mourik, 2011).

C. jejuni must also respond to high oxygen tensions to both protect oxygen sensitive enzymes and to detoxify partially reduced reactive oxygen species (ROS) generated by the stepwise reduction of molecular oxygen. Although *C. jejuni* encodes a complete set of oxidative defence genes, the presence of several key Fe-S cluster enzymes essential to its metabolism render the bacteria highly susceptible to damage by ROS. In order to protect these oxygen sensitive pyruvate and 2-oxoglutarate: acceptor oxidoreductases, *C. jejuni* must regulate the expression of hemerythrin proteins which protect the Fe-S cluster enzymes from inactivation by both molecular oxygen and ROS (Kendall *et al*., 2014). Whilst *C. jejuni* lacks the well characterised oxidative stress regulators SoxR and OxyR found in other bacteria, it does utilise its own regulatory proteins which control the expression of the oxidative stress defence genes (Parkhill *et al*., 2000). These include the essential OmpR-type regulator CosR, the peroxide sensing regulator PerR, two MarR-type regulators RrpA and RrpB and the iron response regulator Fur. The relatively small set of transcription factors found in *C. jejuni* suggests it utilises an intricate regulatory network with overlapping functions, yet how these transcription factors sense and respond to a vast array of environmental challenges faced during transmission between hosts remains unclear.

The small genome size and regulator complement of *C. jejuni* suggests post-transcriptional regulation may be crucial in controlling its adaptive life-cycle, yet few post transcriptional regulators have been characterised in *C. jejuni* to date. Post-transcriptional regulation of genes involved in oxidative stress defence have been described in the case of the *E. coli* Fe-S aconitase proteins AcnA and AcnB (Tang & Guest, 1999) (Austin *et al*., 2015). During oxidant exposure or low intracellular iron levels, $[4Fe\text{-}4S]^{2+}$ clusters are damaged, releasing the catalytic ferrous iron, rendering the enzyme inactive. Upon inactivation, the apo-AcnA and apo-AcnB proteins act as post transcriptional regulators by binding to the 3'UTR of their cognate mRNAs (Tang & Guest, 1999). The binding of the apo protein to *acnA/acnB* transcript increases the mRNA stability which increases the efficiency of the AcnA and AcnB protein synthesis during oxidative damage to Fe-S cluster proteins. Additional regulatory targets of AcnB have been identified in *H. pylori* through examining changes to the proteome in a *acnB* mutant strain using mass spectrometry (Austin *et al*., 2015). The abundance of AhpC was found to be significantly lower in the *acnB* mutant and electrophoretic mobility shift assays show that the apo-AcnB binds to the 3'UTR of the *ahpC* transcript. The decreased AhpC abundance in the *H. pylori acnB* mutant resulted in hypersensitivity towards cumene hydroperoxide and decreased survival upon exposure to O_2 (Austin *et al*., 2015). Although a post transcriptional regulatory role of AcnB has yet to confirmed in *C. jejuni,* the *C. jejuni acnB* mutant has been shown to have an increased sensitivity to $O_2^{\bullet-}$ and

H_2O_2, implying a potential role for apo-AcnB in the regulation of *sodB, ahpC* and/or *katA* (Flint *et al*., 2014).

The carbon starvation regulator CsrA is the most studied global post transcriptional regulator in *C. jejuni* which controls several virulence-related properties, including oxidative stress resistance, motility, adherence, and invasion (Fields *et al*., 2008). Research into CsrA has mainly focused on its control of the major flagellin associated gene *flaA*, as CsrA binds strongly to the 5'UTR of *flaA* mRNA, often at or near the ribosome binding site (Romeo & Babitzke, 2018). Binding of CsrA to the RBS stem loop blocks ribosome access and represses initiation of translation as well as reducing the mRNA stability (Romeo & Babitzke, 2018). *C. jejuni* regulates CsrA activity through the flagellar chaperone FliW, which is released upon secretion of FlaA, allowing binding between CsrA and FliW to alleviate flagellin repression. Proteomic analysis of the *csrA* mutant revealed the global regulatory control of CsrA, with altered abundance of 120–150 proteins involved in diverse cellular processes including several proteins relating to respiration and metabolism (Fields *et al*., 2016). Interestingly the *csrA* mutant showed mild upregulation of *racR*, suggesting a joint role for CsrA and RacR in the regulation of fumarate metabolism, potentially driving the adaption of *C. jejuni* to low oxygen tensions (Taylor & Kelly, 2019). Although the above regulators have been shown to respond to multiple carbon sources to regulate downstream genes, their ability to sense changes in oxygen tensions has not yet been shown.

Although *C. jejuni* is generally considered sensitive to both high and low oxygen tensions, it has a comprehensive response network which alters multiple facets of metabolism, respiration and oxidative stress defence to allow survival under a variety of oxygen concentrations. Given the cyclical exposure to different oxygen tensions during transmission and the complexity of the response oxygen fluctuations, it seems surprising that *C. jejuni* lacks a response regulator that directly binds oxygen and affects expression of downstream genes. Although *C. jejuni* does utilise at least three regulators which control the expression oxidative stress defence genes, these clearly respond to ROS rather than oxygen and do not regulate respiration (Taylor & Kelly, 2019). Other bacteria have been shown to utilise haem-based oxygen sensing regulators such as the *E. coli* direct oxygen sensor (DOS, also known as DosP). The N-terminal haem-bound PAS domain senses changes in oxygen tension to catalyse the conversion of cyclic-di-GMP to linear di-GMP which acts as an important secondary messenger predicted to be critically involved in numerous physiological functions of *E. coli* (Shimizu, 2013). As *C. jejuni* lacks any DosP homologs or any other oxygen sensing transcriptional regulator, we aimed to uncover whether *C. jejuni*

utilises oxygen sensing post transcriptional regulators to control the switch between oxygen tensions.

Recently a new high throughput method has been developed to identify RNA-binding proteins (RBPs) using orthogonal organic phase separation (OOPS). Previously, approaches to identify protein bound RNAs have relied on immunoprecipitation of specific proteins or capture of polyadenylated RNA-binding proteins by UV cross linking. However, these methods were not applicable for high throughput screening and could not be used for bacterial systems which utilise non-polyadenylated RNAs. OOPS purification utilises acidic guanidinium thiocyanate-phenol-chloroform (AGPC) phase partition which enables unbiased recovery of RNA species, generating two distinct phases: the upper aqueous phase containing DNA/RNA, and the lower organic phase containing protein (Sacchi, 2006). UV-cross linking at 254 nm generates RNA-protein adducts with amphiphilic properties which migrate to the aqueous–organic interface shown in Figure 5.1. By isolating and identifying the protein bound RNA at the interface, it is possible to uncover the RNA binding proteome of any given organism (Queiroz *et al*., 2019).

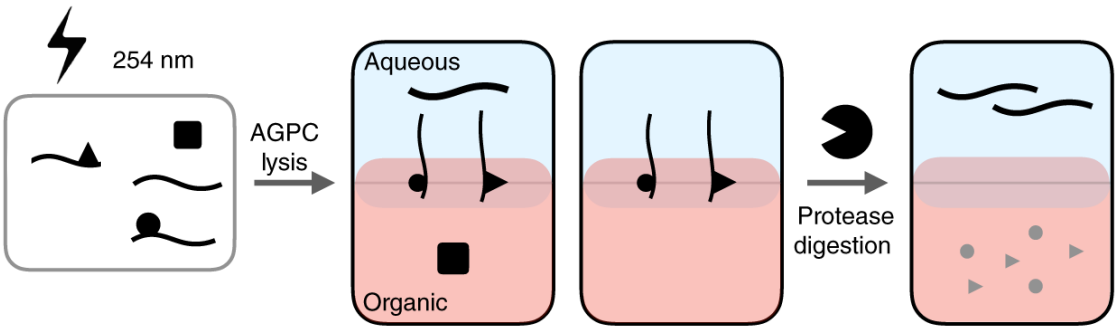

Figure 5.1 – Schematic representation of the OOPS RBP extraction method. Cross linking using 254 nm light induces RNA-protein adducts. During AGPC lysis and separation, proteins migrate to the organic phase and RNA migrates to aqueous phase leaving the amphiphilic RNA-protein adducts at the interphase. Multiple rounds of AGPC separation leave a purified RNA-protein solution at the interphase. Protease digestion and further AGPC separation yields RNA at the aqueous phase (Queiroz *et al*., 2019).

The first study in *E. coli* to use OOPS for the identification of RBPs recovered 364 RBPs representing 8% of the predicted K-12 strain proteome (Queiroz *et al*., 2019). Of the 176 GO annotated RBPs in *E. coli,* 87 were recovered using OOPS separation with a further 277 novel RNA-associated proteins identified which have not previously been annotated with an RNA-related GO term. In this final chapter, we aimed to uncover the *C. jejuni* RBPome using OOPS phase separation and mass spectrometry analysis. Once an initial list of RNA binding proteins has been identified, we aim to measure abundance changes in the *C. jejuni* RBPome upon

exposure to high and low oxygen concentrations to try to uncover new post transcriptional regulators which control the adaption between high and low oxygen environments.

5.2 Results

5.2.1 OOPS efficiently captures *C. jejuni* RBPs

Research in *E. coli* suggests OOPS can be utilised to capture RBPs in bacteria. In order to test if *C. jejuni* RBPs can be captured by OOPS, we measured free RNA and protein bound RNA (PBR) abundance changes following a range of UV cross linking doses followed by 3 rounds of OOPS as described in Section 2.16. UV cross linking at 254 nm generates RNA-protein adducts which migrate to the aqueous-organic interphase. By measuring changes in the abundance of free RNA and PBR, we can assess the cross linking efficiency in the capture of RBPs across a range of UV doses. Figure 5.2 shows that increasing the UV cross linking dose causes a decrease in the abundance of free RNA due to a greater abundance of *C. jejuni* protein bound RNA species migrating to the interphase. To confirm that the decrease in free RNA is due to an increase in PBR at the interphase, we extracted PBR in samples exposed to a range of UV light doses. By incubating the precipitated interphase with proteinase K, cross link bound proteins are removed, releasing the RNA which can then be purified using the standard phenol/chloroform extraction. Figure 5.2 shows that increasing the dose of UV light results in a greater abundance of PBR, yet the abundance of PBR does not rise in consistent increments, suggesting other factors are influencing the cross linking efficiency between samples.

A

Dose J cm^{-2}	Free RNA ng μl^{-1}	PBR ng μl^{-1}	% PBR
0	641.07	136.8	21.33932
150	490.04	182.52	28.47115
400	715.88	84.56	13.19045
650	354.05	282.15	44.01235
900	339.44	383.88	59.88114

B

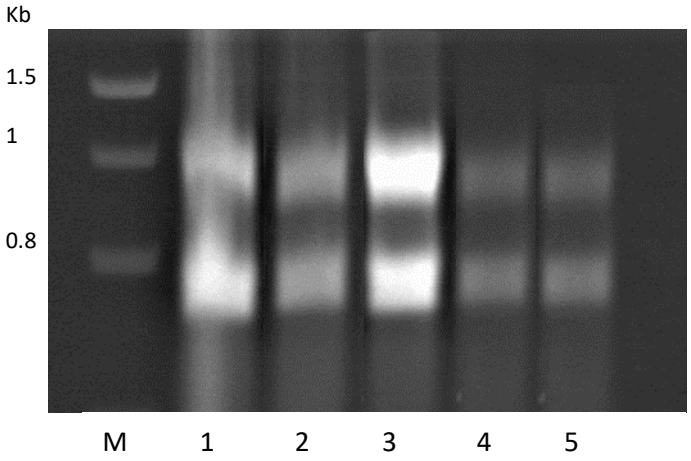

Figure 5.2: Optimisation of UV-cross linking dose. *C. jejuni* cells were grown in a chemostat culture until a steady state of 5 vessel volumes of turnover was achieved before 7 ml of cell culture was collected and immediately cross linked. PBR was extracted following the OOPS protocol outlined in Section 2.16. Free RNA was collected after 1 round of OOPs and the concentration was measured using a NanoDrop. PBR was purified by three rounds of OOPS followed by protease treatment to release bound peptides before RNA concentration was measured. (A) Free RNA and PBR concentrations measured after a range of UV cross linking doses using a NanoDrop. The percentatage PBR was calculated by the following: ((PBR ng μl^{-1}/ non-cross linked free RNA ng μl^{-1}) x 100). (B) Free RNA concentrations visualised on a 1% Agarose gel loading 5 µl per well. M: ladder; followed by UV cross-linkinging at: 1: 0 J cm^{-2}; 2: 150 J cm^{-2}; 3: 400 J cm^{-2}; 4: 650 J cm^{-2}; 5: 900 J cm^{-2}.

5.2.2 Chemostat medium reduces cross linking efficiency

Although UV cross linking increases the abundance of PBR at the interphase, the cross linking efficiency appears highly variable without a clear linear relationship between UV dose and PBR concentration. Studies in *E. coli* assessing RBP retention using OOPS found a clear linear relationship between UV dose and PBR retention with a saturation at around 60%. In order to reduce variables attributed to sample preparation, we altered the original method described by

Queiroz *et al*., 2019 by removing the buffer resuspension step and instead immediately cross linked *C. jejuni* chemostat samples in growth medium (Queiroz *et al*., 2019). By immediately cross linking samples, we hoped to get a more accurate picture of the *C. jejuni* RBPome in growth culture before cells respond to changes in osmilarity between growth medium and buffer and begin adaptations to environmental oxygen saturations. However, as *C. jejuni* growth medium is rich in aromatic amino acids which absorb at 254 nm, we speculated that cross linking directly in chemostat medium may give a quenching effect, reducing the cross linking efficiency. To test this hypothesis, we measured the changes in PBR recovery between samples directly cross linked in chemostat medium and samples diluted in phosphate buffer before UV light exposure. Figure 5.3 shows that samples diluted in buffer have a less variable PBR titration curve than samples directly cross linked in medium suggesting the quenching effect can be alleviated when the concentration of aromatic amino acids is reduced.

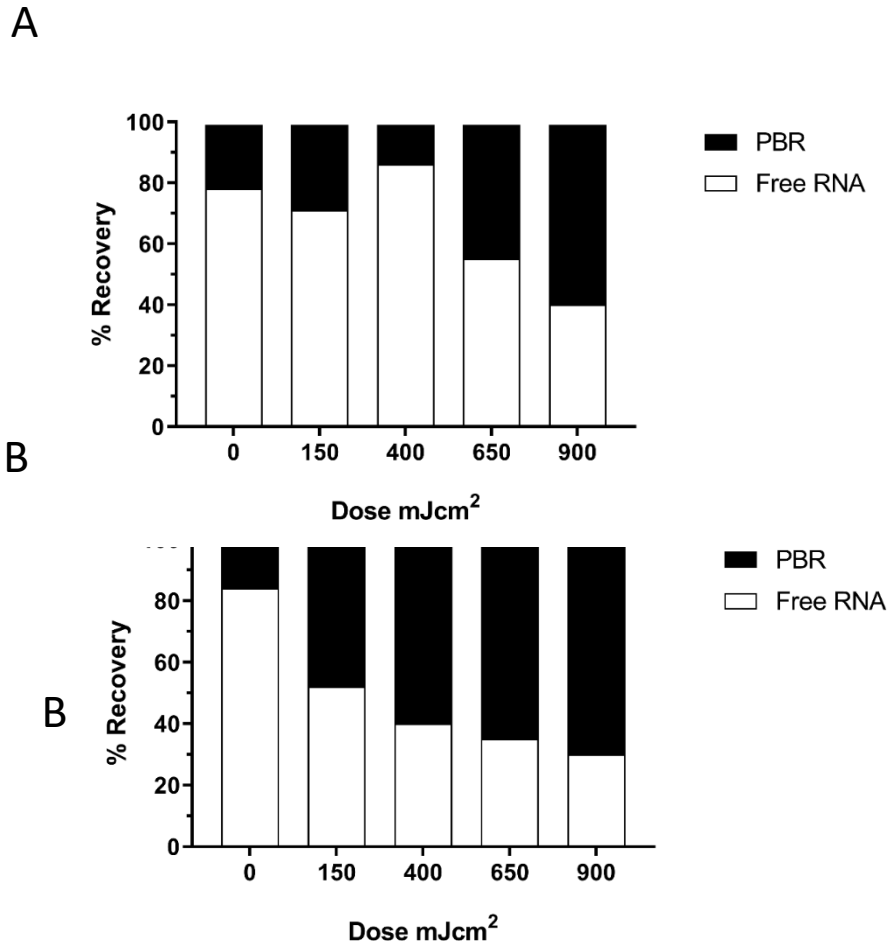

Figure 5.3: Comparison of cross linking efficiency between directly exposed and diluted chemostat culture. *Campylobacter jejuni* in a chemostat culture until a steady state of 5 vessel volumes of turnover was achieved before 7 ml of culture was collected per sample. Cells were immediately cross linked and PBR concentration calculated as described in section 2.16. (A) Cross linking efficiency after direct cross linking without dilution of sample. (B) Cross linking efficiency after 1:1 dilution in sodium phosphate buffer immediately before cross linking.

	Cross Linked (CL)	Non-Cross Linked (NC)
Replicate	**Total Protein (µg)**	**Total Protein (µg)**
1	17.84	18.56
2	19.44	19.68
3	20.88	18.8
4	19.44	18.72
5	21.04	19.44
6	18.32	22.96
7	18.48	20.24

Table 5.1: Total protein concentration after interphase digestion and peptide desalt. Purified PBR interphase samples were resuspended in buffer and solubilised by sonication. Peptide samples were then reduced, alkylated and then digested with Trypsin. Finally, samples were desalted by reverse phase chromatography with samples eluted in 300 µl of 70 % ACN. Peptide quantities were calculated using Qubit™ protein assay kit.

5.2.3 Recovery of RNA binding proteins

In order to determine the *C. jejuni* RNA binding proteome, we compared the RBPs in both cross linked and non-cross linked samples enriched with three rounds of OOPS. We selected a UV cross linking dose of 525 J cm^{-2} which achieved around ~ 50% PBR recovery which is in line with previous reports (Queiroz *et al*., 2019)(Shchepachev *et al*., 2019). The selection of the correct UV cross linking dose is critical in recovering "true" RBPs as over cross linking can result in the recovery of many proteins with no link to RNA metabolism yet if the dose is too small then many known RNA-interacting proteins will be lost (Shchepachev *et al*., 2019). After three rounds of OOPS and subsequent reduction, alkylation, trypsin digestion and desalting steps outlined in section 2.17, digested peptides were quantified by Qubit analysis (Table 5.1). Both cross linked and non-cross linked samples contained sufficient peptide quantities for mass spec analysis (> 10 µg) but despite the samples being soluble in 70% ACN, all samples precipitated when resuspended in 0.1% formic acid which prevented further analysis.

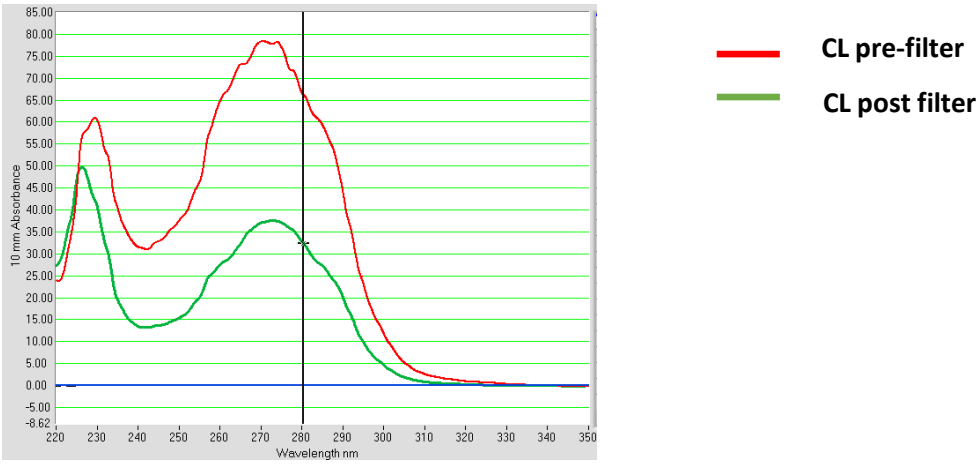

Figure 5.4: Protein quantification before and after peptide clean-up using an Amicon protein filter. Cross-linked (CL) insoluble peptide elute concentration (red line) measured before running through an Amicon Ultra-0.5 centrifugal filter unit with the eluted peptide concentration measured (green line).

5.2.4 Digested RNA binding peptides are insoluble in formic acid

For liquid chromatography-mass spec analysis (LC-MS), peptides must be resuspended in 0.1% formic acid as formic acid is the key component in the supply of protons for reversed-phase LC-MS analysis in the positive ionization mode. However, when soluble cross-linked and non-cross-linked peptides were resuspended in 0.1% formic acid, they formed an insoluble white precipitate which prevented samples being loaded for LC-MS analysis. Attempts to resuspend the precipitate by pipetting and sonication had no effect whilst removing the precipitate by filtration also proved unsuccessful as > 50% of the peptide concentration was lost after passage through a 30 kDa Amicon membrane filter (Figure 5.4). One explanation for this insoluble precipitate found in *C. jejuni* extracts but not in *E. coli* is that *C. jejuni* has an active *N*- and *O*-linked glycosylation system which modifies extracellular flagellar filaments and extra-cytoplasmic proteins. This is of interest in relation to OOPS as glycosylated proteins share the same physiochemical properties as RNA-protein adducts meaning they will migrate to the aqueous-organic interphase during phase separation. One explanation for this insoluble precipitate may be that large portions of the extracellular matrix may migrate to the interphase due to its heavily glycosylated exterior. In order to alleviate this effect, better cell lysis and removal of cellular debris after lysis may reduce the abundance of contaminates at the interphase, preventing the formation of insoluble aggregates after formic acid resuspension.

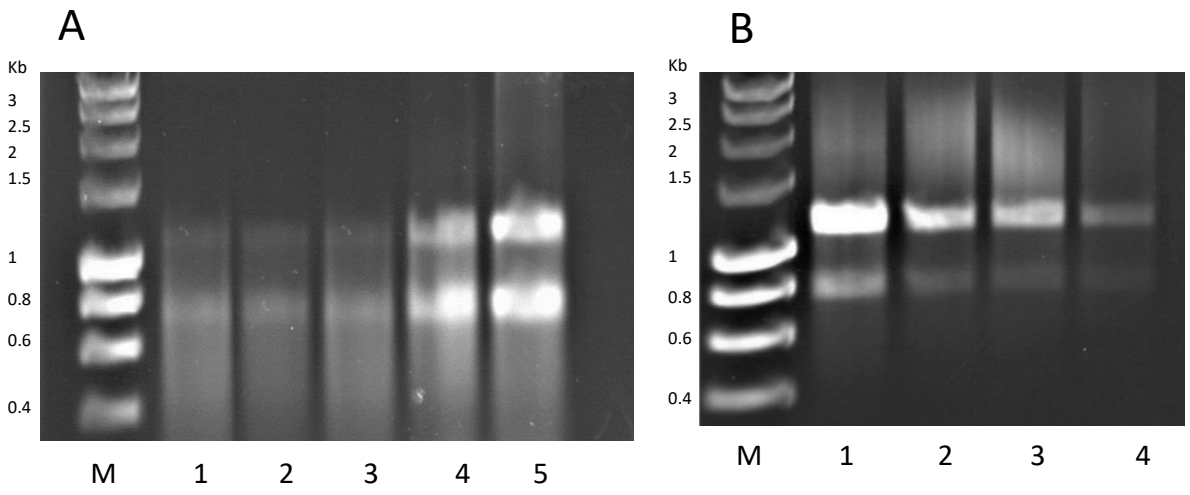

Figure 5.5: Optimisation of precipitate removal. (A) Free RNA concentrations after a variety of cell lysis conditions with 5 µl of aqueous phase taken after cross-linking containing free RNA which was loaded onto a 1% agarose gel. M: ladder; 1: TRIzol only; 2: TRIzol + freeze-dry; 3: TRIzol + 0.5 mm beads + votex; 4: TRIzol + BeadBeater (no beads); 5: TRIzol + beads + BeadBeater. (B) Non cross linked PBR RNA concentrations after increasing spin speeds post cell lysis with 5 µl of extracted RNA was loaded onto a 1 % agarose gel. M: ladder; 1: 0 g; 2: 3,000 g; 3: 6,000 g; 4: 9,000 g.

5.2.5 Optimisation of *C. jejuni* cell lysis

As the *C. jejuni* extracellular membrane is heavily glycosylated, complete cell lysis is essential to both ensure disruption of the bacterial membrane to prevent insoluble aggregates and to prevent the migration of unlysed cells to the interphase. Accumulation of unlysed cells at the interphase could result in an abundance of false positive RBPs being detected giving an inaccurate representation of the *C. jejuni* RBPome. Published work studying the *E. coli* RBPome achieved complete cell lysis using a combination of Trizol®, freeze-drying and 0.5 mm glass beads (Queiroz *et al*., 2019). Our initial experiments found that *C. jejuni* can be effectively lysed using this method although it is possible that the thicker LPS layer and glycoprotein matrix may mean that *C. jejuni* cells require a harsher mechanical disruption to achieve complete cell lysis. Figure 5.5.A shows the comparison between different cell lysis techniques in the total free RNA extracted after treatment. It is clear that although the Trizol® + freeze-dry technique described in *E. coli* does lyse *C. jejuni* cells to allow for RNA extraction, it does not result in complete cell lysis as mechanical disruption by bead beater treatment generates higher free RNA abundances due to better cell lysis.

Another observed difference between *E. coli* and *C. jejuni* PBR concentrations was that *Campylobacter* NC PBR concentrations were much higher than that found in *E. coli.* There are two possible explanations for this phenomenon: first is that *C. jejuni* has a higher abundance of

high affinity RBPs which associate tightly with RNA and will migrate to the interphase without the need for cross linking. The second and more plausible explanation given the small genome size of *C. jejuni* is that unlysed cells or large coagulates of glycosylated membrane debris are migrating to the interphase, trapping and carrying non-protein bound RNA to the interphase. This results in a greater abundance of RNA being extracted from the interphase, falsely implying a greater abundance of PBR. To test this hypothesis, we measured the abundance of PBR after increasing centrifugation speeds, immediately after cell lysis to determine if removal of debris by centrifugation would reduce the abundance of PBR in the non-cross linked samples. Figure 5.5.B shows that applying a 3,000 g spin immediately after cell lysis dramatically reduces the abundance of PBR in non-cross linked samples following OOPS, suggesting that unlysed cells and cellular debris contribute to the high PBR concentrations seen in *C. jejuni* extracts.

5.2.6 The *C. jejuni* RBPome

After optimising the *C. jejuni* cell lysis conditions and including an additional spin step to remove cell debris following TRIzol-beadbeater cell lysis, PBR was extracted by three round of OOPS followed by peptide desalting and trypsin digestion. Peptides were resuspended in 0.1% formic acid and loaded onto an Orbitrap mass spectrometer to compare the peptide abundance between cross-linked and non-cross-linked samples. A total of 445 unique proteins were identified in the label free mass spectrometry run, of which 74 had too many missing values and so were omitted from the analysis. Of the 371 peptides processed, 149 proteins were found to be significantly enriched after cross linking using LIMMA modelling (Linear Models for Microarray and RNA-seq Data) with a further 90 proteins included in the *C. jejuni* RBPome which were not enriched but detected at the interphase (FDR <1%).

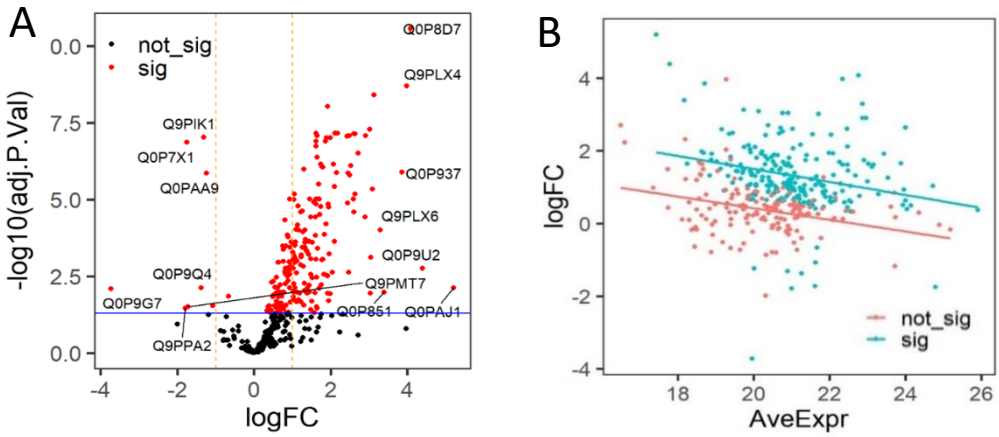

Figure 5.6: Volcano plot displaying the fold change between cross-linked and non-cross-linked samples. **(**A) Volcano plot showing distribution between non-cross linked and cross-linked samples with largest fold change protein UniProt names labelled. Black dots: non-significant proteins (p > 0.01), red dots: significant

proteins isolated from interphase ($p < 0.01$). (B) Plot showing the distribution between average protein expression and log fold change between cross-linked and non- cross-linked samples.

The *C. jejuni* RBPome consists of 235 proteins which pass the false discovery threshold ($p<0.01$), of which 149 show a significant enrichment between cross-linked and non-cross-linked with a point estimate FC > 2 shown in Table 5.2. The full list of 235 OOPS enriched is shown in Supplementary Table 2. There are many more significantly higher abundant proteins in the cross-linked versus non-cross-linked fractions which would be expected given that few proteins will constantly appear in the NC interphase after 3 rounds of OOPS as shown in Figure 5.6.A. To ensure that protein abundance is not the main determinant in controlling the abundance of proteins at the interphase, we plotted the logFC against the average expression/abundance to see if there is any correlation. Figure 5.6.B shows there is no bias to higher abundance proteins when comparing the logFC between cross-linked and non-cross-linked, highlighting that changes seen represent the cross-link driven capture of RBPs.

5.2.7 Functional analysis of the *C. jejuni* RBPome

Of the 235 proteins detected, we recovered 54 of the 89 GO annotated RBPs shown in the Venn diagram in Figure 5.7.A. Of the proteins enriched in the cross-linked samples, we observed an enrichment in RNA associated GO terms, including “RNA binding” and “ribonucleoprotein complex”. It has previously been reported that many glycolytic enzymes and dehydrogenases are good RNA binding proteins as the substrate similarity between NAD(H) and RNA may allow for a dual purpose function (Queiroz *et al*., 2019). The initial *C. jejuni* RBPome obtained using OOPS found that the glycolytic enzymes Enolase, Phosphoglycerate kinase and the probable UDP-glucose 6-dehydrogenase all appear to be RNA binding proteins as they are all significantly enriched after UV cross-linking.

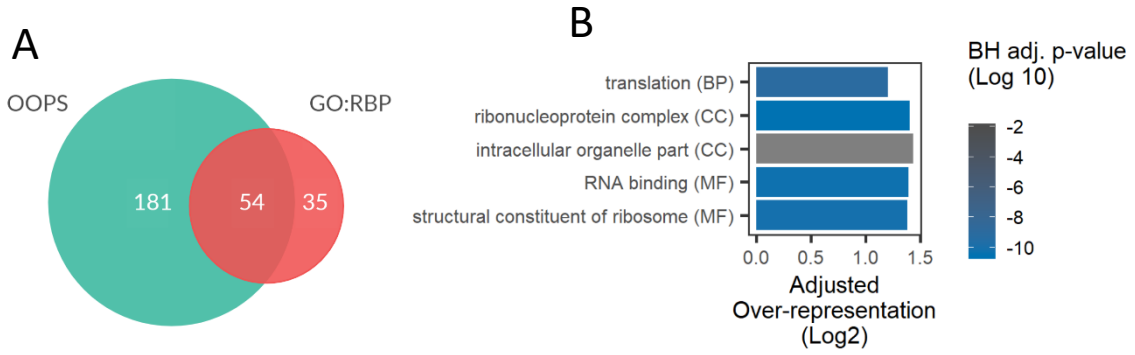

Figure 5.7 Functional analysis of *C.jejuni* RBPome. (A) Venn diagram showing proportion of OOPS identified RBPs which are GO annotated RBPS. (B) Top 5 over-represented GO terms enriched in the cross-linked samples. Benjamin-Huntsman adjusted *p*-value obtained from a modified hypergeometric test to account for protein abundance. (MF, molecular function, BP, biological process, CC cellular component.

Gene	logFC	adj.P.Val
pta	5.21	7.4E-03
trmE	4.39	1.8E-03
rplM	4.07	2.7E-11
rplV	3.98	2.0E-09
Cj1219c	3.86	1.3E-06
nuoC	3.39	1.0E-02
rplV	3.29	9.7E-05
parB	3.13	3.8E-09
nusA	3.09	4.6E-06
Cj0131	3.04	7.8E-04
Cj1237c	3.04	1.1E-02
rpsA	3.02	5.0E-08
rpsG	2.90	8.3E-08
rpsJ	2.90	3.7E-05
peb1C	2.71	3.1E-07
rpsL	2.64	7.1E-08
cjeI	2.63	6.7E-06
rplW	2.61	2.6E-05
rpsB	2.60	7.1E-08
def	2.59	9.6E-06
Cj1542	2.53	8.0E-07
topA	2.49	1.6E-06
Cj0265c	2.48	8.3E-08
Cj1548c	2.47	2.3E-03
Cj0606	2.45	1.4E-06
rpsU	2.44	1.3E-05
pnp	2.43	8.7E-08
Q9PLY5	2.17	7.0E-08
rpoD	2.16	1.3E-06
rpsC	2.11	7.0E-08
ffh	2.10	3.8E-06
mnmG	2.10	2.3E-04
rpmA	2.07	7.1E-07
rpmA	2.05	2.4E-03
argS	1.98	9.8E-08
Cj0118	1.98	1.2E-02
truD	1.96	6.0E-04
rplC	1.95	1.7E-05
recA	1.95	2.0E-02
rpsI	1.93	1.4E-05
cas9	1.92	3.0E-03
Cj0350	1.92	1.1E-02
rpsQ	1.91	9.3E-09
cetB	1.89	2.9E-03
rplP	1.89	9.7E-08
CprR	1.88	6.3E-05
livG	1.86	1.3E-07
infC	1.83	1.3E-04
rloH	1.82	2.7E-03
gltX2	1.80	8.8E-04
hemL	1.80	8.9E-07
rplN	1.77	9.2E-04
kfiD	1.77	8.6E-07
ftsA	1.76	6.1E-03
rplR	1.74	1.7E-05
rplI	1.74	7.0E-07
rnj	1.71	3.1E-05
dnaE	1.70	7.8E-03
cjaA	1.70	9.6E-06
rplU	1.69	3.1E-06
rplJ	1.65	3.9E-04
rpsS	1.65	8.3E-08
rpsK	1.64	4.2E-07
purD	1.64	3.5E-02
uvrA	1.63	3.2E-02
Cj0983	1.63	3.5E-03
Cj1106	1.62	8.9E-04
accA	1.62	1.4E-05
rplT	1.62	1.3E-07
rpsM	1.62	1.8E-07
rpsD	1.62	7.0E-08
infB	1.61	9.6E-06
guaA	1.60	3.7E-05
gne	1.60	1.5E-04
rrc	1.60	1.1E-02
rpsP	1.57	4.9E-02
rplD	1.56	1.2E-05
pgk	1.52	3.5E-03
Cj0807	1.52	2.5E-04
ribB	1.51	2.0E-02
fabG	1.48	2.7E-03
clpP	1.48	3.9E-02
leuS	1.48	8.7E-04
purB	1.47	3.7E-05
rplF	1.46	9.6E-06
Cj1215	1.44	1.0E-02
Cj0372	1.44	2.3E-04
purL	1.44	6.2E-03
cmeA	1.42	6.0E-04
rplE	1.40	7.5E-03
metG	1.39	1.1E-02
proS	1.38	4.8E-04
rpmE	1.36	4.5E-04
dapA	1.35	2.0E-04
rplS	1.33	2.5E-04
mqnE	1.33	3.7E-04
Cj0700	1.32	9.8E-05
nusG	1.32	9.4E-03
glyS	1.31	5.4E-03
pyrC2	1.30	2.8E-02
Cj0706	1.30	1.0E-06
lpxA	1.28	1.5E-03
valS	1.27	1.1E-04
metK	1.26	3.6E-04
rp10	1.26	2.4E-05
aspA	1.24	7.2E-0.4
alaS	1.24	6.4E-04
ilvE	1.22	1.4E-03
mnmA	1.22	2.2E-02
rplK	1.21	2.6E-05
serA	1.19	1.1E-02
hypB	1.17	1.9E-02
tpx	1.16	9.7E-05
secA	1.15	1.6E-05
Cj0054c	1.14	6.9E-05
prs	1.12	1.0E-02
secD	1.12	9.9E-04
mrp	1.11	9.5E-04
pyrD	1.11	2.2E-02
purC	1.10	2.4E-03
Cj1110c	1.09	9.5E-05
dsbI	1.09	2.4E-04
purA	1.08	1.1E-03
ileS	1.07	7.5E-03
glyA	1.06	8.1E-04
ilvC	1.06	3.1E-04
cbrR	1.06	6.7E-06
htpG	1.05	6.6E-04
tig	1.05	7.5E-04
Cj1434c	1.04	1.2E-03
sucD	1.04	1.8E-02
hydB	1.04	1.0E-05
efp	1.04	7.7E-03
pheT	1.04	1.0E-02
thrS	1.03	2.8E-04
thyX	1.03	5.7E-03
rplL	1.03	1.8E-03
pyrG	1.03	1.0E-02
slyD	1.02	8.8E-04
glmS	1.02	1.5E-02
atpA	1.01	5.3E-04

Table 5.2 *C. jejuni* RBPome showing 149 significantly enriched proteins using LIMMA differential protein abundance analysis. Log fold change between non-cross-linked and cross-linked fractions shown in column 2 and the adjusted p value shown in column 3.

5.2.8 Assessment of the RBPome after a change in oxygen tension

To assess the changes in the *C. jejuni* RBPome in a dynamic way upon changes in environmental conditions, we looked for changes in OOPS enriched proteins after a switch in oxygen tension from optimal (7.5% oxygen) to both a high oxygen saturation (17% oxygen) and to low oxygen saturation (1.88% oxygen). This was conducted using a continuous chemostat culture according to a protocol established in our lab and published previously (Guccione *et al.*, 2017). *Campylobacter jejuni* cultures were grown to a steady state after 5 vessel volumes of turnover before the oxygen tension was shifted and samples were taken. To ensure the expected and previously observed physiological changes were taking place after a switch in oxygen tension, RNA samples were extracted, and expression profiles of selected genes diagnostic of adaption to high or low oxygen were measured by qRT-PCR. Extracted RNA samples were screened for the presence of DNA or denatured RNA shown in Figure 5.8.

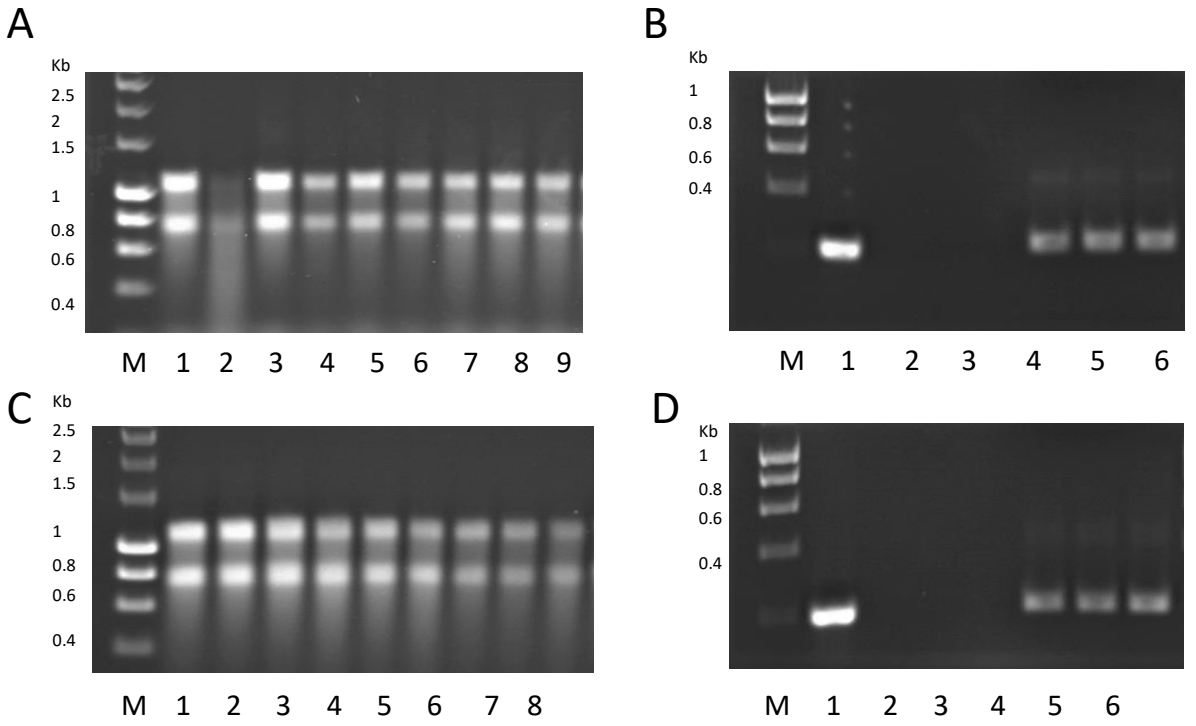

Figure 5.8: RNA purity check of dynamic proteomic samples for qRT-PCR. RNA extracted using TRIzol max bacterial isolation kit and DNAse treated using Turbo-DNA free kit (Ambion) as described in section 2.8.13. (A) RNA integrity check of steady state and low O_2 RNA samples loading 1 µg of RNA per well onto a 1 % Agarose gel. M: ladder; 1: 0 minutes samples 1-3, 10 minutes samples 1-3, 60 minutes samples 1-3. (B) RNA purity check of steady state and low O_2 RNA samples checking for presence of DNA in sample by

MyTaq-Red PCR using *rpoA* screening primers with and without reverse transcriptase (RT). M: ladder; 1: gDNA; 2: 0 minutes; 3: 10 minutes; 4: 60 minutes; 5: 0 minutes RT; 6: 10 minutes RT; 7: 60 minutes RT. (C) RNA integrity check of steady state and high O_2 RNA samples loading 1 µg of RNA per well in same sample order as above. (D) RNA purity check of steady state and high O_2 RNA samples checking for presence of DNA in sample by MyTaq-Red PCR using *rpoA* screening primers with and without reverse transcriptase (RT) in same sample order as above.

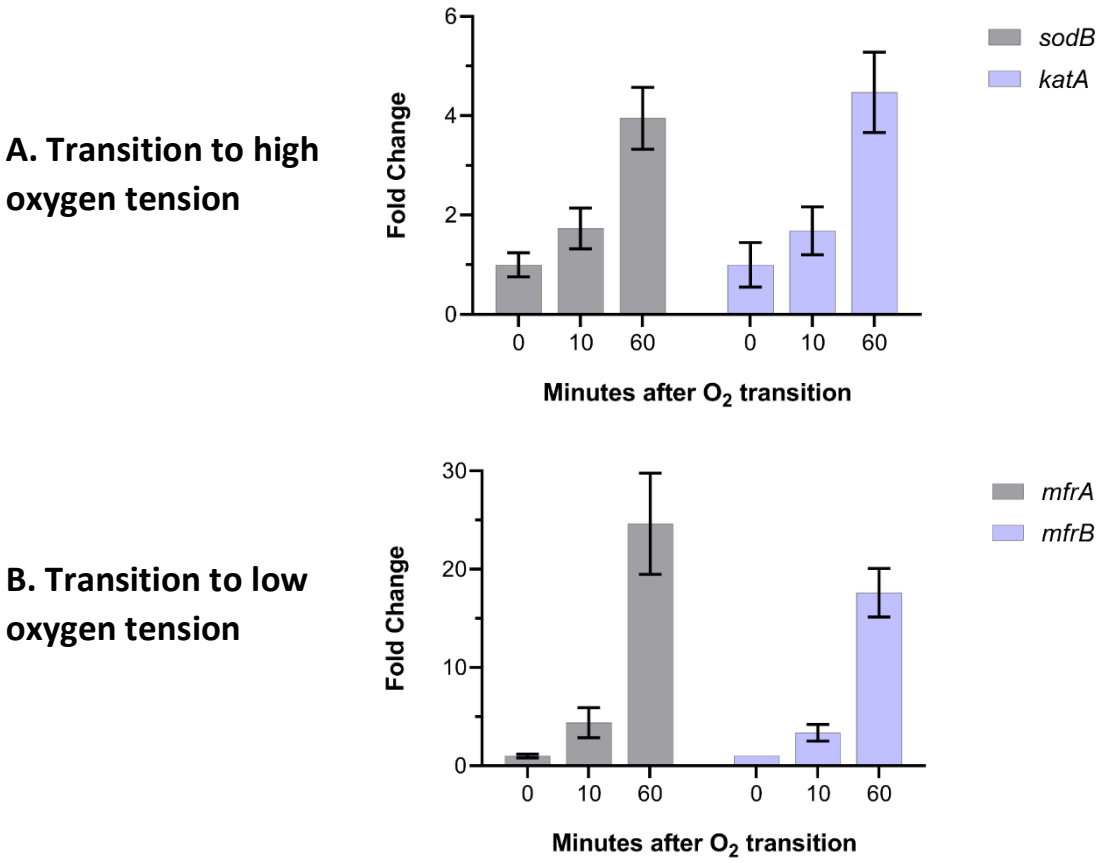

Figure 5.9 Oxygen dependent changes in gene expression. (A) Time dependent increase *sodB* and *katA* expression during the shift from 7.5% to 17% O_2. (B) Time dependant increase in *mfrA* and *mfrB* expression during the shift from 7.5% to 1.88% O_2.

During the transition from steady state to high oxygen tensions, it has been shown that enzymes involved in oxidative stress defence such as superoxide dismutase (*sodB*) and catalase (*katA*) are upregulated (Guccione *et al*., 2017). The expression profiles of these genes were measured after a switch to high oxygen tensions to show physiological adaptations are taking place before RBPs were extracted and analysed. Likewise, the transcription profile was also assessed during the switch to low oxygen tensions by measuring the expression of the methylmenaquinol:fumarate reductase *mfrA* and *mfrB* genes which showed the largest fold change in gene expression after the switch to low oxygen tensions as published by Guccione *et al* (Guccione *et al*., 2017). The methylmenaquinol:fumarate reductase MfrABE, is involved in rapid adaptation to fumarate

respiring conditions which is thought to be driven by RacRS under oxygen limitation in the absence of alternative electron acceptors. The expression profile of *mfrAB* in samples exposed to low oxygen tensions which shows a ~ 25 fold increase in *mfrA* and a ~ 20 fold increase in *mfrB* after 60 minutes at 1.88% O_2 which correlates with previous reports (Guccione *et al.*, 2017). As the selected candidate genes show characteristic expression profiles of cells exposed to high and low oxygen tensions, the dynamic RBPome was determined using TMT labelled mass spectrometry to deduce shifts in the *C. jejuni* RBPome.

To detect dynamic changes in the RBPome after a switch in oxygen tensions, samples at the earlier timepoint, 10 minutes after the change in oxygen tension, were analysed by OOPS to attempt to capture immediate changes in proteins binding or releasing RNA. As well as RBPome analysis, total proteome changes were measured using total cell lysates of the same sample to monitor if changes in OOPs enriched protein abundance correlated with changes in total protein abundance. After tandem mass tag labelling, samples were analysed on an unfractionated Orbitrap Eclipse tribrid mass spectrometer, which detected a total of 4662 peptides in the total RBPome fractions, which associated to 585 master proteins, of which 220 had been previously detected in the preliminary search described above, full dataset shown in Supplementary Table 3.

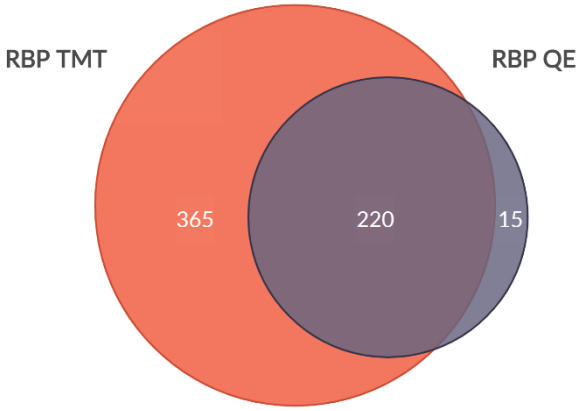

Figure 5.10: Venn diagram comparing RBPs captured using Tandem Mass Tag (TMT) labelling of cross-linked samples plotted against the initial qualitative unfractionated RBPome (QE) to assess the overlap in RBP capture using each method.

5.2.9 RBPome changes under high oxygen concentrations

The sample set which showed the greatest fold change in the RBPome after a switch in oxygen tension was the condition transitioning from steady state to high oxygen saturation. A total of

54 OOPS enriched proteins had a significant change in abundance after the transition from steady state to high oxygen saturations, as shown in Table 5.3**.** Although there are significant changes in the RBPome, the total proteome also showed large scale changes with 337 proteins showing a significant change in abundance after the switch between oxygen tensions.

Gene name	**logFC**	**adj.P.Val**
miaA	-3.06471	0.000513
cstIII	-1.54881	0.000649
Cj1710c	-1.38261	0.000513
lctP	-1.37599	0.003052
sdaC	-1.36318	0.003374
Cj1226c	-1.23865	0.005784
truD	-1.23596	0.001972
rloH	-1.12242	0.001972
Cj1421c	-1.0743	0.001972
Cj0353c	-1.06061	0.001972
Cj0958c	-0.93029	0.003374
Cj1007c	-0.90495	0.00344
Cj1209	-0.89475	0.001972
argS	-0.86175	0.003447
glyS	-0.83719	0.007757
Cj0708	-0.77277	0.004415
hisS	-0.73393	0.005639
Cj1516	-0.65864	0.003052
hslU	0.703874	0.006243
pyrH	0.752761	0.00843
clpP	0.762672	0.003374
Cj0462	0.776694	0.006999
panB	0.790308	0.003551
cheA	0.793829	0.003374
rplM	0.84865	0.002463
Cj1420c	0.87674	0.002463
kpsF	0.88882	0.005794

Gene name	**logFC**	**adj.P.Val**
atpD	0.891645	0.00843
petA	0.92522	0.003051
oorC	0.927564	0.003374
serC	0.931756	0.007955
def	0.949047	0.004955
slyD	0.977045	0.003374
Cj0020c	1.005597	0.003551
Cj0449c	1.015129	0.002961
Cj0448c	1.023731	0.001972
rpsU	1.033318	0.002463
flgR	1.046882	0.001972
ppa	1.053967	0.00344
oorD	1.058516	0.005639
napB	1.082989	0.003347
ccoP	1.134509	0.00344
adk	1.187943	0.002216
cmeA	1.209138	0.00843
rrc	1.210207	0.001984
rpsR	1.23624	0.001972
rpsP	1.334249	0.002625
rpsS	1.372781	0.003374
Cj1164c	1.430385	0.003347
rpsN	1.451017	0.003347
fdxA	1.529827	0.001972
hisJ	1.648751	0.005381
Cj0903c	1.757892	0.001984
dsbI	2.632909	0.00344

Table 5.3: RBPome changes following a switch from steady state to high oxygen saturation after 10 minutes of equilibration. (all pass adjusted p-value threshold of 0.01). Log fold change point estimates show RBP changes from 7.5% O_2 to 17% O_2.

Of the 337 proteins which show a significant change in the total proteome, 190 appear more abundant in the steady state whereas 147 are more abundant 10 minutes after a switch to a high oxygen saturation. Ribosomal and Fe-S cluster proteins appear more abundant in the steady state whereas base excision repair and glycoprotein assembly proteins appear more abundant after a switch to high oxygen saturations.

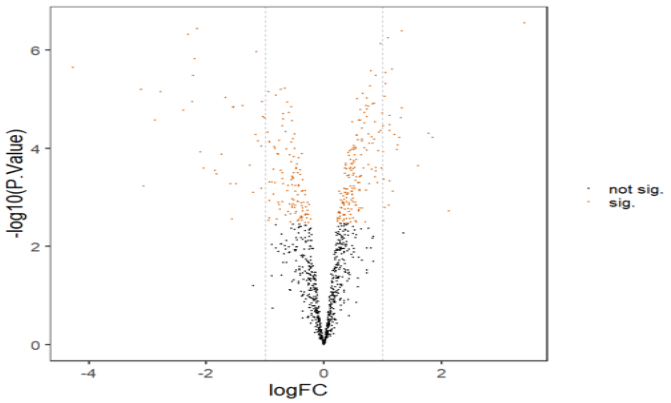

Figure 5.11 Volcano plot showing changes in total protein abundance 10 minutes after a switch from steady state to a high oxygen saturation. Significant fold changes are shown as orange dots with fold changes greater than 2 highlighted outside the black dotted lines. Non-significant peptides are labelled in black.

Of the OOPS enriched RBPs which showed a change in abundance after the transition to a high oxygen concentration, certain pathways were better represented than others. Table 5.4 shows the highest abundant KEGG pathways were ribosomal proteins, tRNA biosynthesis enzymes and proteins involved in oxidative phosphorylation. Proteins with metal, nucleotide and ATP binding sites were all highly abundant.

KEGG PATHWAY	Proteins
Ribosome	8
tRNA biosynthesis	5
Oxidative phosphorylation	4
RNA degradation	2
Purine metabolism	2
Two component system	2

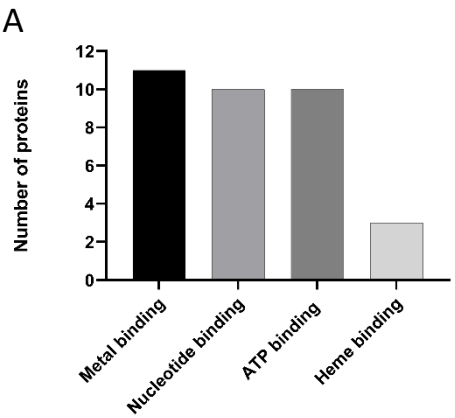

Table 5.4 The most abundant KEGG pathways identified in the dynamic RBPome after a switch to a high oxygen saturation. (A) Chart showing most abundant protein functional groups identifed in dynamic RBPs during high oxygen transition.

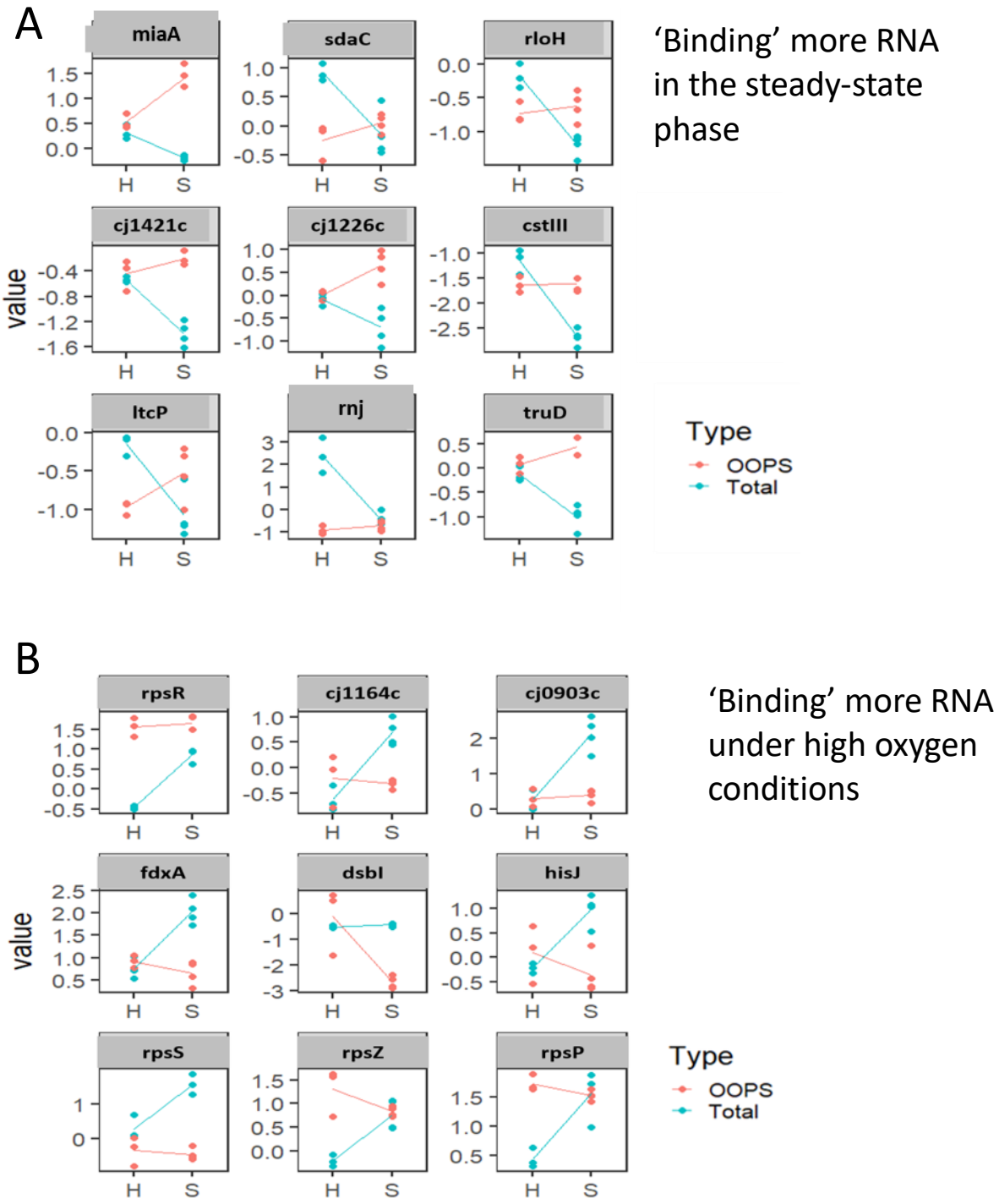

Figure 5.12 Protein abundance plots of OOPS enriched proteins showing greatest fold changes in response to an increase in oxygen saturation plotted with the total proteome changes of the corresponding RBP. (A) OOPS enriched proteins binding more RNA in the steady state phase. (B) OOPS enriched proteins binding more RNA under high oxygen conditions.

Of the proposed RBPs which show the greatest change in abundance after an increase in oxygen concentration, the tRNA dimethylallyltransferase, MiaA and the disulphide bond formation protein DsbI show the largest fold changes, but in opposite directions shown in Figure 5.12. In the case of both MiaA and DsbI, the changes in the RBPome occur independently of changes in the total proteome abundance, suggesting the changes in abundance of the OOPS enriched proteins occurs due to a change in the RNA binding capacity or the target protein.

5.2.9 RBPome changes under low oxygen concentrations

Despite large RBP and total proteome changes occurring in the transition to a high oxygen concentration, comparatively few very little changes were detected after a transition to a low oxygen concentration. A total of 26 proteins showed a significant change in abundance in the total proteome with 5 more abundant in the steady state and 21 proteins more abundant at 1.88% O_2. Only 5 OOPS enriched proteins show a significant change in abundance and these proteins show significant overlap with the RBPs detected in the transition to high oxygen saturation as shown in the PCA plot in Figure 5.13.

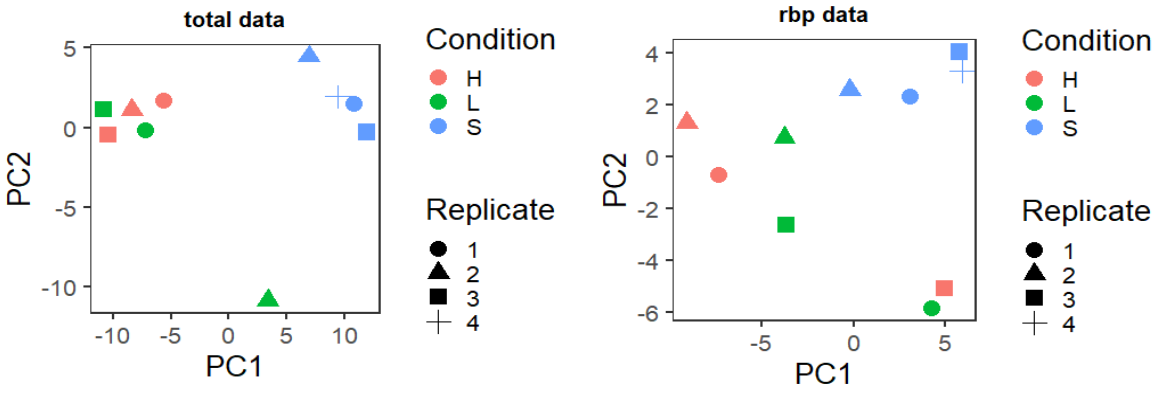

Gene name	Description	log FC	adj.P.Val
miaA	tRNA dimethylallyltransferase	3.359	0.0006782
truD	tRNA pseudouridine synthase	1.419	0.0008021
rnj	Ribonuclease J	1.194	0.0036246
Cj1041c	Putative periplasmic ATP/GTP-binding protein	1.168	0.0021943
dsbI	Disulphide bond formation protein	-2.506	0.0003369

Figure 5.13 Principal component analysis (PCA) plots of total proteome data (left) and RBPome data (right) showing distribution of proteins which show a significant change in abundance between high and low oxygen transitions. Below is table of RBPs which show a significant fold change between steady state and low oxygen saturation and their respective fold changes.

5.3 Discussion

The results published here are the first attempt to generate an RNA binding proteome for *C. jejuni* and outline which RNA binding proteins potentially play a role in the transition between high and low oxygen saturations. As previous prokaryotic OOPS reports have only investigated RBP capture in *E. coli*, we have optimised the original OOPS protocol developed by Queiroz *et al* for use in *C. jejuni* which has a thicker LPS layer and glycoprotein containing cell envelope (Queiroz *et al*., 2019). As AGPC phase separation isolates protein bound RNA based on its amphiphilicity, applying OOPS in a bacteria with an active *N*- and *O*-linked glycosylation system also presents its challenges as glycoproteins are themselves amphiphilic so will migrate to the aqueous organic interphase. To allow accurate identification of RNA-binding glycoproteins, glycans would have to be removed before phase separation, but as only 5 of the 21 annotated *C. jejuni* glycoproteins were OOPS enriched, we simply omitted these proteins from the analysis.

The preliminary dataset outlining the *C. jejuni* RBPome detected 235 proteins OOPS enriched proteins which represents around 14% of the predicted *C. jejuni* proteome, nearly double the coverage seen in *E. coli* (8% of the *K-12* proteome) (Queiroz *et al*., 2019). There was enrichment of classical RNA associated GO terms including ribonucleotide proteins and RNA binding proteins, reinforcing the effectiveness of the method. Of the 235 OOPS enriched proteins, 149 were enriched after cross linking, which suggests *C. jejuni* has 86 tightly associating RBPs which do not require a cross link induced bond for phase separation recovery. Proteins cross linked with RNA are referred to as RBPs as UV cross linking occurs at zero distance, which implies binding, therefore characterisations of the OOPS enriched RBPome needs to account for the total abundance of proteins in the cell. Our results show there is no bias to higher abundance proteins when comparing the logFC between cross-linked and non-cross-linked, highlighting that changes seen correctly represent the cross-link driven capture of RBPs.

Before the analysis was conducted, certain 'positive controls' of previously annotated *C. jejuni* regulatory RNA binding proteins were selected to verify the reliability of the method. CsrA is the most studied regulatory RNA binding protein in *C. jejuni,* yet its small size of only 75 amino acids means detection by unfractionated Orbitrap mass spectrometry was not possible in our initial experiments. Another positive control selected was the Fe-S aconitase proteins AcnA and AcnB, which have been shown to act as post transcriptional regulators in *H. pylori* and *C. jejuni* (Austin *et al*., 2015) (Flint *et al*., 2014). In the initial qualitative *C. jejuni* RBP analysis, AcnB was annotated as an RBP after detection at the interphase (FDR: 0.00704), yet it was not significantly enriched after cross linking (logFC: 0.644, adjusted p value: 0.0147), suggesting the protein maintains a

strong interaction with RNA which is not enhanced by UV cross-linking. This result could have been expected as binding to mRNA by apo-AcnB occurs mainly under conditions of oxidative stress therefore at a steady state growth phase optimal oxygen there may not be an abundance of transiently associated AcnB-mRNA complexes.

The results from the dynamic RBPome analysis show the reproducibility of the OOPS method , with over 94% of the RBPs detected in the initial qualitative analysis being detected again in the quantitative TMT labelled mass spectrometry dataset. Given the increased depth of the TMT labelled mass spectroscopy, a greater abundance of RBPs were detected which totalled 585 proteins or 35% of the total *C. jejuni* proteome. Clearly, it may be considered surprising that the potential RBPome span over a third of the proteome, yet as this is the first time this has been studied in *C. jejuni*, and with the lack of other complete RBPomes in other systems, it could well be the case that the RNA protein interactome is far greater than previously thought.

Despite multiple RBPs showing a significant change in abundance after a switch in oxygen tension, changes often occur alongside large variation in the total protein abundance as shown in Figure 5.12 which is surprising. The purpose of selecting the shorter period of 10 minutes of equilibration was so that large scale proteomic changes following the transcription factor induced translational burst would be avoided and to focus primarily on immediate RBPome changes. However, with over 350 proteins showing a significant change in abundance after 10 minutes of the shift to 17% oxygen, there is clearly a much larger dynamic global proteomic response which we had not anticipated. As the changes occurred over a period of 10 minutes, it seems unlikely to be attributed to a transcriptional burst and more likely a change in RNA or protein turnover. The large overlap in the PCA plots showing the total proteome changes between high and low oxygen conditions in Figure 5.13 shows the response we see is a more general stress response and not one specific to the oxygen saturation. This is plausible given the cells were only equilibrated for 10 minutes at the new oxygen saturation before samples were taken which wouldn't be enough time to induce a tailored transcriptional response.

When looking to validate the results from the dynamic RBPome dataset, some known control proteins were analysed again to give more confidence in the experimental design. Given the proposed role of AcnB in oxidative stress defence, it would be expected that there would be an increase in the OOPS enriched capture of AcnB following a switch to high oxygen saturations to increase stability of the oxidative stress defence enzyme transcripts. qRT-PCR analysis shows there is an upregulation of the oxidative stress defence genes *sodB* and *katA* yet no significant abundance changes of AcnB were detected in the OOPS enriched fractions. Given the greatest fold change in transcript abundance of *sodB* and *katA* was detected after 60 minutes as shown

in Figure 5.9, it is possible that the increase in the RBP capacity of AcnB will come later in the cell response. Although the mass spectrometry analysis of the dynamic proteomic response had a greater depth of detection, CsrA was still not detected despite being it being a known regulator of oxidative stress defence (Fields *et al*., 2016). Given the lack of CsrA in both datasets, we are currently reanalysing the dynamic RBPome using a fractionated mass spectrometry approach to give greater depth and potentially better detection of CsrA if it is indeed an RBP.

Although the results show a clear lack of positive controls of known regulatory RBPs, there were a number of RBPs which showed an unexpected change in abundance after switch in oxygen tensions. One OOPS enriched protein which showed significant changes under both conditions was the disulphide bond formation protein DsbI. The total proteome data shows DsbI abundance remains unchanged following the transition to high or low oxygen saturations yet the abundance of *dsbI* in the OOPS enriched fractions is significantly more abundant (high oxygen logFC: 2.63, low oxygen logFC: 2.51). The Dsb (disulfide bond) family proteins are involved primarily in the formation of disulfide bridges in periplasmic proteins of Gram-negative bacteria. DsbA is a periplasmic protein that catalyses the formation of disulphide bonds in many periplasmic client proteins, while the electrons from this reaction are passed to the cytoplasmic membrane bound DsbB which transfers them to the quinone pool. Some bacteria contain paralogues of DsbA and DsbB, denoted DsbL and DsbI respectively, that appear to be required for disulphide bond formation in a specialised subset of periplasmic proteins (Raczko *et al*., 2005). In *C. jejuni*, the *dsbI* gene is translationally coupled to a small upstream gene called *dba*, of uncertain function (Raczko *et al*., 2005), but it has been confirmed that *dba* expression is required for the synthesis of DsbI and the importance of a secondary *dba-dsbI* mRNA structure for *dsbI* mRNA translation was verified by estimating individual *dsbI* gene expression from its own promoter (Grabowska *et al*., 2011). It may therefore be possible that both Dba and DsbI are RNA binding proteins interacting with their own mRNA to regulate expression in response to changes in cellular redox status caused by changes in ambient oxygen levels.

The OOPS enriched protein which showed the most significant response to oxygen fluctuations was the tRNA dimethylallyltransferase MiaA, which catalyses the transfer of a dimethylallyl group at position 37 in uridine reading tRNAs. It has recently been proposed that MiaA controls the abundance of multiple stress response RBPs including RpoS and Hfq, as their coding sequence is significantly enriched for leucine codons that use MiaA-modified tRNAs (Aubee *et al*., 2017). The total proteome data shows the abundance of MiaA increases under both oxygen saturations (high oxygen logFC: 2.87, low oxygen logFC: 2.91) yet its abundance as an RBP

significantly decreases under both conditions (high oxygen logFC: -3.06, low oxygen logFC: -3.35).

Another known RBP which showed a significant decrease in abundance under both oxygen saturations was the exonuclease ribonuclease J (high oxygen logFC: -1.38, low oxygen logFC: -1.19). After seeing large changes in the total proteome datasets after just 10 minutes of equilibration at both oxygen tensions, we speculated that rapid changes in RNA turnover may contribute to the significant differences seen. It is known that bacteria utilise ribonucleases to allow rapid turnover of the cellular RNA under stress conditions to allow a transcriptome rearrangement and an increase in the transcriptional rate of stress-specific genes. As the OOPS enriched RBPome dataset shows a >2 fold decrease in abundance of ribonuclease J in both conditions, it is possible that this may contribute to the significant increase in total protein abundance due to the significant decrease in RNA degradation.

Overall, we have confirmed that OOPS can be a highly efficient global method for the isolation and identification of RNA-protein complexes. Our results show a clear enrichment of RNA associated GO terms, yet the omission of known RNA binding regulators makes a more detailed interpretation of results in *C. jejuni* problematic. Before the dataset is further scrutinised, we intend to reanalyse the dynamic RBPome using fractionated mass spectrometry to gain better depth and identification of the known RBPs which have been described to play a significant role in *C. jejuni* stress defence.

Chapter 6. Conclusion

The work carried out in this thesis demonstrates the effectiveness of PDI as a novel antimicrobial approach to kill bacterial pathogens. Despite its discovery over a century ago, light activated antimicrobials have been widely ignored and currently only three photo antimicrobial agents have received clinical approval. The main limitations to PDI lies in both the delivery of the photosensitiser to the bacterial target and the delivery of light to the photo antimicrobial agent. If these challenges can be overcome, light activated photosensitisers could provide an innovative, non-antibiotic approach to inactivate pathogenic bacteria.

In Chapter 3 the publication Appleby *et al*. (2020) is presented, which demonstrates the effectiveness of silica bound photosensitisers in the treatment of bacterial pathogens in water. We have shown in this report that silica bound Cu(I) diimine complexes are highly efficient at killing water borne bacterial pathogens when bound to silica. As the Copper complex is immobilised, the photosensitiser can be easily removed prior to consumption, without difficult and costly extraction techniques. We have shown the silica Cu(I) diimine complex is effective at killing both gram negative and Gram -positive bacteria, with log reductions comparable to the approved clinical photosensitiser methylene blue. Typically, Gram negative pathogens are difficult to treat with exogenous photosensitisers as the outer lipid membrane presents an additional permeability barrier for extracellular ROS to penetrate. However, by functionalising the photosensitiser to have an overall positive charge, we found greater killing efficiencies in *E. coli* due to the attraction of the photosensitiser to attraction to the bacterial phospholipid membrane. In order to implement this finding for use as a water disinfection technique, future work will focus on analysing the effectiveness of the silica bound complex in killing a wider range of water borne pathogens, such as *Vibrio cholera* and *Salmonella enterica*.

In Chapter 4 the manuscript by Walker *et al* is presented on the mechanism of photodynamic inactivation in *C. jejuni*. Here we characterise the major endogenous photosensitisers in *C. jejuni* which differentiate it from other non-light sensitive bacteria and identify which enzyme and protein complexes in *C. jejuni* are damaged by photooxidative stress. The global transcriptional response to photooxidative stress shows both the heat shock response proteins and oxidative stress defence enzymes which are involved in protecting the cell against PDI. Given the level of upregulation of *cj1384* and proximity to the major peroxide defence enzyme *katA* , this gene is an ideal target for future analysis. Despite numerous attempts to mutate or overexpress this gene in *C. jejuni* in both this report, and by others, we speculate that this may be an essential gene in *C. jejuni*. Given the gene lies in an operon, upstream of the essential redox enzyme

flavodoxin (FldA), it is possible that attempts to mutate using classical resistance cassette cloning may disrupt the expression of the downstream *fldA*. Alternatively, *cj1384c* may indeed have an unknown function which is essential to *C. jejuni*, but further work is required to ascertain its role.

Finally, we present in Chapter 5 the use of a new RBP capture technique OOPS, to identify novel regulatory RNA binding proteins controlling the switch between oxygen tensions in *C. jejuni*. We successfully optimised the method for use in this glycoprotein containing bacterial pathogen and generated a list of 235 potential RBPs in *C. jejuni*. We followed this up by analysing changes in the *C. jejuni* RBPome after a switch in oxygen tension. The mass spectrometry dataset identified multiple OOPS enriched proteins which showed a significant change in response to oxygen fluctuations, yet these changes occurred amongst a background of high total proteome changes. Before we analyse these findings in more detail, future work must focus on applying a fractionated mass spectrometry analysis to gain better depth, to identify the known regulatory RBPs CsrA and AcnB. Further analysis of OOPS enriched protein DsbI, which showed significant changes after a switch to both high and low oxygen saturations may identify a role for this protein in the transition between oxygen tensions.

Overall, we have shown the potential of PDI in combatting bacterial infections by exploiting both endogenous and exogenous photosensitisers. The primary objective from this thesis was to understand why *C. jejuni* is more susceptible to violet/blue light than other bacterial pathogens. Given *C. jejuni* evolved from deep sea vent bacteria, multiple facets of its physiology remain unique from other canonical pathogens, which are not fitness reducing in their own right, yet in combination with violet/blue light, we have shown these unique physiological differences form the Achilles' heel of this bacteria, resulting in *C. jejuni* being far more sensitive to PDI than other bacterial pathogens.

Chapter 7: References

Ahmed, I. H., Manning, G., Wassenaar, T. M., Cawthraw, S., & Newell, D. G. (2002). Identification of genetic differences between two *Campylobacter jejuni* strains with different colonization potentials. *Microbiology*. *148,* 1203-1212

Alemka, A., Whelan, S., Gough, R., Clyne, M., Gallagher, M. E., Carrington, S. D., & Bourke, B. (2010). Purified chicken intestinal mucin attenuates *Campylobacter jejuni* pathogenicity *in vitro*. *Journal of Medical Microbiology*. *59,* 898-903

Anzaldi, L. L., & Skaar, E. P. (2010). Overcoming the heme paradox: Heme toxicity and tolerance in bacterial pathogens. In *Infection and Immunity*. *20,* 613-620

Arenas, Y., Monro, S., Shi, G., Mandel, A., McFarland, S., & Lilge, L. (2013). Photodynamic inactivation of *Staphylococcus aureus* and methicillin-resistant S*taphylococcus aureus* with Ru(II)-based type I/type II photosensitizers. *Photodiagnosis and Photodynamic Therapy*. *4* 615-625

Atack, J. M., Harvey, P., Jones, M. A., & Kelly, D. J. (2008). The *Campylobacter jejuni* thiol peroxidases Tpx and Bcp both contribute to aerotolerance and peroxide-mediated stress resistance but have distinct substrate specificities. *Journal of Bacteriology 15* 5279-5290

Atack, J. M., & Kelly, D. J. (2008). Contribution of the stereospecific methionine sulphoxide reductases MsrA and MsrB to oxidative and nitrosative stress resistance in the food-borne pathogen *Campylobacter jejuni*. *Microbiology*.*154* 2219-2230

Aubee, J. I., Olu, M., & Thompson, K. M. (2017). TrmL and TusA are necessary for rpoS and miaA is required for hfq expression in *Escherichia coli*. *Biomolecules*. *151,* 2219-2230

Austin, C. M., Wang, G., & Maier, R. J. (2015). Aconitase functions as a pleiotropic posttranscriptional regulator in *Helicobacter pylori*. *Journal of Bacteriology*. *197* 3076-3086

Baillon, M. L. A., Van Vliet, A. H. M., Ketley, J. M., Constantinidou, C., & Penn, C. W. (1999). An iron-regulated alkyl hydroperoxide reductase (AhpC) confers aerotolerance and oxidative stress resistance to the microaerophilic pathogen *Campylobacter jejuni. Journal of Bacteriology*. *186 (16)* 4798-4804

Bartolomeu, M., Rocha, S., Cunha, Â., Neves, M. G. P. M. S., Faustino, M. A. F., & Almeida, A. (2016). Effect of photodynamic therapy on the virulence factors of S*taphylococcus aureus*. *Frontiers in Microbiology*. *36, 829-834*

Bashor, M. P., Curtis, P. A., Keener, K. M., Sheldon, B. W., Kathariou, S., & Osborne, J. A. (2004). Effects of carcass washers on *Campylobacter* contamination in large broiler processing *254,* 247-251

Battisti, A., Morici, P., Signore, G., Ghetti, F., & Sgarbossa, A. (2017). Compositional analysis of endogenous porphyrins from *Helicobacter pylori*. *Biophysical Chemistry*. *254,* 197-215

Baureder, M., & Hederstedt, L. (2013). Heme Proteins in Lactic Acid Bacteria. In *Advances in Microbial Physiology* (1st ed., Vol. 62). *Elsevier Ltd*. *288,* 7618-7625

Beeby, M., Ribardo, D. A., Brennan, C. A., Ruby, E. G., Jensen, G. J., Hendrixson, D. R., & Hultgren, S. J. (2016). Diverse high-torque bacterial flagellar motors assemble wider stator rings using a conserved protein scaffold. *Proceedings of the National Academy of Sciences of the United States of America*. *59,* 458-468

Buchovec, I., Lukseviciūtė, V., Kokstaite, R., Labeikyte, D., Kaziukonyte, L., & Luksiene, Z. (2017). Inactivation of Gram (−) bacteria *Salmonella* enterica by chlorophyllin-based photosensitization: Mechanism of action and new strategies to enhance the inactivation efficiency. *Journal of Photochemistry and Photobiology B: Biology*. *72,* 2430-2436

Bühl, M., & van Mourik, T. (2011). NMR spectroscopy: Quantum-chemical calculations. In *Wiley Interdisciplinary Reviews: Computational Molecular Science*. *67,* 1146-1152

Bull, S. A., Allen, V. M., Domingue, G., Jørgensen, F., Frost, J. A., Ure, R., Whyte, R., Tinker, D., Corry, J. E. L., Gillard-King, J., & Humphrey, T. J. (2006). Sources of *Campylobacter* spp. colonizing housed broiler flocks during rearing. *Applied and Environmental Microbiology*. *60,* 656-657

Burnham, P. M., & Hendrixson, D. R. (2018). *Campylobacter jejuni:* collective components promoting a successful enteric lifestyle. In *Nature Reviews Microbiology*. *44,* 191-199

Butcher, J., Handley, R. A., van Vliet, A. H. M., & Stintzi, A. (2015). Refined analysis of the *Campylobacter jejuni* iron-dependent/independent Fur- and PerR-transcriptomes. *BMC Genomics*. *17,* 203-207

Butzler, J. P. (2004). *Campylobacter*, from obscurity to celebrity. In *Clinical Microbiology and Infection*. *117,* 1146-1148

Cadranel, S., Rodesch, P., Butzler, J. P., & Dekeyser, P. (1973). Enteritis Due to "Related Vibrio" in Children. *American Journal of Diseases of Children*. *124,* 1-18

Caldwell, D. B., Wang, Y., & Lin, J. (2008). Development, stability, and molecular mechanisms of macrolide resistance in C*ampylobacter jejuni*. *Antimicrobial Agents and Chemotherapy*. *69,* 338-344

Cameron, A., & Gaynor, E. C. (2014). Hygromycin B and apramycin antibiotic resistance cassettes for use in *Campylobacter jejuni*. *PLoS ONE*. *69,* 14-18

Chelikani, P., Fita, I., & Loewen, P. C. (2004). Diversity of structures and properties among catalases. In *Cellular and Molecular Life Sciences*.*46, 209-223*

Chomczynski, P., & Sacchi, N. (2006). The single-step method of RNA isolation by acid guanidinium thiocyanate-phenol-chloroform extraction: Twenty-something years on. *Nature Protocols*. *289,* 209-223

Cieplik, F., Steinwachs, V. S., Muehler, D., Hiller, K. A., Thurnheer, T., Belibasakis, G. N., Buchalla, W., & Maisch, T. (2018). Phenalen-1-one-mediated antimicrobial photodynamic therapy: Antimicrobial efficacy in a periodontal biofilm model and flow cytometric evaluation of cytoplasmic membrane damage. *Frontiers in Microbiology*. *289, 8007-8018*

Clauditz, A., Resch, A., Wieland, K. P., Peschel, A., & Götz, F. (2006). Staphyloxanthin plays a role in the fitness of *Staphylococcus aureus* and its ability to cope with oxidative stress. *Infection and Immunity*. *193,* 205-214

Cohn, M. T., Ingmer, H., Mulholland, F., Jørgensen, K., Wells, J. M., & Brøndsted, L. (2007). Contribution of conserved ATP-dependent proteases of *Campylobacter jejuni* to stress tolerance and virulence. *Applied and Environmental Microbiology*. *193,* 205-214

Costa, L., Faustino, M. A. F., Tomé, J. P. C., Neves, M. G. P. M. S., Tomé, A. C., Cavaleiro, J. A. S., Cunha, Â., & Almeida, A. (2013). Involvement of type i and type II mechanisms on the photoinactivation of non-enveloped DNA and RNA bacteriophages. *Journal of Photochemistry and Photobiology B: Biology*. *6,* 343-345

Couri, D., Abdel-Rahman, M. S., & Bull, R. J. (1982). Toxicological effects of chlorine dioxide,

chlorite and chlorate. *Environmental Health Perspectives*. *277,* 327-337

Cox, J. M., & Pavic, A. (2010). Advances in enteropathogen control in poultry production. In *Journal of Applied Microbiology*. *172,* 84-132

Crack, J. C., Green, J., Hutchings, M. I., Thomson, A. J., & Le Brun, N. E. (2012). Bacterial iron-sulfur regulatory proteins as biological sensor-switches. In *Antioxidants and Redox Signaling*. *163,* 305-310

Dai, T., Huang, Y. Y., & Hamblin, M. R. (2009). Photodynamic therapy for localized infections-State of the art. In *Photodiagnosis and Photodynamic Therapy*. *23,* 102-109

Davies, M. J. (2003). Singlet oxygen-mediated damage to proteins and its consequences. *Biochemical and Biophysical Research Communications*. *61,* 1764-1771

De Freitas, L. F., & Hamblin, M. R. (2016). Antimicrobial photoinactivation with functionalized fullerenes. In *Nanobiomaterials in Antimicrobial Therapy: Applications of Nanobiomaterials*. *2,* 1-8

Defty, C. L., & Orpin, S. (2011). Photodynamic therapy: How a "flash" of inspiration was critical in the development of the modern process. *British Journal of Dermatology*.*330,* 81-89

Denkel, L. A., Horst, S. A., Rouf, S. F., Kitowski, V., Böhm, O. M., Rhen, M., Jäger, T., & Bange, F. C. (2011). Methionine sulfoxide reductases are essential for virulence of Salmonella typhimurium. *PLoS ONE*. 4

Domonkos, I., Kis, M., Gombos, Z., & Ughy, B. (2013). Carotenoids, versatile components of oxygenic photosynthesis. In *Progress in Lipid Research*. *6,* 1-12

Dosselli, R., Millioni, R., Puricelli, L., Tessari, P., Arrigoni, G., Franchin, C., Segalla, A., Teardo, E., & Reddi, E. (2012). Molecular targets of antimicrobial photodynamic therapy identified by a proteomic approach. *Journal of Proteomics*. *95,* 189-198

Du, W., Sun, C., Liang, Z., Han, Y., & Yu, J. (2012). Antibacterial activity of hypocrellin A against *Staphylococcus aureus*. *World Journal of Microbiology and Biotechnology*, *28*(11), 3151–3157. *62, 694-700*

Escherich, T. (1886). Ueber das Vorkommen von Vibrionen im Darmcanal und den Stuhlgangen der Sauglinge.(Articles adding to the knowledge of intestinal bacteria. III. On the existence of vibrios in the intestines and feces of babies.). *Beitrage Zur Kenntniss Der Darmbacterien. III*. *62,* 807-809

Esposito, L., Seydel, A., Aiello, R., Sorrentino, G., Cendron, L., Zanotti, G., & Zagari, A. (2008). The crystal structure of the superoxide dismutase from *Helicobacter pylori* reveals a structured C-terminal extension. *Biochimica et Biophysica Acta - Proteins and Proteomics*. *56,* 1560-1566

European Commission. (2004). Regulation (EC) N° 853/2004 of the European Parlamient and of the Council of 29 April 2004 laying down specific hygiene rules for on the hygiene of foodstuffs. *Official Journal of the European Union*, *L 139*(853), *74,* 4698-4707

Ewing, C. P., Andreishcheva, E., & Guerry, P. (2009). Functional characterization of flagellin glycosylation in *Campylobacter jejuni* 81-176. *Journal of Bacteriology*. *24,*1551-1557

Faraj Tabrizi, P., Wennige, S., Berneburg, M., & Maisch, T. (2018). Susceptibility of sodA- and sodB-deficient: *Escherichia coli* mutant towards antimicrobial photodynamic inactivation via the type I-mechanism of action. *Photochemical and Photobiological Sciences*, *17*(3), 352–362.

Faulkner, M. J., Ma, Z., Fuangthong, M., & Helmann, J. D. (2012). Derepression of the bacillus subtilis perr peroxide stress response leads to iron deficiency. *Journal of Bacteriology*. *183,* 3953-3959

Fields, J. A., Li, J., Gulbronson, C. J., Hendrixson, D. R., & Thompson, S. A. (2016). *Campylobacter jejuni* CsrA regulates metabolic and virulence associated proteins and is necessary for mouse colonization. *PLoS ONE*.*4,* 1-9

Fields, J. A., & Thompson, S. A. (2008). *Campylobacter jejuni* CsrA mediates oxidative stress responses, biofilm formation, and host cell invasion. *Journal of Bacteriology*. *63,* 462-468

Flint, A., Sun, Y. Q., Butcher, J., Stahl, M., Huang, H., & Stintzi, A. (2014). Phenotypic screening of a targeted mutant library reveals *Campylobacter jejuni* defenses against oxidative stress. *Infection and Immunity*. *150,* 1957-1964

Garénaux, A., Guillou, S., Ermel, G., Wren, B., Federighi, M., & Ritz, M. (2008). Role of the Cj1371 periplasmic protein and the Cj0355c two-component regulator in the *Campylobacter jejuni* NCTC 11168 response to oxidative stress caused by paraquat. *Research in Microbiology*. *16,* 1105-1121

Gaynor, E. C., Cawthraw, S., Manning, G., MacKichan, J. K., Falkow, S., & Newell, D. G. (2004). The Genome-Sequenced Variant of *Campylobacter jejuni* NCTC 11168 and the Original Clonal Clinical Isolate Differ Markedly in Colonization, Gene Expression, and Virulence-Associated Phenotypes. *Journal of Bacteriology*. *70,* 2800-2812

Georgsson, F., orkelsson, Á. E., Geirsdóttir, M., Reiersen, J., & Stern, N. J. (2006). The influence of freezing and duration of storage on *Campylobacter* and indicator bacteria in broiler carcasses. *Food Microbiology*. *101,* 953-963

Golden, N. J., & Acheson, D. W. K. (2002). Identification of motility and autoagglutination *Campylobacter jejuni* mutants by random transposon mutagenesis. *Infection and Immunity*. *314,* 1148-1150

Gollmer, A., Felgentraeger, A., Maisch, T., & Flors, C. (2017). Real-time imaging of photodynamic action in bacteria. *Journal of Biophotonics*. *271,* 47-55

Gomes, M. C., Silva, S., Faustino, M. A. F., Neves, M. G. P. M. S., Almeida, A., Cavaleiro, J. A. S., Tomé, J. P. C., & Cunha, Â. (2013). Cationic galactoporphyrin photosensitisers against UV-B resistant bacteria: Oxidation of lipids and proteins by 1O2. *Photochemical and Photobiological Sciences*. *79,* 3718-3741

Guccione, E., Del Rocio Leon-Kempis, M., Pearson, B. M., Hitchin, E., Mulholland, F., Van Diemen, P. M., Stevens, M. P., & Kelly, D. J. (2008). Amino acid-dependent growth of *Campylobacter jejuni*: Key roles for aspartase (AspA) under microaerobic and oxygen-limited conditions and identification of AspB (Cj0762), essential for growth on glutamate. *Molecular Microbiology*.*38,* 898-899

Guccione, E., Hitchcock, A., Hall, S. J., Mulholland, F., Shearer, N., van Vliet, A. H. M., & Kelly, D. J. (2010). Reduction of fumarate, mesaconate and crotonate by Mfr, a novel oxygen-regulated periplasmic reductase in Campylobacter jejuni. *Environmental Microbiology*. *36,* 3421-3428

Guccione, E. J., Kendall, J. J., Hitchcock, A., Garg, N., White, M. A., Mulholland, F., Poole, R. K., & Kelly, D. J. (2017). Transcriptome and proteome dynamics in chemostat culture reveal how *Campylobacter jejuni* modulates metabolism, stress responses and virulence factors upon changes in oxygen availability. *Environmental Microbiology*. *186,* 88-98

Guerry, P., Ewing, C. P., Schirm, M., Lorenzo, M., Kelly, J., Pattarini, D., Majam, G., Thibault, P.,

& Logan, S. (2006). Changes in flagellin glycosylation affect *Campylobacter* autoagglutination and virulence. *Molecular Microbiology*. *52,* 174-180

Gundogdu, O., Bentley, S. D., Holden, M. T., Parkhill, J., Dorrell, N., & Wren, B. W. (2007). Re-annotation and re-analysis of the *Campylobacter jejuni* NCTC11168 genome sequence. *BMC Genomics*. *76,* 2114-2145

Gundogdu, O., da Silva, D. T., Mohammad, B., Elmi, A., Mills, D. C., Wren, B. W., & Dorrell, N. (2015). The Campylobacter jejuni MarR-like transcriptional regulators RrpA and RrpB both influence bacterial responses to oxidative and aerobic stresses. *Frontiers in Microbiology*. *74,* 48-89

Hamblin, M. R., & Hasan, T. (2004). Photodynamic therapy: A new antimicrobial approach to infectious disease? In *Photochemical and Photobiological Sciences*. *31,* 297-300

Hamblin, M. R., Viveiros, J., Yang, C., Ahmadi, A., Ganz, R. A., & Tolkoff, M. J. (2005). *Helicobacter pylori* accumulates photoactive porphyrins and is killed by visible light. *Antimicrobial Agents and Chemotherapy*. *6,* 1-14

Hanahan, D. (1983). Studies on transformation of *Escherichia coli* with plasmids. *Journal of Molecular Biology*. *28,* 1255-1260

Hendrixson, D. R., & DiRita, V. J. (2004). Identification of *Campylobacter jejuni g*enes involved in commensal colonization of the chick gastrointestinal tract. *Molecular Microbiology*. *298,* 1778-1789

Hessling, M., Spellerberg, B., & Hoenes, K. (2017). Photoinactivation of bacteria by endogenous photosensitizers and exposure to visible light of different wavelengths - A review on existing data. In *FEMS Microbiology Letters*. *104,* 1-13

Hoang, K. V., Stern, N. J., & Lin, J. (2011). Development and stability of bacteriocin resistance in *Campylobacter* spp. *Journal of Applied Microbiology*. *72,* 211-227

Hoffman, P. S., & Goodman, T. G. (1982). Respiratory physiology and energy conservation efficiency of *Campylobacter jejuni*. *Journal of Bacteriology*. *12,* 4052-4062

Holmes, K., Mulholland, F., Pearson, B. M., Pin, C., McNicholl-Kennedy, J., Ketley, J. M., & Wells, J. M. (2005). *Campylobacter jejuni* gene expression in response to iron limitation and the role of Fur. *Microbiology*. *244,* 258-259

Hong, Y. H., Ku, G. J., Kim, M. K., & Song, K. Bin. (2008). Effect of aqueous chlorine dioxide treatment on the microbial growth and quality of chicken legs during storage. *Journal of Food Science and Nutrition*. *52,* 702-706

Imlay, J. A. (2006). Iron-sulphur clusters and the problem with oxygen. In *Molecular Microbiology*. *20,* 1154-1162

Imlay, J. A. (2013). The molecular mechanisms and physiological consequences of oxidative stress: Lessons from a model bacterium. In *Nature Reviews Microbiology*. *11,* 1971-1981

Jackson, R. J., Elvers, K. T., Lee, L. J., Gidley, M. D., Wainwright, L. M., Lightfoot, J., Park, S. F., & Poole, R. K. (2007). Oxygen reactivity of both respiratory oxidases in *Campylobacter jejuni*: The cydAB genes encode a cyanide-resistant, low-affinity oxidase that is not of the cytochrome bd type. *Journal of Bacteriology*. *183,* 1607-1616

Jesionek A, T. von H. (1905). Zur Behandlung der Hautcarcinome mit fluoreszierenden Stoffen. *Dtsch Arch Klin Med*, *85:*223–239.

Johnson, M., Zaretskaya, I., Raytselis, Y., Merezhuk, Y., McGinnis, S., & Madden, T. L. (2008).

NCBI BLAST: a better web interface. *Nucleic Acids Research*. *10,* 178-189

Jones, A. M., & Elliott, T. (2010). A purified mutant HemA protein from *Salmonella enterica* serovar Typhimurium lacks bound heme and is defective for heme-mediated regulation *in vivo*. *FEMS Microbiology Letters*. *282,* 1584-1598

Jones, M. A., Marston, K. L., Woodall, C. A., Maskell, D. J., Linton, D., Karlyshev, A. V., Dorrell, N., Wren, B. W., & Barrow, P. A. (2004). Adaptation of *Campylobacter jejuni* NCTC11168 to high-level colonization of the avian gastrointestinal tract. *Infection and Immunity*. *457,* 343-347

Karlyshev, A. V., Linton, D., Gregson, N. A., & Wren, B. W. (2002). A novel paralogous gene family involved in phase-variable flagella-mediated motility in *Campylobacter jejuni*. *Microbiology*.*11,* 1109-1150

Kasimova, K. R., Sadasivam, M., Landi, G., Sarna, T., & Hamblin, M. R. (2014). Potentiation of photoinactivation of Gram-positive and Gram-negative bacteria mediated by six phenothiazinium dyes by addition of azide ion. *Photochemical and Photobiological Sciences*. *11,* 133-138

Kelly, D. J. (2001). The physiology and metabolism of *Campylobacter jejuni* and *Helicobacter pylori*. *Journal of Applied Microbiology Symposium Supplement*. *87,* 77-89

Kendall, J. J., Barrero-Tobon, A. M., Hendrixson, D. R., & Kelly, D. J. (2014). Hemerythrins in the microaerophilic bacterium *Campylobacter jejuni* help protect key iron-sulphur cluster enzymes from oxidative damage. *Environmental Microbiology*. *91,* 57-65

Kere Kemp, G., Aldrich, M. L., Guerra, M. L., & Schneider, K. R. (2001). Continuous online processing of fecal- and ingesta contaminated poultry carcasses using an acidified sodium chlorite antimicrobial intervention. *Journal of Food Protection*. *465,* 419-450

Khademian, M., & Imlay, J. A. (2017). *Escherichia coli* cytochrome c peroxidase is a respiratory oxidase that enables the use of hydrogen peroxide as a terminal electron acceptor. *Proceedings of the National Academy of Sciences of the United States of America*. *105,* 871-888

Kim, C., Hung, Y. C., & Russell, S. M. (2005). Efficacy of electrolyzed water in the prevention and removal of fecal material attachment and its microbicidal effectiveness during simulated industrial poultry processing. *Poultry Science*. *184.* 4178-4191

Kim, J. C., Oh, E., Kim, J., & Jeon, B. (2015). Regulation of oxidative stress resistance in *Campylobacter jejuni*, a microaerophilic foodborne pathogen. In *Frontiers in Microbiology*. *101,* 909-923

King, E. O. (1957). Human infections with vibrio fetus and a closely related vibrio. *Journal of Infectious Diseases*.*76,* 5269-5277

King, E. O. (1962). The laboratory recognition of vibrio fetus and a closely related vibrio isolated from cases of human vibriosis. *Annals of the New York Academy of Sciences*. *76,* 5298-5301

Lauro, F. M., Pretto, P., Covolo, L., Jori, G., & Bertoloni, G. (2002). Photoinactivation of bacterial strains involved in periodontal diseases sensitized by porphycene-polylysine conjugates. *Photochemical and Photobiological Sciences*. *45,* 960-967

Lawes, J. R., Vidal, A., Clifton-Hadley, F. A., Sayers, R., Rodgers, J., Snow, L., Evans, S. J., & Powell, L. F. (2012). Investigation of prevalence and risk factors for *Campylobacter* in broiler flocks at slaughter: Results from a UK survey. In *Epidemiology and Infection*. 2

LEVY, A. J. (1946). A gastro-enteritis cutbreak probably due to a bovine strain of vibrio. *The Yale Journal of Biology and Medicine*.*2,* 9-11

Line, J. E., Svetoch, E. A., Eruslanov, B. V., Perelygin, V. V., Mitsevich, E. V., Mitsevich, I. P., Levchuk, V. P., Svetoch, O. E., Seal, B. S., Siragusa, G. R., & Stern, N. J. (2008). Isolation and purification of enterocin E-760 with broad antimicrobial activity against Gram-positive and Gram-negative bacteria. *Antimicrobial Agents and Chemotherapy*. *10,* 699-711

Liu, Y. W., & Kelly, D. J. (2015). Cytochrome c biogenesis in *Campylobacter jejuni* requires cytochrome c6 (CccA; Cj1153) to maintain apocytochrome cysteine thiols in a reduced state for haem attachment. *Molecular Microbiology*, *96*(6), 1298–1317.

Maisch, T., Bosl, C., Szeimies, R. M., Lehn, N., & Abels, C. (2005). Photodynamic effects of novel XF porphyrin derivatives on prokaryotic and eukaryotic cells. *Antimicrobial Agents and Chemotherapy*. *69,* 2468-2482

Maisch, Tim, Baier, J., Franz, B., Maier, M., Landthaler, M., Szeimies, R. M., & Bäumler, W. (2007). The role of singlet oxygen and oxygen concentration in photodynamic inactivation of bacteria. *Proceedings of the National Academy of Sciences of the United States of America*. *63,* 4280-4298

Mancini, S., & Imlay, J. A. (2015). The induction of two biosynthetic enzymes helps Escherichia coli sustain heme synthesis and activate catalase during hydrogen peroxide stress. *Molecular Microbiology*. *32,* 1102-1109

Meyer, J. (2008). Iron-sulfur protein folds, iron-sulfur chemistry, and evolution. In *Journal of Biological Inorganic Chemistry*. *23,* 55-59

Miller, C. E., Williams, P. H., & Ketley, J. M. (2009). Pumping iron: Mechanisms for iron uptake by *Campylobacter*. In *Microbiology*. *6,* 11-22

Mongkolsuk, S., & Helmann, J. D. (2002). Regulation of inducible peroxide stress responses. In *Molecular Microbiology*. *13,* 48-61

Morgan, P. E., Dean, R. T., & Davies, M. J. (2004). Protective mechanisms against peptide and protein peroxides generated by singlet oxygen. *Free Radical Biology and Medicine*. *187,* 6630-6645

Muraoka, W. T., & Zhang, Q. (2011). Phenotypic and genotypic evidence for L-fucose utilization by Campylobacter jejuni. *Journal of Bacteriology*. *187,* 778-795

Murdoch, L. E., MacLean, M., MacGregor, S. J., & Anderson, J. G. (2010). Inactivation of *Campylobacter jejun*i by exposure to high-intensity 405-nm visible light. *Foodborne Pathogens and Disease*. *5,* 458-487

Nitzan, Y., & Kauffman, M. (1999). Endogenous porphyrin production in bacteria by δ-aminolaevulinic acid and subsequent bacterial photoeradication. *Lasers in Medical Science*. *72,* 5420-5465

Nothaft, H., Davis, B., Lock, Y. Y., Perez-Munoz, M. E., Vinogradov, E., Walter, J., Coros, C., & Szymanski, C. M. (2016). Engineering the *Campylobacter jejuni* N-glycan to create an effective chicken vaccine. *Scientific Reports*. *181*-6371-6376

Nothaft, H., Liu, X., McNally, D. J., Li, J., & Szymanski, C. M. (2009). Study of free oligosaccharides derived from the bacterial N-glycosylation pathway. *Proceedings of the National Academy of Sciences of the United States of America*. *53,* 235-245

Nyati, K. K., & Nyati, R. (2013). Role of *Campylobacter jejuni* infection in the pathogenesis of

Guillain-Barré syndrome: An update. In *BioMed Research International*. *12,* 440-458

O Cróinín, T., & Backert, S. (2012). Host epithelial cell invasion by *Campylobacter jejuni*: trigger or zipper mechanism? In *Frontiers in cellular and infection microbiology*. *298,* 96-102

Oelschlaeger, T. A., Guerry, P., & Kopecko, D. J. (1993). Unusual microtubule-dependent endocytosis mechanisms triggered by *Campylobacter jejuni* and *Citrobacter freundii*. *Proceedings of the National Academy of Sciences of the United States of America*. *13,* 113-132

Palyada, K., Sun, Y. Q., Flint, A., Butcher, J., Naikare, H., & Stintzi, A. (2009). Characterization of the oxidative stress stimulon and PerR regulon of *Campylobacter jejuni. BMC Genomics*. *52,* 78-85

Panek, H., & O'Brian, M. R. (2002). A whole genome view of prokaryotic haem biosynthesis. In *Microbiology*. *221,* 1-15

Panel, E., & Biohaz, H. (2010). Scientific Opinion on Quantification of the risk posed by broiler meat to human campylobacteriosis in the EU. *EFSA Journal*, *8*(1), 1–89.

Parkhill, J., Wren, B. W., Mungall, K., Ketley, J. M., Churcher, C., Basham, D., Chillingworth, T., Davies, R. M., Feltwell, T., Holroyd, S., Jagels, K. (2000). The genome sequence of the food-borne pathogen Campylobacter jejuni reveals hypervariable sequences. *Nature*. *65,* 1-18

Pascoe, B., Williams, L. K., Calland, J. K., Meric, G., Hitchings, M. D., Dyer, M., Ryder, J., Shaw, S., Lopes, B. S., Chintoan-Uta, C., Allan, E., Vidal, A., Fearnley, C., Everest, P., Pachebat, J. A., Cogan, T. A., Stevens, M. P., Humphrey, T. J., Wilkinson, T. S., … Sheppard, S. K. (2019). Domestication of campylobacter jejuni NCTC 11168. *Microbial Genomics*, *5*(7).

Pedigo, L. A., Gibbs, A. J., Scott, R. J., & Street, C. N. (2009). Absence of bacterial resistance following repeat exposure to photodynamic therapy. *Photodynamic Therapy: Back to the Future*. *5,* 655-679

Poly, F., Noll, A. J., Riddle, M. S., & Porter, C. K. (2019). Update on Campylobacter vaccine development. *Human Vaccines and Immunotherapeutics*, *15*(6), 1389–1400.

Prather, K. L. J., & Martin, C. H. (2008). De novo biosynthetic pathways: rational design of microbial chemical factories. In *Current Opinion in Biotechnology*. *8,* 665-679

Putnam, C. D., Arvai, A. S., Bourne, Y., & Tainer, J. A. (2000). Active and inhibited human catalase structures: Ligand and NADPH binding and catalytic mechanism. *Journal of Molecular Biology*. *8,* 120-128

Queiroz, R. M. L., Smith, T., Villanueva, E., Marti-Solano, M., Monti, M., Pizzinga, M., Mirea, D. M., Ramakrishna, M., Harvey, R. F., Dezi, V., Thomas, G. H., Willis, A. E., & Lilley, K. S. (2019). Comprehensive identification of RNA–protein interactions in any organism using orthogonal organic phase separation (OOPS). *Nature Biotechnology*. *270,* 554-568

Raczko, A. M., Bujnicki, J. M., Pawłowski, M., Godlewska, R., Lewandowska, M., & Jagusztyn-Krynicka, E. K. (2005). Characterization of new DsbB-like thiol-oxidoreductases of Campylobacter jejuni and *Helicobacter pylori* and classification of the DsbB family based on phylogenomic, structural and functional criteria. *Microbiology*. *95,* 5289-5297

Raphael, B. H., Pereira, S., Flom, G. A., Zhang, Q., Ketley, J. M., & Konkel, M. E. (2005). The *Campylobacter jejuni* response regulator, CbrR, modulates sodium deoxycholate resistance and chicken colonization. *Journal of Bacteriology*. *34,* 647-689

Regensburger, J., Maisch, T., Felgenträger, A., Santarelli, F., & Bäumler, W. (2010). A helpful

technology - The luminescence detection of singlet oxygen to investigate photodynamic inactivation of bacteria (PDIB). *Journal of Biophotonics*. *2,* 9-11

Ridley, K. A., Rock, J. D., Li, Y., & Ketley, J. M. (2006). Heme utilization in *Campylobacter jejuni. Journal of Bacteriology*. *89,* 175-189

Riedel, C. T., Brøndsted, L., Rosenquist, H., Haxgart, S. N., & Christensen, B. B. (2009). Chemical decontamination of *Campylobacter jejuni* on chicken skin and meat. *Journal of Food Protection,* 2, 188-198

Roche, B., Aussel, L., Ezraty, B., Mandin, P., Py, B., & Barras, F. (2013). Iron/sulfur proteins biogenesis in prokaryotes: Formation, regulation and diversity. In *Biochimica et Biophysica Acta - Bioenergetics*. *32,* 1022-1044

Romeo, T., & Babitzke, P. (2018). Global Regulation by CsrA and Its RNA Antagonists. *Microbiology Spectrum*. *218,* 167-174

Rosenquist, H., Boysen, L., Galliano, C., Nordentoft, S., Ethelberg, S., & Borck, B. (2009). Danish strategies to control *Campylobacter* in broilers and broiler meat: Facts and effects. *Epidemiology and Infection*. *6,* 11-22

Rosenquist, Hanne, Nielsen, N. L., Sommer, H. M., Nørrung, B., & Christensen, B. B. (2003). Quantitative risk assessment of human campylobacteriosis associated with thermophilic *Campylobacter* species in chickens. *International Journal of Food Microbiology*. *13,* 48-61

Scherer, K., Bartelt, E., Sommerfeld, C., & Hildebrandt, G. (2006). Comparison of different sampling techniques and enumeration methods for the isolation and quantification of *Campylobacter* spp. in raw retail chicken legs. *International Journal of Food Microbiology*. *285,* 213-219

Sellars, M. J., Hall, S. J., & Kelly, D. J. (2002). Growth of *Campylobacter jejuni* supported by respiration of fumarate, nitrate, nitrite, trimethylamine-N-oxide, or dimethyl sulfoxide requires oxygen. *Journal of Bacteriology*. *187,* 664-659

Sharma, M., Visai, L., Bragheri, F., Cristiani, I., Gupta, P. K., & Speziale, P. (2008). Toluidine blue-mediated photodynamic effects on staphylococcal biofilms. *Antimicrobial Agents. 31,* 889-899

Shchepachev, V., Bresson, S., Spanos, C., Petfalski, E., Fischer, L., Rappsilber, J., & Tollervey, D. (2019). Defining the RNA interactome by total RNA -associated protein purification. *Molecular Microbiology*. *92,* 88-91

Shimizu, T. (2013). The heme-based oxygen-sensor phosphodiesterase Ec DOS (DosP): Structure-function relationships. In *Biosensors*.*10,* 699-722

Skarp, C. P. A., Hänninen, M. L., & Rautelin, H. I. K. (2016). Campylobacteriosis: The role of poultry meat. In *Clinical Microbiology and Infection*. *64,* 57-74

Smith, T. (1919). The etiological relation of spirilla (vibrio fetus) to bovine abortion. *Journal of Experimental Medicine*. *95,* 1889-1921

St. Denis, T. G., Dai, T., Izikson, L., Astrakas, C., Anderson, R. R., Hamblin, M. R., & Tegos, G. P. (2011). All you need is light, antimicrobial photoinactivation as an evolving and emerging discovery strategy against infectious disease. *Virulence*, *2*(6), 509–520.

St. Denis, T. G., Huang, L., Dai, T., & Hamblin, M. R. (2011). Analysis of the bacterial heat shock response to photodynamic therapy-mediated oxidative stress. *Photochemistry and Photobiology*. *101,* 897-899

Stahl, M., Friis, L. M., Nothaft, H., Liu, X., Li, J., Szymanski, C. M., & Stintzi, A. (2011). L-fucose utilization provides *Campylobacter jejuni* with a competitive advantage. *Proceedings of the National Academy of Sciences of the United States of America*. *76,* 5268-5289

Sun, J., Zhang, Y., Su, J., Dai, T., Chen, J., Zhang, L., Wang, H., Liu, W., Huang, M., & Chen, Z. (2020). Naftifine enhances photodynamic therapy against Staphylococcus aureus by inhibiting staphyloxanthin expression. *Dyes and Pigments*. *11,* 601-624

Szymanski, C. M., Ruijin, Y., Ewing, C. P., Trust, T. J., & Guerry, P. (1999). Evidence for a system of general protein glycosylation in Campylobacter jejuni. *Molecular Microbiology*. *11,* 1971-1978

Szymanski, C. M., & Wren, B. W. (2005). Protein glycosylation in bacterial mucosal pathogens. In *Nature Reviews Microbiology*. *45,* 654-658

Tang, Y., & Guest, J. R. (1999). Direct evidence for mRNA binding and post-transcriptional regulation by *Escherichia coli* aconitases. *Microbiology*. *365,* 1361-1369

Tavares, A., Carvalho, C. M. B., Faustino, M. A., Neves, M. G. P. M. S., Tomé, J. P. C., Tomé, A. C., Cavaleiro, J. A. S., Cunha, Â., Gomes, N. C. M., Alves, E., & Almeida, A. (2010). Antimicrobial photodynamic therapy: Study of bacterial recovery viability and potential development of resistance after treatment. *Marine Drugs*. *51,* 702-732

Tavares, A., Dias, S. R. S., Carvalho, C. M. B., Faustino, M. A. F., Tomé, J. P. C., Neves, M. G. P. M. S., Tomé, A. C., Cavaleiro, J. A. S., Cunha, Â., Gomes, N. C. M., Alves, E., & Almeida, A. (2011). Mechanisms of photodynamic inactivation of a Gram-negative recombinant bioluminescent bacterium by cationic porphyrins. *Photochemical and Photobiological Sciences 10,* 481-497

Taxonomy of the Family Campylobacteraceae. (2014). In *Campylobacter, Third Edition*.

Taylor, A. J., & Kelly, D. J. (2019). The function, biogenesis and regulation of the electron transport chains in *Campylobacter jejuni:* New insights into the bioenergetics of a major food-borne pathogen. In *Advances in Microbial Physiology* (Vol. 74).

Tegos, G. P., Masago, K., Aziz, F., Higginbotham, A., Stermitz, F. R., & Hamblin, M. R. (2008). Inhibitors of bacterial multidrug efflux pumps potentiate antimicrobial photoinactivation. *Antimicrobial Agents and Chemotherapy*. *65,* 1-14

Thöny-Meyer, L. (1997). Biogenesis of respiratory cytochromes in bacteria. *Microbiology and Molecular Biology Reviews : MMBR*. *5,* 988-999

Tustin, J., Laberge, K., Michel, P., Reiersen, J., Dadadóttir, S., Briem, H., Hardardóttir, H., Kristinsson, K., Gunnarsson, E., Fridriksdóttir, V., & Georgsson, F. (2011). A National Epidemic of Campylobacteriosis in Iceland, Lessons Learned. *Zoonoses and Public Health*. *76,* 297-311

van der Stel, A. X., van Mourik, A., Łaniewski, P., van Putten, J. P. M., Jagusztyn-Krynicka, E. K., & Wösten, M. M. S. M. (2015). The *Campylobacter jejuni* RacRS two-component system activates the glutamate synthesis by directly upregulating γ-glutamyltranspeptidase (GGT). *Frontiers in Microbiology*. *285,* 1534-15836

Van Vliet, A. H. M., Baillon, M. L. A., Penn, C. W., & Ketley, J. M. (1999). Campylobacter jejuni contains two fur homologs: Characterization of iron-responsive regulation of peroxide stress defense genes by the PerR repressor. *Journal of Bacteriology*. *193,* 1-14

Vegge, C. S., Jansen van Rensburg, M. J., Rasmussen, J. J., Maiden, M. C. J., Johnsen, L. G., Danielsen, M., MacIntyre, S., Ingmer, H., & Kelly, D. J. (2016). Glucose metabolism via the

entner-doudoroff pathway in campylobacter: A rare trait that enhances survival and promotes biofilm formation in some isolates. *Frontiers in Microbiology*. *52,* 575-587

Velayudhan, J., Jones, M. A., Barrow, P. A., & Kelly, D. J. (2004). L-Serine Catabolism via an Oxygen-Labile L-Serine Dehydratase Is Essential for Colonization of the Avian Gut by *Campylobacter jejuni*. *Infection and Immunity*.*322,* 1437-1456

Velayudhan, J., & Kelly, D. J. (2002). Analysis of gluconeogenic and anaplerotic enzymes in *Campylobacter jejuni:* An essential role for phosphoenolpyruvate carboxykinase. *Microbiology*. *312,* 1526-1530

Véron, M., Lenvoisé-Furet, A., & Beaune, P. (1981). Anaerobic respiration of fumarate as a differential test between Campylobacter fetus and Campylobacter jejuni. *Current Microbiology*.*24,* 954-965

Wainwright, M. (2008). Photodynamic Therapy: The Development of New Photosensitisers. *Anti-Cancer Agents in Medicinal Chemistry*. *314,* 114-149

Weerakoon, D. R., Borden, N. J., Goodson, C. M., Grimes, J., & Olson, J. W. (2009). The role of respiratory donor enzymes in *Campylobacter jejuni* host colonization and physiology. *Microbial Pathogenesis*. *53,* 853-859

Weingarten, R. A., Grimes, J. L., & Olson, J. W. (2008). Role of Campylobacter jejuni respiratory oxidases and reductases in host colonization. *Applied and Environmental Microbiology*. *150,* 476-798

Wilkinson, F., Helman, W. P., & Ross, A. B. (1995). Rate Constants for the Decay and Reactions of the Lowest Electronically Excited Singlet State of Molecular Oxygen in Solution. An Expanded and Revised Compilation. *Journal of Physical and Chemical Reference Data*. *23,* 1135-1156

Woodall, C. A., Jones, M. A., Barrow, P. A., Hinds, J., Marsden, G. L., Kelly, D. J., Dorrell, N., Wren, B. W., & Maskell, D. J. (2005). Campylobacter jejuni gene expression in the chick cecum: Evidence for adaptation to a low-oxygen environment. *Infection and Immunity*. *6,* 1-14

Wright, J. A., Grant, A. J., Hurd, D., Harrison, M., Guccione, E. J., Kelly, D. J., & Maskell, D. J. (2009). Metabolite and transcriptome analysis of *Campylobacter jejuni in vitro* growth reveals a stationary-phase physiological switch. *Microbiology*. *43,* 23-56

Yamakoshi, Y., Umezawa, N., Ryu, A., Arakane, K., Miyata, N., Goda, Y., Masumizu, T., & Nagano, T. (2003). Active Oxygen Species Generated from Photoexcited Fullerene (C 60) as Potential Medicines: O2-. versus 1O2. *Journal of the American Chemical Society*. *456,* 1154-1159

Yeaman, M. R., & Yount, N. Y. (2003). Mechanisms of antimicrobial peptide action and resistance. In *Pharmacological Reviews*. *84(5),* 435-58

Ziegelhoffer, E. C., & Donohue, T. J. (2009). Bacterial responses to photo-oxidative stress. *Nature Reviews Microbiology*, *306* 575-576.

Supplementary Tables:

Supplementary table 1 :

RNAseq analysis of photooxidative stress response

https://drive.google.com/file/d/1acHCeRzGzqkj723o9h8rMEYlGAGYzVXl/view?usp=sharing

Supplementary table 2 :

Initial *C. jejuni* RBPome

https://drive.google.com/file/d/14TebwcuH46tdK3WfOMly2FPn5gmSeAPK/view?usp=sharing

Supplementary table 3 :

Dynamic TMT labelled *C. jejuni* RBPome

https://drive.google.com/file/d/10ZUgRRQeYEAnVoHA1mjgxG7dGGzxVSRL/view?usp=sharing